University of Cagliari University of Sassari

PhD Degree in Chemical Science and Technology

Cycle XXXIII

DEVELOPMENT OF ELECTROCHEMICAL BIOSENSORS FOR THE DETERMINATION OF ANALYTES OF ALIMENTARY AND BIOMEDICAL INTEREST

Scientific Disciplinary Sectors: CHIM/03-CHIM/01

PhD Thesis of

Francesca Meloni

Supervisor

Prof. Antonio Zucca

Co-Supervisor

Prof. Maria Itria Pilo

Coordinator

Prof. Stefano Enzo

Final Exam. Academic Year 2019-2020

Thesis Defence: May 2021 Session

This PhD work is also the result of an 8-month collaboration with the research group of **Prof. Joanna Cabaj** of the Wrocław University of Science and Technology in which I spent the period abroad required by the PhD regulations.



UNIVERSITA' DEGLI STUDI DI CAGLIARI

Francesca Meloni gratefully acknowledges Sardinian Regional Government for the financial support of this PhD scholarship (P.O.R. Sardegna F.S.E. – Operational Programme of the Autonomous Region of Sardinia, European Social Fund 2014-2020 – Axis III Education and Training, Thematic goal 10, Investment Priority 10ii, Specific Goal 10.5) and the Mobility Grants Erasmus+ Placedoc.

Once the storm is over you won't remember

how you made it through, how you manage to survive.

You won't even be sure, in fact, whether the storm is really over.

But one thing is certain. When you come out of the storm

you won't be the same person who walked in.

That's what this storm's all about.

Haruki Murakami, Kafka on the Shore

TABLE OF CONTENTS

INTRODUCTION 10

CHAPTER 1 – STATE OF THE ART 15

1.1 Biosensors: Historical Background 16

1.2 Classification of Biosensors 20

1.2.1 Classification of Biosensors based on Recognition Method 20

1.2.1.1 Biocatalytic Recognition Biosensors 20

Recognition by Enzymes 22

1.2.1.2 Biocomplexing or Bioaffinity Recognition Biosensors 23

1.2.2 Classification of Biosensors based on Transducers 24

1.2.2.1 Electrochemical Biosensors 25

Amperometric Biosensors 25

Potentiometric Biosensors 33

Conductometric Biosensors 36

Impedimetric Biosensors 37

1.2.2.2 Optical Biosensors 39

1.2.2.3 Calorimetric Biosensors 42

1.2.2.4 Mass-based Biosensors 43

1.3 Enzyme-based Amperometric Biosensors for Histamine and Epinephrine: an Overview 45

1.3.1 Histamine 48

1.3.2 Epinephrine 63

1.4 Enzymes 72

1.4.1 Introduction 72

1.4.2 Classification of Enzymes 75

1.4.3 Enzyme Kinetics 77

1.4.4 Effects of pH and Temperature on Enzyme Reactions 81

1.4.5 Enzymes in Biosensors 82

1.4.6 Diamine Oxidase (DAO) 83

1.4.7 Tyrosinase (Tyr) 85
1.4.8 Immobilization Techniques 88
1.4.8.1 Adsorption 89
1.4.8.2 Entrapment 90
Entrapment via Electropolymerization 90
1.4.8.3 Cross-linking 91
Cross-linking with Glutaraldehyde 91
1.4.8.4 Immobilization by Covalent Bond 96
Activation of Carboxylic Groups 96
Activation of Amino Groups 97
1.5 Conducting Polymers and Metallopolymers 98
1.5.1 Conducting Polymers 98
1.5.2 Conductive Mechanism 102
1.5.3 Doping Processes 106
1.5.3.1 Formation of Solitons, Polarons and Bipolarons 107
1.5.4 Polythiophenes (PThs) 110
1.5.4.1 Structure and Properties 111
1.5.4.2 Chemical Synthesis 112
1.5.4.3 Electrochemical Synthesis 115
Cathodic Reduction 115
Anodic Oxidation 115
1.5.5 Conducting Metallopolymers 119
CHAPTER 2 – EXPERIMENTAL 123
2.1 Electrochemical Techniques 124
2.1.1 Cyclic Voltammetry 124
2.1.2 Differential Pulse Voltammetry 128
2.1.3 Chronoamperometry 129
2.2 Instruments and Reagents 131
2.2.1 Instruments 131
2.2.2 Reagents 131

2.3 Synthesis of Monomers 132

2.3.1 Sonogashira-Hagihara Cross-Coupling Reactions 132

2.3.2 Suzuki-Miyaura Cross-Coupling Reactions 135

2.3.3 Synthesis of 4,4′-([2,2′-bithiophene]-4-4′-diyl)bis(2-methylbut-3-yn-2-ol) (1) and 4-(4′-bromo-[2,2′-bithiophen]-4-yl)-2-methylbut-3-yn-2-ol (2) 139

2.3.4 Synthesis of 4,4′-diethynil-2,2′-bithiophene (3) 141

2.3.5 Synthesis of 4,4′-([2,2′-bithiophene]-4,4′-diylbis(ethyne-2,1-diyl))dianiline (4) 143

2.3.6 Synthesis of 4,4′-([2,2′-bithiophene]-4,4′-diylbis(ethyne-2,1-diyl)) dibenzoic acid (5) 147

2.3.6.1 Synthesis Attempt 1 148

2.3.6.2 Synthesis Attempt 2 148

2.3.6.3 Synthesis Attempt 3 152

2.3.6.4 Synthesis Attempt 4 153

2.3.6.5 Synthesis Attempt 5 157

2.3.6.6 Synthesis Attempt 6 158

2.3.6.7 Synthesis Attempt 7: One-Pot Sonogashira Method 159

2.3.7 Synthesis of 4′-(2,2′:5′,2′′-terthien-3′-ethynyl)-2,2′:6′,2′′-terpyridine (TAT) . 160

2.3.8 Synthesis of of [(TAT)Ru(TpyCOOH)][PF_6]$_2$ 166

CHAPTER 3 – RESULTS AND DISCUSSION 169

3.1 Electrochemical Characterization of Monomers and of Their Corresponding Polymers 170

3.1.1 4,4′-([2,2′-bithiophene]-4-4′-diyl)bis(2-methylbut-3-yn-2-ol) (1) 170

3.1.2 4-(4′-bromo-[2,2′-bithiophen]-4-yl)-2-methylbut-3-yn-2-ol (2) 173

3.1.3 4,4′-diethynil-2,2′-bithiophene (3) 175

3.1.4 4,4′-([2,2′-bithiophene]-4,4′-diylbis(ethyne-2,1-diyl))dianiline (4) 180

3.1.5 4′-(2,2′:5′,2′′-terthien-3′-ethynyl)-2,2′:6′,2′′-terpyridine (TAT) 184

3.1.6 [(TAT)Ru(TpyCOOH)][PF_6]$_2$ 186

3.1.7 4,7-bis(5-(pyridin-2-yl)thiophen-2-yl)benzo[c][1,2,5]thiadiazole (TBT) 189

3.1.8 Bis(4-(thiophen-2-yl)tetraphenylsilane (TTP) 193

3.2 Spectroscopic Characterization 195

3.2.1 Dithiophene-based Monomers **195**
3.2.2 4′-(2,2′:5′,2′′-terthien-3′-ethynyl)-2,2′:6′,2′′-terpyridine (TAT) **197**
3.2.3 Bis(4-(thiophen-2-yl)tetraphenylsilane (TTP) **197**
3.2.4 Poly[(TAT)Ru(TpyCOOH)] **198**
3.2.5 Poly(TTP) **199**
3.3 Biosensors Assembly **200**
3.3.1 General Procedures for Biosensors Assembly **200**
3.3.2 Preparation of Diamine Oxidase (DAO) Solution and Immobilization Procedure **201**
3.3.3 Preparation of Tyrosinase (Tyr) Solution and Immobilization Procedure **201**
3.4 Biosensors for Histamine Detection **202**
3.4.1 Pt/PEDOT/DAO **202**
3.4.2 Pt/Poly[(TAT)Ru(TpyCOOH)]/DAO **205**
3.5 Biosensors for Epinephrine Detection **208**
3.5.1 Au/Poly(TBT)/Tyr **208**
3.5.2 Poly[(TAT)Ru(TpyCOOH)]/Tyr-based Biosensors **214**
3.5.2.1 Au/Poly[(TAT)Ru(TpyCOOH)]/Tyr 215
3.5.2.2 GC/Poly[(TAT)Ru(TpyCOOH)]/Tyr 225
3.5.3 Poly(TTP)/Tyr-based Biosensors **231**
3.5.3.1 Au/Poly(TTP)/Tyr 231
3.6 Biosensors for Dopamine Detection **237**
3.6.1 Au/Poly(TTP)/Tyr **238**
3.6.2 GC/Poly(TTP)/Tyr **242**
FINAL SUMMARY **250**
REFERENCES **258**
AKNOWLEDGEMENTS **268**

INTRODUCTION

Biosensors are defined as analytical devices that use biorecognition elements (such as enzymes, antibodies, nucleic acids, aptamers, cells, tissues etc.) to interact with the target analyte in order to produce an input biochemical signal. This signal is then converted, by the transducer element, into a different output signal (electric, optical, acoustic etc.), proportional to the concentration of the analyte[1-3].

Even though scientists started talking about biosensing in the early 1900s, it is only in the past fifty years that this interest has increased significantly. A Scopus study reveals that since 1972 to 2014 the number of publications about biosensors has shown exponential growth[2,4].

The growing appeal is mainly due to the need to realize simple, rapid, cost-effective and portable analytical tools for the detection of pollutants in the environment, markers that are indicators of a disease in bodily fluids and potentially toxic molecules in food stuff (figure 1), in order to minimize health risks, improving the quality of life[2,5-7].

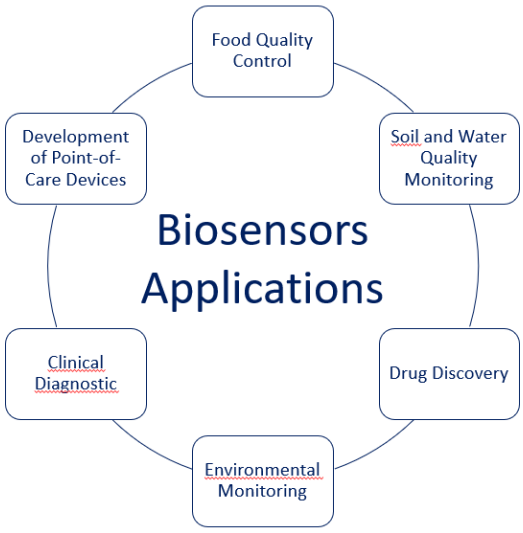

Figure 1: main applications of biosensors

Until few years ago, this type of analysis was mainly carried out using classical techniques, such as chromatography (gas chromatography, reversed phase high performance liquid chromatography with pre-column, ion exchange chromatography etc. often coupled with mass spectrometry), optical methods, calorimetry etc. These conventional techniques are highly sensitive and selective, but they are also expensive, sometimes complicated, and time consuming, since often, before the analysis, complex extraction, purification and/or derivatization steps of the sample under examination are required[7,8]. For these reasons, traditional techniques cannot be used by non-specialized operators and they are not the best solution for daily and repetitive analyses, both from an economic and saving time point of view.

Biosensors, at least ideally, have all the advantages of the just mentioned techniques, which are combined with the features of rapid analysis, low costs, possibility of use in places other than laboratory and, in some instances, by unskilled users. Typical example of biosensors with all these characteristics are the so-called point-of-care diagnostic devices such as the glucometer (for detection of glucose in blood), whose first commercial piece, developed by Yellow Spring Instruments (YSI), dates back to 1975[2,7].

However, unlike biosensors developed for some biomedical applications, those used in different fields (in particular in the alimentary and environmentally sectors) are currently not commercially available because they often have several drawbacks. The biorecognition element can be selective for a specific analyte or for an entire class of analytes, allowing the analysis of a single analyte or of all the various analytes belonging to the same class, respectively. This aspect can be problematic depending on the type of required analyses. Furthermore, another barrier to the development of efficient biosensors is the uncertain stability of the bio-material which could undergo degradation phenomena depending on pH, temperature, immobilization or anchoring processes to which it is subjected[9].

As a result of what has been said so far, the goal, but also the challenge, of this work has been to try to develop efficient biosensors that can be used in food and biomedical fields. The biosensors, designed and assembled by our research group, are enzyme-based electrochemical devices.

Among the various types of biosensors, the electrochemical ones are the most common and also the most promising in the fields of our interest. Indeed, as evidenced in literature papers, electrochemical biosensors present several advantages: versatility, ease of assembly and miniaturization, robustness, possibility of use in small volumes of various matrices (even complex and turbid), low limits of detection (LoD), low instrumentation and reagents costs and rather long-life times. In particular, the latter two characteristics are very important as regards, respectively, the development of the so-called "single shot" analysis tools for applications requiring disposable devices (food quality monitoring, clinical analysis etc.) and the development of the so-called "long-term monitoring" analysis tools for applications (such as pollution monitoring) requiring devices that should operate from a few hours to several days.

In addition, among electrochemical biosensors, the enzyme-based ones are the cheapest and fastest and, thanks to the enzyme features of extreme chemical specificity and intrinsic signal amplification, they are also the most sensitive and selective. Particularly, the most used enzymes are those of the oxidoreductase type which are widely studied and are easily available on the market[2,7,10-13].

Thanks to all these worthwhile features, this PhD thesis work was oriented in this direction, also considering the previous experience of the research group on construction of enzyme-based electrochemical biosensors for detection of glucose, polyphenols and 5-hydroxymethyl-2-furaldehyde (HMF) in food matrices[9]. On the other hand, the research group where this work has been carried on possesses a long experience in synthesis of monomers (both completely organic molecules and transition metal complexes) for the generation

of conducting (metallo)polymers to use as modifying agents for electrode surfaces.

For these reasons the plan of this work starts from the design and synthesis of new thiophene-based monomers, suitable to give polymer films on electrode surfaces by electrochemical deposition. Then, the enzyme immobilization is achieved by means of the polymer film, and finally the obtained biosensors are tested in the determination of target molecules.

The target analytes taken into account are mainly histamine and epinephrine, as well as dopamine. A part of the research work has been developed in collaboration with the group of Prof. Joanna Cabaj of the Wrocław University of Science and Technology, during the traineeship period included in the PhD programme.

Histamine is one of the most toxic biogenic amines, responsible of the so-called scombroid syndrome, and its concentration is used as an index to evaluate the freshness and quality of different food products. Epinephrine and dopamine, well-known neurotransmitters and hormones of the catecholamine family, may be considered markers of presence of possible various diseases (Parkinson's disease, schizophrenia, depression, Alzheimer's disease, presence of tumours).

Summarizing schematically, the topics covered during this three-year work are:

1. Design and synthesis of new thiophene-based monomers containing different functionalities such as triple bonds, and carboxylic and amino groups, allowing an adequate anchoring of specific enzymes.
2. Development of a biosensor based on diamine oxidase (DAO) immobilized on a terthiophene-based metal-polymer film for histamine detection.
3. Development of biosensors based on tyrosinase immobilized on different conducting polymer-based films for epinephrine detection.
4. Development of biosensors based on tyrosinase immobilized on thiophene-based film for dopamine detection.

CHAPTER 1

STATE OF THE ART

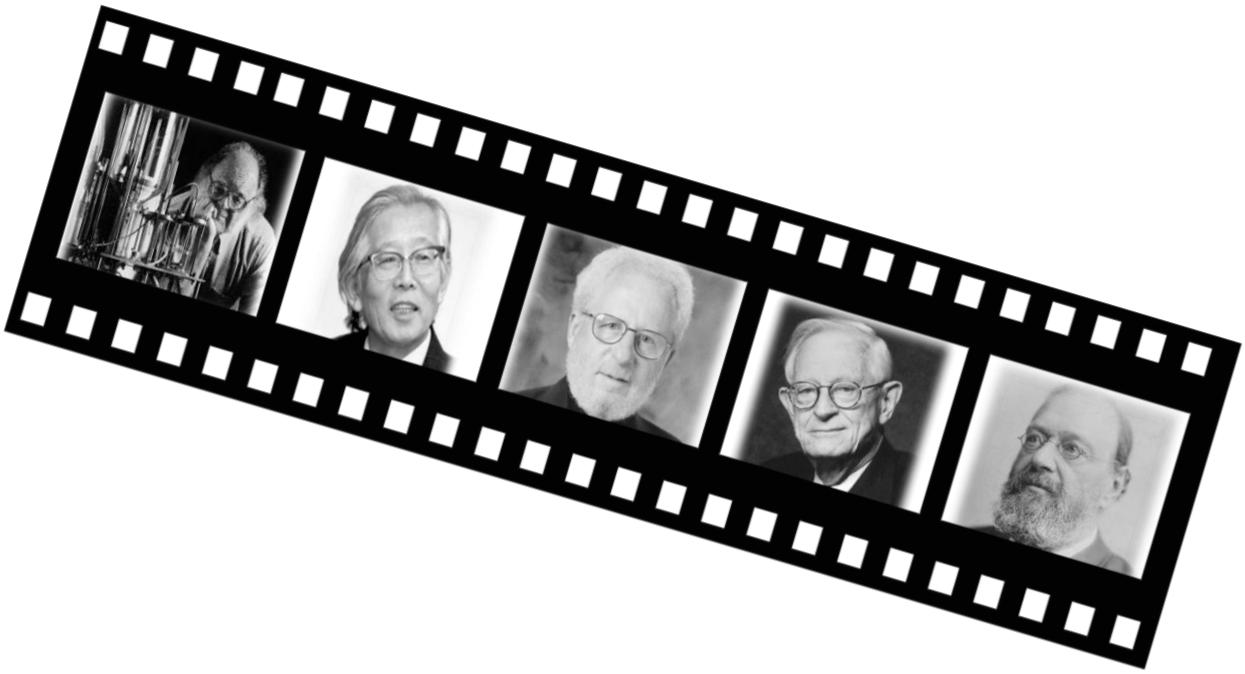

From left to right: Leland Clark, Hideki Shirakawa, Alan Heeger, Alan McDiarmid and Jaroslav Heyrovský

1.1 Biosensors: Historical Background

Chemical sensors are small devices that convert chemical information, such as the presence and/or the concentration of one or more specific analytes, into analytically useful signal. They are made up of three main elements (figure 2):

1. A chemical-type recognition element, also called chemical receptor, which is responsible for detecting the input signal, undergoing some chemical modifications or transformations by interaction or reaction with the analyte.
2. A chemical-physical transducer that converts the incoming chemical signal into a different quantifiable one (electrical, optical, calorimetric, piezoelectric etc.), making it associable with a quantitative determination.
3. An electronic component consisting of a signal amplification system, a display, a data processing and a storage system.

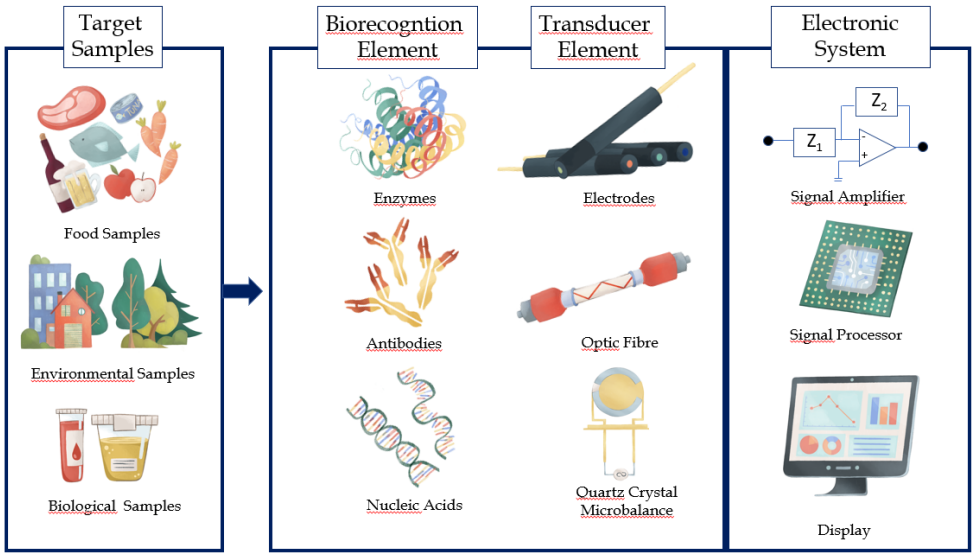

Figure 2: schematic representation of a biosensor

In 1977, Karl Cammann coined the term "biosensor" and defined it as: "A chemical sensor in which the recognition system utilises a biochemical mechanism". In 1992, the International Union of Pure and Applied Chemistry

(IUPAC) defines a biosensor as: "A device that uses specific biochemical reactions mediated by isolated enzymes, immunosystems, tissues, organelles or whole cells to detect chemical compounds usually by electrical, thermal or optical signals", thus incorporating the antecedent and provisional definition of "enzyme electrode" defined as: "A sensor in which an ion-selective electrode is covered with a coating that contains an enzyme, which causes the reaction of an organic or inorganic substance (substrate) to produce a species to which the electrode responds"[3,14-17].

Finally, in 2001, two divisions of the IUPAC Organization, namely Physical Chemistry (Commission I.7 on Biophysical Chemistry formerly Steering Committee on Biophysical Chemistry) and Analytical Chemistry (Commission V.5 on Electroanalytical Chemistry) defined an electrochemical biosensor: "An electrochemical biosensor is a self-contained integrated device, which is capable of providing specific quantitative or semi-quantitative analytical information using a biological recognition element (biochemical receptor) which is in direct spatial contact with an electrochemical transduction element"[14]. The definition was, then, extended by IUPAC to all types of biosensors: "A biosensor is a self-contained integrated device which is capable of providing specific quantitative or semi-quantitative analytical information using a biological recognition element (biochemical receptor) which is in direct spatial contact with a transducer element. A biosensor should be clearly distinguished from a bioanalytical system which requires additional processing steps, such as reagent addition. Furthermore, a biosensor should be distinguished from a bio-probe which is either disposable after one measurement, e.g., single use, or unable to continuously monitor the analyte concentration"[10].

Scientists started talking about sensing and biosensing in the first two decades of the 1900s. In 1906 Max Cremer, in his investigation about glass electrodes, proved that the electric potential that occurs between parts of the fluid located on

opposite sides of the glass membrane is proportional to the concentration of acid[18].

In 1916 the first enzyme immobilization was performed: J.M. Nelson and Edward G. Griffin immobilized the enzyme invertase on gelatinous aluminium hydroxide and charcoal[19].

Successively, in 1922, after the introduction of pH concept by Søren P. L. Sørensen, an electrode for pH measurements was realised by W. S. Hughes. In 1956 the first amperometric sensor was designed and realised by Leland C. Clark, Jr.: this is a device for O_2 detection, known as "Clark sensor" or "Clark cell". Only six years later, Clark and Champ Lyons developed the first enzyme-coupled amperometric biosensor for determination of glucose in blood samples. This new device is a modification of the Clark sensor with a semipermeable membrane in which glucose oxidase (GOx) is entrapped. The mechanism is based on the following catalysed reaction:

$$\text{Glucose} + \text{FAD} + H_2O \longrightarrow \text{Gluconic Acid} + FADH_2$$

$$FADH_2 + O_2 \longrightarrow H_2O_2 + \text{FAD}$$

where FAD and $FADH_2$ are the oxidized and reduced form of flavin adenine dinucleotide, respectively.

The working electrode potential is set to a proper value in order to cause the reduction of H_2O_2 to H_2O that is proportional to oxygen consumption and glucose concentration. The innovation of Clark and Lyons is followed by an even greater news: S.J. Updike and G.P. Hicks designed and developed the first enzyme-based amperometric biosensor in which the enzyme is immobilized on a polyacrylamide gel, simplifying the preparation of the electrode and improving the operational stability of the GOx[19,20].

In 1969, a further innovation in the field of electrochemical biosensors was achieved thanks to the work of George G. Guilbault and Joseph G. Montalvo, Jr that assembled

the first potentiometric biosensor for urea detection. It is a glass electrode coupled with urease enzyme, whose operating principle is based on the determination of the pH variations as the catalysed reaction proceeds.

In 1975 Yellow Springs Instruments produced the first commercial glucometer based on the patent of Clark. One year later La Roche introduced the first second-generation enzyme-based amperometric biosensor, that is the lactate analyser, "LA 640": it used redox mediator (specifically, hexacyanoferrate) between the active site of lactate dehydrogenase and the electrode. According to analogous principles, Anthony Cass and collaborators proposed the use of ferrocene derivatives (ferricenium ion) as electronic shuttles for oxidoreductases and developed a biosensor for glucose determination[21,22].

In 1992 an enormous progress was achieved with the launch of the i-STAT handheld blood analyser, and from that moment on, research in the field of biosensing grew exponentially, as proved by the above-mentioned Scopus study and confirmed by a research on "Web of Science" that counts in its database over 84000 papers on the topic about biosensors (from 2005 to 2015), with approximately 72000 dating back to the last five years[2,4,9].

1.2 Classification of Biosensors

Biosensors can be classified according to the recognition method or to the transduction process or, alternatively, on a combination of both of these two (figure 3).

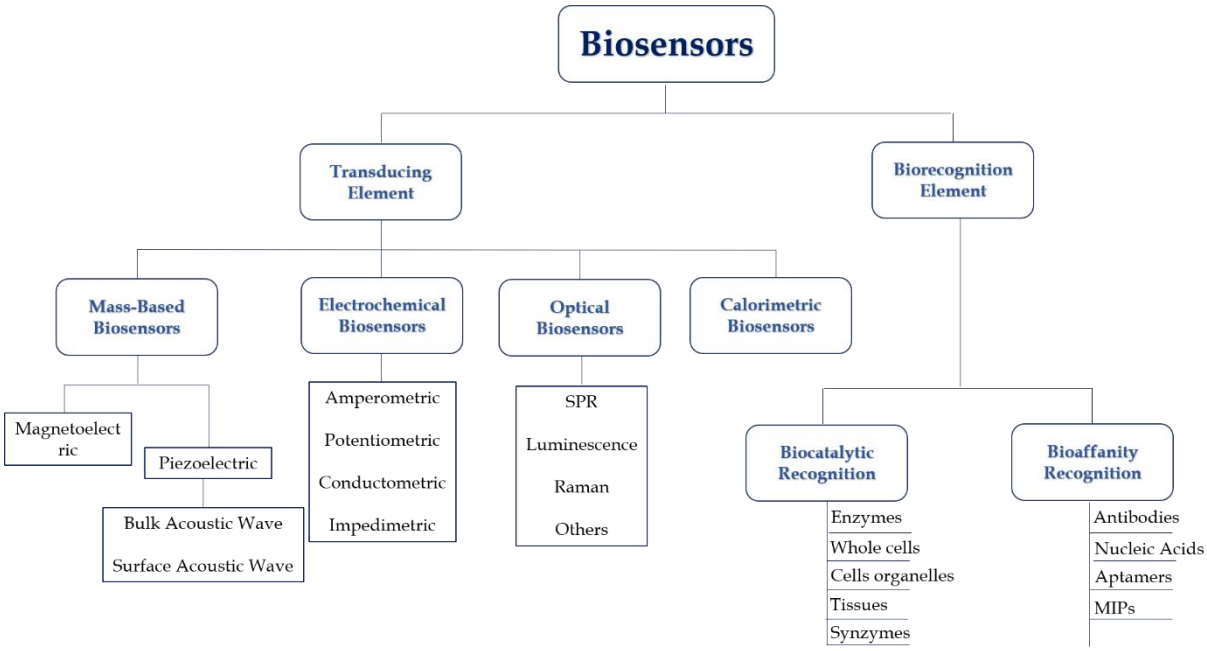

Figure 3: schematic representation of the classification of biosensors

1.2.1 Classification of Biosensors based on Recognition Method

As regards the classification based on recognition method, two main categories of biosensors can be distinguished: the most studied biocatalytic recognition biosensors and biocomplexing or bioaffinity biosensors[23,24].

1.2.1.1 Biocatalytic Recognition Biosensors

This type of biosensors includes devices based on a reaction, generally redox, catalysed by macromolecules that commonly are enzymes, whole cells (bacteria, fungi, eukaryotic cells or yeasts), cell organelles or particles (mitochondria, cell walls), or tissues (plant or animal tissue segments)[23].

In a nutshell, the operating mechanism of this kind of biosensors provides a reaction between the analyte (or substrate S) and a co-substrate (S') by the action of the biocatalyst to give one or several products (P and P') according to the following reaction:

$$S + S' \longrightarrow P + P'$$

The consumption of the analyte can be monitored by different strategies:

- Detection of the co-substrate S' consumption; the most common example is O_2 consumed by enzymes isolated or incorporated in cells or tissues or by bacteria or yeast reacting layers. In this case, the monitored signal undergoes a decrease with respect to the starting one.
- Recycling of the product P; the most common examples are H_2O_2, NH_3, CO_2 etc. deriving from the action of several types of enzymes (oxidoreductase, lyase etc.). In this case the monitored signal undergoes an increase.
- Detection of the state of the active site, of the cofactor (coenzyme or metal ion) or of the prosthetic group evolution of the biocatalyst in the presence of S by recording a signal of an additional species (called mediators or electronic shuttles), which rapidly exchange electrons between the biocatalyst and an electrochemical transducer. The additional species are generally ferrocene derivatives, organic salts, quinones, metal complexes in polymer matrices etc.
- Direct electron transfer between the active site of an enzyme and an electrochemical transducer[9,23,24].

Since, in this work, enzymes have been used as recognition elements, recognition by enzymes will be further explored in the next paragraph.

Recognition by Enzymes

Since in this work the developed biosensors are enzyme-based, it is necessary to pay particular attention to the recognition mechanism promoted by the latter.

Isolated enzymes are the most common biorecognition elements, although recently researchers realized that enzymes within biological materials such as cells and/or tissues can improve the enzymatic performances, as they are in their original environment[24]. Another class of materials, which are not enzymes but which perform the same function and which can be used instead of enzymes, are the so-called synzymes or synthetic enzymes[25]. The advantage in their use is that, compared to the native ones, they can be ideally designed in order to be less delicate, cheaper, chemically adaptable etc.

The recognition process supported by enzymes consists of three main steps:

1. The target analyte interacts with the active site of the enzyme yielding provisional analyte-enzyme complex.
2. The bound analyte undergoes a chemical transformation, often with the support of some co-reagents (e.g., O_2).
3. Products are released and the active site of the enzyme is restored to its active form.

This cycle is reiterated as long as the analyte and co-reagents are present.

The concentration of the analyte can be measured in different ways, according to the coupled transduction method, that is often an electrochemical method.

Enzyme-based biosensors can be used to determine the concentration of a target analyte exploiting either the catalytic activity of the enzyme towards the substrate, or its inhibition when the target molecules are species capable of negatively influencing its activity[24].

Thanks to their versatility of use and the wide variety of enzymes (isolated or in "masked" forms), enzyme-based are among the most developed biosensors.

1.2.1.2 Biocomplexing or Bioaffinity Recognition Biosensors

This type of biosensors is based on affinity interactions (ionic bonds, hydrogen bonds, Van der Waals interactions) that can be established between an analyte and the biorecognition system which, in this case, may be represented by antibodies, antigens, nucleic acids, aptamers etc.

The product of an affinity interaction is called molecular association complex and for this reason the recognition process is also called biocomplexing recognition. The molecular complex is the species detected by the transducer[23,24].

The most common recognition element, in this context, are antibodies (monoclonal or polyclonal) that are glycoproteins produced by the immune system to recognize and counteract bacteria or viruses; the part of microorganisms that interact with the antibody is called antigen. On the other hand, using an antigen as a receptor it is possible to detect a specific antibody. This type of biosensors is known as immunosensors.

Regarding nucleic acids, they are more stable than antibodies. In this case, the recognition process can occur by the so-called hybridization. This kind of affinity interaction involves only hydrogen bonds between guanine-cytosine and adenine-thymine in DNAs and or guanine-cytosine and adenine-uracil in RNAs. This allows to obtain a double-strand association complex between a short nucleic acid, normally used as a receptor (also called "capture probe") and the target nucleic acid. These devices are used for the detection of genetic anomalies, recognition of pathogen microorganisms and, in forensic field, to identify individuals by their DNA profiles[9,23,24].

Recently, around the 90s, scientists have also started developing biomimetic sensors: aptasensors and molecular imprinting polymer (MIP)-based biosensors belong to this category. The aptasensors exploit aptamers, that are small molecules of DNA or RNA with very high affinity for a particular target molecule, as a recognition element. Using SELEX process (Systematic Evolution of Ligands by EXponential enrichment process)

it is possible to obtain the aptamers with desired specific activity[26,27]. The use of aptamers is advantageous because they are very stable, suitable for using in real matrices (they can be easily functionalized and modified) and besides, thanks to their small dimensions (30-1000 nucleotides), they can be immobilized with high density[9,24,28]. MIPs are polymer materials including cavities with proper shape and dimensions to match the target analyte. They also mimic the behaviour of bioaffinity original molecules. Unlike antibodies, they are robust and stable and can be used in the presence of acids and organic solvents and can withstand also in particular pression and temperature conditions. MIPs have been developed for pesticides, amino acids, steroids and sugars[10].

However, compared to biosensors based on biocatalytic recognition, those based on bioaffinity recognition still have some drawbacks. They have usually a very limited linear range because they are based on equilibrium reactions, some of these devices cannot operate in biological matrices, others are not capable to monitor continuously the analyte concentration and, in some cases, they require additional reagents to perform the quantification[23].

1.2.2 Classification of Biosensors based on Transducers

Based on transduction method, biosensors can be classified as[28,29]:

- Electrochemical biosensors (amperometric, potentiometric, conductometric and impedimetric)
- Optical biosensors (SPR, Raman FTIR, fibre optic etc.)
- Calorimetric biosensors or bio thermistors
- Mass-based biosensors (piezoelectric and magnetoelectric)

1.2.2.1 Electrochemical Biosensors

Among different types of biosensors, the electrochemical ones are, currently, the most advanced and the most promising. As a matter of fact, they exhibit several advantages such as ease of assembly and miniaturization, robustness, possibility to operate in complex and turbid media, possibility to use in small volumes, rapid response and low LoD, thanks to several electroanalytical techniques (square wave voltammetry, differential pulse voltammetry, chronoamperometry) that can reach LoDs between 10^{-7} and 10^{-9} M. Besides, required instrumentation is simple and cheap if compared with that necessary for other types of biosensors such as the optical ones[13,30].

For the analysis with this type of devices, a classical electrochemical cell connected to a potentiostat or galvanostat is used.

The operating mechanism of electrochemical sensors is based on the determination of measurable electrical property: current (amperometric detection), potential or charge accumulation (potentiometric detection), conductivity change of a medium between electrodes (conductometric detection) and impedance change (impedimetric detection)[29,31].

Thanks to their worthwhile features and versatility of use, these analytical tools are used in many different fields: food quality monitoring (detection of glucose, biogenic amines, microorganisms etc.), industrial bioprocesses monitoring (detection of amino acids, lactic acid, ethanol, yeasts etc.), environmental monitoring (pesticides, gaseous analytes such as CO and CO_2, fertilizers etc.), clinical diagnostic (glucose level in blood, hormones, neurotransmitters etc.), and finally in forensic science (detection of doping and toxic substances, pathogens etc.)[9].

Amperometric Biosensors

Amperometric biosensors are the most widespread, numerous and successful electrochemical devices, from a commercial point of view, as they are highly sensitive,

reliable, cheap and rapid. Commonly, the amperometric technique relies on measuring the current flowing in an electrochemical cell when a constant potential value is applied on the working electrode. The potential is set in such a way as to produce a faradic process (oxidation or reduction) of the target molecule[32]. The current value is related to the concentration of the analyte according to the following mathematical equation:

$$i = nFAk_mC$$

in which:

i = limiting current [A];
n = number of exchanged electrons;
F = Faraday constant [C mol^{-1}];
A = working electrode area [cm^2];
k_m = mass transport coefficient [cm s^{-1}];
C = concentration of electroactive species [mol cm^{-3}];

The working electrodes are commonly made of platinum, gold, graphite or modified from these with conducting polymer films, metal nanoparticles etc. Polymer films are particularly suitable for immobilization of a biomolecule, offering a more proper environment than bare metal surfaces[9].

On the basis of the type of the immobilized biomolecule and of the material constituting the working electrode, the acquired current signal can be attributed to faradic processes that directly or indirectly concern the electroactive species. Particularly, when the immobilized biomolecule is an enzyme, it is possible to distinguish different classes of amperometric biosensors that differ one from each other for the identity of the recorded current signal[33]. In the first class the recorded signal is the oxidation/reduction current of one of the by-products of the enzyme

reaction; in the second class the detected current is due to the oxidation/reduction of the used redox mediator; in the third one, the current is that of a redox process directly associated with the active site of the enzyme.

The reason why most enzyme-based biosensors are coupled with an electrochemical (and in particular amperometric) transducer is to be found in the fact that many enzymatic reactions tend to either produce or consume protons and/or electroactive species.

Most of enzyme-based biosensors employ a class of enzymes called oxidoreductase and among these, two subclasses stand out: oxidases and dehydrogenases.

Their reaction sequences can be described by the following general reactions:

$$S_{red} + E_{ox} \longrightarrow S_{ox} + E_{red}$$

$$S'_{ox} + E_{red} \longrightarrow S'_{red} + E_{ox}$$

In which S is the substrate, S' can be a by-product, a mediator or the electrode itself and E_{ox} and E_{red} is the enzyme in its oxidized and reduced form, respectively.

Starting from this scheme, it is possible to classify three classes, known as generations, of biosensors[11,32,34].

1. First-generation biosensors:

First-generation biosensors, or mediatorless amperometric biosensors, are devices based on the measurement of concentration of analyte or products of enzyme reaction, that diffuse to the electrode surface generating an electrical response (figure 4).

The reaction mechanism can be sketched as follows:

$$S + E_{ox} \longrightarrow P + E_{red}$$

$$O_2 + E_{red} \longrightarrow H_2O_2 + E_{ox}$$

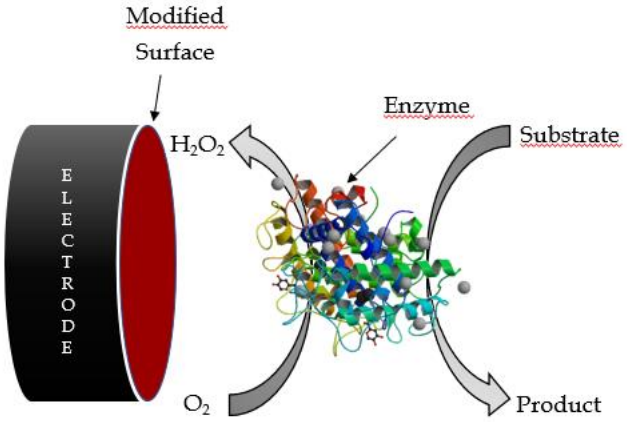

Figure 4: schematic representation of a first-generation biosensor

The most commonly used oxidases are the so-called copper-containing oxidases and those that contain flavin adenine dinucleotide (FAD) as a co-factor[11,24]. First-generation oxidases biosensors can measure either the consumption of O_2 by applying a constant cathodic potential (about -0.7 V *vs*. Ag/AgCl) or the formation of hydrogen peroxide (H_2O_2) by applying a constant anodic potential (about +0.7 V *vs*. Ag/AgCl). The first approach is, however, a little bit disadvantageous because it requires two measurements of O_2 concentration: before and after the enzymatic reaction. On the other hand, measurement of hydrogen peroxide is simpler, but the potential required for the oxidation of H_2O_2 is quite high and this can lead to the oxidation of other reducing species, such as ascorbic and uric acids, and some electroactive drugs. Nevertheless, it is possible to minimize interferences using permselective coatings that restrict these compounds to accessing to the electrode surface. As permselective coatings can be used electropolymerized films, in particular polyphenol and overoxidized polypyrrole, Nafion, size-exclusion cellulose acetate films, hydrophobic alkanethiol and lipid layers[8,11,35]. To minimize interferences, an alternative may be the use of a second enzyme, commonly horseradish peroxidase (HRP) that allows to determine H_2O_2 reducing it at a potential value where contributions of easily oxidable substances are eliminated and O_2 is not yet reduced. In this case it is more correct to speak of a third-generation biosensor, as it is possible to monitor the reduction of H_2O_2

at lower potentials thanks to the direct electron transfer between the peroxidase and the electrode[32,34,36], as shown in figure 5.

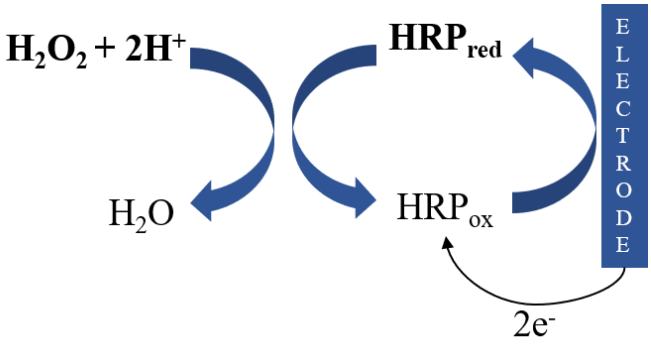

Figure 5: scheme of direct reduction of HRP

The most common co-factor in dehydrogenase enzymes is the oxidized form of nicotinamide adenine dinucleotide (NAD^+), and the reaction mechanism can be sketched as:

$$S + NAD^+ \longrightarrow P + NADH + H^+$$

$$NADH \longrightarrow NAD^+ + H^+ + 2e^-$$

For this type of biosensors, the reduced form of nicotinamide adenine dinucleotide (NADH) concentration is directly proportional to the concentration of the target analyte.

First-generation biosensors are highly sensitive and are characterized by a very short response-times (about one second). On the other hand, first-generation devices that use oxidases are oxygen dependent and, for this reason, if the dissolved O_2 is present in low concentration a decreased sensibility and a reduced linearity range could be obtained. Moreover, prolonged use can lead to a fouling of the biosensor surface, causing the need of a pre-treatment in order to generate a reproducible surface and sensor response[11].

2. Second-generation biosensors:

Second-generation biosensors, or mediator amperometric biosensors, exploit redox mediator as electron shuttle to transfer electrons between the enzyme active site and the transducer (figure 6).

The operating mechanism of this type of biosensor is based on the following general reactions sequences:

$$S + E_{ox} \longrightarrow P + E_{red}$$

$$E_{red} + M_{ox} \longrightarrow E_{ox} + M_{red}$$

$$M_{red} \longrightarrow M_{ox} + e^-$$

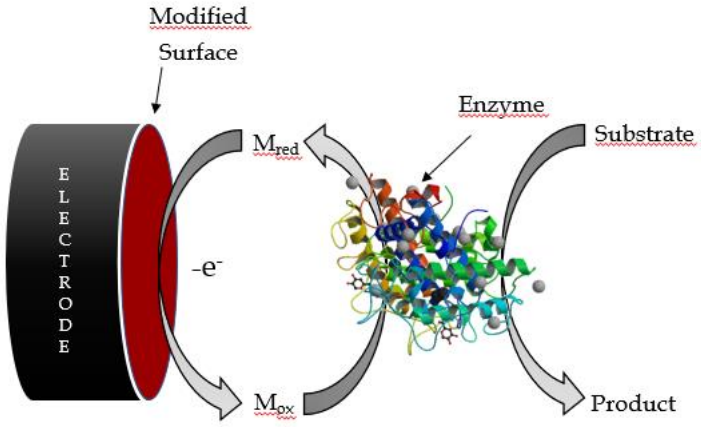

Figure 6: schematic representation of a second-generation biosensor

where M_{ox} and M_{red} are the oxidized and the reduced form of the mediator.

The reduced form of the mediator is re-oxidized at the electrode, giving a current signal proportional to the target analyte concentration.

Common redox mediators are ferrocene derivatives and ferricyanides, organic dyes such as methylene blue, methyl violet, phenazines, Alizarin yellow, Prussian blue, thionine, azure A and C and toluidine blue, conducting organic salts, quinone

compounds, transition metal complexes[35]. Mediators can be added in solution or immobilized on the electrode surface. In the latter case, it is very important that the mediator is entrapped close to the enzyme. A mediator should be stable under the required working conditions and should not participate in possible side reactions during electron transfer. The choice of this compound should be done in such a way to obtain a working redox potential lower than the other electroactive species in the sample. In addition, the redox potential of the mediator should be, compared to the redox potential of the enzyme active site, more positive for oxidative biocatalysis and more negative for reductive biocatalysis. The redox properties of the mediators, and the choice of the suitable mediator, are evaluated on the basis of cyclic voltammetry investigations. In the table 1 some examples of common redox mediators with their typical potential value *vs*. Ag/AgCl in aqueous solution are reported.

Table 1: typical mediators in second-generation biosensors and their redox potential

Mediator	**Potential *vs*. Ag/AgCl**
Ferricyanide (hexacyanoferrate (III))	+0.45 V
2,6 – dichlorophenol	+0.24 V
Indophenol	+0.24 V
Ferrocene	+0.17 V
Methylene blue	+0.04 V
Phthalocyanine	-0.02 V
Benzyl violet	-0.36 V
Methyl violet	-0.46 V

This approach allows to obtain devices that can operate at low potential values, avoiding O_2 dependence and the influence of interferences[11,32,33,35].

3. Third-generation biosensors

Third-generation biosensors are based on a process called bioelectrocatalysis that provides a direct electron transfer between enzyme and electrode (figure 7). The operating mechanism is, therefore, based on the following reaction sequences:

$$S + E_{ox} \longrightarrow P + E_{red}$$

$$E_{red} \longrightarrow E_{ox}$$

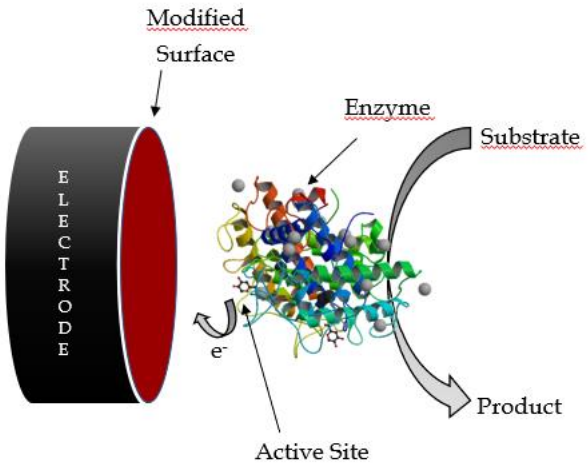

Figure 7: schematic representation of a third-generation biosensor

The realization of a third-generation device is, however, not so easy because, to establish an electric contact between the enzyme active site and the electrode, the use of specific materials for electrode surface modification is often required. These materials have to facilitate the electron transfer acting as electron channels or electron wires. According to the theory of electron transfer, in fact, the rate constant of direct electrochemical interaction between donor and acceptor is determined by potential drop between the enzyme redox-centre and electrode and mostly by the distance between the two. In this case, peptide environment separates spatially enzyme active site (donor) and the electrode (acceptor) as very often the active site is located in the

centre of the enzyme and this means that the active site is electrically isolated. Therefore, to make electric contact between redox-protein and electrode, such mediators as electron carriers and different modified electrode surfaces are used[32].

First demonstrations of direct electron transfers date back to 1977, when Peter Yeh and Theodore Kuwana[37] and Mark Eddowes and Allen Hill[38] proved direct electron transfer between cytochrome-c and tin-doped indium oxide, and cytochrome-c and gold electrode modified with bis(4-pyridil), respectively. After these works, scientists developed some strategies to facilitate direct electron transfers, for example using organothiol-gold coatings, conducting polymers, lipid bilayers and rafts, layer by layer assemblies etc. or modifying the active sites of enzymes with redox associated components.

Third-generation biosensors are still less common than others, but development in polymer science and nanotechnology are making them more widespread. Their diffusion is desirable as they are characterized by short response time and completely independent of O_2 and/or redox mediators' concentration[11].

Although the topic of this thesis concerns amperometric biosensors, a brief mention of the other classes of biosensors is useful.

Potentiometric Biosensors

Potentiometric biosensors are based on measurement of a potential difference between a working electrode and a reference electrode or between the two surfaces of a suitable membrane interested in ion exchange phenomena, in equilibrium conditions (when zero or no significant current flows between the system). The potential difference is a function of the activity of the species, and just for dilute solutions it is possible to assume that activity and concentration are equal[39]. The equation that correlates the measured potential difference and the activity of the analyte is the Nernst equation:

$$E_{cell} = E^0_{cell} - \left(\frac{RT}{nF}\right) lnQ$$

where:

E_{cell} is the observed cell potential at zero current [V];

E^0_{cell} is the standard cell potential [V];

R is the universal gas constant = 8.3143 [J K^{-1} mol^{-1}];

T is the absolute temperature [K];

n is the charge number of electrode reaction;

F is the Faraday constant = $9.6487 \cdot 10^4$ [C mol^{-1}];

Q is the ratio of ion activity at the anode to ion activity at the cathode;

The most commonly used potentiometric transducers are ion-selective electrodes (ISEs), based on thin films or selective membranes. With these types of electrodes (properly connected with an electronic voltmeter) it is possible to determine a wide variety of ions such as: H^+, K^+, Na^+, Ca^{2+}, NH_4^+, F^-, I^-, CN^-, or gas such as CO_2 or NH_3.
The coupling of these transducers with biological elements such as enzymes, antibodies etc. makes these devices real biosensors[9].
An example of ISE modified with an enzyme is the potentiometric biosensor for urea detection: urease enzyme is immobilized on a membrane which is placed over an ion-selective electrode. In this specific case it is an ammonium selective electrode, as urease catalyses the degradation of urea according to the following reactions:

$$CO(NH_2)_2 + H_2O \xrightarrow{\text{urease}} CO_2 + 2NH_3$$

At physiological pH, CO_2 and NH_3 dissociate in:

$$CO_2 + H_2O \longrightarrow HCO_3^- + H^+$$

$$NH_3 + H_2O \longrightarrow NH_4^+ + OH^-$$

Other examples of enzyme-based potentiometric biosensor are shown in table 2:

Table 2: examples of enzyme-based potentiometric biosensors

Analyte	Enzyme	ISE
Creatinine	Creatininase	Glass or polymer for NH_4^+ or sensor for NH_3
L-glutamate	Glutamate decarboxylase	Sensor for CO_2
Glucose	Glucose oxidase	Glass or polymer for H^+
Amygdaline	β-glucosidase	Solid state for CN^-

An evolution of ISEs is represented by ion-sensitive field-effect transistors (ISFETs). In this type of devices, the metal gate is coated with an insulating layer of silicon nitride (Si_3N_4) in direct contact with the analyte solution. This type of sensors works in a very similar way to glass electrodes for pH detection. However, this Si_3N_4 layer can be covered with different polymers containing molecules that can form complexes with species other than H^+ ion[40].

ISFETs, like ISEs, can be coupled with biological elements. In this context, the most widespread biological elements are enzymes, giving the so-called enzyme-FETs (ENFETs) and antibodies, giving immunosensitive FETs (immunoFETs)[39].

Advantages of ISFET are multiples: background noise reduction, robustness, small size and fast response times.

Another type of potentiometric devices that can be coupled with biorecognition elements (generally enzymes) is represented by light-addressable potentiometric sensors (LAPs)[40]. LAPs belong to semiconductor-based sensors utilising the interaction of a particular analyte with a transducer layer by forming a Nernstian potential. Variations of a specific analyte in the solution will produce a change in the surface potential of a transducer layer. These additional local variations of the surface

potential will be superimposed with the applied bias voltage, and hence modify the underlying space charge region, located at the insulator-semiconductor interface. A modulated light beam is used to illuminate a certain area of the LAP's structure, allowing to determine the variation of the space-charge region.
The light beam will create electron-hole pairs, separated within the electric field in the semiconductor, resulting in an externally detectable photo-current[41]. Measuring the photo-current as a function of the polarization potential it is possible to determine the surface potential correlated to the analyte concentration.

Conductometric Biosensors

Conductometric transducers are miniaturized systems of two electrodes that, connected to a conductometer, allow to measure the conductivity of thin electrolyte layer adjacent to the electrode surface. The conductivity of an electrolytic solution is determined by the chaotic motion of the present ions and can be expressed as:

$$\Lambda = \frac{1}{R}$$

where R is the resistance of the solution.

When a potential difference is applied between the electrodes, an electric field is generated, inducing an ordered and opposite movement of the ionic species, based on their charge: those with negative charge move towards anode, whereas those with positive charge move towards cathode.
The coupling of a biomolecule to a conductometric transducer results in the so-called conductometric biosensors. The most common biological elements used with these devices are, again, enzymes. Many enzymatic reactions produce or deplete charged species and it is, therefore, possible to associate the variation in conductivity of the

tested sample with the concentration of the species responsible for it. Nevertheless, when enzymatic reactions produce only hydrogen and hydroxyl ions (H^+ and OH^-) as charged species and the assay is performed in buffered solution, it is not possible to use a conductometric transduction because these ions are neutralized by buffer components and do not contribute to the transport of electric charges. Anyway, there are many enzymatic reactions that produce, in addition to the ions just mentioned, other charged species[24]. Examples are reported in table 3:

Table 3: examples of enzymatic reactions resulting in ionic products for application in conductometric enzymatic sensors

Enzyme	Produced Species
Amidases	$-RCOO^- + NH_4^+$
Serine dehydratase	$CH_3(CO)COO^- + NH_4^+$
Lactate oxidase	$CH_3COO^- + HCO_3^- + 2H^+$
Sulfatase	$CH_3OH + SO_4^{2-}$

Devices of this type have several advantages: thin film electrodes are, for example, suitable for miniaturization and can be produced on a large scale using inexpensive technology[9,42].

Impedimetric Biosensors

Impedimetric biosensors are based on the use of a technique called electrochemical impedance spectrometry. Electrical impedance indicates the opposition that an electrical circuit presents to the passage of an alternating current (AC) when an alternating voltage is applied, and can be defined as follows:

$$Z = \frac{V(t)}{I(t)} = \frac{1}{y} = \frac{V_0 \sin(2\pi f t)}{I_0 \sin(2\pi f t + \varphi)}$$

where:

V(t) and I(t) are voltage-time and current-time functions, respectively

y is the complex conductance or admittance

V_0 and I_0 are the maximum voltage [V] and current [A] signals

f is the frequency of the sine wave AC [s^{-1}]

t is the time [s]

φ is the phase shift between the voltage-time and current-time functions.

Electrochemical impedance spectrometry is an advanced method that allows to investigate the response of an electrochemical cell when it is exposed to small perturbations, such as a small amplitude sinusoidal voltage or current covering a broad frequency range, typically from 10 mHz to 100 kHz[9,24,43].

Usually, this technique allows to obtain information about three main parameters of the electrochemical cell: ohmic resistance of the solution, capacitance of the electrode/solution interface, and rate constant of the electrochemical reaction.

When a biorecognition element is immobilized on the electrode surface and the recognition process occurs, these parameters will be influenced. This method is, indeed, valid to monitor recognition processes, and lets them correlate with the concentration of a target analyte responsible for the interaction with the biomolecule[24].

Particularly, impedimetric biosensors are promising tools for foodborne pathogenic detection thanks to portability, sensibility and rapidity. The most commonly used biorecognition elements in impedimetric biosensors are antibodies and nucleic acids. Since 2007 have been reported a wide variety of the so-called impedimetric immunosensors for different bacteria detection[43].

Even though electrochemical impedance spectrometry is mostly coupled with affinity reactions, it is also possible using this transduction method with enzymes. For

example, in impedimetric enzyme biosensors a signal can be generated by precipitation of the product of a peroxidase reaction. An evident example is a bienzymatic impedimetric biosensor with glucose oxidase: glucose oxidation produces hydrogen peroxide, which reacts with a peroxidase substrate to form an insoluble product that precipitate on the electrode surface and causes a change in the impedance. The response is related to glucose concentration[44].

Another application of the biocatalytic impedimetric biosensors is based on electrodes coating with biodegradable polymers: their degradation can occur directly due to the enzymatic effect on the polymer, or indirectly due to the effects of the products of the enzymatic reaction. The alteration of the thickness of the polymer film can be monitored by impedance measurements. These can be associated with the concentration of enzyme substrates or inhibitors[24].

1.2.2.2 Optical Biosensors

Optical biosensors, known as bio-optodes, are devices based on the interaction between an electromagnetic radiation and the sample under investigation, and the information arise from the measurement of photons (instead of electrons, as occurs in the case of electrochemical sensors)[45].

The main components of an optical biosensor are: a light source, an optical transmission medium (fibre, waveguide etc.), an immobilized biorecognition element (commonly enzymes, antibodies, nucleic acids), and an optical detection system[28].

Optical biosensors can be classified in two main categories: label-free and label-based. In a nutshell, in a label-free detection the signal is directly generated by the interaction between the target molecule and the transducer, whereas in label-based mode either the target analyte or biorecognition element are labelled and the signal is generated by a colorimetric or luminescent response. The first type of detection is easy and cost-effective, the second one requires the presence of an additional reagent (the label) but

is very sensitive. In particular in the case of fluorescence-based detection it is possible to reach very low LoDs[28,46].

To detect the optical signal, it is possible to use several spectrochemical transduction methods such as: light absorption, diffuse reflectance, luminescence (fluorescence, phosphorescence, chemiluminescence, bioluminescence), fluorescence quenching, Raman, surface plasmon resonance (SPR), interferometry[24].

The most widely used optical biosensors are SPR-based biosensors (figure 8).

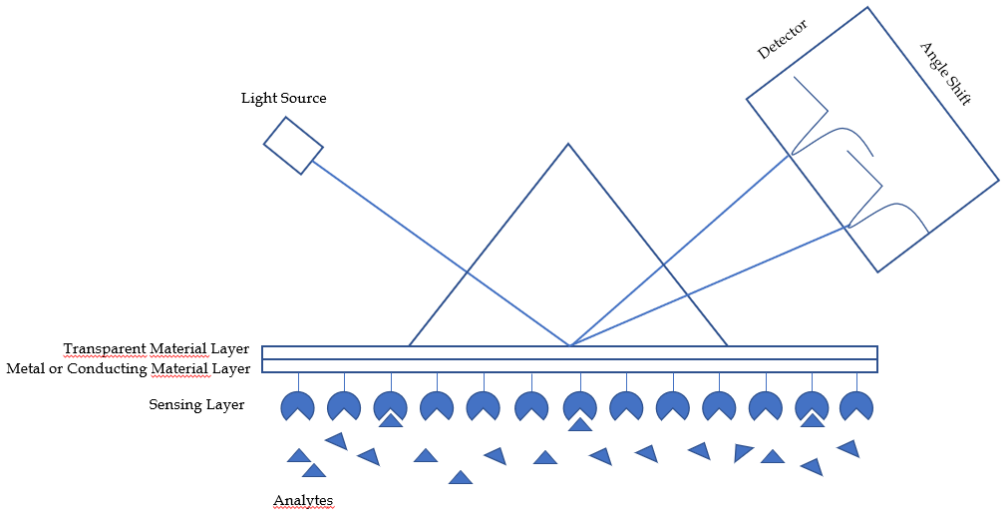

Figure 8: principle of operation of SPR instrument

The SPR phenomenon occurs on the surface of a metal (or other conducting materials) at the interface of two transparent media with different refractive indexes, when it is illuminated by polarized light at a specific angle called "resonance angle". This generates surface plasmons (large groups of electrons in an oscillation state) and consequently a reduction of the intensity of reflected light. The surface plasmon waves are extremely sensitive to the refractive index changes at the sensor surface and are proportional to the sample mass. In the SPR-based biosensors, biomolecules (the most common are antibodies) are immobilized on the surface of the transducer, and the recognition event causes a variation in SPR signal[29,47]. The unit signal of the SPR is defined as a resonance unit (RU), equivalent to a critical angle shift of 10^{-4} degrees[48]

which corresponds approximately to 1 pg (picogram)/mm^2 of analyte bound of surface area[29]. At the beginning of the experiment, in absence of the target analytes, the initial RU value coincides to the resonance angle. The change in refractive index within a layer of thickness h can be calculated as:

$$\Delta n_d = (\frac{dn}{dc})_{vol} \frac{\Delta \Gamma}{h}$$

where:

$(\frac{dn}{dc})_{vol}$ is the increase of refractive index n with the volume concentration of analyte c; $\Delta\Gamma$ is the concentration of the bound target on the surface.

SPR-based biodevices have many advantages such as rapid response, label-free, cost effective[47,48]. Other commonly used optical biosensors are optical fibres coupled with absorption, luminescence, Raman etc. An optical fibre is a flexible, transparent and very thin fibre made of silica glass or plastic that works as a waveguide to transmit the electromagnetic radiations between the two ends of the fibre. This type of biosensors can be sensitive to changes in absorbance, variations of intensity of fluorescence etc. and all these signals can be related, through the classic optical laws, to the target analyte concentration. For example, in the case of absorbance measurements, when an interaction between analyte and biomolecule occurs, a change in absorbance takes place and it can be related to the concentration of the target molecule by Lambert-Beer's law. The incorporation of an optical fibre into a biochemical sensor proved several advantages that are well described in the work of M.D. Marazuela and M.C. Moreno-Bondi[49].

1.2.2.3 Calorimetric Biosensors

Calorimetric biosensors are devices based on measurement of changes in temperature caused by interactions between a target analyte and a biorecognition element. In order to convert temperature variations into an electric signal it is possible to use two different types of transducer: resistive transducers (resistance thermometers and thermistors) and transducers based on the thermoelectric effect (thermopiles). Thermometric transduction is very suitable when the biorecognition elements are enzymes: in fact, most of enzyme-catalysed reactions are exothermic processes, so the heat generated can be measured and associated to the concentration of the target analyte. A thermal enzymatic biosensor can be seen as a microcalorimeter with the biological element closely integrated with a temperature transducer. The most commonly used thermal sensors are thermistors, but also examples of thermopile-based enzymatic sensors are reported. It is important to note that in enzyme-based calorimetric biosensors, even if the substrate reaction is not thermally efficient, it is possible to use subsequent enzymatic reaction that generate more heat[24,47].

Usually, LoD of single-enzyme thermal biosensors is rather mediocre, about 10^{-4} M. Nevertheless, sensitivity can be enhanced by increasing the heat output based on substrate or coenzyme recycling in multienzyme systems. A typical example is the catalysed oxidation of lactate using co-immobilized lactate oxidase, lactate dehydrogenase and catalase: the last enzyme enhances the heat effect by decomposition of hydrogen peroxide generated by the reaction catalysed by lactate oxidase. The catalytic reaction generates also pyruvate which, in turn, is converted back to lactate thanks to the presence of lactate dehydrogenase (figure 9).

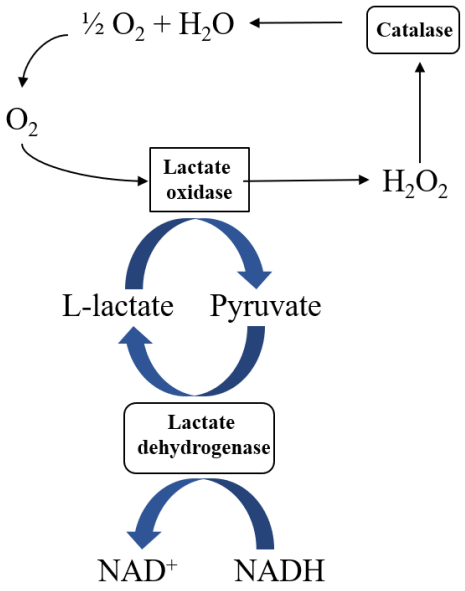

Figure 9: catalytic mechanism of lactate oxidation using co-immobilized lactate oxidase, lactate dehydrogenase and catalase

Moreover, in order to minimize heat dissipation and consequently to enhance sensitivity, it is desirable that the sensor-solution system should be as small as possible and it is preferable the use of organic solvents (when it is possible) that have thermal capacities lower than water[24].

1.2.2.4 Mass-based Biosensors

Mass-based biosensors are devices sensitive to mass changes, which can be determined by changes in resonance frequency, beam deflection or electrical resistance from the mass on the surface of the sensor[50]. As the mass change can be below the μg, extremely sensitive mass transducers are required. These ultrasensitive transducers are based on vibrating piezoelectric crystals. Piezoelectric biosensors are the most widely used mass-based biosensors, also called acoustic wave biosensors as vibrations are perceived as sounds. This type of devices is based on piezoelectric effect which is a particular property of certain crystals to develop electrical polarization under an applied mechanical stress. The most common material that presents this effect is

crystalline quartz. Other piezoelectric materials are zinc oxide, lithium niobate and lithium tantalate[24].

The piezoelectric biosensors rely on measurement of changes in oscillating crystal resonance frequency, due to biorecognition element and target analyte interactions. In this type of biosensors, the transducer is covered by the biosensing material. Piezoelectric materials have no centre of symmetry and generate an electric signal when they are stressed mechanically. When crystal is covered with some biorecognition element its frequency depends on the mass of the crystal and on the coating. In presence of a target analyte, a change in oscillation frequency occurs and it is proportional to the amount of a target analyte mass. There are two main types of piezoelectric (bio)sensors: bulk acoustic wave (BAW), where the acoustic wave expands throughout the whole volume of the vibrating device, and surface acoustic wave (SAW), where the acoustic wave develops only at the surface of the vibrating device. The most commonly used BAW devices are the thickness-shear mode (TSM) resonator, being the quartz crystal microbalance (QCM) one of the best-known TSM resonator. QCM lets information related to the elasticity and viscosity of various materials such as synthetic and biological polymers used in the development of chemical sensors[9,24,28].

Piezoelectric transduction is very convenient as it is cost-effective, allows free-label detection and it is suitable for large scale use. These devices allow also to reach very low LoDs, down to the picogram level. The main drawback is the possibility of interferences at sensor surface. The most commonly used biorecognition elements are antibodies, antigens and enzymes[28,29].

Another type of mass-based biosensors is the magnetoelastic ones, that are based on magnetoelasticity instead of piezoelectricity. A magnetoelastic material modifies its dimensions when it is subjected to a magnetic field. A thin film of a magnetoelastic material forms a resonator, which exposed to a short magnetic pulse excites, and starts to oscillate emitting a magnetic field. The frequency, amplitude and damping of this emitted magnetic field give information about the status of the sensor and the coating

or media surrounding it. This type of devices presents several advantages: wireless detection, low sensor cost (so they are suitable for disposable sensors), and no batteries or other power supplies are required[28].

1.3 Enzyme-based Amperometric Biosensors for Histamine and Epinephrine: an Overview

As already mentioned in the introduction, the ultimate goal of this research work is the realization of enzyme-based electrochemical biosensors for detection of histamine in food samples and epinephrine in biological ones. Both these species, as well as other molecules of alimentary and biomedical interest, are usually detected through classical techniques, especially chromatographic and spectrophotometric.

In the last decades, biosensing technologies have been developed and improved, resulting in commercial production of versatile and portable analytical tools for different fields of application such as environmental monitoring, food quality control, food safety, and mainly biomedical and clinical analysis[51].

As regards biomedical sector, many prototypes of biosensors have been enhanced and commercialized in order to replace some of the more expensive and time-consuming routine tests, mainly due to the growth of population and increase in people with various diseases (diabetes, obesity, cancer, cardiac pathologies etc.) which require periodic monitoring[52].

In table 4 some of the commercially available clinical biosensors are reported. It is important to note that, to the best of our knowledge, no biosensor for epinephrine detection has yet been marketed.

Table 4: some examples of commercially available clinical biosensors

Company	Model	Analyte
Yellow Spring Instruments, USA	23A	Glucose
Pulsatum Health Care Ltd, India	Glucometer	Glucose
Abbott, USA	FreeStyle Life FreeStyle InsuLinx	Glucose Insulin
Bayer, Canada	Contour Meter	Glucose
ApexBio, Taiwan	Eclice Alc UASure	Haemoglobin Uric Acid
Nova Biomedical, USA	Stat Strip CREAT Stat Strip LAC	Creatinine Lactate
Pts Diagnostics, China	CardioChek	Cholesterol

Concerning biosensors for food industry, food quality control and safety, a Web of Science study reports that between 2005 and 2010, out of 12155 publications on biosensors, only 4% was related to biosensors for food applications[53] (figure 10). After 2010, the number of food-related biosensors papers has increased, but just few devices are commercially available[51,52], maybe due to still high costs. Moreover, many biosensors producers have focused their interest on the so-called "money-rich" life sciences, by dedicating themselves mainly to the R&D area and therefore neglecting routine tests, that are the backbone of the food sector[53].

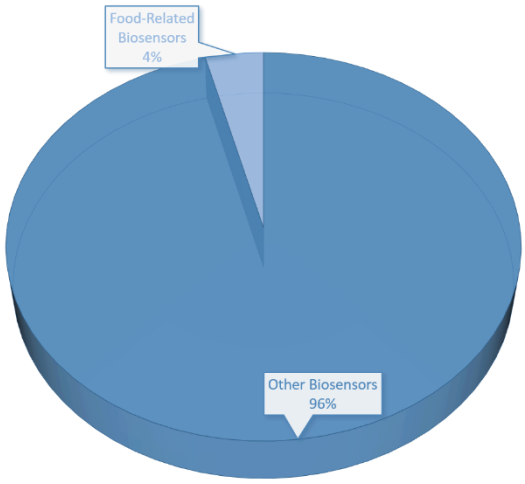

Figure 10: biosensors publication in the period between 2005-2010

A large number of the few commercial devices for food analysis are for glucose, lactose, lactate etc.; they are available in different forms such as autoanalyzers, manually laboratory instruments and portable systems. Some biosensors for food applications are reported in table 5.

Table 5: some examples of biosensors for food applications

Company	Analyte
Oriental Electric Co., Japan	Fish Deterioration Tracking
Pegasus Biotechnology, Canada	Fish Deterioration Tracking
Gwent Sensors, UK	Glucose
Biacore AB, Sweden	Water Soluble Vitamins, Chemical Veterinary Residues, Mycotoxins
Universal Sensors, USA	Ethanol, Methanol, Glucose, Sucrose, Lactose, L-AAS, Glutamine, Ascorbic Acid, Oxalate
Michigan State University's Electrochemical Biosensor, USA	*E. coli* O157:H7 and *Salmonella* in Meat Products
IVA Co. Ltd	Heavy Metals
Texas Instruments, Inc., USA	Peanut Allergens, Antibiotics

Among these, it is possible to note two biosensors for monitoring fish freshness, of which biogenic amines and in particular histamine are important markers, developed by the Japanese company Oriental Electric Co. and by the Canadian company Pegasus Biotechnology, respectively. Nevertheless, both systems are based on the monitoring of ATP degradation and not on the determination of the biogenic amines content[54,55]. To the best of our knowledge, biosensors for histamine detection are not yet commercially available.

1.3.1 Histamine

Biogenic amines (BAs) are low molecular weight basic compounds, with one or more amine groups. They can be aliphatic (e.g., putrescine, cadaverine, spermine and spermidine), aromatic (e.g., tyramine and phenylethylamine) or heterocyclic (e.g., histamine and tryptamine).

The most common BAs that can be found in food and beverages are histamine, tyramine, putrescine, cadaverine, tryptamine and β-phenylethylamine, originating from the precursor amino acids: histidine, tyrosine, ornithine and lysine, tryptophan and phenylalanine respectively[8,56,57] (figure 11).

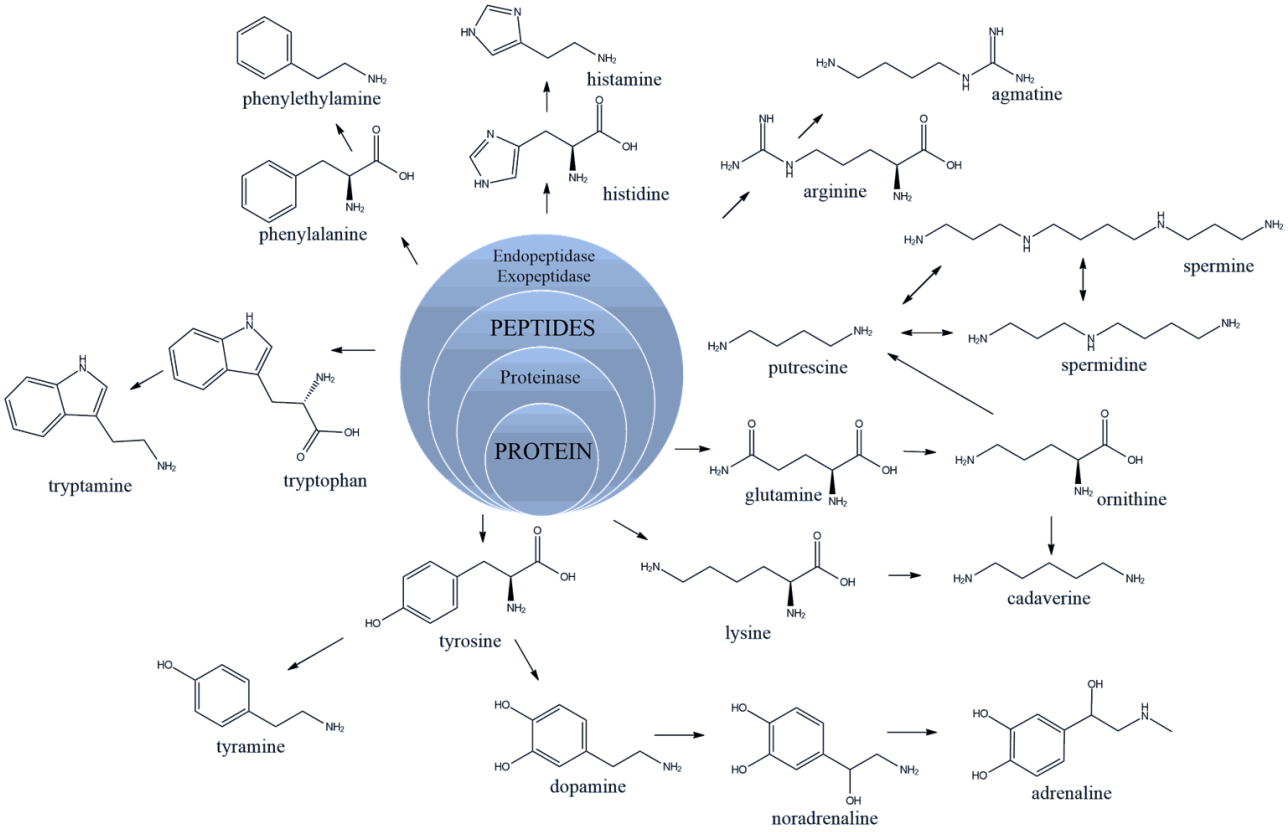

Figure 11: mechanism of formation of biogenic amines

They are mainly generated by microbial decarboxylation of free amino acids due to positive decarboxylase bacteria such as *Morganella morganii*, *Klebsiella pneumonia*, *Hafnia alvei*, *Proteus*, *Clostridium*, *Enterobacter aerogenes*, *Bacillus spp.*, *Staphylococcus* in fishes, *Lactobacillus buchneri*, *Lactobacillus 30a*, *Lactobacillus casei*, *Streptococcus*, *Bacillus macerans*, *Enterobacteriaceae*, *Pseudomonas*, *Micrococcus* in cheeses, meat and meat products[57]. Furthermore, the formation of BAs can occur through other three mechanisms: (i) transamination and/or (ii) reductive amination of aldehydes and ketones, and (iii) degradation of certain precursor amino compounds[56-59]. Requirements for the synthesis of BAs promoted by positive decarboxylase microorganisms are: (i) availability of free amino acids (closely related to the presence of proteases), (ii) presence of permeases, (iii) presence of cofactor (pyridoxal phosphate or B6 vitamin), (iv) optimal pH values (between 5.0 and 6.5 depending on decarboxylase type), (v) optimal temperature for enzymatic activity (20-35 °C)[60,61]. In particular, two mechanisms through which decarboxylation occurs have been

identified: a pyridoxal phosphate dependent reaction and a non-pyridoxal phosphate dependent reaction described in detail by R.R. Eitenmiller and S.C. De Souza[62] and E.E. Snell and P.A. Recsei[63]. BAs are present in traces in the human body (endogenous amines) where they carry out important biological functions in the nervous and cardiovascular systems. They are also sources and precursors of hormones, proteins, nucleic acids and alkaloids and regulate body temperature and digestion[56]. They are present in low concentrations in non-fermented food (fruits, vegetables, chocolate, milk) and in slightly higher concentrations in fermented and aged foods (wine, beer, fish and fish products, meat), as a matter of fact decarboxylase activity has been found both in altering and useful microflora microorganisms.

BAs formation is "species specific", so putrescine and cadaverine are mainly formed in meat and fish (particularly in poultry meat and white-muscle fishes), tyramine is normally formed in ripened cheese, while histamine is present in dark-muscle fishes or histidine-rich fishes. Their quantification is useful for determining the quality and freshness of the products where they are detected, and it is then regarded as an index of fish quality and freshness[56]. Some of these amines are also found in wine of all kinds and beers, in particular histamine and tyramine are common in beers and red wine, often combined with the presence of agmatine and ethanolamine[64]. When present in high concentrations, these compounds can cause health hazard because of their toxic effect. Furthermore, BAs are also potential precursors of carcinogenic nitrosamines due to their ability to react with nitrates and nitrites. In particular these reactions occur in products with added nitrites and nitrates as preservatives and also, contrary to all expectations, in salted products as it is not uncommon that sea or rock salts contains nitrites and/or nitrates as impurities[56,61,65,66].

Among the several biogenic amines, histamine is one of the most toxic. It is responsible of the so-called scombroid syndrome as the fishes commonly implicated in histamine fish poisoning (HFP) belong to scombroid species (mackerel, tuna and saury);

nevertheless, also non-scombroid species (sardines, anchovies, bluefish, marlin etc.) can contain high quantity of histamine[67].

According to EU Commission Regulation EC No. 1019/2013 histamine limits in fishery products are set at 200 mg/kg for fresh fish with high histidine content and 400 mg/kg for fish sauce obtained by fermentation of fishery products[68]. Histamine fish poisoning can cause a series of allergic reactions: headache, nausea, tachycardia, loss of sight, hypotension or hypertension, bronchoconstriction, respiratory disorders and, in the extreme cases, also death[56,69-76]. Furthermore, its toxic effects can be amplified by other biogenic amines such as putrescine, cadaverine and tyramine (responsible of the so-called cheese syndrome) that inhibit histamine-detoxifying enzyme (DAO). Moreover, the toxic effects can be enhanced by the assumption of several drugs such as clavulanic acid, metoclopramide, verapamil etc. which inhibits DAO in the intestinal tract[56,70,71].

Since histamine is one of the most toxic and is present, above all, in fishery products, these latter are the most investigated matrices from the point of view of biogenic amines. Meat products and their derivatives, wines, cheeses and beers containing other biogenic amines in addition to histamine, less important from the point of view of toxicity but quite significant as regards to the taste of the products, are also investigated[66] (figure 12).

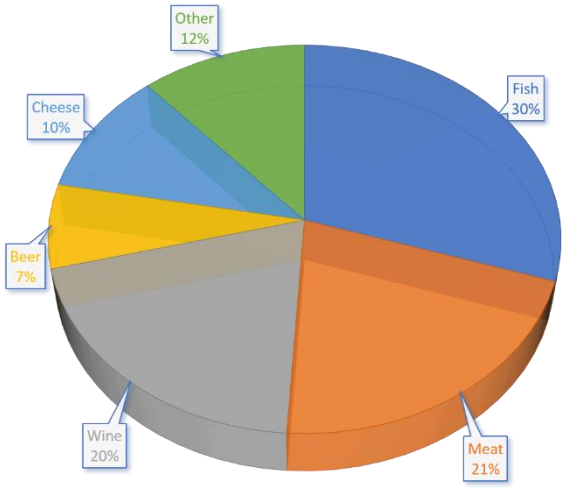

Figure 12: distribution of food products in published articles concerning biogenic amine analysis in 2011 and 2012

Hence, biogenic amines detection and overall histamine detection are useful in the context of quality control and food safety for the evaluation of food freshness and quality and to minimize health risks[64].

Until a few years ago, methods for histamine (and other biogenic amines) detection in food products were commonly based on chromatographic techniques often coupled with fluorimetry, conductometry, amperometry and mass spectrometry.

One of the first chromatographic methods for histamine determination in fish samples was developed in 1981 by J.D. Henion[77]. He used gas-chromatography coupled with mass spectrometry to analyse fresh tuna tissues. Histamine has been derivatized *in situ* by silylation with N,O-Bis-(trimethylsilyl)-trifluoroacetamide (BSTFA). The trimethylsilyl derivative of histamine has been resolved by the high resolution 12-m SP-2100 fused-silica capillary column and detected with a mass spectrometer ion source, that operated in the positive ion chemical ionization mode using methane as reactant gas. The technique described by Henion allows to determine all the components of the fish extract in 15 minutes and the sensitivity of the procedure is sufficient for the detection of 10^{-9} g levels of histamine in fish extracts.

Differently, H.S. Marks and C.R. Anderson[78] used liquid chromatography coupled with fluorimetry for the determination of putrescine and cadaverine in canned tuna, frozen tuna loin, frozen raw shrimp and other seafood. The method proved to be useful for histamine. The technique required a previous homogenization of fish tissue, extraction of biogenic amines into borate-trichloroacetic acid solution, centrifugation and derivatization of supernatant with 1-pyrenebutanoic acid succinimidyl ester. The derivatized species are fluorescent and can be determined with high specificity. This method allows determining putrescine and cadaverine even when these are present in concentration of few ppm. Concerning histamine, the method permits the detection of concentrations from 50 ppm upwards.

In 2012, H. Zhai et al.[79] and R. Romero-González et al.[80], developed two other methods for the determination of histamine (and other BAs) in fishery products, both based on liquid chromatography. In particular, Zhai and co-workers developed a high-

performance liquid chromatography (HPLC)-based method combined with fluorescence to determine eight biogenic amines, including histamine, in 13 species of fish and 49 fishery products commonly consumed in southern China. This method required a derivatization step of BAs with dansyl chloride before the column injection. The research group of Romero-González elaborated an advanced method based on ultra-high-performance liquid chromatography (UHPLC) coupled with tandem mass spectrometry (UHPLC-MS/MS), using an electrospray ionization source (ESI) in positive ion mode. This method, in addition to the various advantages attributable to the use of UHPLC interfaced MS/MS, does not require derivatization steps then saving time of analysis. It allows to determine four biogenic amines (putrescine, cadaverine, histamine and tyramine) and three volatile amines (trimethylamine, triethylamine and tripropylamine) in anchovies. Limits of quantification (LoQs) are 25 μg/kg for all amines with the exception of trimethylamine, which is, instead, 60 μg/kg.

As reported by B.M. De Borba and J.S. Rohrer[81], HPLC-based techniques and in particular reverse phase (RP)-HPLC are commonly used also to determine BAs in alcoholic beverages (wines and beers). In most cases, these methods require pre- or post-column chemical derivatization: o-phtalaldehyde (OPA) combined with a thiol compound such as 2-mercaptoethanol (MCE) is a common derivatizing agent for determining BAs in wine and beer. In this regard, G.J. Soleas and co-workers[82] developed a HPLC-based method with pre-column derivatization with OPA, using a gradient elution and fluorescence detection for determination of nine BAs including histamine, putrescine, cadaverine etc. They analysed 73 monovarietal wines from five red and six white cultivars. The method can be considered an upgrade to that of Lehtonen[83] resulting in a greater sensitivity.

Tang and co-workers[84] determined BAs in beers using a method based on RP-HPLC with UV diode array detection. The column injection was preceded by a derivatization step with 4-chloro-3,5-dinitrobenzotrifluoride (CNBF).

The research group of Li[85] developed a likewise method based on HPLC coupled with fluorescence, using as fluorescent reagent 8-phenyl-(4-oxy-acetic acid N-

hydroxysuccinimide ester)-4,4-difluoro-1,3,5,7-tetramethyl-4-bora-3a,4a-diaza-s-indacene (TMPAB-OSu) synthesized by themselves. Analogously to the procedure developed by Tang[84], the method set a pre-column derivatization. The described technique allows to determine varies BAs in pericarp and pulp of mature and immature apples and in wine, with LoDs between 0.1-4 nM depending on considered amine. In spite of the excellent LoD values obtained, the method has the disadvantage of being time consuming due to the derivatization step that, moreover, adds complexity to the analysis, requiring additional skilled work and sometimes producing by-product interferences.

De Borba and Rohrer[81] developed a new method based on cation-exchange chromatography coupled with either suppressed conductivity, integrated pulsed amperometry (IPAD), UV or a combination of these, to determine BAs in several kinds of wines and beers. This method allows to reach LoDs in the range of 0.004-0.08 mg/L using suppressed conductivity, 0.021-0.39 mg/L for IPAD and 0.090-1.1 mg/L for IPAD after suppression. The described ionic chromatography (IC) method coupled with suppressed conductivity proved good precision and recovery for many of the BAs and superior sensitivity if compared with other previous reported works.

In 2008, an innovative method for BAs detection, based on coupling of a highly selective electrochemical biosensor to a weak cation-exchange column, was developed by L. Mureşan et al.[86]. The technique consisted in two steps: (i) BAs separation on column and (ii) online detection of individual BAs using an amperometric bienzymatic biosensor based on amine oxidase from *grass pea* (GPAO) and commercial horseradish peroxidase (HRP). The biosensor operated at applied potential of -50 mV *vs*. Ag/AgCl, where biases from interferences are minimal. The development of such a system was a real novelty since it requires a minimal sample pre-treatment and relatively fast response. On the other hand, it demands expensive instrumentation and skilled personnel additionally combined with the impossibility of carrying out the analysis outside an equipped laboratory.

Biosensors, as already mentioned above, ideally represent a cheaper, faster and portable and valid alternative to the just described methods, possessing all their advantageous characteristics[87,88]. Biosensors for biogenic amines detection so far developed use as biorecognition element one or more enzymes, antibodies[89,90] and aptamers[91], and from the point of view of the transducer are reported several electrochemical (amperometric and impedimetric) and optical devices[90,92]. Among these, electrochemical biosensors perform a leading position, and in particular the enzyme-based amperometric ones stand out.

One of the first enzyme-based amperometric biosensors for biogenic amines detection dates back to 1997 thanks to the work carried out by P. Bouvrette and co-workers[93]. This research group developed a device based on a platinum electrode modified with an Immunodyne membrane, on which diamine oxidase from *porcine kidney* (purified over 2300-fold with an activity of 1 U/mg) has been immobilized exploiting a cross-linking mechanism with glutaraldehyde. It is a first-generation biosensor where a potential of 0.7 V was applied to the working electrode in order to detect H_2O_2 released during the reaction between an amine and the enzyme, according to a simplified reaction scheme (figure 13).

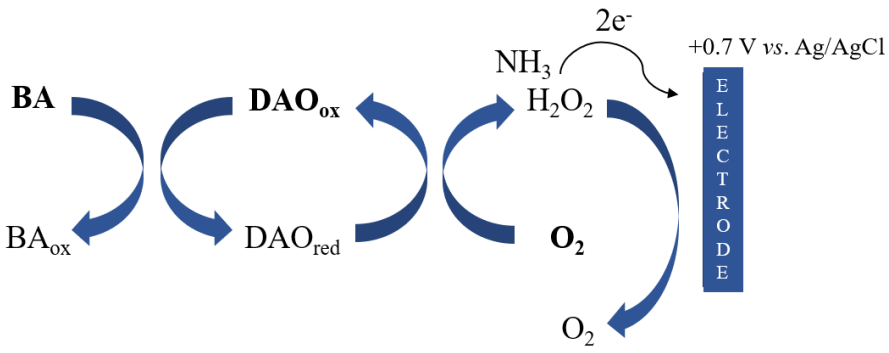

Figure 13: operating mechanism of the first-generation biosensor developed by P. Bouvrette et al.

The described biosensor allows to determine putrescine, cadaverine and histamine with a LoD of 25 μM. As in most first-generation biosensors, the main problem is the

use of high potential values which, inevitably, expose the device to possible interferences.

A good solution to minimize the effect of interfering substances was devised, one year later, by S. Tombelli and M. Mascini[94]. They realized, a biosensor with a bienzymatic configuration in which DAO was coupled with HRP (1100 U/mg of solid protein) on a glassy carbon electrode; this system used a ferrocene monocarboxylic acid (FcA) as a mediator, giving a second-generation biosensor. This arrangement allows to work at lower potential value (0.0 V than the usual 0.7 V *vs*. Ag/AgCl used for the oxidation of H_2O_2) based on the measurement of the reduction current of the ferrocinium ion, according to the scheme reported in figure 14.

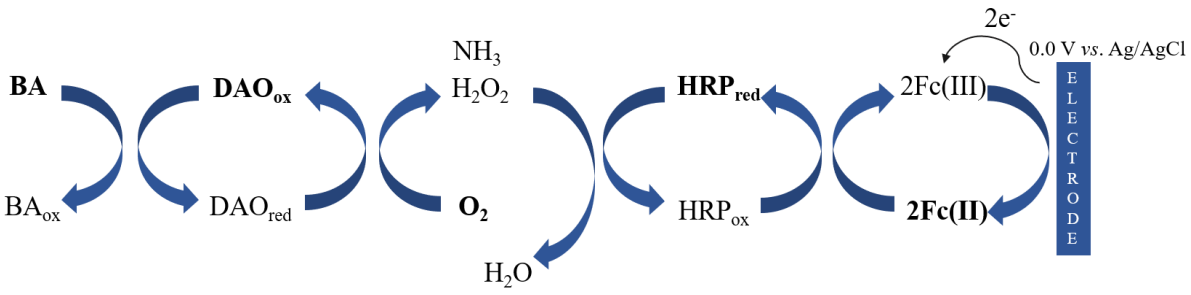

Figure 14: operating mechanism of a second-generation biosensor developed by S. Tombelli and M. Mascini

The obtained LoD is 0.1 μM. Therefore, the presence of a second enzyme makes the system very sensitive and the presence of the mediator makes it highly selective.

Along the lines of Tombelli and Mascini, Alonso-Lomillo and co-workers[95] conceived two disposable biosensors based on monoamine oxidase (MAO)-HRP and DAO-HRP both covalently immobilized (with N-hydroxysuccinimide (NHS) followed by the addition of and N-(3-dimethylaminopropyl)-N'-ethylcarbodiimide hydrochloride (EDC)) on screen printed carbon electrodes previously modified with an aryl diazonium salt; the investigating sample was added with hydroxymethylferrocene as mediator. The detection can be performed at 0.25 V *vs*. Ag/AgCl by measuring the cathodic current of the reduction of the mediator.

Inversely, Al Layla and collaborators[8] developed another first-generation biosensor based on DAO entrapped in a film of poly(3,4-ethylenedioxythiophene) (PEDOT). The current responses have been recorded at 0.7 V *vs.* Ag/AgCl, but the innovative element is that, to minimize the interferences, an over oxidized film of polypyrrole was introduced. This allowed to considerably reduce the interference from ascorbic acid.

C.M. Keow et al.[96] realised a first-generation biosensor for histamine detection different from the usual ones as it is based on the electrode oxidation of the imidazoleacetaldehyde to imidazoleacetic acid (figure 15).

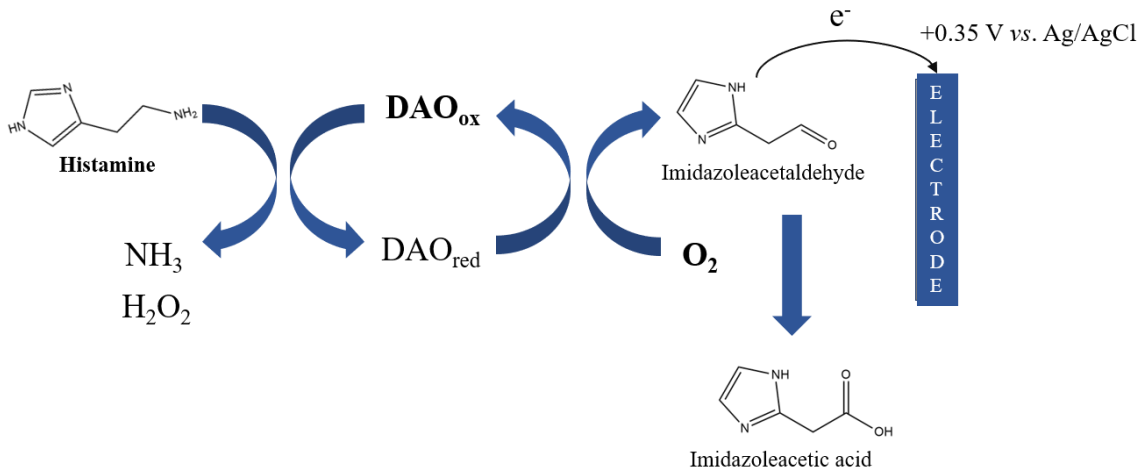

Figure 15: operating mechanism of a first-generation biosensor developed by C.M. Keow et al.

In this way, it is possible to work at lower potential values (0.35 V *vs.* Ag/AgCl), avoiding the classical interferences of ascorbate and urate. Moreover, interferences from other biogenic amines have proved to be negligible, in particular in the investigated tiger prawn samples. The developed device was a carbon paste screen printed electrode where a photocured membrane entrapping DAO was deposited. It showed a LoD of 0.65 ppm and a very fast response time (< 1 min).

Other second-generation biosensors have been developed by M. Niculescu et al.[69] and K. Zeng et al.[97]. The former was based on graphite electrode modified with an Os-bipyridine redox polymer that acts as redox mediator, on which amine oxidase (AO) from *grass pea* (isolated and purified) has been immobilized. The working electrode

was held at +0.2 V *vs*. Ag/AgCl for histamine detection. The latter, instead, was based on gold minielectrode modified with a polypyrrole film on which methylamine dehydrogenase (MADH) from *Paracoccus denitrificans* has been immobilized. The device was used in presence of ferricyanide as mediator and the amperometric response of histamine was recorded at 0.245 V *vs*. Ag/AgCl. The LoD was set at 25 μM and the linear range was 25 μM–4 mM allowing the histamine detection in alimentary matrices (e.g., fishes).

Equally based on polypyrrole, MADH from *Paracoccus denitrificans* and ferricyanide, another biosensor, starting from a graphite electrode, was developed by Bao and co-workers[98]. The substantial difference with the device made by Zeng[97] is that MADH is not used in its native form but in a αF55A mutated form, that is phenylalanine 55 on the α subunit was converted in alanine. Using the mutated form, the sensor exhibited a LoD of about 5 μM, 5-fold lower than that reached by Zeng with MADH native form.

Finally, there is also an example of third-generation biosensor for histamine detection. Niculescu and her group[69] described, in fact, another device based on a direct electron transfer (DET) between the enzyme active site and the electrode, realized directly immobilizing amine oxidase (AO) on a graphite electrode. The mechanism is shown in figure 16 and details are exhaustively reported in the article of Niculescu et al.[99].

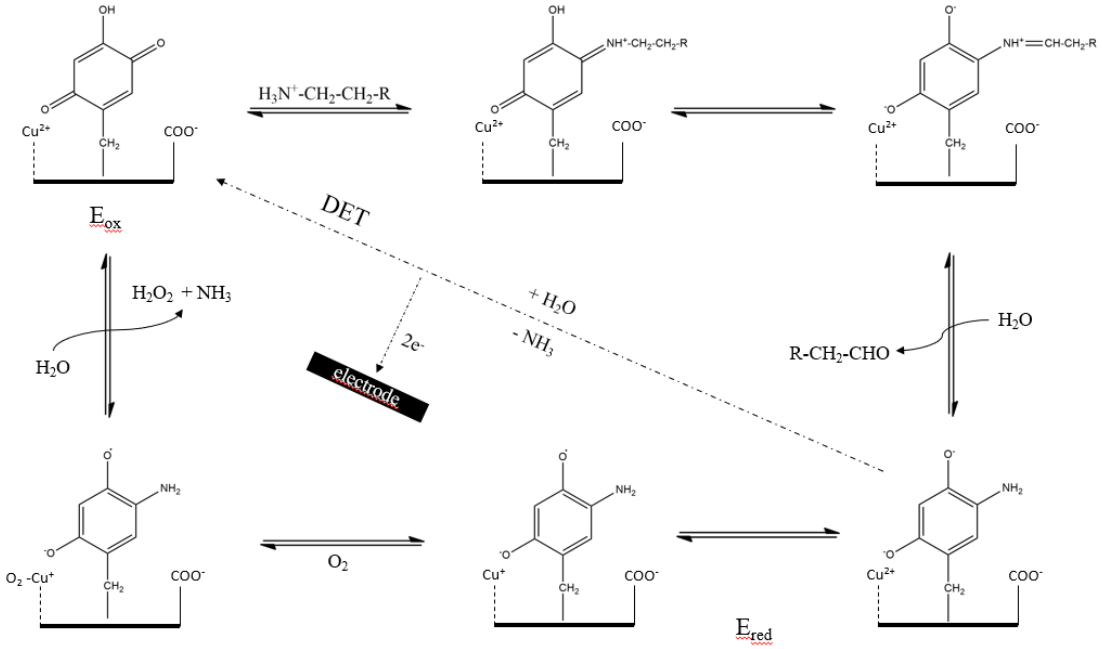

Figure 16: mechanism of the reaction catalysed by plant copper amine oxidase. The dashed line shows the proposed "short circuit" in the catalytic mechanism caused by a DET between the enzyme's active site and an oxidative electrode

Table 6 summarizes some biosensors for histamine and biogenic amines (including histamine) detection, along with their main analytical characteristics.

Table 6: biosensors for biogenic amines detection

Biogenic Amine	Enzyme	Working Electrode	Mediator	Immobilization	Applied Potential	pH	LoD [μM]	Linear Range [μM]	Ref.
BAs	MAO/HRP DAO/HRP	SPCE	Hydroxymethyl ferrocene	Covalent Binding	+250 mV	9.3	0.40 ±0.04 0.18 ± 0.01	0.4-2.4 0.2 -1.6	95
His	DAO	SPCE	-	Physical Entrapment	+350 mV	7.4	5.85	0-540	96
His, Cad, Put	DAO DAO/HRP	Pt	FcA	Cross-Linking with GA	+700 mV 0 mV	7.4	0.6 0.1	1-100	94
His	DAO	SPCE/PtNPs/graphene/chitosan	-	Physical Adsorption	+400 mV	7.4	0.025	0.1-300	102
His and Put	HMD	SPCE/TTF	Tetrathiafulvalene (TTF)	Cross-Linking with GA and BSA	+130 mV	6.8	8.1 ± 0.7	8-60	103
His	MADH	Au/PPy/Ferricyanide/Nafion	Ferricyanide	Physical Entrapment	+245 mV	7.5	25	25-4000	97
His	Mutated MADH	GC/PPy/Ferricyanide/Nafion	Ferricyanide	Physical Entrapment		7.5	5.2 ±1.7	-	98
His, Put, Cad	DAO	Pt/Immunodyne™ membrane/GA	-	Copolymerization with GA	+700 mV	7.4	25	25-6000	93

His	AO	Graphite/PVI$_{13}$-dmeOs/PEGDGE	PVI$_{13}$-dmeOs	Physical Entrapment	+200 mV	7.2	2.2	10-200	69
His	-	Pt-Cu	-	-	+200 mV	10.0	0.33	1-750	104
His	-	GC/pAHNSA/ MWCNTs	-	-		7.0	0.076	0.1-100	105

BAs: histamine (His), cadaverine (Cad), putrescine (Put), spermine (Spm), spermidine (Spd), tryptamine (Trypt); MAO: monoamine oxidase; HRP: horseradish peroxidase; DAO: diamine oxidase; FcA: ferrocene monocarboxylic acid; GA: glutaraldehyde; SPCE: screen printed carbon electrode; PtNPs: platinum nanoparticles; HMD: histamine dehydrogenase; BSA: bovine serum albumin; MADH: methylamine dehydrogenase; PPy: polypirrole; PVI$_{13}$-dmeOs: [osmium (4,4'-dimethylbipyridine)$_2$Cl]$^{+/2+}$ complexed with poly (1-vinylimidazole); PEGDGE: poly (ethylene glycol) (400) diglycidyl ether; p – AHNSA: poly (4-amino-3-hydroxynapthalene sulfonic acid); MWCNTs: multi- walled carbon nanotubes.

A glance at the table 6 lets to note that no second-generation biosensors based on DAO have been developed. Bouvrette and co-workers[93] reported, in this regard, that seven well-characterized mediators tested by them (1,1′-dimethylferrocene-2–hydroxypropyl–β–cyclodextrin complex (HPBC); tetrathiafulvalene–HPBC inclusion complex; N,N,N′,N′–tetramethyl–1,4–phenylenediamine x 2 HCl; 4-aminodiphenylamine x HCl; ferrocene carboxylic acid HPBC complex; 2,6–dichlorophenolindophenol; potassium ferricyanide $K_3Fe(CN)_6$), that usually efficiently work with FAD containing oxidases, were not able to promote the electron transfer from the DAO active site to the electrode. To confirm this, A. Boffi[100] and Verma[88] reported that commonly used redox mediators are unable to shuttle electrons between the enzyme redox centre of an amine oxidases and the electrode. The reason can be attributable to the fact that the active site of diamine oxidase is located in the centre of the enzyme, thus being hardly accessible to mediator molecules.

In this work we attempted to realize a second-generation biosensor both by trying to use potassium ferricyanide ($K_3Fe(CN)_6$) as redox mediator and, according to the method used by Niculescu et al.[69], a conducting metallo-polymer film based on ruthenium(II): poly[(TAT)Ru(TpyCOOH)] (TAT = 4′-[(2,2′:5,2′′-terthien-3′-ethynyl]-2,2′:6,2′′-terpyridine; TpyCOOH = 4,4′,4′′-tricarboxylate-2,2′:6,2′′–terpyridine)[101]. Unfortunately, in both cases the biosensors did not show significant responses, confirming what was stated in the aforementioned papers[88,93,100]. Nevertheless, using poly(3,4-ethylenedioxythiophene) (PEDOT) and poly[(TAT)Ru(TpyCOOH)] both in combination with DAO, two first-generation biosensors have been developed showing, however, not too exciting results.

1.3.2 Epinephrine

Epinephrine (also known as adrenaline or "fight or flight hormone", EP) belongs to the catecholamine or biogenic amines group and exhibits the properties of a chemical neurotransmitter and a hormone[106]. Most of it is biosynthesized in the adrenal medulla and in sympathetic nerve terminals, and it is also secreted by the suprarenal gland, as well as norepinephrine[107]. It plays an essential role in the functioning of renal, cardiovascular, hormonal and central nervous systems, both of animals and of humans. Epinephrine has a very short life time, its half-live is about 1-3 minutes and it is degraded mainly in the liver and in the kidney, by the action of several enzymes like catecholamine O-methyl transferase (COMT) and a combination of monoamine oxidase (MAO) and aldehyde oxidase based on the mechanism[108] depicted in figure 17.

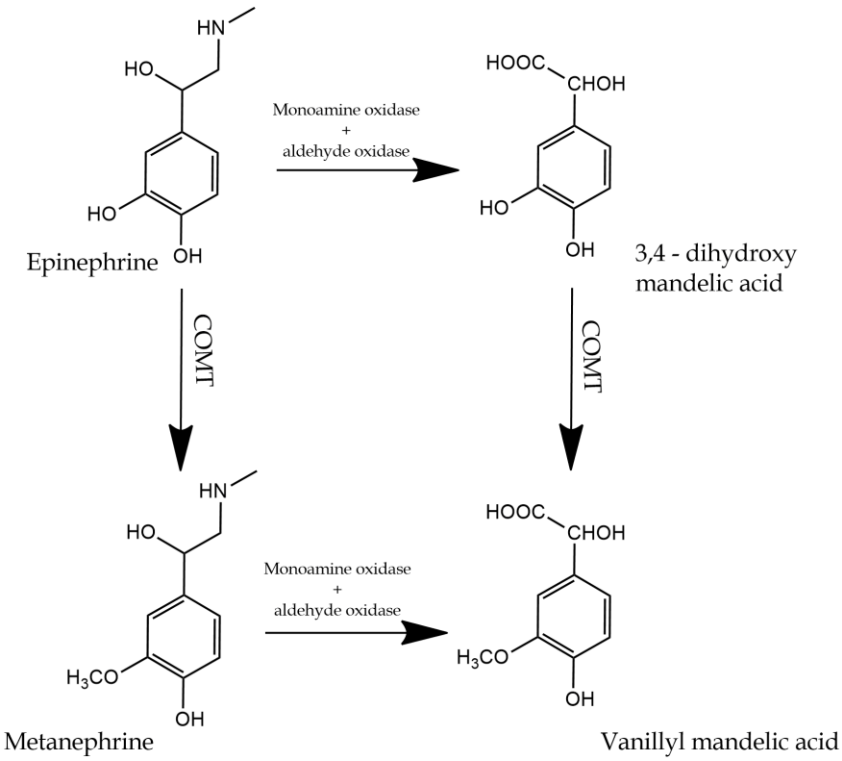

Figure 17: pathways for metabolism of epinephrine

Epinephrine regulates blood pressure, immune system, heartbeat rate, lipolysis and glycogen metabolism and it is a potent vasoconstrictor. Moreover, it is released in response to stressful, exciting, dangerous or threatening situation. It is a drug used in medicine in the treatment of allergic emergencies, heart attack (being a cardiac stimulant), bronchial asthma (being a bronchodilator) and cardiac surgery[106,109-111]. Nevertheless, EP, in combination with dopamine (DOP) and norepinephrine (NOR), is wrongly and illegally used by some athletes as energy stimulators, resulting in an increase in the concentration of DOP and EP in urine[112].

Abnormalities of EP levels can represent symptoms of several diseases: low levels can be associated with Parkinson disease and orthostatic hypotension, whereas slightly high levels are observed in stress and thyroid hormone deficiency, or can be connected with the presence of tumours (e.g., pheochromocytoma)[111,113].

Typically, endogenous plasma EP concentrations are below 10 ng/L (0.054 nM) for healthy people, but the concentration can increase by a factor of 10 after physical activity and by a factor of 50 during stress times. Moreover, in patients with pheochromocytoma, levels of EP can reach concentrations between 5.5 and 54.4 nM, while in acute-care cardiac patients, the parenteral administration can provide concentrations in the range of 54.59-545.85 nM[114].

It is, therefore, clearly evident the importance of monitoring changes in the concentration levels of EP in biological fluids (blood plasma, urine and extracellular fluid of the brain) in order to make possible the detection of potential pathologies, but also for the doping control of the athletes[112]. Moreover, when EP is used as a drug, it is also important to control its concentration in pharmaceutical formulations and monitor it in the production process as well as during the therapeutic treatment, in order to avoid side effects of overdosage[114,115].

Due to the low physiological concentration of epinephrine, a highly sensitive and selective method to conduct a quantitative analysis in biological samples is necessary. In this regard, several determination methods, including liquid chromatography, flow injection analysis, capillary electrophoresis, fluorimetry, are used. With this type of

methods, LoD values in the range of 10^{-7}–10^{-9} M have been reported. Nevertheless, methods with higher LoDs (in the micromolar range) are commonly used for pharmacological samples investigations[111,114]. In this context, P. Solich and co-workers[116] described a flow injection spectrophotometric method for the determination of epinephrine and isoprotenerol in pharmaceutical formulations. The method is based on the formation of their coloured complexes of Fe(II) in aminoacetic carbonate buffer. The signal was measured at the maximum wavelength (λ_{max}) of 530 nm. This method allows to obtain a LoD of 4.4 μM.

Similarly, M. H. Sorouraddin and co-workers[117] developed a spectrophotometric method, with a LoD of 0.26 μM, for the determination of epinephrine and norepinephrine in marketed pharmaceutical formulations and in dosage forms. The method was based on the reaction between the two catecholamines and sodium bismuthate, which yields red products exhibiting absorption peak at 486 nm for EP and 482 for NOR.

More sensitive methods have been developed and described by the research groups of W. K. Adeniyi[118], V. Carrera[119] and Y. Zhao[120] who determined EP in human serum, EP secreted by bovine chromaffin cells cultures and EP in human urine samples, respectively.

The method reported by Adeniyi is a fluorometric method. Classical fluorometric techniques allow generally to reach very good sensitivity, but the reactions of EP with other compounds, to enhance the emission intensity, are frequently long. The novelty, in this case, is that the investigation is carried out without the conventional derivatization or use of fluorophores by diazotization. It is, in fact, a method based on the optimization of experimental parameters and a careful selection of surfactant to increase fluorescence intensity. LoD was found to be $2.7 \cdot 10^{-7}$ M.

Carrera and her research group developed, instead, an HPLC-MS method for the simultaneous determination of epinephrine, norepinephrine, dopamine and 5-hydroxytryptamine. Chromatographic separation was achieved by injecting the sample, without any derivatization treatment, into a reverse-phase column; the signal

was recorded in signal ion mode. The described method allows to reach a LoD of $1.04 \cdot 10^{-8}$ M.

Finally, one of the most sensitive method was elaborated by Zhao and co-workers. It is a capillary electrophoresis method based on use of cadmium telluride quantum dots (CdTe QDs) which permits to reach a LoD of $9.3 \cdot 10^{-9}$ M.

As already seen also in the case of histamine, most of these techniques are characterized by high sensitivity and selectivity but tend to be expensive, complicated, sometimes time-consuming, due to the need of derivatization or extraction steps, and often they require high cost of equipment or analysis and cannot be used to perform measurements out of the laboratory. Hence, in this context, it is very useful to realize commercial, rapid, low-cost and portable analytical tools, possibly with the high sensitivity and selectivity of the aforementioned methods. A proper solution can be represented by electrochemical (bio)sensors[114,115].

Several types of electrodes (glassy carbon, carbon paste, gold, platinum, composite electrodes) properly modified are employed for electrochemical EP determination in different matrices. It was observed that LoDs reached with (bio)sensors varies within the range of 10^{-6} and 10^{-9} M as observed for the other methods, but with the above-mentioned advantages.

Electrochemical sensors for EP detection are often based on metal oxide films[112,121] or metal nanostructures[109,114,122,123] which possess the capability to mediate electron transfer reactions, resulting in electrocatalytic activity. Many of these mentioned sensors have proven to be particularly suitable for the quantification of EP in biological matrices (human blood plasma, human blood serum and human urine) having LoDs in the nanomolar range even reaching values of 5 nM[121] and 0.15 nM[123], and a very good selectivity, except in the presence of dopamine[109,121,123] and in some cases of ascorbic acid[109].

Electrochemical biosensors for EP detection are commonly based on the use of enzymes, especially tyrosinase and laccase. In this regard, I.M. Apetrei and C. Apetrei[115] realized a biosensor based on tyrosinase immobilized on a single-walled

carbon nanotube-modified glassy carbon electrode (figure 18). Tyrosinase catalyses the oxidation of EP to epinephrine quinone (EP-quinone) according to the following reaction:

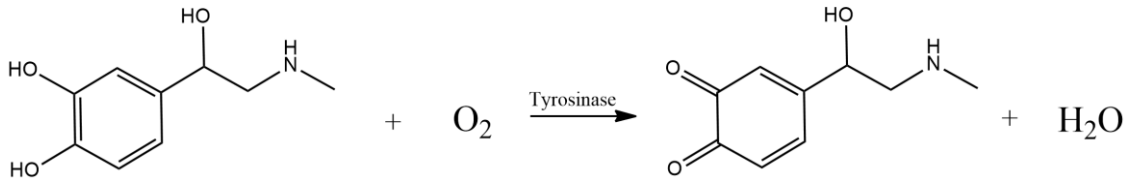

The EP-quinone is then reduced on the electrode surface at -0.07 V *vs*. Ag/AgCl.

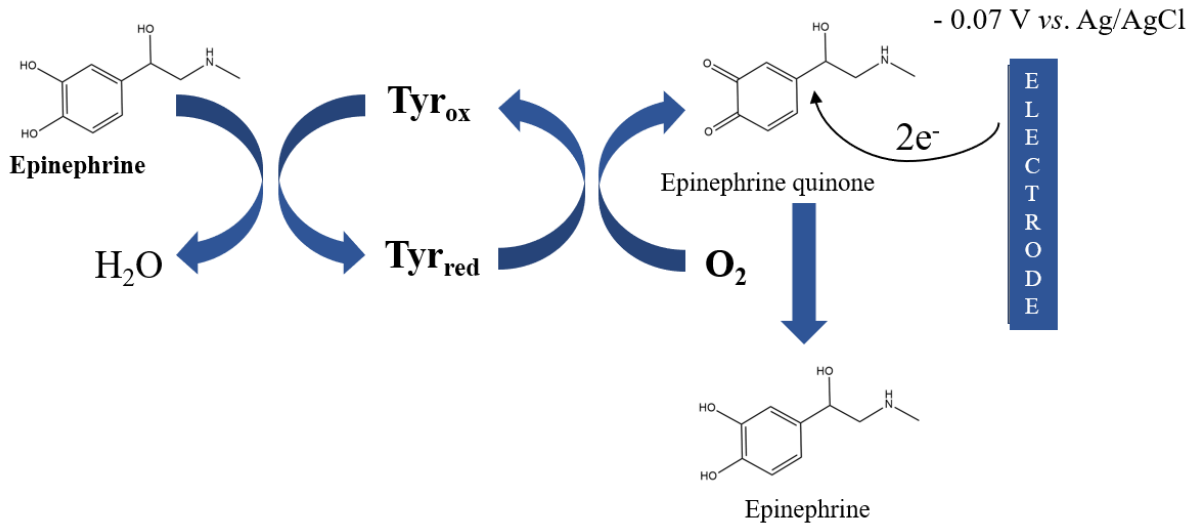

Figure 18: operating mechanism of a first-generation biosensor developed by I. M. Apetrei and C. Apetrei

The biosensor showed a good selectivity and a LoD of 2.54 μM which is adequate for EP determination in pharmaceutical preparation.

Analogously, Ş. Alpat and co-workers[111] developed a biosensor based on carbon paste electrode modified with a multi-walled carbon nanotube, tyrosinase and Nafion membrane. The electrode process is based, as the previous, on the reduction of EP-quinone, which is reduced at -0.33 V *vs*. Ag/AgCl. This biosensor allows the detection of EP in pharmaceutical samples exhibiting a linear dynamic range from $5.0 \cdot 10^{-6}$ to

$5.0 \cdot 10^{-4}$ M, with LoD $3.0 \cdot 10^{-7}$ M. In addition, the Nafion layer proved useful for limiting ascorbic and uric acids interferences.

Biosensors based on the use of laccase are reported by D. Brondani et al.[106] and by S. Baluta et al.[113]. The first one, which dates back to 2009, is based on carbon paste electrode modified with platinum nanoparticles dispersed in 1-butyl-3-methylimidazolium hexafluorophosphate ionic liquid (Pt-BMI.PF_6) and laccase. Laccase, like tyrosinase, catalyses the oxidation of EP to EP-quinone which is then reduced at -0.21 V *vs*. Ag/AgCl. LoD was found to be $2.93 \cdot 10^{-7}$ M which results suitable for detection of EP in pharmaceuticals.

More recently (2018), Baluta and co-workers reported a device based on the catalytic oxidation of EP to EP-quinone, thanks to the presence of laccase. The process was investigated using cyclic voltammetry in cathodic direction and monitoring the EP oxidation peak at about 0.5 V *vs*. Ag/AgCl. It was observed that in presence of laccase, the EP oxidation signal (observed also without the biocatalyst) becomes more intense, proving the catalytic activity of the immobilized enzyme. The biosensor, consisting of a glassy carbon electrode modified with graphene quantum dots (GQDs) and laccase, showed a LoD of 83 nM and a linear range from $1 \cdot 10^{-6}$ to $120 \cdot 10^{-6}$ M.

A biosensor adopting a different enzyme was conceived by F. S. Felix et al.[107] who modified a carbon paste electrode with plant tissues from fruits of a common palm tree in Brazil (*Livistona chinensis*) with a high content of polyphenol oxidase enzymes (PPO). PPO catalyses the same reaction of tyrosinase and laccase, and the electrode process is, thus, based on the reduction of EP-quinone at 0.10 V *vs*. Ag/AgCl. Estimated LoD was $1.5 \cdot 10^{-5}$ M.

A tyrosinase-based third-generation biosensor, based on a direct electron transfer between enzyme and electrode, is reported by A.B. Moghaddam et al.[124] (figure 19). The device is based on a glassy carbon electrode modified with nickel oxide nanoparticles and tyrosinase. The so-modified electrode tested with cyclic voltammetry, in absence of any analytes, showed a reductive peak at -275 mV and a corresponding oxidative peak at 67 mV *vs*. Ag/AgCl which are attributable to the redox

reaction of tyrosinase electroactive sites. Thus, the behaviour of the biosensor was investigated using differential pulse voltammetry, in the absence and presence of EP. In particular, an increase in the oxidation peak current was observed for each subsequent addition of EP. This signal should be attributable to the active site of tyrosinase which is present in its reduced form due to the reaction with the substrate and then is re-oxidized at the electrode surface.

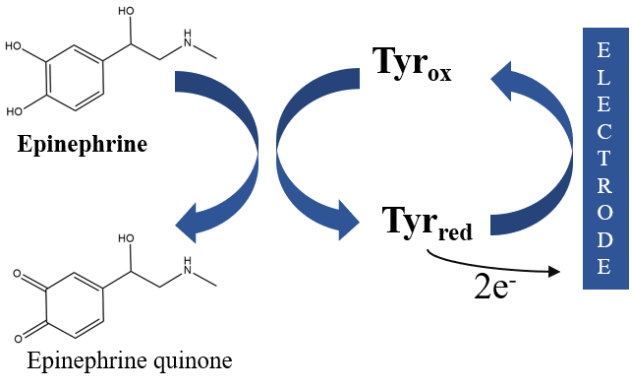

Figure 19: operating mechanism of a third-generation biosensor developed by A. B. Moghaddam et al.

Table 7 summarizes some biosensors for epinephrine detection, along with their main analytical characteristics.

Table 7: some examples of biosensors for epinephrine detection

Catechol-amine	Enzyme	WE	Immobilization	Applied Potential	pH	LoD [μM]	Linear Range [μM]	Target Samples	Ref.
EP	PPO	CPE	Entrapment	-0.10 V *vs*. Ag/AgCl	4.4	15	50-350	Pharmaceutical Formulations	107
EP	Lac	GQDs/ GCE	Physical Absorption + Cross-Linking with GA	-0.2-0.8 V *vs*. Ag/AgCl	5.2	0.083	1-120	Pharmaceutical Formulations	113
EP	Lac	PtNPs in $BMI.PF_6$/ CPE	Entrapment	-0.21 V *vs*. Ag/AgCl	6.5	0.29	0.999–213	Pharmaceutical Formulations	106
EP	Tyr	CPE/ MWCNT/ Nafion	Physical Absorption	-0.33 V *vs*. Ag/AgCl	7.0	0.3	5.0–500	Pharmaceutical Formulations	111
EP	Tyr	GCE/ SWCNT	Drop and Dry + Cross-Linking with GA	-0.07 V *vs*. Ag/AgCl	7.0	2.54	10-110	Pharmaceutical Formulations	115
EP	-	Nanostructured Au Electrode	-	-0.36-0.6 V and -0.1-1 V *vs*. SCE	7.0	2.8 7.3	10-150, 60-600	Pharmaceutical Formulations	114
EP	-	MnO_2/ GCE/ Nafion	-	0.36 V *vs*. SCE	0.0	0.005	0.03-10, 10-100	Pharmaceutical Formulations	121
EP	-	CPE/ MWCNT	-	0.224 V *vs*. SCE	7.0	0.029	0.5-10, 10-100	Human Blood Serum and Pharmaceutical Formulations	122

EP + NOR	-	MWCNT/ EPPGE	-	0.15 V *vs.* Ag/AgCl	7.2	0.00015	0.0005-0.1	Human Blood Plasma and Urine	123
EP + UA + FA	-	EBNBH-modified double-walled carbon nanotube paste electrode	-	0.185 V *vs.* Ag/AgCl	7.0	0.216	0.7-1200	Human Blood Serum and Pharmaceutical Formulations	109

CPE: carbon paste electrode; Lac: laccase; GCE: glassy carbon electrode; Tyr: Tyrosinase; SCE: saturated calomel electrode; EPPGE: plane pyrolytic graphite electrode; UA: uric acid: FA: folic acid; EBNBH: 2,2′-[1,2 – ethanediylbis(nitroloethylidyne)]-bis-hydroquinone;

1.4 Enzymes

1.4.1 Introduction

Enzymes are protein compounds that perform the function of biological catalysts, and are also known as biocatalysts. They are structured in such a way to bind and to act on a particular molecule (substrate) to convert it by a catalytic mechanism, lowering the activation energy of the reaction without effects on the chemical equilibrium (figure 20). They can increase the reaction rate up to a factor of 10^6–10^{12}.

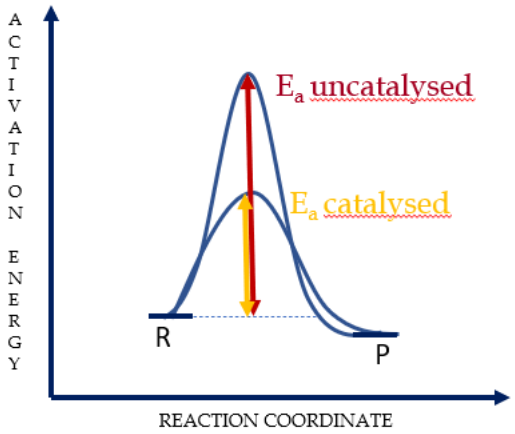

Figure 20: effect of an enzyme on reducing the activation energy required to start a reaction

Biological catalysis was identified and described, for the first time, at the end of 18th century in studies on the digestion of meat by gastric secretions. The term enzyme derives from the Greek words *en* = within and *zume* = yeast, and it was coined by the German physiologist Wilhelm Kühne in 1878, when he was describing the capability of yeast to produce alcohol from sugars[9,125].

In the late 1800s and early 1900s, enzymes were extracted, characterized and used for commercial purposes, but it was only in 1926 that J. B. Sumner isolated and crystallized the enzyme urease revealing that it is a protein compound[126]. The idea that enzymes

were protein compounds was accepted only in 1930 when JH. Northrop and M. Kunitz crystallized other enzymes such as pepsin and trypsin, confirming that they had a protein nature[9]. For the subsequent sixty years it was believed that all enzymes were proteins but, afterwards, it was found that some ribonucleic acid molecules (RNAs) possess catalytic effects; these RNA molecules have been called ribozymes. In the same period (about 1980s) biochemists also developed the technology to generate antibodies with catalytic properties and called them abzymes. However, much of classical enzymology is focused on the proteins that have catalytic activity[125].

Amino acids-based enzymes are globular proteins ranging in size from less than 100 to more than 2000 amino acid residues, with molecular mass between 12000 and 1000000 Dalton[127]. These amino acids can be arranged as one or more polypeptide chains that are folded and bent to form a specific three-dimensional structure, incorporating a small area called active site, which is the part involved in the substrate bond, forming the so-called enzyme-substrate (ES) complex (figure 21).

E = enzyme; S = substrate; ES = enzyme-substrate complex; P = enzyme reaction product;

Figure 21: representation of substrate binding to the active site of an enzyme molecule

In the ES complex, substrate conversion is facilitated by several factors: the interaction can cause in fact a weakening of a key chemical bond in the substrate which then becomes prone to further modifications and, secondly, the enzyme tends to stabilize the reaction intermediate, preventing its reconversion to the initial form. Based on the shape and charge of the active site, the enzyme is specific for a well-defined substrate. The hypothesis that enzyme specificity depends on the complementary nature between substrate and the enzyme active site was first proposed by the German

chemist Emil Fischer in 1894 and it is known as "Fischer's lock and key hypothesis". In 1958 Daniel Edward Koshland extended Fischer's theory with his "induced fit model" of substrate and enzyme binding, in which the enzyme molecule changes slightly its shape to adapt itself to the substrate. This is known as "hand-in-glove model". The part other than the active site is, therefore, not responsible for the specificity, but its role is to stabilize the active site and ensure a suitable environment for interaction of the site with the substrate. It is important to note that, although a large number of enzymes consist only of proteins, most of them also have a non-protein component, called co-factor, which is necessary for the catalytic activity. The co-factor can be a small organic or metalloorganic molecule, the so-called coenzyme, or it may be an inorganic molecule, characteristically a metal ion such as iron, copper, cobalt, zinc etc. (figure 22). These latter are attached to the protein side chains by coordination or electrostatic bonds. When the enzyme requires a co-factor for its activity, the inactive protein component is called apoenzyme whereas the apoenzyme plus co-factor is called holoenzyme. When a coenzyme is strongly and permanently bound to the apoenzyme it is called prosthetic group, instead when it is weakly bound it is called co-substrate[9,24,125].

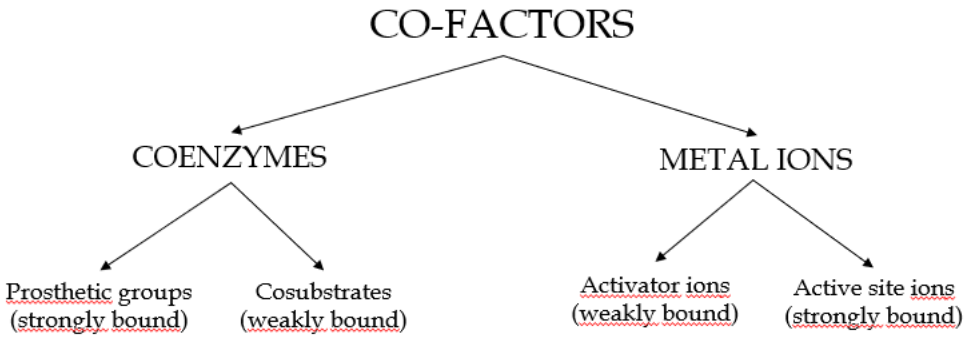

Figure 22: different co-factors and their interaction with proteins

By free diffusion, coenzymes contribute to the transport of electrons, atoms or groups of atoms between molecules. An activator metal ion obliges the active site to adopt a

favourable configuration or can be involved in binding the substrate to the active site; in some cases, it can act as an electron shuttle. The so-called active site ions are structural constituents of the active site[24].

1.4.2 Classification of Enzymes

Many enzymes have common names (often called "trivial names") which refers to the reaction that they catalyse, adding the suffix *-ase* (e.g., oxidase, dehydrogenase, hydrolase), although individual proteolytic enzymes have the suffix *-in* (e.g., trypsin, pepsin, papain). Sometimes, the trivial name also shows the substrate on which the enzyme acts (e.g., glucose oxidase, diamine oxidase) but in other cases they are more generic and provide little information (e.g., invertase, catalase).

Due to the growing complexity and to avoid confusion, the International Union of Biochemistry set up the Enzyme Commission (EC). The sixth edition of the Enzyme Commission Report was published in 1992 and contains details of nearly 3200 different enzymes; supplements published annually have, now, extended this number to over 5000. Within this system, each enzyme has a recommended name, suitable for common use, a systematic name which denotes the reaction it catalyses and a four-digit classification number (preceded by the EC acronym): for example, glucose oxidase is denoted EC 1.1.3.4 and has the systematic name "β-D-glucose: oxygen 1-oxidoreductase". The first number indicates the enzyme membership class, the second identifies the subclass, the third indicates the sub-subclass and the last represents the systematic name. There are six major classes and a series of subclasses (table 8 and table 9):

Table 8: main classes of enzymes in enzyme classification system

First EC Digit	Enzyme Class	Reaction Type	Systematic Name
1	Oxidoreductases (Oxidases and Dehydrogenases)	Oxidation/Reduction	Donor: acceptor oxidoreductase
2	Transferases	Atom/Group Transfer	Donor: acceptor group transferase
3	Hydrolases	Hydrolysis	Substrate X-hydrolase
4	Lyases	Group Removal	Substrate group lyase
5	Isomerases	Isomerization	Reaction type + suffix *-ase*
6	Ligases	Joining of molecules linked to the breakage of a pyrophosphate bond	A:B ligase

Table 9: secondary and tertiary classes of oxidoreductase enzymes in enzyme classification system

Oxidoreductases: Second EC Digit	Hydrogen or Electron Donor	Oxidoreductases: Third EC Digit	Hydrogen or Electron Acceptor
1	Alcohol (CHOH)	1	NAD^+ or $NADP^+$
2	Aldehyde or ketone (C=O)	2	Fe^{3+}
3	CH-CH	3	O_2
4	Primary amine ($CHNH_2$ or $CHNH_3^+$)	4	Other
5	Secondary amine (CHNH)		
6	NADH or NADPH (when another redox catalyst is the acceptor)		

1.4.3 Enzyme Kinetics

To understand the underlying principles of enzyme biosensors it is very important to know how the enzymes work. To study the action mechanism of enzymes it is possible to evaluate different experimental approaches, among which, the most used one is the enzymatic kinetics.

A wide diversity of reaction mechanisms is possible for enzyme-catalysed reactions. The simplest enzyme mechanism was first described by Leonor Michaelis and Maud Menten in 1913 and it is a representative one, highlighting some essential features of enzyme kinetics. Denoting by E, S and P the enzyme, the substrate and the product, respectively, Michaelis-Menten mechanism can be formulated as a two-step process:

$$E + S \underset{k_{-1}}{\overset{k_1}{\rightleftharpoons}} ES \xrightarrow{k_2} E + P$$

Central to their derivation is the concept that reaction occurs *via* the formation of the ES complex which, then, can either dissociate to release product or dissociate in the reverse direction to generate substrate and enzyme again. The Michaelis-Menten model is based on two important assumptions:

1. We consider the initial rate of the reaction (v_0) when the product concentration is negligible ([S] >> [P]), in this way we can ignore the possibility of any product reverting to substrate;
2. The concentration of S is much higher than that of E ([S]>> [E]).

According to what abovementioned:

$$v_0 = \frac{d[P]}{dt} = k_2[ES]$$

[ES] is an intermediate and, therefore, its concentration is unknown, but it is possible to express it in terms of known values. In a steady-state approximation (Briggs-Haldane assumption) we can assume that [ES] remains constant. The rate of formation of the ES complex and that of its breakdown must, therefore, be balanced:

$$Rate\ of\ ES\ complex\ formation\ =\ k_1[E][S]$$
$$Rate\ of\ ES\ complex\ breakdown\ =\ (k_{-1}\ +\ k_2)[ES]$$

At steady-state:

$$k_1\,[E][S] = (k_{-1} + k_2)\,[ES]$$

$$[ES] = \frac{k_1[E][S]}{k_{-1} + k_2}$$

The Michaelis-Menten constant K_M can be defined as follows:

$$K_M = \frac{k_{-1} + k_2}{k_1}$$

$$[ES] = \frac{[E][S]}{K_M}$$

Since in the second assumption [S] >> [E], the concentration of uncombined [S] is almost equal to the total concentration of substrate, and the concentration of uncombined enzyme, [E], is equal to the total enzyme concentration $[E]_T$ minus that combined with S, [ES]:

$$[ES] = \frac{[E]_T\,[S]}{[S] + K_M}$$

Substituting in v_0:

$$v_0 = k_2 \frac{[E]_T[S]}{[S] + K_M}$$

When all the active sites are saturated by the substrate, the maximum rate is reached and $k_2[E]_T$ is V_{max} (also called saturation rate), therefore Michaelis Menten equation can be written as follows:

$$v_0 = \frac{V_{max}[S]}{[S] + K_M}$$

Michaelis-Menten constants have been determined for many commonly used enzymes and are typically in the lower millimolar range. Generally, K_M is considered as a measure of the affinity of the enzyme for its substrate, then a low K_M value indicated a high affinity and vice versa. It is important to note that enzymes that catalyse the same reaction, but which derive from different organisms, can have different K_M values. In addition, an enzyme with multiple substrates can have quite different K_M values for each substrate[9,125].

There are various methods for determining K_M and V_{max}, mainly:

- from a direct plot of rate against substrate concentration which is an equilateral hyperbola, but very often this can be hard;
- using the plot of double reciprocal or Lineweaver-Burk plot: this plot linearizes the hyperbolic curved relationship and the produced line is easy to extrapolate, allowing the evaluation of V_{max} and K_M.

As already said, Michaelis-Menten kinetics is the simplest and it is valid just in some cases. However, in a large number of cases two or more substrates are involved. Multi-substrate reactions are often represented by schemes proposed by W. W. Cleland[128] for the double displacement mechanism, also called *ping-pong* mechanism. This

mechanism can occur in reactions involving coenzymes. During such a process, the enzyme alternates between two states (e.g., oxidized and reduced forms in the case of an oxidase). The *ping-pong* mechanism is characterized by the following equation:

$$v = V_{max}(1 + \frac{K_{M1}}{[S1]} + \frac{K_{M2}}{[S2]})^{-1}$$

where S1 and S2 are the two substrates, K_{M1} and K_{M2} are specific constants to each of the substrates. If the concentration of S2 is sufficiently high and $K_{M2}/[S2] \ll K_{M1}/[S1]$ the kinetic equation reduces to the Michaelis-Menten equation in [S1], if the above inequality is reversed, K_{M2} can be determined in a similar way[24].

The kinetic approach allows to derive several physical parameters of the enzymes. When the conversion of ES to product involves several distinct steps, k_2 should be replaced with k_{cat} (rate constant at enzyme saturation):

$$k_{cat} = \frac{V_{max}}{[E]_T}$$

This constant is often referred to as the turnover number of the enzyme [s^{-1}] and represents the number of catalytic cycles that each active site undertakes per unit under saturation conditions. Sometimes, when the enzyme is not pure, but there are also other (inactive) protein species, the turnover number can be ambiguous, and the quantity of enzyme is preferably expressed in empirical way by means of the enzyme activity. Enzyme activity is the amount of the enzyme preparation that catalyses the conversion of a given quantity of substrate per unit time, under specified conditions of pH, temperature and ionic strength. The SI unit for enzyme activity is the katal which represents the amount of enzyme preparation that converts 1 mole of substrate per second. A commonly used value is the enzyme unit (U) that denotes the amount of enzyme that converts 1 μmole of substrate per minute (1U = 16,67 nanokatals).

Activity is an extensive quantity, hence, in order to characterize it independently of its amount, specific activity was introduced:

$$Specific\ Activity = \frac{Activity}{Amount\ of\ Enzyme}$$

The SI unit for specific activity is katal kg^{-1} but, more often, μmol mg^{-1} min^{-1} is used. The specific activity is a pointer of enzyme purity[24].

1.4.4 Effects of pH and Temperature on Enzyme Reactions

The enzyme active sites can possess acid or base groups, then an optimum pH at which the rate of the catalysed reaction is maximal exists, and above and below it the reaction rate decreases. The pH value, determining the protonation state of the active site, affects the stability of the ES complex and is essential in the progress of the reaction. However, effects of pH are often reversible but, in extreme acidic or alkaline conditions, the enzyme can undergo irreversible changes in its conformation, completely and definitely losing its catalytic activity. Charged substrates can also influence the pH dependence of the reaction rate, as they affect the local ionic strength and thereby the thermodynamics activity of the reactants. In addition, the transduction process itself can be affected and the response of an enzyme biosensor can be strongly dependent on pH. Therefore, this parameter should be controlled using a pH buffer system whose components do not participate in the enzyme reaction.

The effects of temperature on enzyme activity are complex, indeed there are two forces that act simultaneously but in opposite directions. Like any chemical reaction, the rate of an enzyme catalysed reaction increases as the temperature is raised, but at the same time a progressive inactivation caused by denaturation of the enzyme occurs. Thermal denaturation is time dependent, and for enzyme the term "optimum temperature" has little real meaning unless the duration of exposure to that temperature is recorded. The

temperature at which denaturation becomes important varies from one enzyme to another. Normally, denaturation is negligible below 30°C and starts to be appreciable above 40°C. It is important to note that, typically, enzymes derived from microbial sources show much higher thermal stability than those from mammalian ones. There are also enzymes derived from extremely thermophilic microorganisms (e.g., thermolysin from *Bacillus thermoproteolyticus*) that are thermostable at 70°C and still retain good levels of activity even at 100°C[24,125].

1.4.5 Enzymes in Biosensors

Among the various types of enzymes, several have proved useful for bioanalytical purposes and for designing enzyme biosensors. For this latter aim most important enzymes are oxidases, dehydrogenases, hydrolases and lyases. In this work, oxidase type enzymes have been used, in particular diamine oxidase and tyrosinase which will be described in detail in the next paragraphs.

Enzyme biosensors are widely used to determine the enzyme itself or its substrate. The application of enzymes in biosensors design is based on their specificity for a substrate analyte. Therefore, in order to assembly an enzyme biosensor, the enzyme should be immobilized as part of a recognition layer at the surface of a proper transducer so as to measure the concentration of detectable species. The substrate and any additional reactants undergo, first of all, diffusion from the solution into the recognition layer in which the enzyme is immobilized. The transducer allows the monitoring of the occurrence of the reaction by detecting either a product or the excess of reactant that escaped the enzyme reaction. Moreover, also physical effects (e.g., heat evolution) are suitable to monitor the rate of the enzyme reaction and, indirectly, the substrate concentration (figure 23).

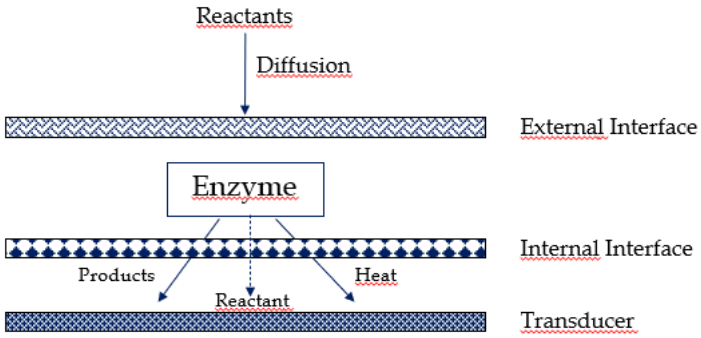

Figure 23: typical configuration of an enzymatic biosensor

Sometimes, perm-selective membrane can be incorporated to control the diffusion of only some reactants and to avoid the diffusion of possible interfering substances. Enzyme-based biosensors, either with isolated enzymes or with enzymes incorporated in living materials, are often called "metabolism sensors"[24].

1.4.6 Diamine Oxidase (DAO)

Amine oxidases are a class of enzymes (EC 1.4.3.6 and EC 1.4.3.13) widely distributed in mammals, plants and microorganisms and their structure, selectivity and biological functions are very different depending on the isolation source: in prokaryotes the presence of the enzyme permits the microorganisms to use amines as a carbon and nitrogen sources, whereas in both plants and animals their main role is in detoxification processes by catabolizing the toxic mono- and diamines and in the regulation of fundamental cellular processes (tissue differentiation, tumour growth and programmed cells death)[69,99,129].

The copper-containing amine oxidases (EC 1.4.3.6) [amine: oxygen oxidoreductase (deaminating) (copper containing)][129] catalyse the oxidative deamination of histamine and other biogenic amines by dioxygen reduction to generate aldehydes, hydrogen peroxide and ammonia:

$$R\text{-}CH_2\text{-}NH_2 + H_2O + O_2 \longrightarrow R\text{-}CHO + H_2O_2 + NH_3$$

In particular, DAO (also known as histaminase) is mainly selective for histamine but catalyses also the deamination of diamines such as putrescine and cadaverine. DAO from *porcine kidney* is a homodimer protein consisting of two equal subunits with a molecular weight of 87 kDa each, containing in its catalytic site a tightly bound copper centre and an organic cofactor with a quinoid structure (topa quinone,TPQ)[69,93,99,130] (figure 24).

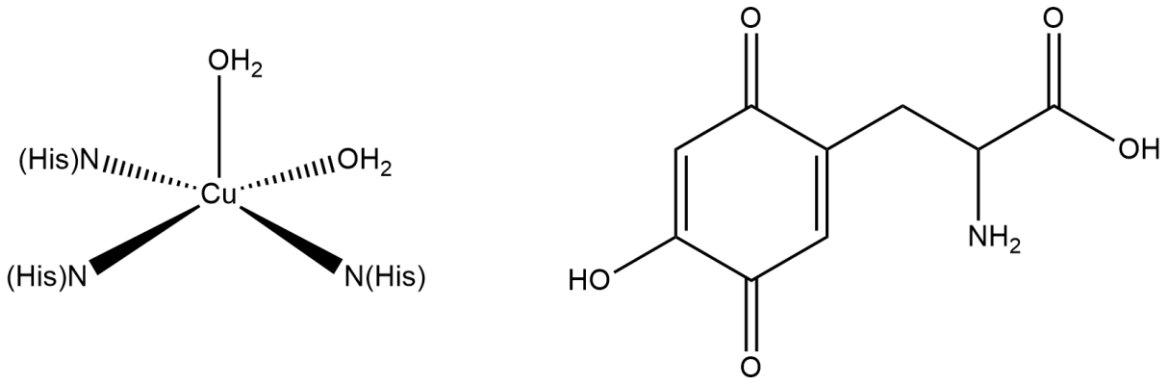

Figure 24: catalytic site of diamine oxidase from porcine kidney: (left) type II copper centre and (right) TPQ

The kinetic mechanism of the catalysed reaction has been extensively studied since 1960, but it was only quite recently completely understood[69,99]. It is a *ping-pong* mechanism articulated in three steps (figure 25):

1. amine substrate binding with C4 quinone group of topa forming a ketoimine that undergoes a proton abstraction from the α-carbon of the amine by a nucleophilic agent (a side chain carboxylate group of an Asp residue present in the active site);
2. hydrolysis and release of the aldehyde product;
3. transfer of an electron between the reduced topa and Cu^{2+}, mediated by an integrated network of water. At this point, O_2 forms a complex with Cu^{+} and in presence of water environment, H_2O_2 and NH_3 are released, while the oxidized form of the topa quinone is regenerated.

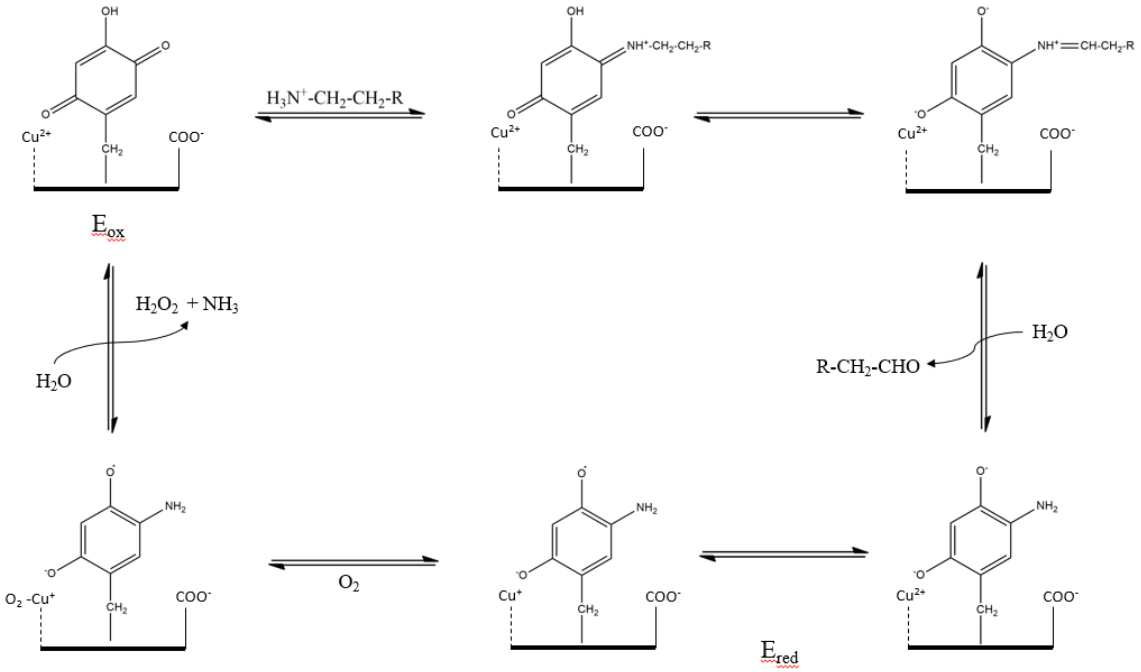

Figure 25: enzymatic mechanism of histamine oxidation

1.4.7 Tyrosinase (Tyr)

Tyrosinases (EC 1.14.18.1) are metalloenzymes that can be found in multiple sources like bacteria, fungi, arthropods, plants and mammals. In mammals tyrosinases are responsible for the formation of melanin in skin and hair colour as well as browning in fruits and vegetables. In plants, sponges and many invertebrates tyrosinases are useful for wound healing and primary immune responses. In bacteria, tyrosinases protect DNA from UV damage, and in arthropods they play a role in sclerotization. Using molecular oxygen, tyrosinase catalyses two sequential enzyme reactions:

1. orthohydroxylation of monophenols (monophenolase or cresolase activity);
2. oxidation of *o*-diphenols to the corresponding *o*-quinones (diphenolase or catecholase activity).

Tyrosinases belong to the "type III copper" family. The overall structure of tyrosinase can be divided in three domains: the central domain, the N-terminal domain and the

C-terminal domain. The active site is placed in the central domain and it consists in a binuclear type III copper centre containing two copper ions (Cu_A and Cu_B) with six histidine residues which are located in a four helical bundle, coordinating the two copper ions[131,132].

The properties of tyrosinase are determined by four oxidation states of its active site: met, oxy, deoxy and deactivated forms (figure 26). Oxy-tyrosinase (E_{oxy}) consists of two tetragonal Cu(II) ions, each coordinated by two strong equatorial and one weaker N_{His} ligand. The exogeneous oxygen molecule is bound as peroxide and is located between the two Cu centres. Met-tyrosinase (E_{met}), like the oxy form, contains two tetragonal Cu(II) ions antiferromagnetically coupled through an endogenous bridge, although hydroxide endogenous ligands other than peroxide are bound to the copper sites. This derivative can be converted in the oxy-tyrosinase by addition of peroxide. Deoxy-tyrosinase (E_{deoxy}) has a bicuprous structure Cu^I-Cu^I. Finally, the deactivated form occurs when a catecholic group molecule is oxidized through the phenolic oxidative mechanism which leads to the reduction of Cu^{2+} to Cu^0 (inactivation suicide)[131,133].

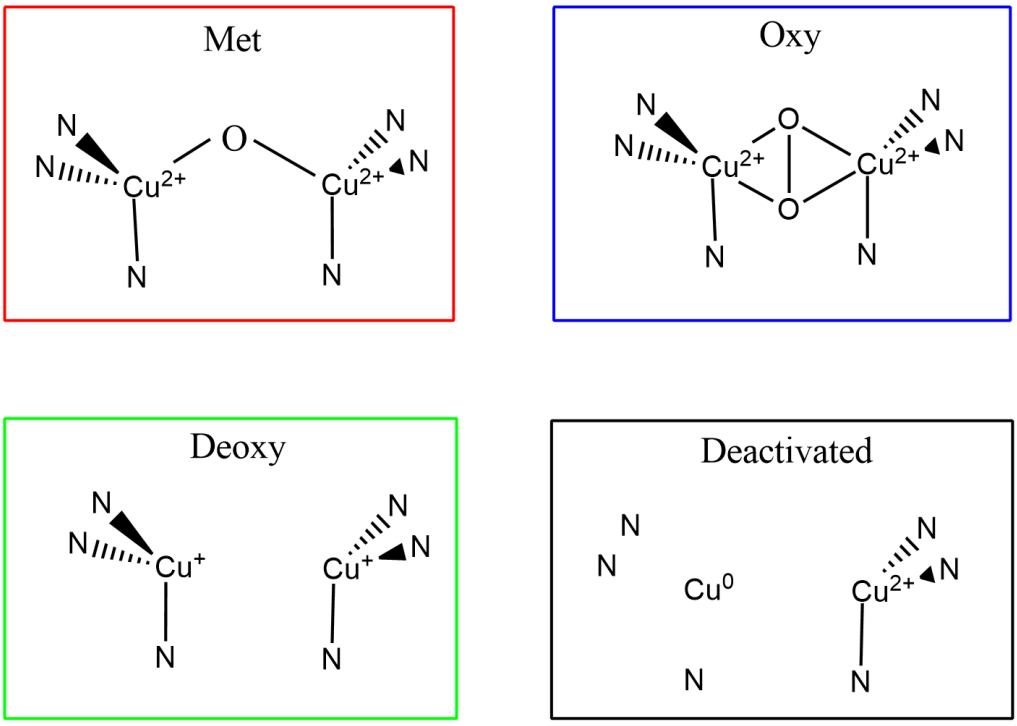

Figure 26: four discrete states of the active site of tyrosinase

If only diphenol is present, the tyrosinase mechanism (figure 27) can be described as follows: the diphenol binds the E_{oxy} form to give E_{oxy}-D, which oxidizes the diphenol to *o*-quinone and yields the antiferromagnetically coupled tetragonal Cu(II) form of the enzyme in met form E_{met}. This form transforms another *o*-diphenol molecule to *o*-quinone and is reduced to the deoxy form E_{deoxy}[133].

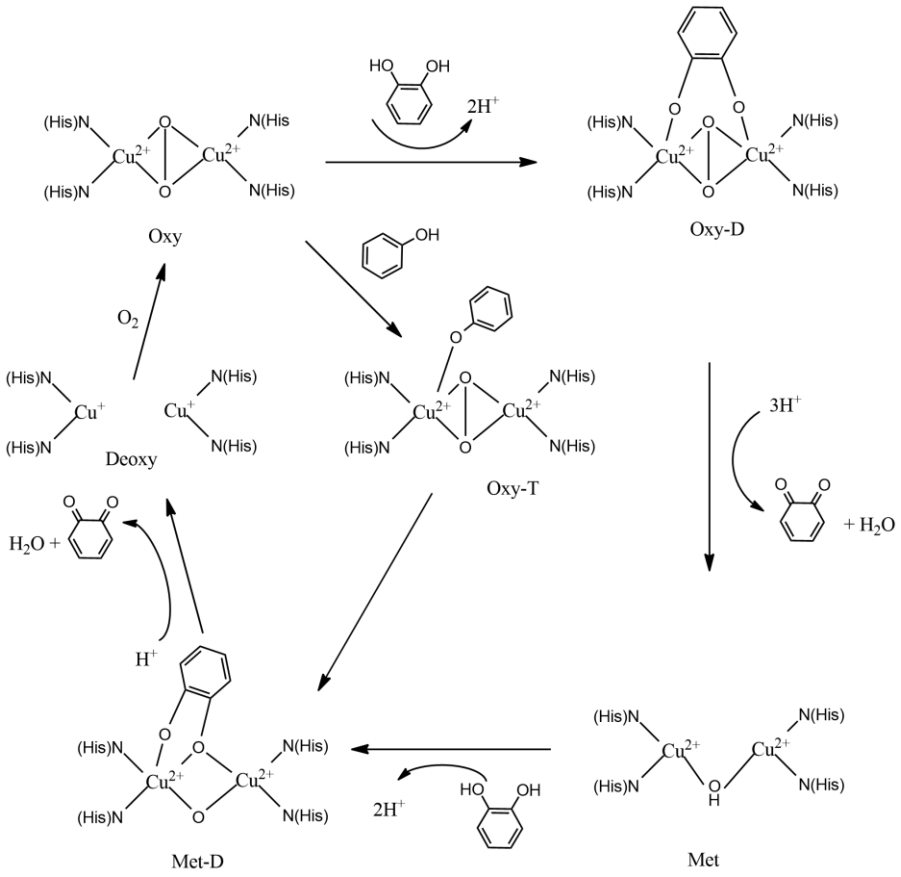

Figure 27: mechanism for diphenolase activity of tyrosinase

Summarizing, the diphenolase activity involves the oxidation of two *o*-diphenols to two *o*-quinones with a concomitant 4 electrons reduction of O_2 which yields two molecules of water.

1.4.8 Immobilization Techniques

Immobilization of enzymes is one of the most important and crucial features in designing the biorecognition part of enzyme-based biosensors, indeed a proper immobilization method should be chosen depending on the desired usage biosensor, the enzyme nature and the transduction, and its associated detection mode[134,135]. This process is a real key-step for developing efficient biosensor with suitable performances such as a good operational and shelf time stability, high sensitivity, high selectivity, high reproducibility and short response time. Immobilized enzymes have to keep their structure and their function to consequently retain their biological activity. Moreover, the immobilization step should ensure that the enzyme remain strongly bound to the surface without undergoing desorption processes, during the use of the biosensor and should be stable for long-term application.

Each immobilization technique possesses advantages and drawbacks. The best method of enzyme immobilization varies according to specific analytic requirements of the biosensor (e.g., maximum sensitivity or stability). Sensitivity decreases if immobilization causes enzyme denaturation or misfolding, especially on its active site. Reproducibility, cost and difficulty of the immobilization process also need to be considered[134].

Various approaches in classifying immobilization techniques are reported, one of the most used is showed in figure 28, based on:

1. physical or reversible methods: (i) adsorption and (ii) disulphide bond formation;
2. chemical or irreversible methods: (i) entrapment, (ii) cross-linking and (iii) covalent bonding[136].

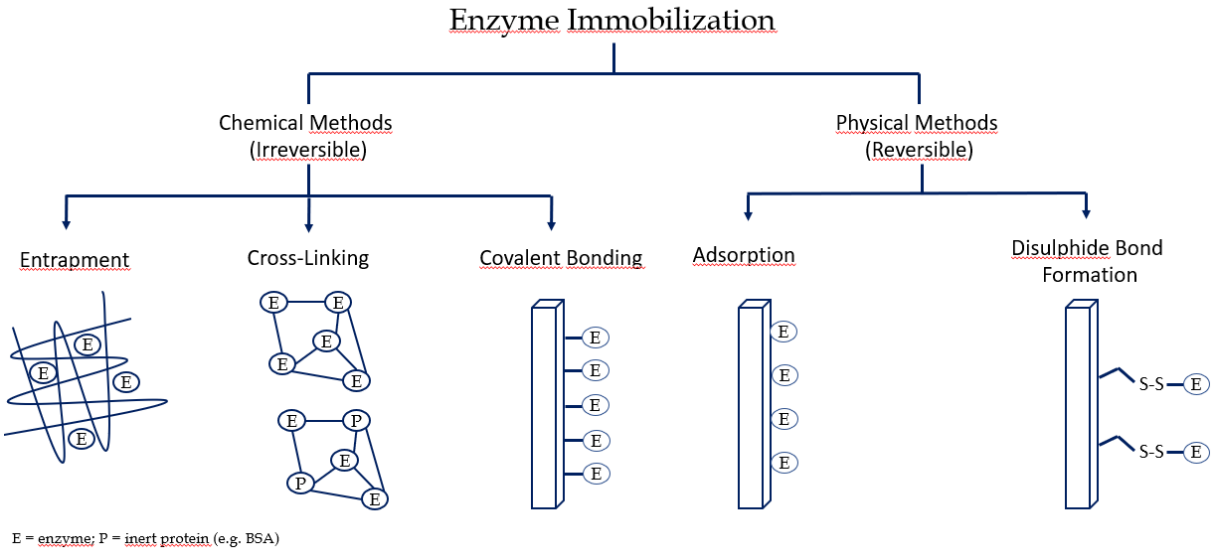

Figure 28: classification of different enzyme immobilization techniques

1.4.8.1 Adsorption

Enzyme adsorption onto solid supports is the easiest method of physical immobilization and it is the method of choice in preliminary investigations. The enzyme is dissolved in solution and the support is placed in contact with the enzyme solution for a fixed period of time; the unadsorbed enzyme is then removed by washing with a buffer solution. The adsorption mechanism is based on weak bonds such as Van der Waals's forces and electrostatic and/or hydrophobic interactions. If the isoelectric point of the enzyme is lower than the pH of solution, enzyme is negatively charged and thus can be bound to a positively charged support. Another strategy can be the immobilization by electrochemical doping: by controlling pH, the negatively or positively charged enzymes can be doped into a conductive polymer film during its oxidation or reduction processes, respectively.

This technique does not require any functionalization of the support and not even any additional reagents, and it is generally conservative from the point of view of enzyme activity. Although this method causes little or no enzyme inactivation, the desorption of enzyme resulting from changes in temperature, pH and ionic strength is possible. In addition, biosensors based on adsorbed enzymes suffer from poor operational and

storage stability and they are, therefore, particularly suitable for disposable sensors which are exposed to sample solution for only short periods of time[24,134]. A detailed section dedicated to conducting polymers will be discussed in the next paragraph.

1.4.8.2 Entrapment

Enzyme entrapment allows enzymes, possible mediators and additives to be simultaneously deposited in the same sensing layer. Enzymes can be entrapped in three-dimensional matrices as electrogenerated polymer films, amphiphilic networks composed of poly-dimethylsiloxane (PDMS), photopolymers, or silica gel. This technique should allow to preserve enzyme activity. Furthermore, this type of biosensors is often characterized by increased operational and storage stability if compared to devices in which the enzyme is adsorbed. Nevertheless, possible drawbacks can be the leaching of the biomolecule and possible diffusion barriers that can restrict the performances of the systems.

Entrapment via Electropolymerization

Entrapment in electrogenerated films is one of the most attractive approach in this context. It is a one-step method which consists in applying a proper potential or current to the electrode in an aqueous solution containing both enzyme and monomer. Monomer oxidation yields to a radical cation which can either react with a second radical cation or with a neutral monomer, in such a way to obtain a dimer that is, then, re-oxidized. Finally, a polymer is formed at electrode surface. Enzyme molecules in the immediate vicinity of the electrode surface are physically incorporated into the growing polymer film. Most of electropolymerized films used for enzyme entrapment are conducting polymers such as PEDOT, polypirrole and polyaniline. This technique does not involve any chemical reaction between the monomer and the enzyme that could affect its activity. Moreover, this method allows to have the exact control of the

thickness of the polymer film and, hence, the modulation of the immobilized amount of enzyme. Nevertheless, this method sometimes requires high concentration of monomer (0.05 – 0.5 M) and enzyme (0.2-3.5 mg mL^{-1}) and it is difficult to estimate the amount of the entrapped enzyme[134]. It is also important to note that this approach can only be used if the monomer is soluble in an aqueous medium, since the enzyme cannot be solubilized in organic solvents without being damaged.

1.4.8.3 Cross-Linking

One of the most commonly used immobilization methods is cross-linking with glutaraldehyde or other bifunctional coupling agents (e.g., glyoxal or hexamethylenediamine). Molecules of an enzyme can be either cross-linked one to each other or with a functionally inert protein such as bovine serum albumin (BSA). This method is very attractive due to its simplicity and the strong chemical binding achieved between biomolecules. The main disadvantage of this method is the possibility of activity losses due to the possible distortion of the enzyme conformation and the chemical alterations of the active site during cross-linking[134].

Cross-Linking with Glutaraldehyde

Glutaraldehyde, the most used coupling agent, is a linear 5-carbon dialdehyde. It is a clear, colourless to pale straw-coloured, pungent oily liquid that is soluble in all proportions in water and alcohol, as well as in organic solvents. It is mainly available as acidic aqueous solutions (pH 3.0–4.0), ranging in concentration from less than 2% to 70% (w/v). Glutaraldehyde is widely used for enzyme immobilization for a whole series of advantages: commercial availability, low costs, high reactivity with amine groups at around neutral pH. Moreover, glutaraldehyde is more efficient than other aldehydes in generating thermally and chemically stable crosslinks. In spite of the success of this reagent, its chemistry has been quite controversial. In fact, the simple

structure of glutaraldehyde is not indicative of the complexity of its behaviour in aqueous solution and its reactivity.

Glutaraldehyde, therefore, can be present in an aqueous solution in at least thirteen different forms (figure 29) depending on the conditions of pH, concentration and temperature, hence the cross-linking mechanisms are not yet fully understood. Considering also the peculiar characteristics of each single enzyme, probably the cross-linking mechanisms are always different and multiple at the same time.

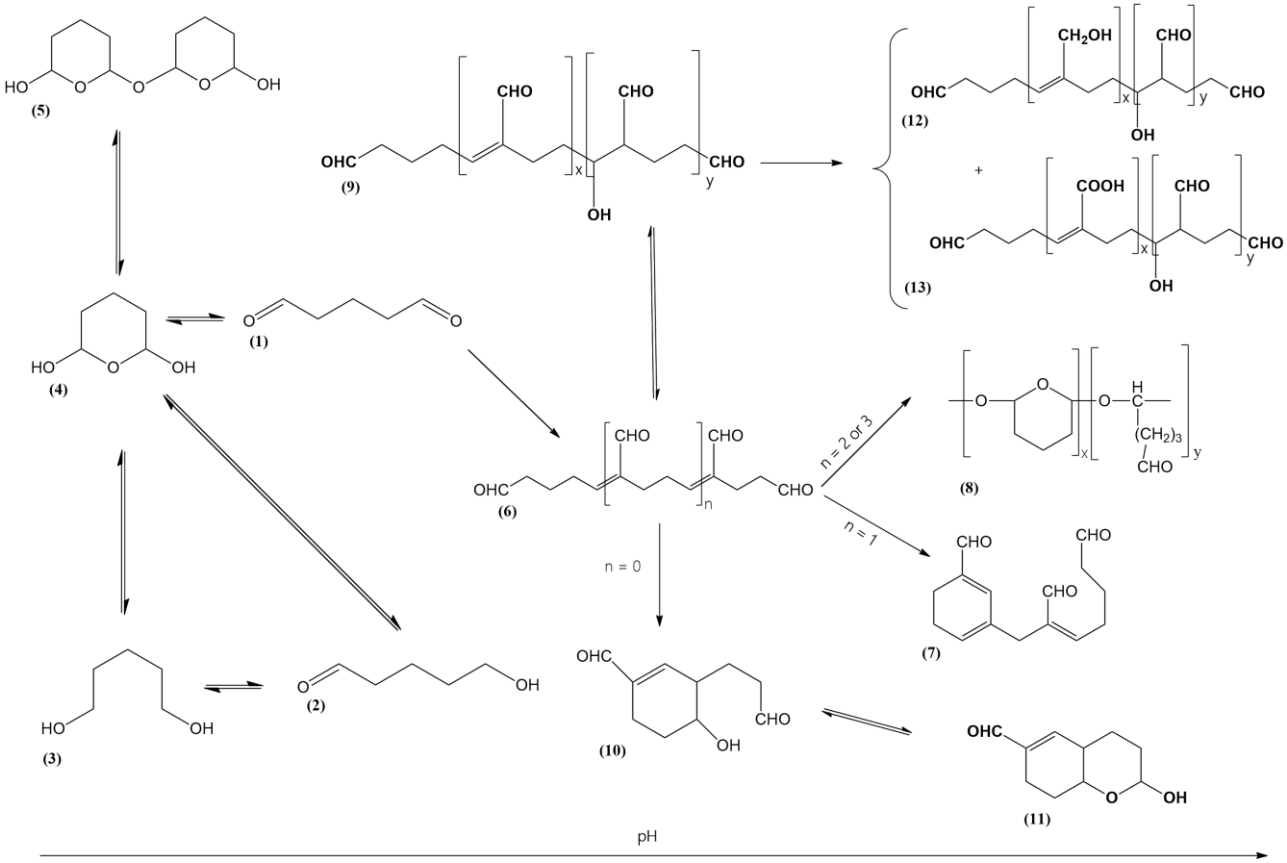

Figure 29: forms of glutaraldehyde in an aqueous medium at different pH values

Glutaraldehyde was used for the first time at the beginning of the 1960s for the fixation of tissues, and since this time many other applications have been developed. The high reactivity between glutaraldehyde and proteins at neutral pH is based on the presence of several reactive residues in proteins and molecular forms of glutaraldehyde in aqueous solution, leading to many different possible reaction mechanisms. The

crosslinking of proteins, either to a carrier (solid support) or between protein molecules (carrier-free), generally involves the ε-amino group of lysine residues which are usually located on protein surface and are not involved in the catalytic site, allowing to preserve protein conformation and consequently its biological activity.

Aldehydes are expected to form Schiff bases upon nucleophilic attack by the ε-amino groups of lysine residues. Schiff bases are, however, unstable under acidic conditions and tend to break down to generate again the starting aldehyde and amine. Thus, a simple Schiff base with both ends of monomeric glutaraldehyde has been excluded as a mechanism for cross-linking between glutaraldehyde and enzymes[137]. F. M. Richards and J. R. Knowles[138] and P. Monsan et al.[139] postulated, instead, alternative pathways both involving the reaction of the protein amino group with α,β-unsaturated aldehydes formed by aldol condensation of glutaraldehyde. Richards and Knowles[138] proposed a Michael type addition between the enzyme amino groups and the ethylenic double of the α,β-unsaturated oligomers found in the commercial aqueous solutions of glutaraldehyde. Conversely, Monsan et al.[139] proposed a mechanism in which an addition reaction occurs on the aldehydic part of the α,β-unsaturated polymers and poly-glutaraldehyde to give a Schiff base stabilized by conjugation (figure 30).

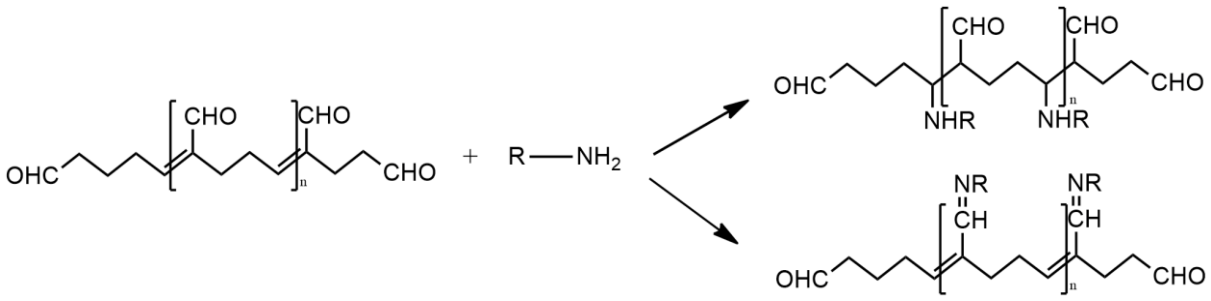

Figure 30: Michael-type (up) and Schiff base (down) reactions of glutaraldehyde with proteins

A few years later, other mechanisms were proposed by P. M. Hardy et al.[140,141] (figure 31), T. Tashima et al.[142] (figure 32) (for alkaline conditions) and by D. R. Walt and V. Agayn[143] (figure 33) (for neutral or acidic conditions).

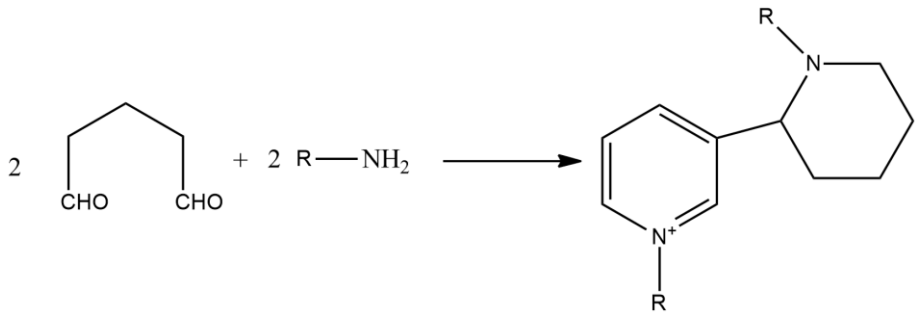

Figure 31: crosslinking of proteins with glutaraldehyde giving a quaternary pyridinium compound

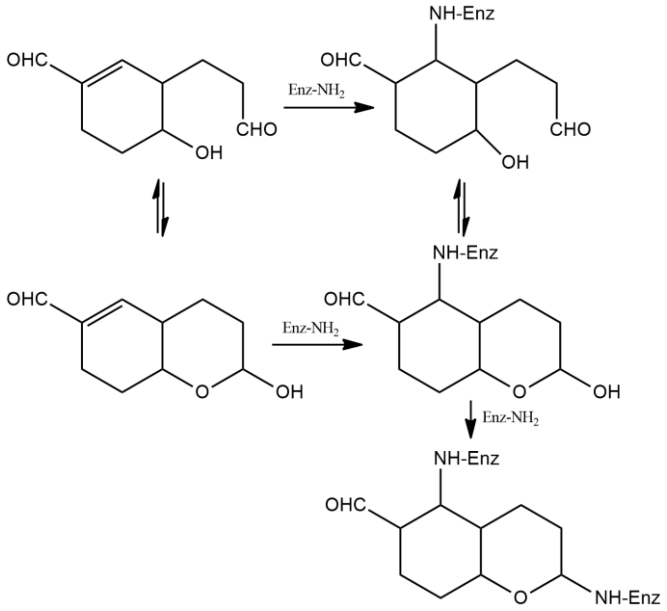

Figure 32: reaction of dimeric cyclic glutaraldehyde with proteins under basic conditions

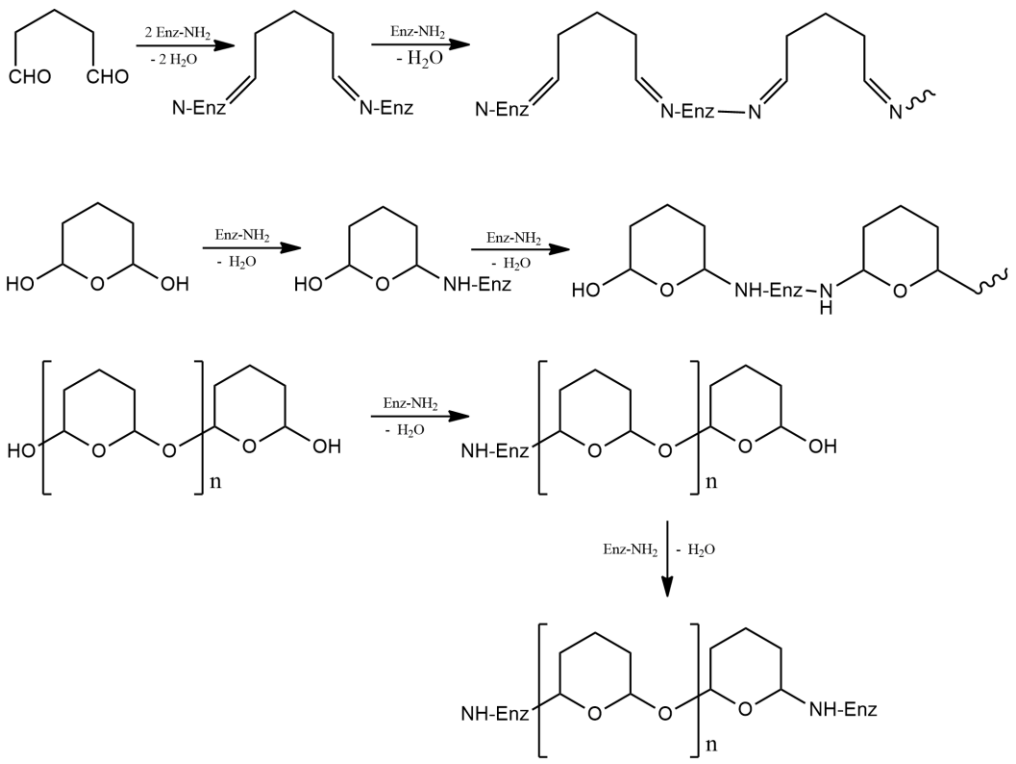

Figure 33: reactions of glutaraldehyde with proteins under acidic or neutral conditions

In conclusion, since mechanisms are multiple and not completely understood, and a number of parameters can influence immobilization by cross-linking with glutaraldehyde, an efficient immobilization requires a correct balance between concentration of both enzyme and reagent, pH, ionic strength, temperature, reaction time. Furthermore, the nature of the enzyme, especially its lysine content, has to be carefully considered. In particular, the concentration of enzyme and glutaraldehyde is one of the most critical parameters: too low concentrations tend to induce intramolecular cross-linking rather than the desired intermolecular cross-linking; on the other hand, too high concentrations can cause too large intermolecular cross-linking causing distortions of the enzymatic structures and consequently loss of the enzymatic activity[137].

1.4.8.4 Immobilization by Covalent Bond

Covalent coupling between enzymes and polymer matrices is a common chemical immobilization method. In this case, biocatalysts are bound to the support through their functional groups, that are not essential for their catalytic activity. The binding of the enzymes to the support is, generally, carried out by initial activation of the surface using multifunctional reagents (e.g., glutaraldehyde or carbodiimide), followed by enzyme coupling to the activated support, and finally removal of unbound biomolecules. The solid matrix can either be an inorganic material (e.g., pore glass), a natural (cellulose) or synthetic (nylon) polymer or pre-activated membranes (e.g., Immunodyne, or UltraBind)[134].

Activation of Carboxylic Groups

Carbodiimides permit the binding between the carboxylic groups of a support and the amino function of an enzyme or, conversely, the amino groups of a support and the carboxyl function of enzyme[134]. Sometimes, N-hydroxysuccinimide (NHS) can be associated to carbodiimide in order to improve immobilization efficiency (figure 34).

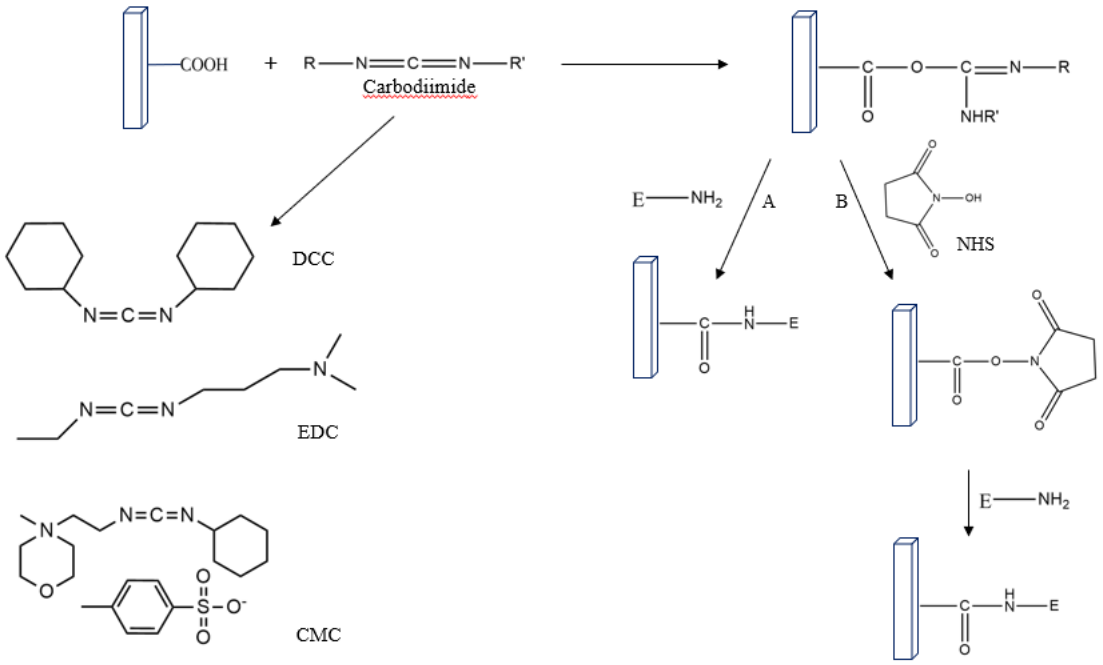

Figure 34: enzyme immobilization on carboxylated surface by carbodiimide coupling (A) without or (B) with NHS

The most easily available and commonly used carbodiimides are 1-ethyl-3-(3-dimethylaminopropyl) carbodiimide (EDC) and 1-cyclohexyl-(2-morpholinoethyl) carbodiimide metho-p-toluene sulfonate (CMC), both water soluble, and dicyclohexylcarbodiimide (DCC), soluble in organic solvents[9,134] (figure 34).

Activation of Amino Groups

Amino groups can be activated either by carbodiimides or by glutaraldehyde. In the latter case, a Schiff-base reaction occurs between an aldehyde group of glutaraldehyde and an amine function of the support. Then, the second aldehyde group of glutaraldehyde reacts with an amine function of the enzyme (figure 35).

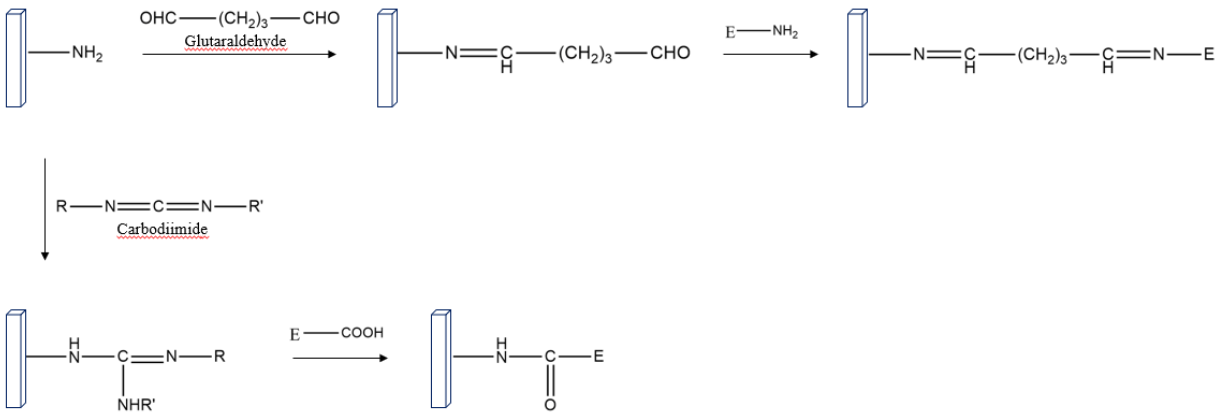

Figure 35: enzyme immobilization on an aminated surface by (down) carbodiimide or (right) glutaraldehyde coupling

Enzymes can also be immobilized on functionalized nanotubes present on an electrode surface[134].

1.5 Conducting Polymers and Metallopolymers

1.5.1 Conducting Polymers

Based on their electrical properties, materials can be divided into three main categories: insulators, semiconductors and conductors. Insulators have conductivity lower than 10^{-7} S m^{-1}, materials with conductivity in the range of 10^{-7}-10^{3} S m^{-1} (depending on the doping level) can be considered semiconductors, while conductivity values higher than 10^{3} S m^{-1} are typical of metals[144].

Conducting polymers (CPs), also known as "synthetic metals", are organic polymers that can conduct electricity. They can go up to conductivity values typical of metals (doped conjugated polymers) or behave like semiconductors (conjugated polymers) (figure 36).

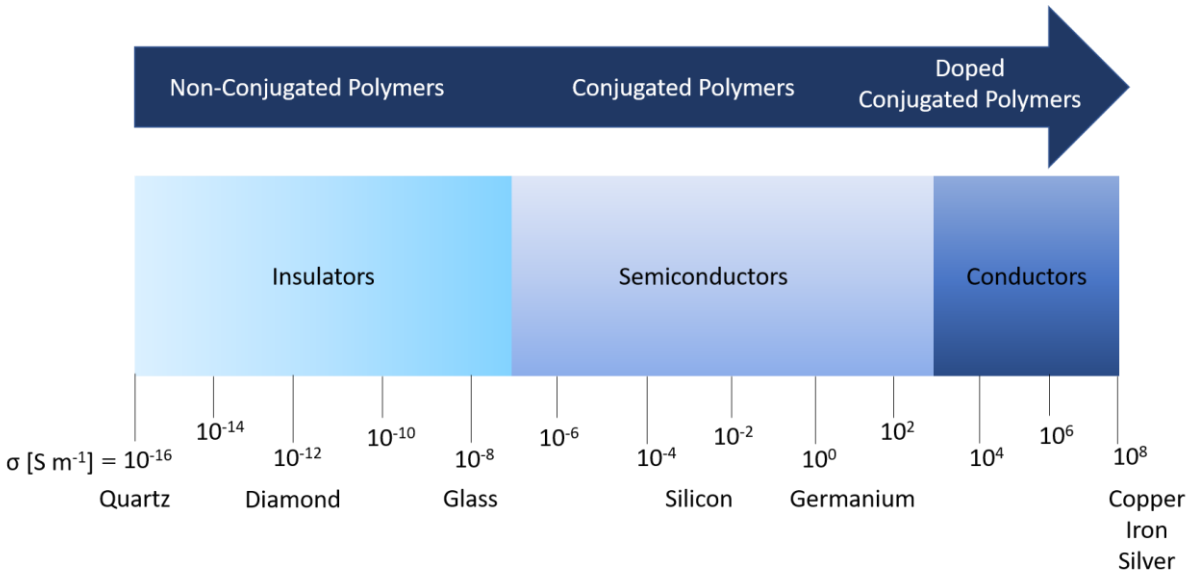

Figure 36: conductivity of conjugated and doped conjugated polymers compared with those of other materials

In addition to the conductivity properties, CPs exhibit electronic, magnetic, wetting, and optical properties (figure 37) which, combined with the mechanical properties and processability of conventional polymers, make these materials suitable for multiple applications.

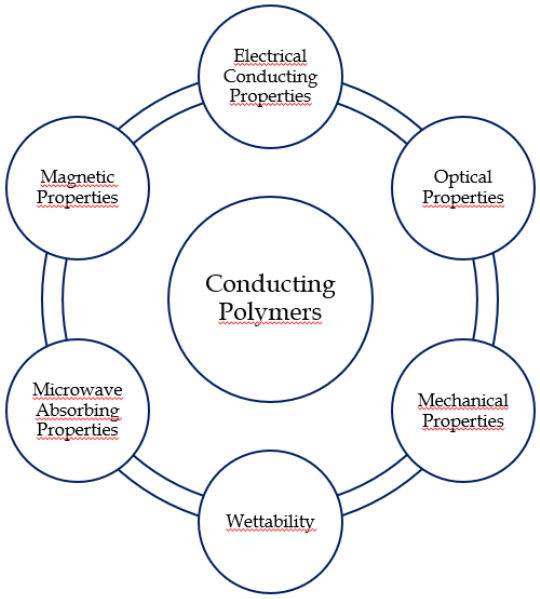

Figure 37: properties of conducting polymers

Among the various applications (figure 38), the use of CPs stands out in the realization of different devices such as sensors and biosensors, rechargeable batteries, organic light emitting diodes (OLEDs), smart windows, electrochromic devices[145-147].

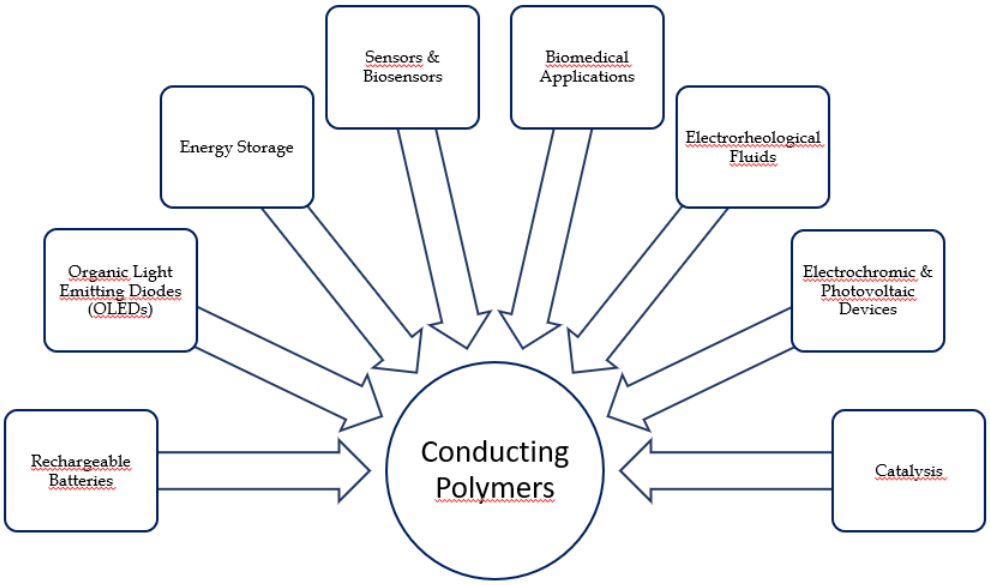

Figure 38: applications of conducting polymers

The term "polymer" is associated with a huge number of substances, both synthetic and natural. The synthetic development dates back to the beginning of 20th century. The idea of associating the electrical properties of metals with the mechanical properties of polymers was born approximately in 1950s through the incorporation into polymers of conductive charges (e.g., black smoke, metal fibres or carbon fibres) generating the so-called extrinsically conducting polymers (ECPs). At the end of the 70s, another class of conductive materials was discovered and studied: intrinsically conducting polymers (ICPs). In 1977, in fact, Alan J. Heeger of University of California, Alan G. McDiarmid of University of Pennsylvania and Hideki Shirakawa of University of Tsukuba (Nobel Prizes in Chemistry in 2000 for their work on CPs) accidentally discovered that silvery films of semiconductive polymer trans-polyacetilene (PA) could become conductive afterward doping with molecular chlorine, bromine or

iodine vapour, increasing their conductivity markedly (over seven orders of magnitude in the case of iodine doping, about 3000 S m^{-1})[148].

In the 1980s, Narmann and Theophilou of BASF AG, Ludwigshafen, Germany, further increased the conductivity of polyacetylene reaching, after doping, conductivity similar to that of metallic copper at room temperature[147].

So, starting from the 80s, various types of new conducting polymers have been synthesized. They are mainly unsaturated polymers with electrons that can easily be removed or added to the polymer chains[149]. Typical examples are: polypyrrole (PPy), polythiophene (Pth), poly(3,4-ethylenedioxythiophene) (PEDOT), polyfuran (PF), polyaniline (PANI) (figure 39).

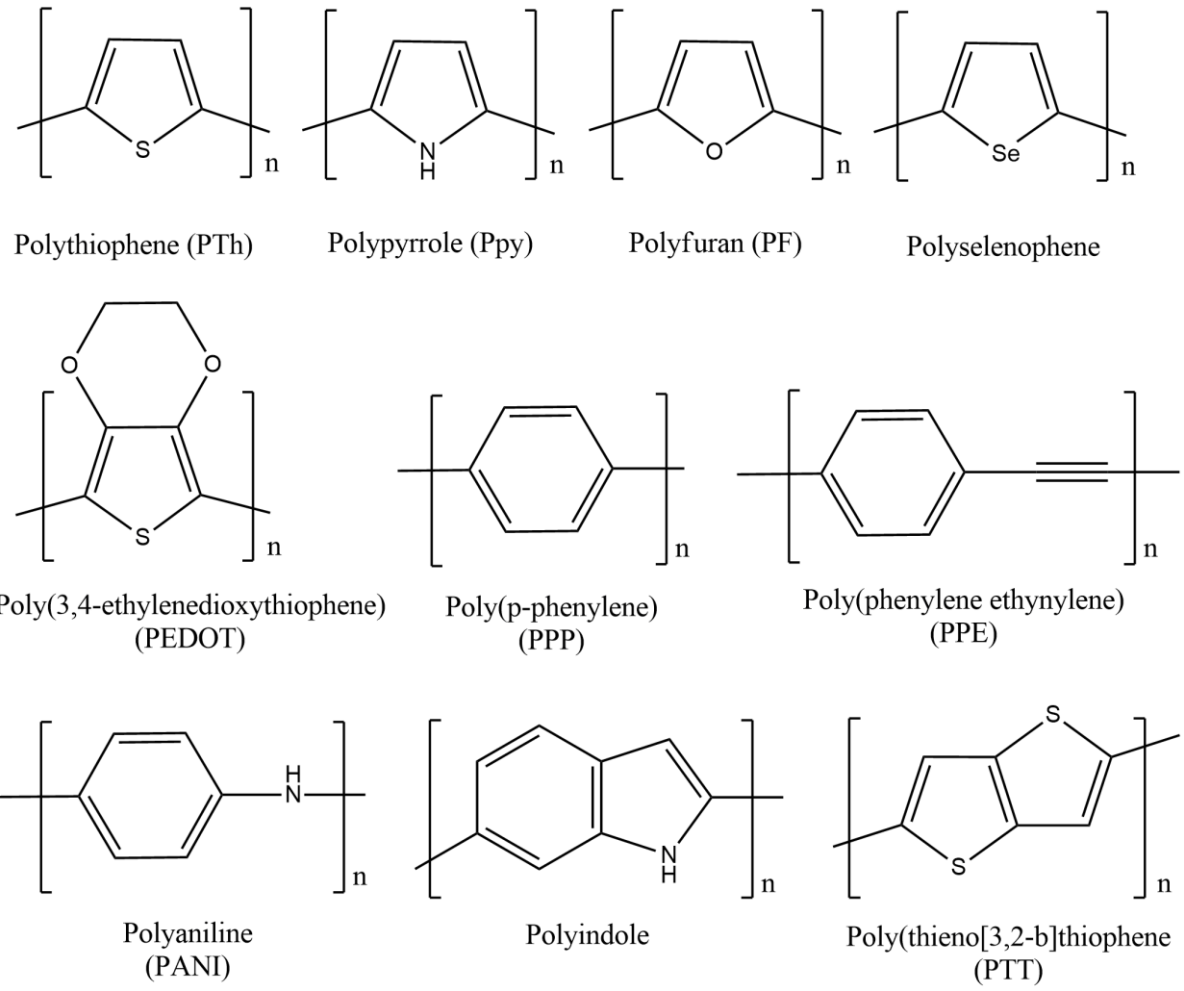

Figure 39: typical structures of conducting polymers

Although polyacetylene remains the most crystalline CP, it is not the first to be commercialised because of its sensitivity to humidity and its ease to be oxidized by the oxygen in air. Conversely, polypyrrole and polythiophene are stable in both doped and undoped states and can be synthesized directly in the doped form. However, their conductivity is not so high (about 10^4 S m^{-1}), but enough for many practical purposes[144].

1.5.2 Conductive Mechanism

The main characteristic of the CPs is the conjugation, they are in fact made up of a network of alternating double bonds along the polymer backbone (figure 40) which generates an electronic delocalization, fundamental for conductivity.

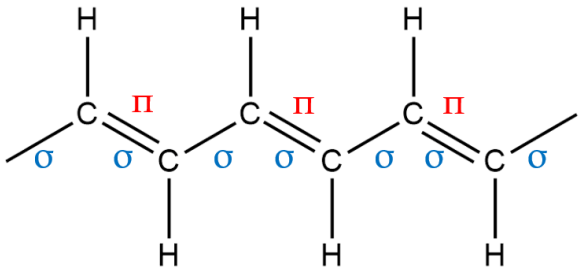

Figure 40: the structure of polyacetylene

The π-bond between the first and second carbon atoms is transferred to the position between the second and third. In turn, the π-bond between the third and fourth propagates to the next carbon, and so on. As a result, the electrons in the double bonds move along the carbon chain. In this way, double bonds allow electric flow. However, conjugated bonds do not make polymer materials highly conductive, but they only confer semiconductor features.

A useful and easy way to visualize the differences among conductors, semiconductors and insulators is to consider the energy band theory. The difference between the valence (VB) and conduction (CB) bands of a material is known as "band gap" or "energy gap" (E_g). In the case of insulators, the E_g is too large (8÷10 eV) to be crossed

by electrons and therefore they do not conduct electricity. Semiconductors have small band gap (1÷4 eV) and excited electrons can reach the conduction band, leaving a hole in the VB. Both electrons and holes are charge carriers thus contributing to the conduction. Finally, conductors have the VB overlapped on the CB, in this way electrons are free to move and propagate in the CB[150] (figure 41).

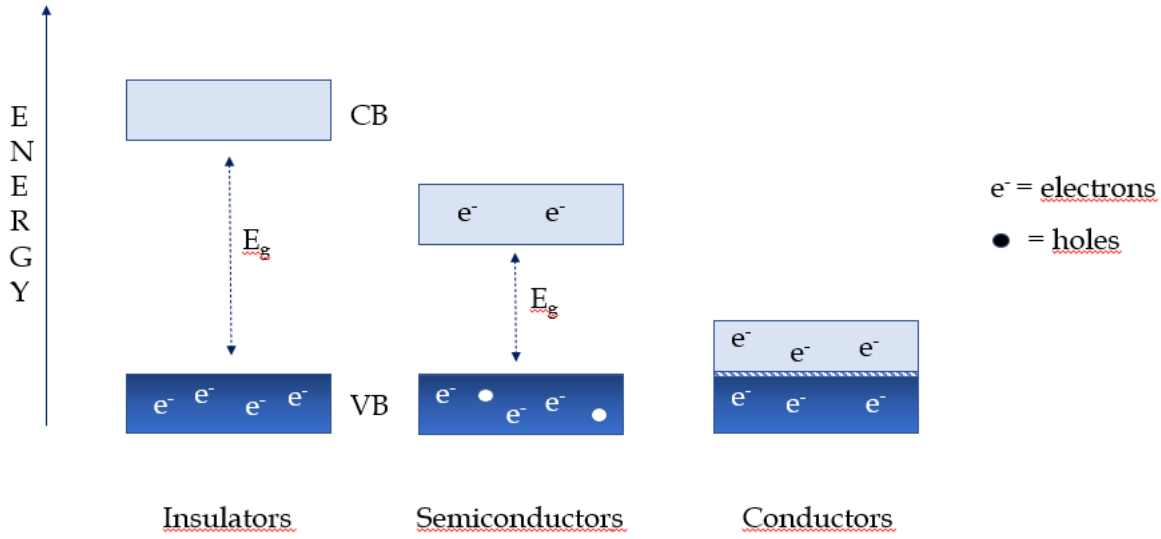

Figure 41: valence and conduction bands in insulators, semiconductors and conductors

At the beginning the electrical conductivity of polymers was explained on the basis of the "band model" similar to that of inorganic semiconductors. In a conducting polymer the increase of conjugation leads to the formation of electronic bands (figure 42), similarly to what happens in an inorganic conductor, in which the insertion of the unit cell with all its neighbours leads to the same result.

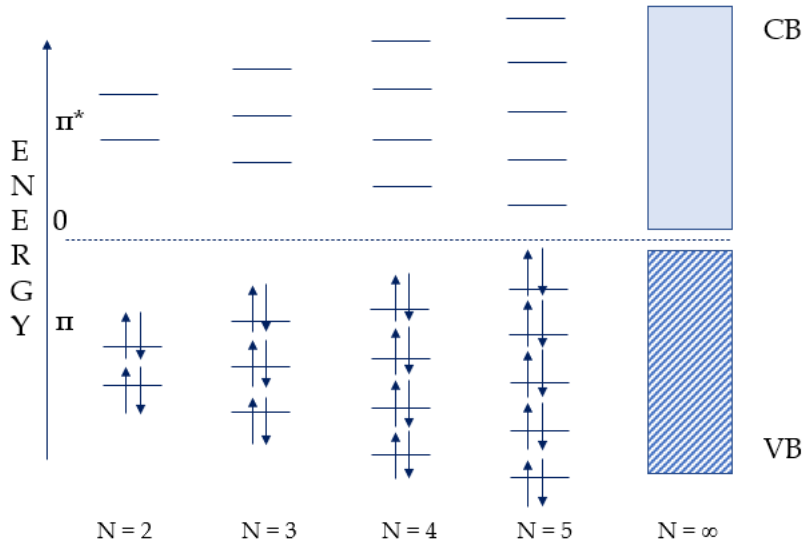

Figure 42: formation of bands: decrease of E_g as conjugation increases

The E_g value of about 1-4 eV is responsible for the semiconductor characteristics of conjugated polymers.

However, this model does not explain the fact that conductivity is associated with zero spin charge carriers and not with delocalized electrons. As a matter of fact, while in an inorganic semiconductor the charge carriers are holes and electrons, in CPs they are quasiparticles called solitons, polarons (radical ions) and bipolarons (dications or dianions) shown in figure 43, whose characteristics are summarized in table 10.

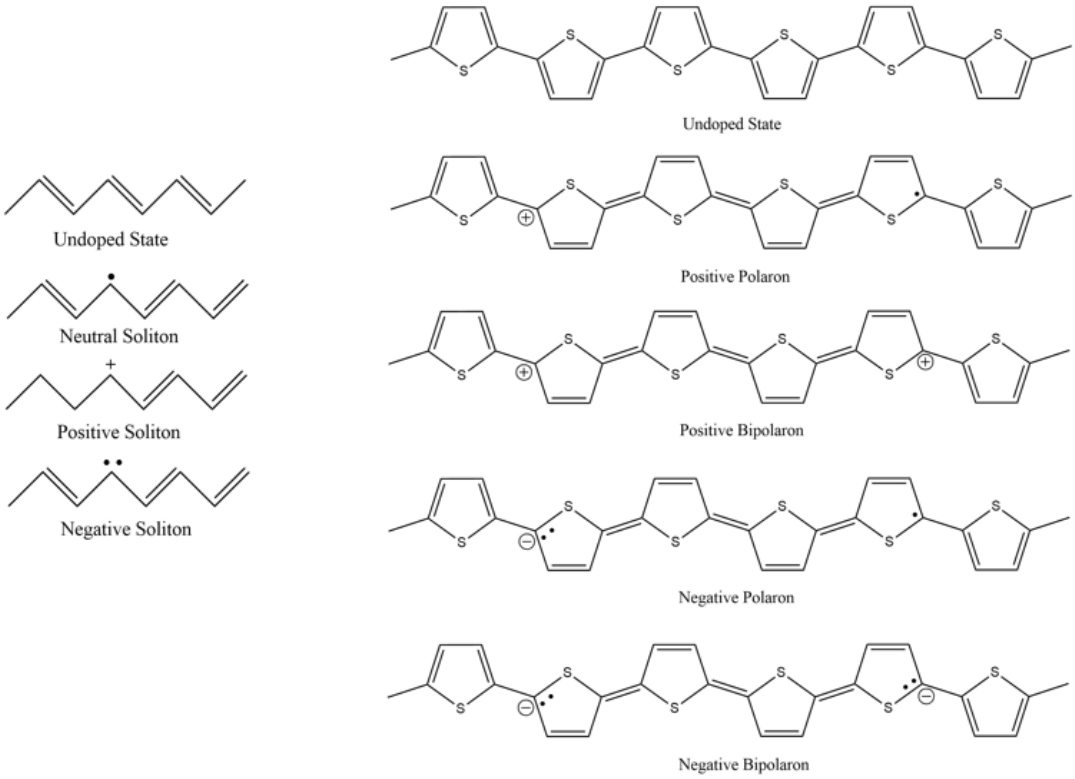

Figure 43: solitons in trans-polyacetylene (left) and polarons and bipolarons and in polythiophenes (right)

Table 10: charge carriers in conducting polymers

Charge Carriers	Type	Charge	Spin
Positive soliton	Cation	$+e^-$	0
Negative soliton	Anion	$-e^-$	0
Neutral soliton	Neutral radical	0	½
Positive polaron	Radical cation	$+e^-$	½
Negative polaron	Radical anion	$-e^-$	½
Positive bipolaron	Dication	$+2e^-$	0
Negative bipolaron	Dianion	$-2e^-$	0

1.5.3 Doping Processes

To obtain polymers with conductive behaviour, the conjugated polymer chains have to be oxidized or reduced by charge transfer with doping molecules (oxidizing or reducing agents) or by electrochemical way through polarization in suitable cells. These oxidation/reduction processes are called p-doping and n-doping, respectively. With regard to electrochemical doping processes:

- an anodic polarization will induce p-doping processes accompanied by the insertion of anions from the electrolytic solution, according to the following scheme:

$$P + yX^- \leftrightharpoons P(X)_y + ye^-$$

- a cathodic polarization will induce n-doping processes accompanied by the insertion of cations from the electrolytic solution, according to the following scheme:

$$P + yM^+ + ye^- \leftrightharpoons P(M)_y$$

In a nutshell, dopants (chemical or electrochemical) in the polymer undergo redox processes in which charges are transferred with subsequent formation of the already mentioned charge carriers. A simple explanation of the effect of doping is that electrons are extracted from the valence band (in the case of oxidation) or transferred to the conduction band (in the case of reduction). These processes create the quasiparticles, whose motion along the polymer chains generates conductivity. Generally, the negatively charged carriers in n-doping are not as stable as positively charged forms, so p-doping is more common. In particular, solitons are known to be charge carriers in degenerate systems (systems that possess two identical geometric structures in the ground state) whereas polarons and bipolarons serve as the charge

carriers in both degenerate and non-degenerate systems (systems that exhibit two different structures with different energies in the ground state)[149,150].

1.5.3.1 Formation of Solitons, Polarons and Bipolarons

As already said, solitons are charge carriers in degenerate systems. Trans-polyacetylene is a typical CP with degenerate ground state.
When the chain is composed of an odd number of carbon atoms, the single and double bonds can exchange electrons, leading to two geometric structures (phase A and phase B) with the same energy (figure 44).

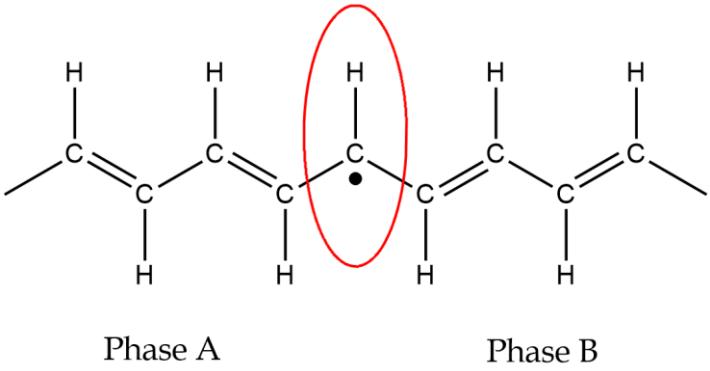

Figure 44: geometric structure of a neutral soliton on a trans-polyacetylene chain

The radical form between the two phases contains an unpaired π electron which is called a neutral soliton. The soliton has a certain mobility that allows its delocalization along the polymer backbone. When the neutral soliton meets one another, they can be destroyed by generating a double bond. Moreover, solitons with charge become more stable as they can be delocalized over the polymer chain; a positive or negative soliton (figure 45) can be obtained oxidizing or reducing a neutral soliton using a dopant.

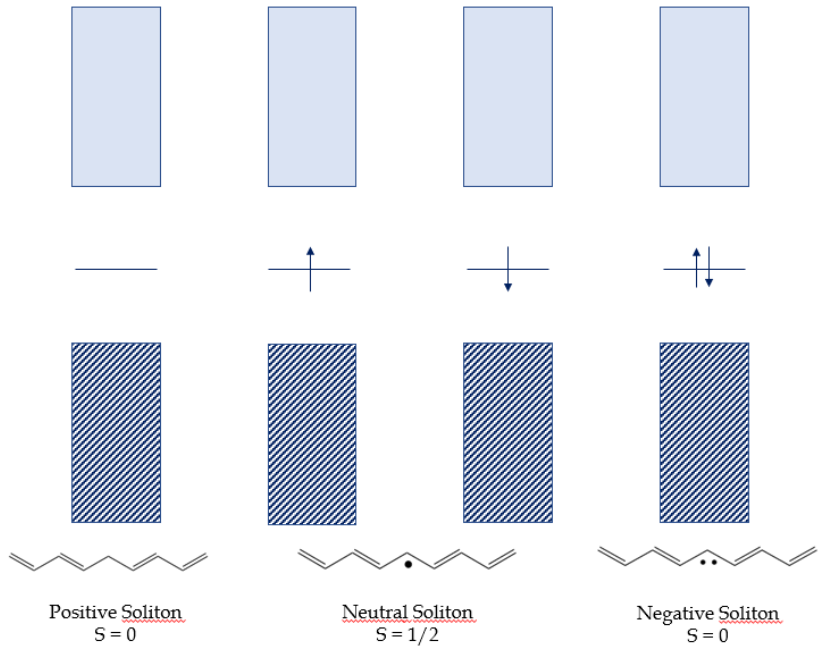

Figure 45: the band structures of trans-polyacetylene containing a positively charged soliton, a neutral soliton and a negatively charged soliton

In the backbone, the π electrons propagate over a long distance and the regions of individual charged solitons can overlap. This generates the so-called soliton band that is located in the middle of HOMO and LUMO and become larger with an increase in doping level.

Regarding polarons and bipolarons, they are the charge carriers in both degenerate and non-degenerate systems (figure 46), such as PPy and PTh.

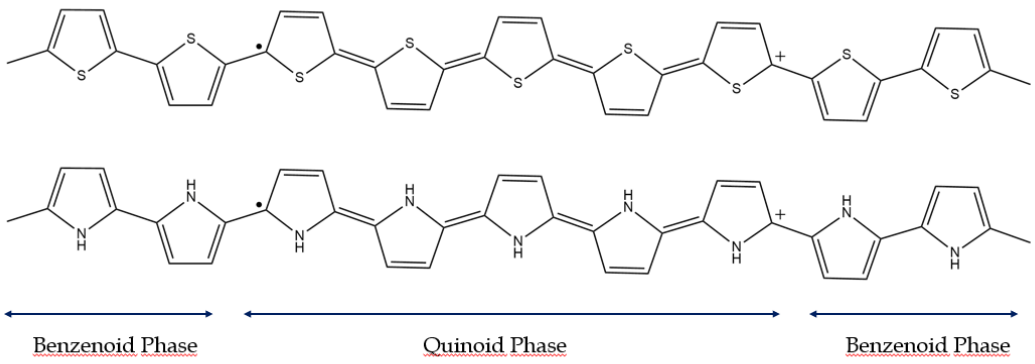

Figure 46: benzenoid and quinoid phases in PTh and PPy

If we consider p-doping of PPy, it has four distinct electronic band structures with different doping levels. In the undoped state Le et al.[150] calculated for PPy an E_g of 3.16 eV. Upon oxidation a π electron is removed and a local deformation from the benzenoid structure to a quinoid one occurs, generating a polaron. With the formation of polaron, two new energy levels are produced within the band-gap: the one with the lowest energy is occupied and is called singly occupied molecular orbital (SOMO)[151]. A further oxidation can remove a second electron and either a second independent polaron may be created or, if it is the unpaired electron of the first polaron that is removed, a bipolaron is formed (figure 47).

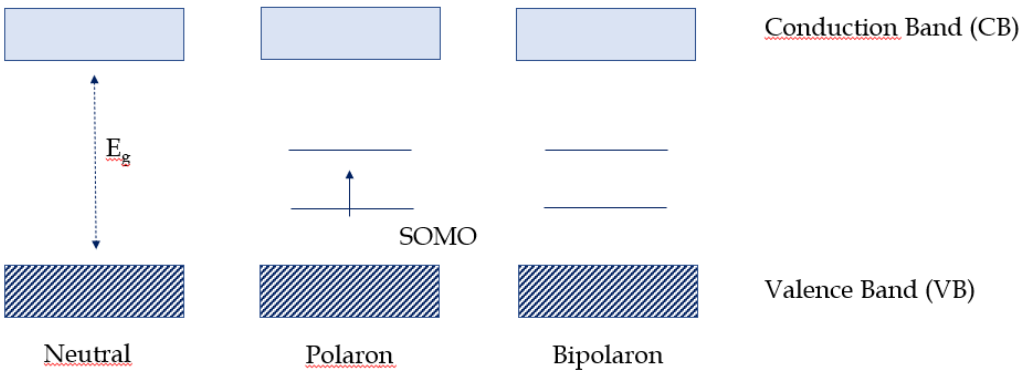

Figure 47: electronic structure of a conducting polymer based on its doping level

The two positive charges of the bipolaron are not independent but move as a pair[144]. As the polymer is further oxidized, an overlap between bipolarons occurs, leading to the formation of two narrow bipolaronic bands and a decrease in E_g to 1.4 eV (figure 48).

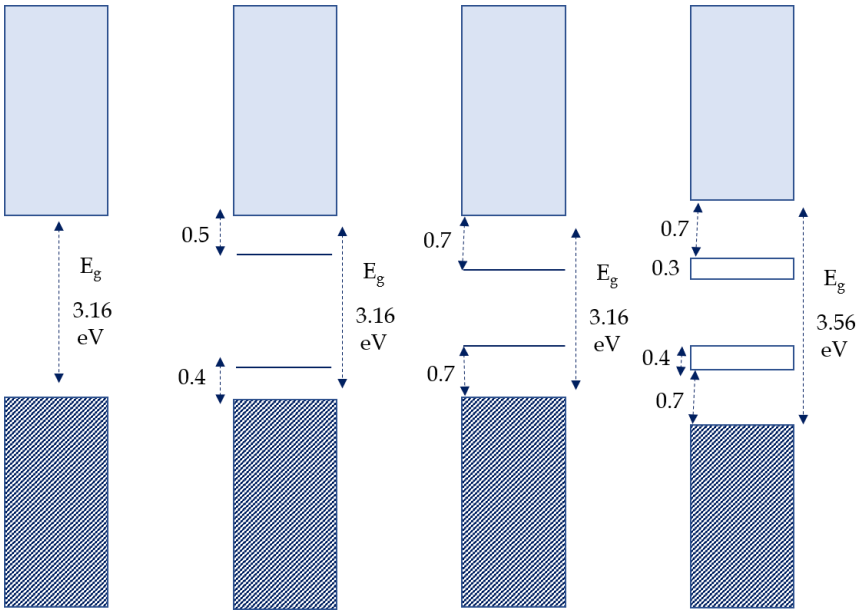

Figure 48: electronic bands of (a) undoped, (b) polaron, (c) bipolaron and (d) fully doped states of PPy

CPs conductivity is, however, also influenced by environmental factors such as temperature[150].

1.5.4 Polythiophenes (PThs)

Among the numerous CPs, PThs have become object of considerable interest thanks to their high environmental stability of both its doped and undoped states, in combination with its structural versatility that have led to develop multiple applications. These applications concern: antistatics and electromagnetic interference (EMI) shielding, gas sensors, photoelectrodes for photoelectrochemical solar cells, photovoltaic cells, photochargeable devices, Schottky diodes. Moreover, recently, several substituted PThs have been investigated as possible electrode materials. Selective modified electrodes and electrochemical devices appear as one of the most promising fields of application of PThs[152].

1.5.4.1 Structure and Properties

Thiophene behaves as an aromatic compound with respect to its structure, physical properties and reactivity. The sulphur atom in this five-membered ring acts as an electron-donating centre, by contributing with two electrons to the aromatic sextet and so, thiophene is considered to be an electron-rich heterocycle[153]. *Ab initio* calculations indicate accumulation of negative charge on the carbon atoms and positive charge on sulphur. Protonation and other electrophilic reactions occur preferentially at the 2- and 5- carbon positions[154] (figure 49).

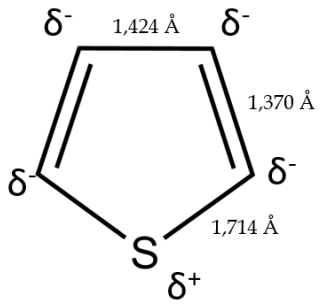

Figure 49: structure of thiophene

Prior to 1960, bithiophenes, polythiophenes and their derivatives were not easily prepared, and were often obtained as by-products in standard reactions. Since 1960, thanks to the work of S. Gronowitz and S. O. Lawesson, synthesis of bithiophenes (figure 50) became easily available. In particular, 3,3' bithiophene was prepared through the coupling of 3-thienyllithium with (i) cupric chloride or (ii) with 3-ketotetrahydrothiophene followed by dehydration and aromatization of the intermediate tertiary alcohol[155].

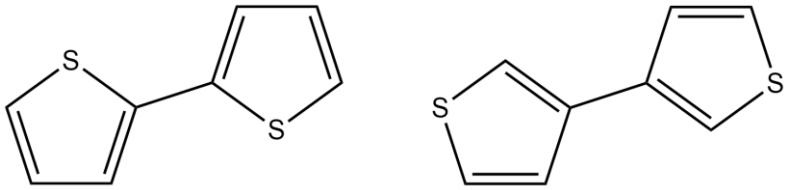

2,2'-bithiophene 3,3'-bithiophene

Figure 50: structures of 2,2'-bithiophene and 3,3'-bithiophene

However, despite the fact that the development of polymer materials from thiophene and its derivatives has been known since 1960s, it was only in 1980s that research, aimed at optimizing the preparation of PThs, was started. PThs are essentially prepared by two main methods: (i) chemical and (ii) electrochemical synthesis[152-154,156].

1.5.4.2 Chemical Synthesis

Regarding chemical synthesis, it is possible to consider two different approaches[152]:

1. metal-catalysed coupling reactions:
2. chemical oxidative polymerization.

Thiophene oligomers have been prepared by several methods and some of them have been proposed as a general procedure for the preparation of polymers. Thus, mixtures of several thiophene oligomers have been obtained by reaction of 2-iodothiophene with copper-bronze. Terthiophene has been prepared by cyclization of 1,4-diketones containing one or more thiophene rings. Quater- and sexithiophene have been synthesized by coupling of a-lithiated thiophenes in presence of cupric chloride or organoboranes[152]. However, one of the best-known chemical synthesis is that which involves the use of transition metal complexes as catalysts. Transition metal complexes catalyse reactions that involve thiophene-based monomers with halogens in 2- and 5-positions. One of the first synthesis of the unsubstituted PTh dates back to 1980 and was carried out, independently, by two different research groups[157,158]. In both cases,

the PTh synthesis provides a polycondensation of 2,5-dibromo thiophene catalysed by a metal complex. The synthesis of Yamamoto et al.[157] was carried out using Mg in tetrahydrofuran (THF) as solvent in presence of $Ni(bipy)Cl_2$ (bipy = 2,2'-bipyiridine), whereas in the synthesis of Lin and Dudek[158] the catalyst is $M(AcAc)_2$ (AcAc = acetylacetonate) with M = Ni, Co or Fe (figure 51).

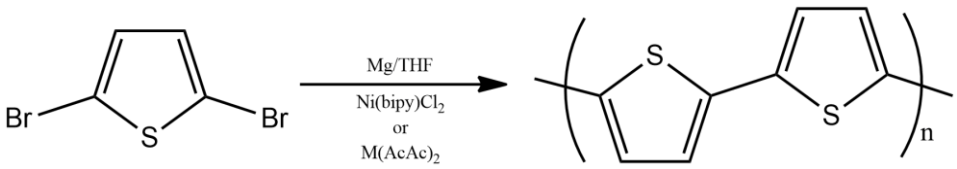

Figure 51: polycondensation of 2,5-dibromo thiophene catalysed by a metal complex

Mg reacts with one of the two bromine atoms leading to the formation of Grignard reagent in 2- or 5- position which, by coupling reaction catalysed by the metal complex, leads to the formation of a thiophene dimer with a -MgBr group and a bromine atom. The reaction continues by forming polymer films of low molecular weight (figure 52).

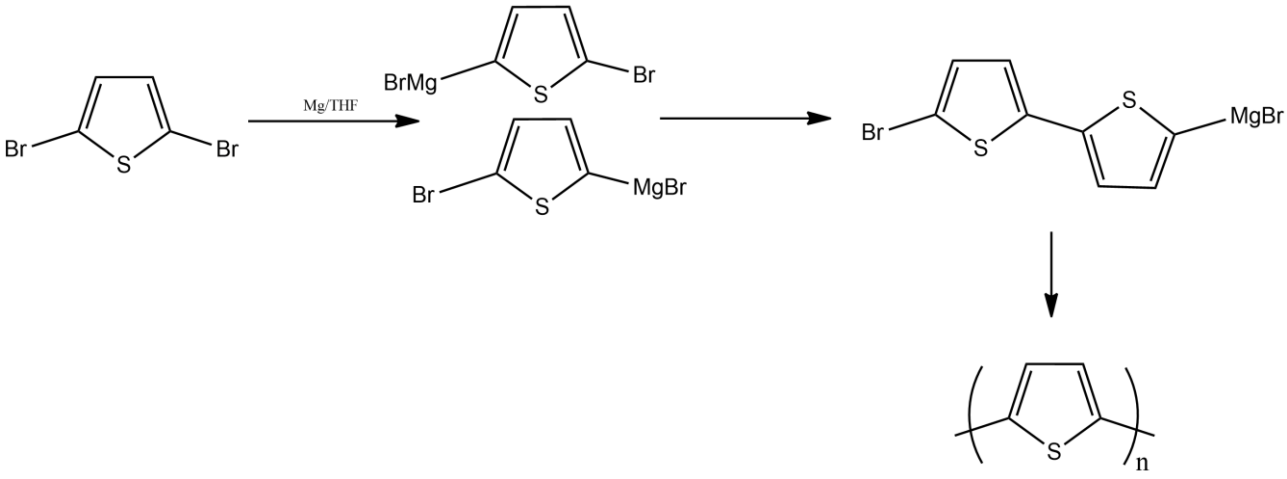

Figure 52: schematic mechanism of polycondensation of 2,5-dibromo thiophene

The polymerization process is an extension of Kumada coupling reaction between aryl halides and Grignard reagents[159].

Thiophene and 3-alkylthiophene oligomers have been also synthesized by $NiCl_2$(dppp) (dppp = diphenilphosphino propane) coupling of Grignard compounds with the appropriate halothiophenes[9,152] (figure 53).

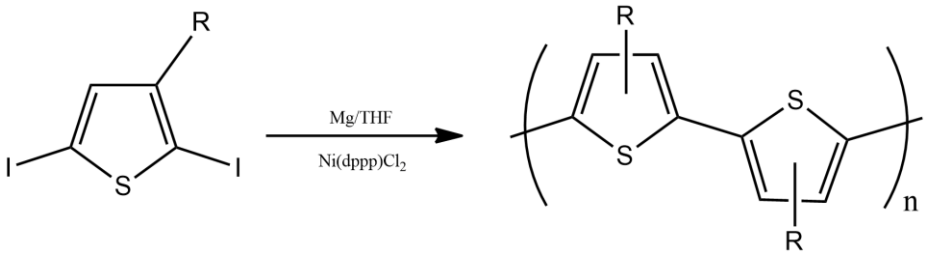

Figure 53: synthesis of thiophenes and 3-alkylthiophene oligomers with $NiCl_2$(dppp) catalyst

Regarding the chemical oxidative polymerization, the most popular technique uses $FeCl_3$ as oxidizing agent. The first synthesis of this type was carried out by Sugimoto and Yoshino[9,151] (figure 54).

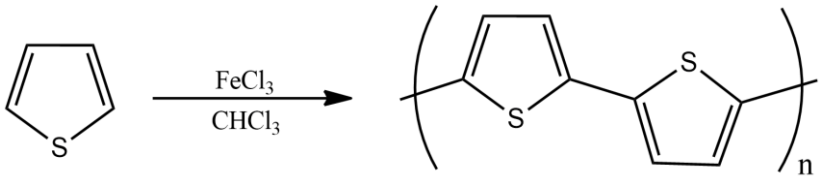

Figure 54: chemical oxidative polymerization of thiophene with $FeCl_3$

Based on this, oxidative synthesis of substituted PThs was also developed. This also provides the use of $FeCl_3$ or alternatively $MoCl_5$ or $RuCl_3$. The reaction occurs by 2-5 thiophen units coupling which consists in the oxidation of 3-alkylthiophenes to radical cations followed by chain propagation[9] (figure 55).

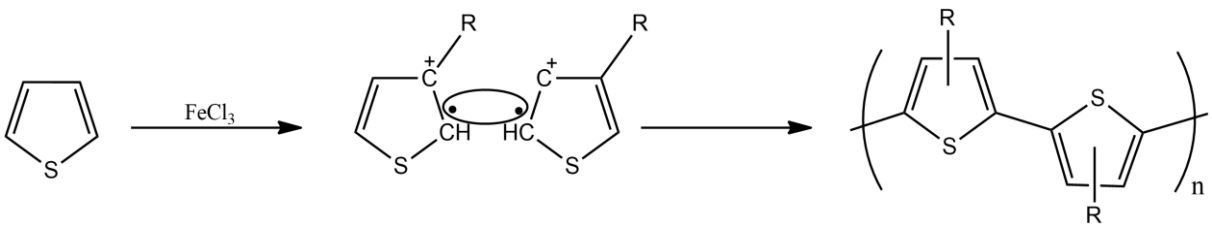

Figure 55: schematic mechanism of chemical oxidative polymerization of thiophene

1.5.4.3 Electrochemical Synthesis

Although chemical syntheses seem to be the most suitable methods for the preparation of oligomers with well-defined structures, it is thanks to the electrochemical syntheses that it has been possible to obtain the most conjugated and most conductive PThs.
PThs can be electrochemically prepared by two main routes: by cathodic reduction or, more conveniently and more often, by anodic oxidation.

Cathodic Reduction

One of the best known cathodic route involves the electroreduction of the complex (2-bromo-5-thienyl)triphenylnickelbromide in acetonitrile. It is a similar method to one already used for the synthesis of poly(*p*-phenylene). The main drawback of this method is that the polymer is mainly generated in its neutral insulating form which leads, rapidly, to a passivation of the electrode limiting the film thickness to ca. 100 nm. Conversely, this technique is useful when working with electrodes subject to anodic corrosion such as semiconductors with small band gap[152].

Anodic Oxidation

The anodic route possesses several advantages: absence of catalyst, direct grafting of the doped conducting polymer onto the electrode surface, easy control of the thickness by the deposition charge, and possibility to perform a first *in situ* characterization of the growing process or of the polymer by electrochemical and/or spectroscopic techniques.
The first report of the anodic electropolymerization of thiophene appeared in the 1980s[160]. Despite the large amount of work devoted to electrogenerated PThs, the mechanism of the electropolymerization of thiophene was poorly considered. A fundamental aspect is that the anodic electropolymerization involves a reaction

sequence in which each coupling step has to be activated by two species. It proceeds with electrochemical stoichiometry with n values in the range 2.07-2.6 F mol^{-1}. The oxidation of monomer requires $2e^-$/molecule whereas the excess of charge is normally used for the reversible partial oxidation of the conjugated polymer. As the potential needed for the oxidation of the monomer is always higher than the charging of oligomeric intermediates or the resulting polymer, the two processes, polymer formation and its doping, occur at the same time.

Figure 56 shows the proposed mechanism for the electropolymerization of heterocycles, based on the already known coupling reactions of aromatic compounds.

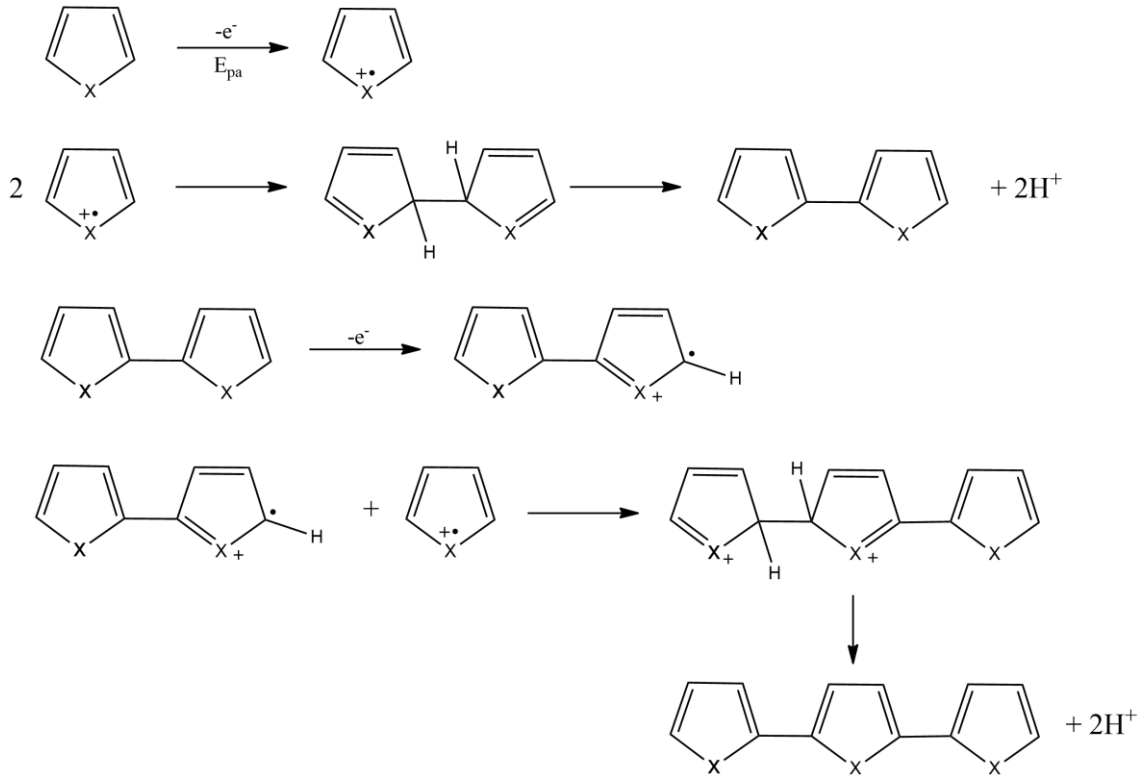

Figure 56: hypothetical mechanism of electropolymerization of 5-membered heterocycles

The first step is an electrochemical step (EC) and consists in the oxidation of the monomer to its radical cation. Since the electron transfer reaction is faster than the diffusion of the monomer from the bulk solution, a high concentration of radicals is continuously maintained near the electrode surface. The second step, that is a chemical

step (C), consists in the coupling of two radicals to produce a dihydro dimer dication which, losing two protons, rearomatizes leading to the formation of a dimer. The rearomatization is the driving force of this chemical step. Due to the applied potential, the dimer, which is oxidized more easily than the monomer occurs in its radical form and undergoes a further coupling with a monomer radical. Electropolymerization proceeds through the succession of chemical and electrochemical steps, according to a general $E(CE)_n$ scheme, until the oligomers become insoluble in the electrolytic medium and precipitate onto the electrode surface[152,161]. However, this mechanism is still uncertain but what is firmly established is the oxidation of the monomer to its radical cation and the fact that the electropolymerization process is not diffusion limited[152].

The electropolymerization is a complex process that depends on multiple variables, which are interdependent, such as: solvent, temperature, concentration of monomers, supporting electrolyte, cell geometry, nature and shape of the electrodes and applied electrical conditions. These parameters can influence the structure and the properties of the resulting polymer.

The solvent has to satisfy some requirements: high dielectric constant, to ensure the ionic conductivity of the electrolytic medium, and good electrochemical resistance against decomposition at the high potentials required to oxidize the thiophene ring (≈ 1.4-2.3 V *vs*. SCE depending on substituents on the ring). The most conductive PThs have been obtained in rigorously anhydrous aprotic solvents with high dielectric constant and low nucleophilicity such as acetonitrile (powdery deposits or brittle films with conductivities of about 0.02-10 S cm^{-1} for PTh and 0.1-50 S cm^{-1} for PMeTh), benzonitrile, nitrobenzene (compact free-standing films with conductivities of about 100 S cm^{-1}). However, electropolymerization of 3-methylthiophene has been reported in aqueous medium[162] despite several works report that the presence of traces of water in the synthesis medium can have deleterious consequences for what concerns conjugation length and conductivity of the polymer.

Regarding supporting electrolytes, PThs are generally electrogenerated in the presence of small anions, derived from strong acids, such as ClO_4^-, PF_6^-, BF_4^- and AsF_6^- associated with lithium or tetraalkylammonium cations. It is very important to note that the nature of anion strongly affects the morphology and the electrochemical properties of PThs prepared in acetonitrile, and that electrolytes containing aromatic anions such as halo- or alkylbenzene sulfonates or naphthalene sulfonates yield no or little polymer with low doping level and conductivity.

The temperature of electropolymerization affects the extent of the conjugated system and consequently the optical and electrical properties of the polymer. In particular, it has been reported[163] that films obtained at 40 °C had a shorter mean conjugation length than those obtained at 5 °C.

As regards the anode materials, PThs generally grow on noble metals such as platinum and gold but also on optically transparent electrodes such as tin oxide and indium-tin oxide (ITO) coated glass. However, PThs have been also deposited on titanium and iron. Until now, the most conductive polymers have been generated on bulk platinum, probably because thiophene adsorbs more efficiently on platinum. Moreover, platinum possesses a larger number of potentially active sites leading to a high density of initial nucleation sites and to more compact materials.

The applied electrical conditions represent the most important parameter and that with the most considerable effects on the structure and properties of electrodeposited PThs. Electrical conditions affect not only the electrochemical and optical properties of the films but also the mechanical ones and the orientation of the polymer chains. PThs can be deposited in potentiostatic, potentiodynamic or galvanostatic conditions. Although, from a thermodynamical point of view, the applied potential is the most relevant electrical parameter, the most homogeneous and conducting films are generally obtained in galvanostatic conditions at potential of ca. 0.5 V more positive than the oxidation potential of the monomer. Although the role of this overpotential is not fully explained, it has been observed that highly conducting films can be obtained

at the potential corresponding to the onset of electropolymerization but it should be initiated by a short pulse at high potential.

Another critical parameter is the monomer concentration. Keeping constant the electrical conditions (2 mA cm^{-2}), it has been reported[152,164] that high monomer concentrations (0.5-1 M) produce poorly conducting films containing a big amount of soluble oligomers. The decrease of monomer concentration improves both the cohesion of the films and their conductivity (500 S cm^{-1} for 0.1 M). On the other hand, it is possible to define the best electrical conditions for a fixed monomer concentration. It is important to note that, beyond the optimal current density, it has been observed a decrease in conductivity, probably related to the fact that PThs are unstable at the potentials required for their formation. This fact is called "polythiophene paradox" and the consequence is that the degradation of the polymer may compete with its electrodeposition, in particular at highly anodic potentials or when the monomer concentration is too low to sustain the rate of polymer deposition[152,156].

1.5.5 Conducting Metallopolymers

Conducting metal-containing polymers or metallopolymers represent an important class of conjugated polymers in which metal centres are incorporated. They can contain several metal centres belonging to the main group metals (e.g., Sn, Pb), transition metals (e.g., Ru, Fe, Pt, Os) and also lanthanides (e.g., Eu)[165].

Examples can be metal complexes of poly(2,2′-bipyridine)[166] or poly(4′-(2,2′:5′,2′′-terthien-3′-ethynyl)-2,2′:6′,2′′-terpyridine[101,146] (figure 57).

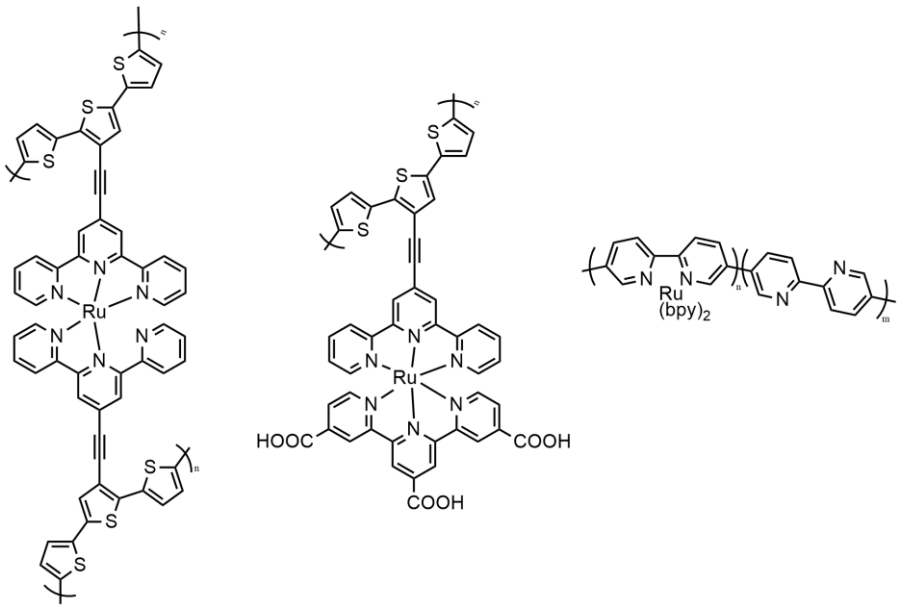

Figure 57: examples of structures of metal complexes of poly(4′-(2,2′:5′,2′′-terthien-3′-ethynyl)-2,2′:6′,2′′-terpyridine and poly(2,2′-bipyridine)

The key feature of this class of materials is that the metal is directly coordinated to the conjugated backbone of the polymer or forms a link in a backbone and, in this way, there are synergistic electronic interactions between the electroactive metal centres and the electroactive polymer backbone. This can improve electron transport in the polymer, its electrocatalytic activity and leads to new electronic, optic and electrochemical properties.

Regarding the improvement of electron transport, it depends on the electronic interactions between the polymer's π-system and the metal's d-orbitals. The source of extra electrons can be the polymer backbone itself or the metal centres (or their ligands). d-π interactions would be expected to enhance the rate of electrons transfer in both cases[166]. Electron transfer between the metal centres and the polymer backbone in a metallopolymer can be described with different models. P. G. Pickup[166] outlines three different mechanisms (figure 58): (i) electron transfer between metal sites, (ii) electron transfer through the polymer backbone *via* a metal-metal electronic interaction (superexchange pathway), (iii) electron transfer *via* polymer-based charge carriers (polymer mediated pathway).

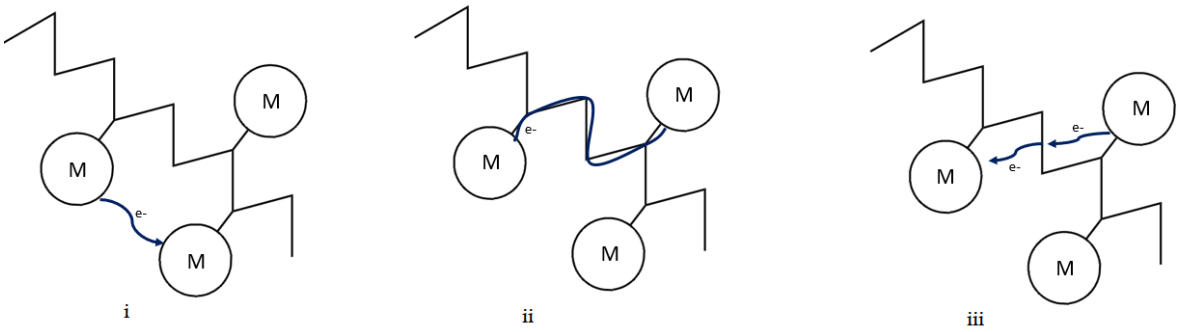

Figure 58: schematic diagram of the three electron transfer pathways between metal centres in redox polymers: (i) outer sphere electron transfer, (ii) superexchange pathway and (iii) mediated polymer pathway

In the first mechanism redox-active metal centres or complexes that decorate the outer edge of the conducting polymer chain have no direct interaction with the delocalized orbitals of the conducting organic polymer backbone.

The superexchange pathway can occur *via* two mechanisms: electron-type superexchange and hole-type superexchange (figure 59).

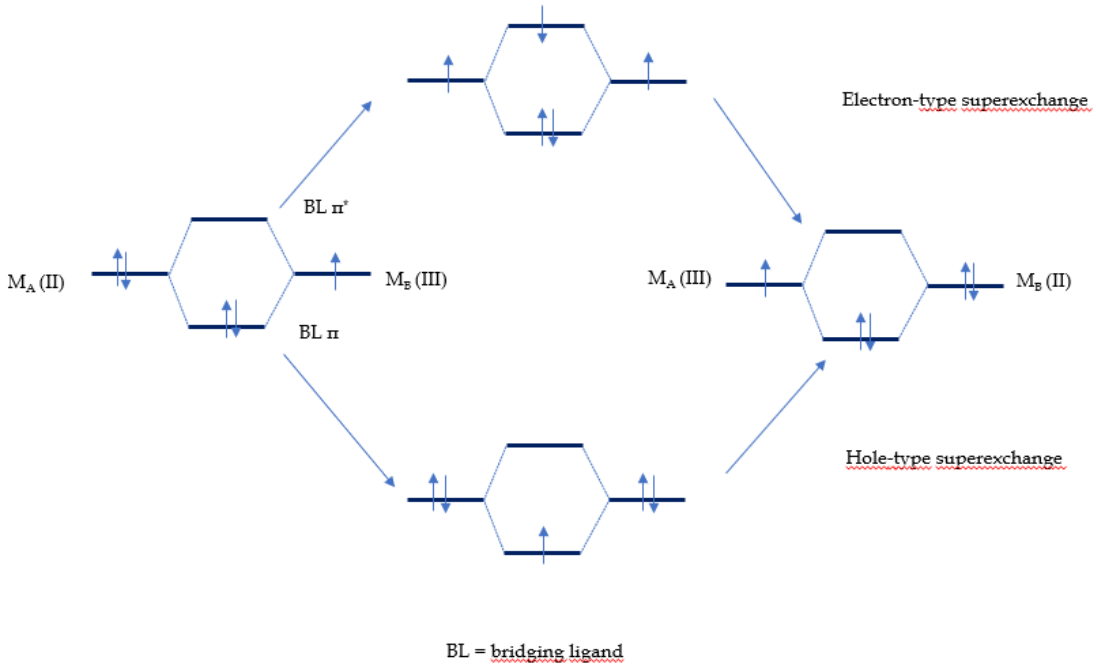

Figure 59: superexchange mechanisms

In the former, the greatest contribution to the metal-metal interaction is the mixing of π^* LUMO of the polymer with the metal d-orbitals, while in the latter is the mixing of π HOMO of the polymer and the metal d-orbitals. The redox potential for p-doping and n-doping of the polymer indicates the energies of its π and π^* orbitals, respectively; the redox potential of the complex provides a relative measure of the energy of its d-orbitals. The third pathway requires that the polymer backbone is electronically conductive (p-doped or n-doped at potentials close to the formal potential of the metal).

In a similar way, B. J. Holliday and T. M. Swager[167] distinguish between two mechanisms called *outer sphere* and *inner sphere*. In the first one, analogous to the first mechanism described by Pickup[166], redox active metal centres or complexes are linked to the polymer chain but have no direct interaction with it. This mechanism is similar to the hopping mechanism of the conventional redox polymer (polymers containing groups that can be reversibly reduced or oxidized). Inner sphere mechanism involves the incorporation of the metal centres into the conducting polymer chain with strong coupling between the orbitals of the conducting polymer backbone and the metal orbitals[161,167]. Superexchange and mediated electron pathways can be incorporated into the inner sphere mechanism.

CHAPTER 2

EXPERIMENTAL

2.1 Electrochemical Techniques

All the experiments were performed using cyclic voltammetry (CV), differential pulse voltammetry (DPV) and chronoamperometry (CA).

In particular, both cyclic voltammetry and chronoamperometry have been used for the electrochemical polymerization of the monomers on the electrode surfaces. Cyclic voltammetry has been then used for the characterization of the obtained polymer films, and chronoamperometry and differential pulse voltammetry for quantitative analysis of histamine and epinephrine.

2.1.1 Cyclic Voltammetry

Voltammetric techniques (linear sweep voltammetry (LSV), square wave voltammetry (SWV), cyclic voltammetry (CV), anodic and cathodic stripping voltammetry (ASV and CSV)) are a series of controlled potential electroanalytical techniques developed following the discovery of polarography by the Czechoslovakian chemist Jaroslav Heyrovskỳ. By these techniques, a large number of information can be obtained: reversibility of redox processes, stability of the electrogenerated species, presence of chemical reactions subsequent to the electron transfer, quantitative information.

CV is the most suitable technique for the electrochemical characterization of a compound, a biological material or a modified electrode surface. CV can be considered an evolution of LSV (figure 60a). It consists in applying, to the working electrode dipped in a quiescent solution, a ramp (usually linear) of potentials that varies over time according to a triangular trend (figure 60b).

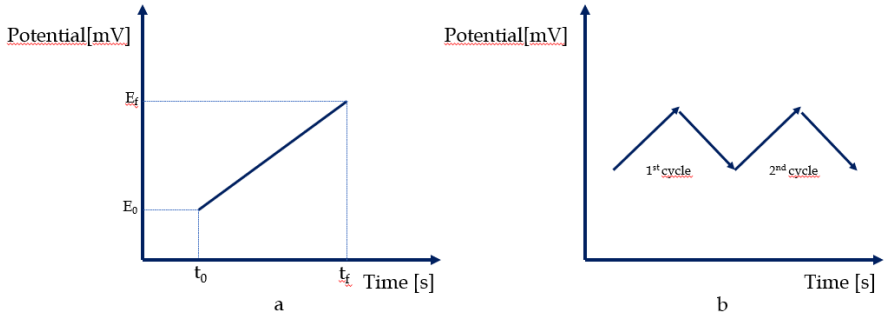

Figure 60: (a) application of potential in LSV and (b) application of potential in CV

The used device is a potentiostat with a three-electrode configuration:

- a working electrode (WE), usually of platinum, gold, graphite
- a counter electrode (CE), usually a platinum wire or mesh or a graphite rod
- a reference electrode (RE), saturated calomel electrode (SCE), silver chloride electrode (Ag/AgCl), standard hydrogen electrode (SHE), that have to be unpolarizable and with constant potential over time and in the most varied operating conditions.

In this configuration, a voltage generator imposes a difference of potential (ddp) between WE and CE and a galvanometer, placed between these two electrodes, measures the current. The variation of potential is recorded by a voltmeter placed between WE and RE in a circuit in which an appreciable amount of current does not pass.

Usually, the potential ramp is applied starting from the open circuit potential (OCP), and then proceeds towards the catho-anodic window of interest. Once the electrogenerated species have been obtained, if these are stable enough and if the redox process is reversible or quasi-reversible, by inverting the potential, it is possible to oxidize or reduce the species again, with the appearance of an associated peak. The result is a current-voltage diagram called cyclic voltammogram (figure 61).

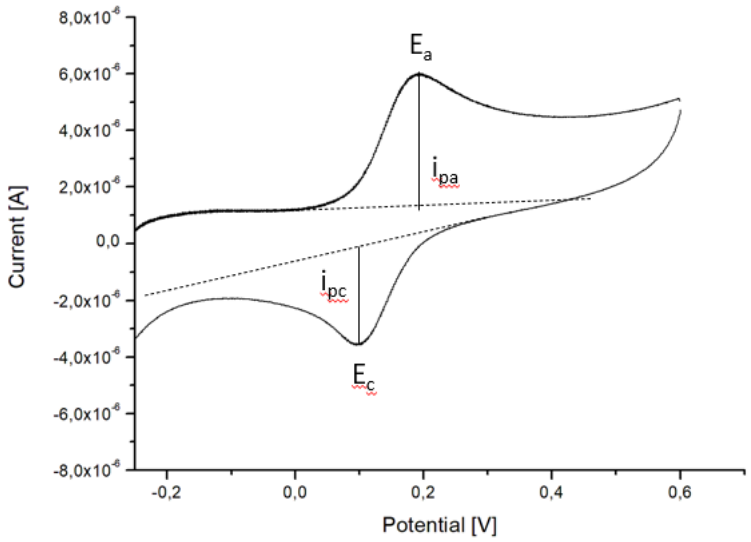

Figure 61: example of a cyclic voltammogram

The absence of an associated peak denotes an irreversibility condition, which can be of a chemical or electrochemical type (this can be identified by increasing the scanning rate of the potential). Some specific parameters can be considered in the analysis of the voltammetric response. In particular, the reversibility of the redox process can be investigated by the potential difference (ΔE) between the cathodic (E_c) and the anodic peak potential (E_a):

$$\Delta E = |Ec - Ea|$$

For completely reversible systems $\Delta E\,[mV] \approx \frac{59,1}{n}$ with n = number of exchanged electrons.

The peak current, for a reversible system, is described by the Randles-Sevcik equation:

$$i_p = (2,69 \cdot 10^5) n^{3/2} A D^{1/2} C v^{1/2}$$

where i_p = peak current [A], n = number of electrons, A = electrode area (cm^2), D = diffusion coefficient ($cm^2\ s^{-1}$), C = concentration of the species ($mol\ cm^{-3}$) and v = scan rate ($V\ s^{-1}$).

In quasi-reversible responses, a slow exchange of electrons is observed between the redox species and the working electrode, and the Randles-Sevcik equation is not applicable.

The faradic current that flows at any time within a cell is a direct measure of the electrochemical reaction that occurs at the electrode. Furthermore, the same current depends on two factors: the rate of the mass transport from the solution to the electrode, governed by the laws of mass transport, and the rate of the electron transfer between the solution and the electrode surface. These two processes affect the current flow. The transport of the mass towards the electrode surface can take place through three mechanisms: diffusion, migration and convection, but only diffusion can be related to the concentration of the electroactive species as it depends on the gradient of concentration, which in turn depends on the initial concentration of the species. Diffusion is governed by Fick's laws:

$$1^{st}\text{ Fick's Law: } \frac{dN}{dt} = DA\frac{\delta C(x;t)}{\delta x}$$

$$2^{nd}\text{ Fick's Law: } \frac{\delta C(x;t)}{\delta t} = D\ \frac{\delta^2 C(x;t)}{\delta x^2}$$

Fick's first law describes a flow of matter towards the surface A due to a concentration gradient; the second law expresses the dependence of the concentration on time and distance from the electrode.

The electrochemical experiments must, therefore, be designed and conducted in such a way as to eliminate the contributions to the current related to migration and convection. To do this, it is necessary to work in the presence of an inert supporting electrolyte in a concentration 10-100 times greater than the concentration of the analyte to limit migration phenomena, and in a quiescent and thermostated solution to limit convection.

Usually, solvents such as methylene chloride, acetonitrile and N,N dimethylformamide are used, as these possess a catho-anodic window suitable for most electroanalytical needs. Concerning supporting electrolytes, they must be chemically inert towards the partners of the electrode processes, soluble in the selected solvent and must have a high degree of purity and anhydricity (when operating in a non-aqueous solvent), as well as a high catho-anodic window of potential. In the case of polar solvents, inorganic salts such as $NaClO_4$ or $NaBF_4$are preferred, whereas tetraalkylammonium salts (perchlorate, hexafluorophosphate, tetrafluoborate) are mainly used with low polar solvents.

However, CV is not only used for analytical purposes, thermodynamic or kinetic studies but also to carry out processes such as electrochemical polymerizations. In this case, from the point of view of the voltammogram it is observed that the current peaks increase in intensity with each subsequent scan[9,39,168].

2.1.2 Differential Pulse Voltammetry

In DPV, to a linear scan of potentials, a periodic series (every 0.5-5 s) of pulses of duration between 40-60 ms and amplitude between 5-250 mV is applied to the working electrode (figure 62a). The duration and amplitude of pulses are keeping constant during the analysis. More recently a staircase ramp is preferred instead of a linear scan as it is simpler to implement in digital instruments (figure 62b).

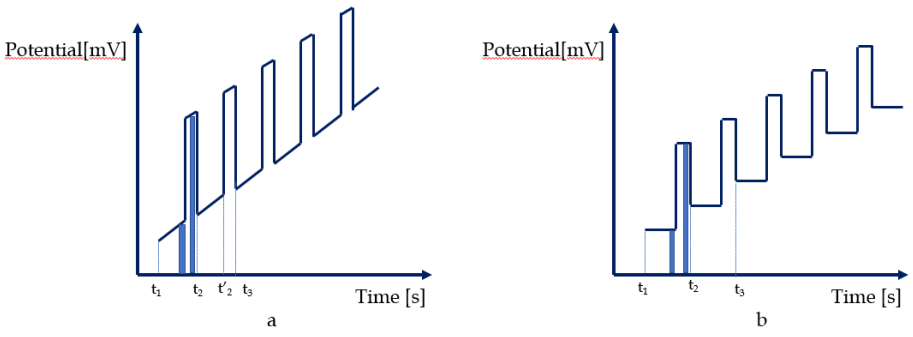

Figure 62: application of potentianl in DPV (a) linear scan and (b) staircase scan

DPV measures the difference between two currents, just before the end of the pulse and just before pulse application (as evidenced in figure 62). In this way the contribution of the capacitive current is minimized and this makes the technique very sensitive. LoDs can reach values up to 10 μg/L.

The resulting voltammogram is a differential voltammogram with very well defined and symmetrical peaks (it depends on the reversibility of the system)[39,168].

2.1.3 Chronoamperometry

Chronoamperometry is a simple controlled-potential electroanalytical technique, where the current flowing through the electrode is measured as a function of time, when the potential is sharply brought from a value E_0, where no faradic process occurs, to a value E_1, where the electronic transfer begins (figure 63).

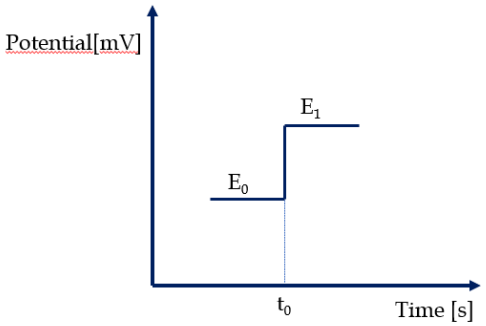

Figure 63: application of potential in chronoamperometry

It is a particularly proper technique for mechanistic investigations such as the study of the reversibility of a process. At value E_1, for any reversibility level of the analysed system, C_0^0 (concentration of the analyte on the electrode) tends to 0 and the process will be under diffusion control: the current will vary as a function of time according to the Cottrell equation:

$$i(t) = \frac{nFAD_0C_0^b}{(\pi D_0 t)^{1/2}}$$

where n = number of electrons, F = Faraday's constant [C mol^{-1}], A = electrode area [cm^2], D_0 = diffusion coefficient [cm^2 s^{-1}], C_0^b = concentration of the analyte in the bulk of the solution [mol cm^{-3}], t = time [s].

The current decays exponentially over time as at t = 0 (as soon as the potential E_1 is applied) the whole electroactive species around the electrode is reduced and at subsequent times the concentration gradient become gradually larger, the species near the electrode is gradually less concentrated due to the fact that the flow of matter arrives from further away, thus taking longer time (hence, $i = \frac{dq}{dt}$ decreases).

The theoretical trend described by Cottrell is not respected in an excessively short time or in a rather long time. The period of time available for observations, in the best experimental conditions (optimal cell geometry and electrode), is always within the range between 20 μs and 200 s, but it is often two or three orders of magnitude smaller.

If the potential applied to the electrode is such that $C_0^0(t) \neq 0$, two cases are distinguished, according to the reversibility of the process. If the process is reversible the current trend is given by:

$$i(t) = \frac{nFD_o^{1/2}\pi^{1/2}t^{-1/2}}{1 + (\frac{D_O}{D_R})^{\frac{1}{2}}e^{\frac{nF}{RT}(E - E^0)}}$$

where D_o and D_R are the diffusion coefficients of oxidized and reduced species, respectively.

Moreover, if the process is completely reversible, the product $it^{1/2}$ is constant for any potential value applied to the electrode and proportional to the number of exchanged electrons in the process. If, on the other hand, the process is irreversible and the potential not sufficient to reach the limiting current region, the trend of the current will

not simply depend on the kinetic parameters of charge transfer (β and $K_{s,h}$) and on the electrode potential. The product $it^{1/2}$ will not be constant over time[9,168].

2.2 Instruments and Reagents

2.2.1 Instruments

All electrochemical tests were carried out using a CHI-650 potentiostat interfaced with a PC using the specific software CHI-650 in a conventional three-electrodes voltammetric cell.

NMR spectra were acquired using Bruker Avance III 400 MHz spectrometer.

UV–Vis spectra were acquired using Hitachi U-2010 spectrophotometer.

Scanning electron microscopy (SEM) analyses were performed on a SEM Fei Quanta 200 instrument.

2.2.2 Reagents

Methylene chloride (CH_2Cl_2), diethyl ether (Et_2O), ethyl acetate, hexane, methanol (MeOH), petroleum ether, diisopropylamine, triethylamine (NEt_3), acetonitrile (CH_3CN), 1,2-dimethoxyethane (DME), N,N-dimethylformamide (DMF), trifluoroacetic acid (≥ 99%, TFA), diamine oxidase from *porcine kidney* (≥ 0.05 unit/mg solid protein, stored at -20 °C, DAO), tyrosinase from *mushroom* (lyophilized powder ≥ 1000 U/mg solid protein, stored at -20 °C, Tyr), glutaraldehyde (technical 50% in H_2O, 5,6 M), histamine (analytical standard), (-)–epinephrine, 3,4-ethylenedioxythiophene (EDOT), 4-iodobenzoic acid, N-boc-4-iodoaniline, 2,3,5-tribromothiophene, bis(triphenylphosphine)palladium(II)dichloride ($Pd(PP_3)_2Cl_2$), 2-methyl-3-butin-2-ol, copper iodide (CuI), magnesium sulphate ($MgSO_4$) from Sigma-Aldrich. Methyl-4-iodobenzoate, 4'-chloro-2,2':6',2''-terpyridine, 4-iodoaniline, 4,4'-dibromo-2,2'-

bithiophene, 1,8-diazabicyclo[5,4,0]-7-undecene (DBU, 2,thiopheneboronic acid, tetrakis(triphenylphosphine)palladium(0) ($Pd(PPh_3)_4$), trimethylsilylacetylene, [1,1'-bis(diphenylphosphino)-ferrocene]palladium(II) dichloride dichloromethane adduct ($Pd(dppf)Cl_2 \cdot CH_2Cl_2$), dopamine hydrochloride from TCI. Triphenylphosphine (PPh_3), ammonium chloride (NH_4Cl), potassium fluoride dihydrate ($KF \cdot 2H_2O$), potassium carbonate (K_2CO_3) from Carlo Erba. Sodium dodecyl sulphate (SDS) from BDH. Sodium chloride (NaCl) and sodium bicarbonate ($NaHCO_3$) from Fluka. Sodium hydroxide from Merck. 1,4-dioxan from Riedel-de Haën.

2.3 Synthesis of Monomers

The plethora of transition-metal catalysed cross-coupling reaction, in particular those palladium-catalysed, can be considered, nowadays, a milestone in the field of organic synthesis. As a matter of fact, several palladium-catalysed cross-coupling reactions such as Heck[169], Suzuki-Miyaura[170,171], Sonogashira-Hagihara[172-178], Stille[179], Hiyama, Negishi, Kumada, Murahashi and Buchwald-Hartwig have been developed over the years[180]. This type of reactions is used to obtain complex and functionalized organic molecules[180,181].

In particular, the molecules synthesized in this thesis work exploit Sonogashira-Hagihara and Suzuki-Miyaura cross-coupling reactions. In addition, two molecules synthesized by Dr. Dorota Zając of Wrocław University of Science and Technology, obtained *via* Stille reaction, were also used.

2.3.1 Sonogashira-Hagihara Cross-Coupling Reactions

Sonogashira-Hagihara cross-coupling (or simply Sonogashira coupling) is the most popular procedure for the alkynylation of aryl or alkenyl halides or triflates with terminal alkynes. The first reaction of this type dates back to 1975 by the Japanese

scientist Kenkichi Sonogashira[175]. The general reactivity order on sp^2 species is: vinyl iodide ≥ vinyl triflate > vinyl bromide > vinyl chloride > aryl iodide > aryl triflate ≥ aryl bromide >> aryl chloride.

It is important to note that even primary alkyl bromides and iodides and a secondary alkyl bromide have been alkynylated using Sonogashira protocol, but this type of sp^3-sp coupling is very recent and still unexplored.

The reaction is normally carried out with a palladium catalyst ($Pd(PPh_3)_4$, $Pd(PPh_3)_2Cl_2$, $Pd(dppf)Cl_2$, $Pd(dppe)Cl_2$, $Pd(dppp)Cl_2$) and an amine base (diisopropylamine and triethylamine are the most commonly used), with or without the presence of a copper(I) as a co-catalyst, according to the figure 64:

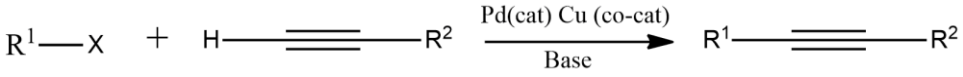

Figure 64: generic scheme of Sonogashira-Hagihara reaction

The exact mechanism of the homogeneous copper-co-catalysed Sonogashira reaction is still unknown, but some techniques[181,182] (e.g., solid state NMR and high-resolution magic angle spinning NMR (HRMAS-NMR)) developed to study this coupling process using heterogeneous catalysts in order to isolate reaction intermediates, the mechanism is thought to occur through two independent catalytic cycles: Pd-cycle and Cu-cycle (figure 65).

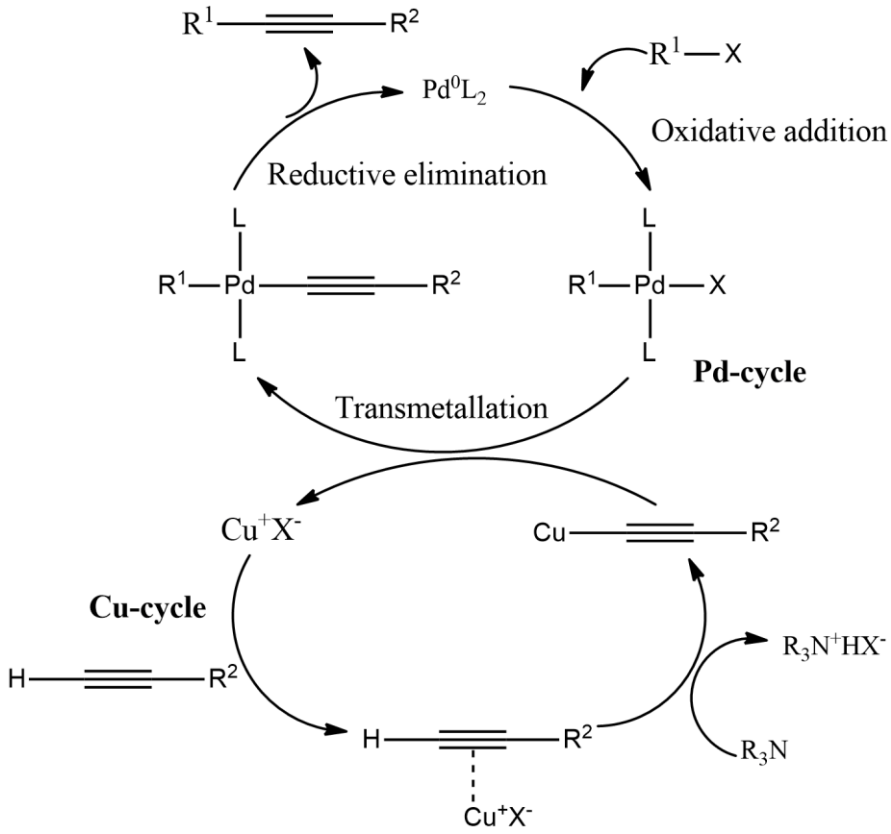

Figure 65: possible catalytic mechanism of the homogeneous copper co-catalysed Sonogashira reaction

The first reaction is the fast oxidative addition of R^1-X (R^1 = aryl, vinyl or heteroaryl; X = I, Br, Cl or OTf) to the actual catalyst generated from the initial palladium complex. In this step, the features of R^1-X substrate are crucial, and the reaction is facilitated when X = I or OTf and the electronic density on the C-X bond is reduced by the presence of electron-withdrawing groups. The second step should be connected with the copper-cycle. Thus, a usually rate-determining trans-metallation from the copper acetylide formed in the Cu-cycle should generate a species that, after *trans*/*cis* isomerization and reductive elimination yields the final coupled product with regeneration of the catalyst. The Cu-cycle is still poorly understood: it is supposed that the base (the amine) abstracts the acetylenic proton of the terminal alkyne thus forming a copper acetylide. It should point out that the generally employed amines are usually not basic enough to deprotonate the alkyne but, probably, the formation of π-alkyne-Cu complex makes the alkyne proton more acidic, allowing an easier abstraction.

These copper acetylides could also be the responsible of the formation of the initial Pd^0L_2. However, although π-alkyne-Cu complex has never been proved, NMR studies have shown the existence of π-alkyne-Ag complexes in Sonogashira silver-co-catalysed.

The use of copper salts as co-catalysts in the classical Sonogashira protocol increases the efficacy of the reaction, but also exhibits some drawbacks as it is an environmentally unfriendly and difficult to recover reagent. Furthermore, one of the major drawbacks is that *in situ* generation of copper acetylides under the reaction conditions often generates homocoupling products of the terminal alkynes, the well-known Glaser coupling[181] (figure 66).

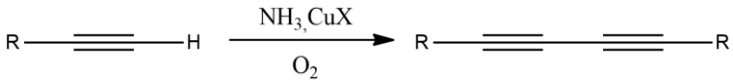

Figure 66: generic scheme of Glaser reaction

However, Glaser coupling can be widely reduced by working in an inert atmosphere, preferably in Schlenk tubes[177], and slowly adding the alkyne[176]. Moreover, significant efforts have being dedicated to developing coupling procedures working in the absence of copper salts. These methodologies are usually called copper-free Sonogashira couplings. However, the copper-free processes require the use of excess of amine, so diminishing the environmental and economic advantages of the methodology. Thus, the development of methods which allow the elimination of both copper and amine is desirable.

2.3.2 Suzuki-Miyaura Cross-Coupling Reactions

Suzuki-Miyaura cross-coupling reaction, more commonly known as "Suzuki coupling reaction", is one of the most useful reaction between aryl or vinyl boronic acid or boronic ester with aryl or vinyl halides and also with different reagents such as

alkenes, alkynes, amines. The first reaction of this type dates back to 1979 by the Japanese scientists Akira Suzuki and Norio Miyaura[183,184]. The reaction is usually carried out with a palladium(0) catalysts ($Pd(PPh_3)_4$ is the most common, but $Pd_2(dba)_3$ and $Pd(OAc)_2$ are also used) in the presence of a base (preferably aqueous solution of $NaHCO_3$, Na_2CO_3, NaOH, KOH, K_3PO_4) at temperature range of 60-80°C with usually excellent yields[171].

The general accepted Suzuki-Miyaura catalytic mechanism for the homogeneous-phase reaction is shown in figure 67:

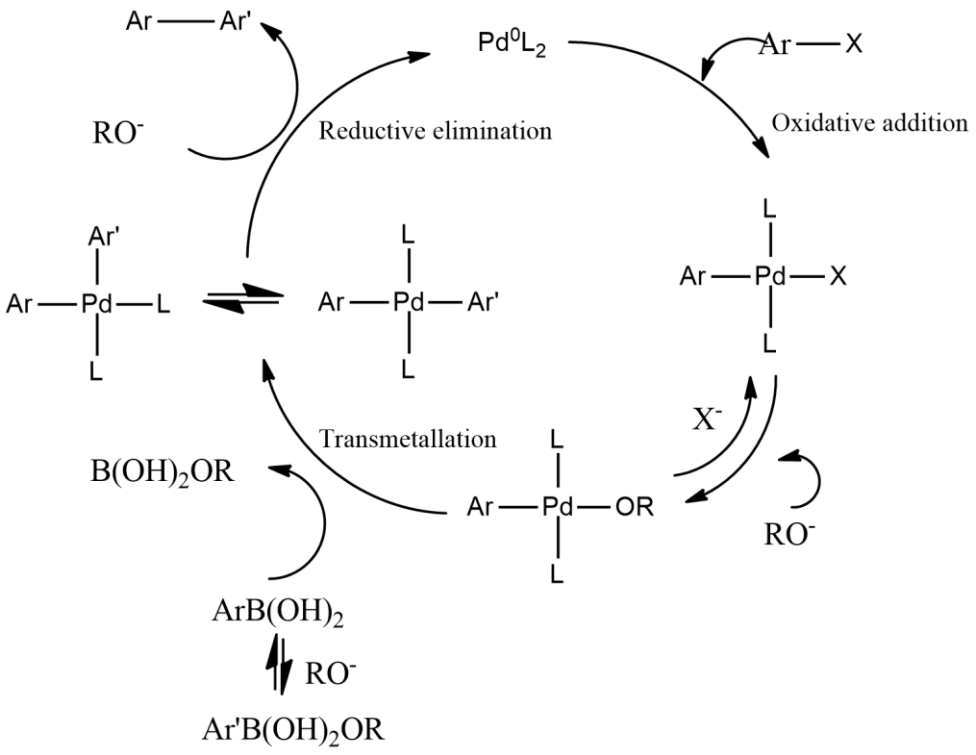

Figure 67: catalytic mechanism of the homogeneous phase Suzuki reaction

The catalytic cycle occurs through oxidative addition, transmetallation and reductive elimination. After formation of the catalytic species Pd(0), generated *in situ* starting from Pd(II) or Pd(0) derivatives, oxidative addition of the aryl halide R-X yields the Pd-complex $ArPdXL_n$. The transmetallation step occurs by conversion of the Pd-halide in the presence of the base RO^- to a nucleophilic Pd-alkoxy complex. This complex subsequently reacts with a neutral organoboron compound to give the biaryl complex

in a *cis-trans* equilibrium. Then, reductive elimination of the *cis* form gives the biaryl derivative Ar-Ar' and regenerates the Pd(0) catalyst[180].

Like in Sonogashira coupling, side reactions are possible, mainly protodeboration (figure 68), oxidation and palladium catalysed homocoupling.

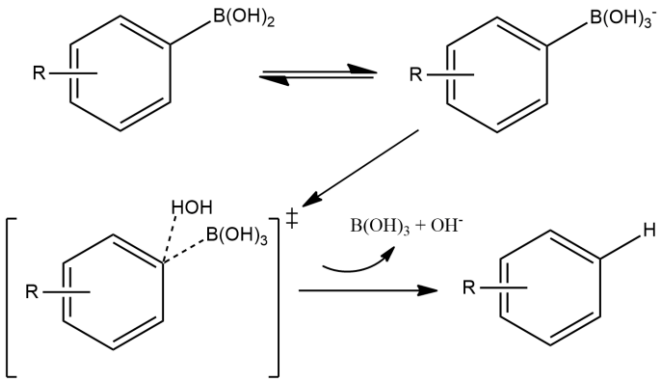

Figure 68: base-catalysed protodeboration of arylboronic acids

Concerning the oxidation, aerobically-generated peroxide-type oxidants can readily form in many ethereal solvents, and boronic acids are highly susceptible towards oxidation by these species under Suzuki coupling conditions. Arylboronic acids form phenols following a 1,2-migration of the aryl moiety to an electrophilic oxygen atom (figure 69).

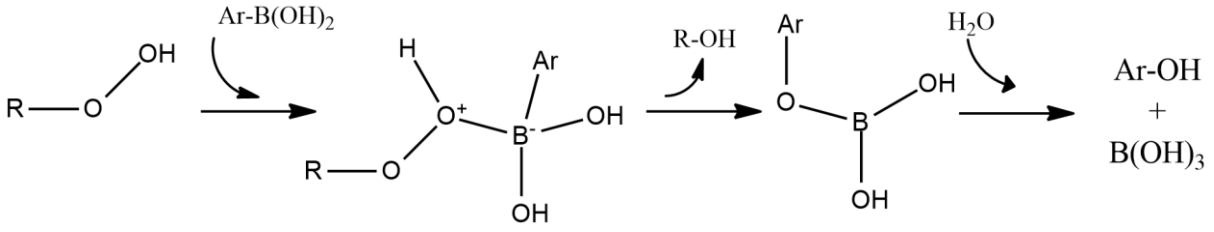

Figure 69: oxidation of boronic acids from organic peroxides

Regarding instead the homocoupling process, there are two general conditions under which Pd(II) mediates boronic acid homocoupling occurs. The first involves reductive activation of a Pd(II) pre-catalyst, consuming two boronic acid molecules (figure 70a).

The second common homocoupling process (figure 70b) occurs when accidental oxygen enters the system[185].

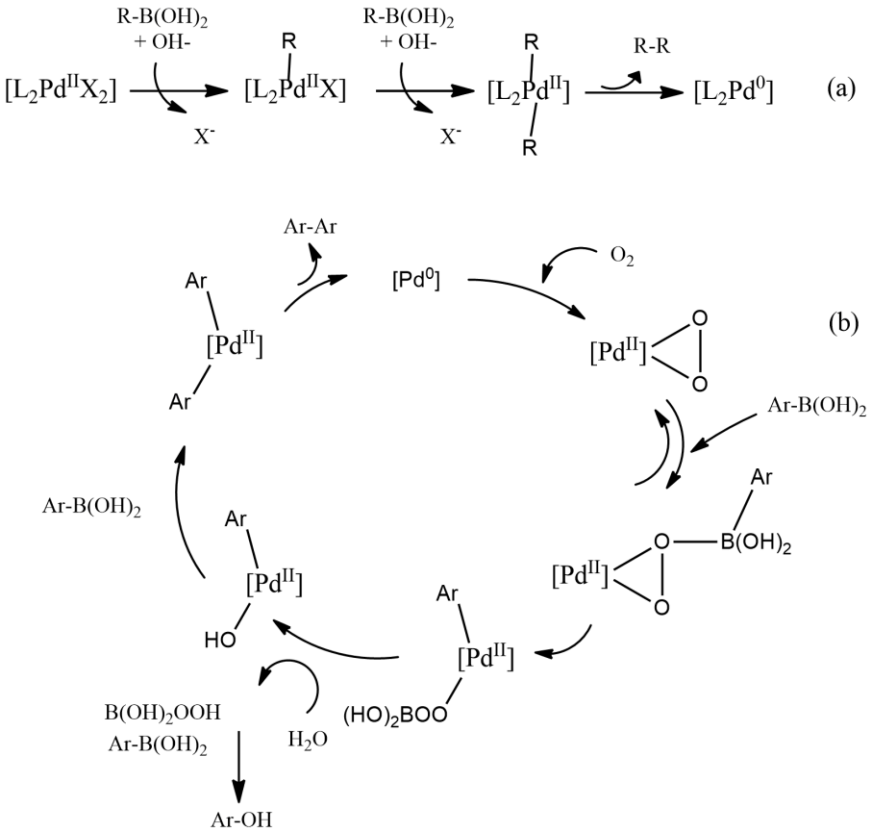

Figure 70: (a) reductive activation of a Pd(II) precatalyst resulting in homocoupling and (b) mechanism of the oxidative homocoupling of arylboronic acids by palladium peroxo-complex

2.3.3 Synthesis of 4,4′-([2,2′-bithiophene]-4-4′-diyl)bis(2-methylbut-3-yn-2-ol) (1) and 4-(4′-bromo-[2,2′-bithiophen]-4-yl)-2-methylbut-3-yn-2-ol (2)

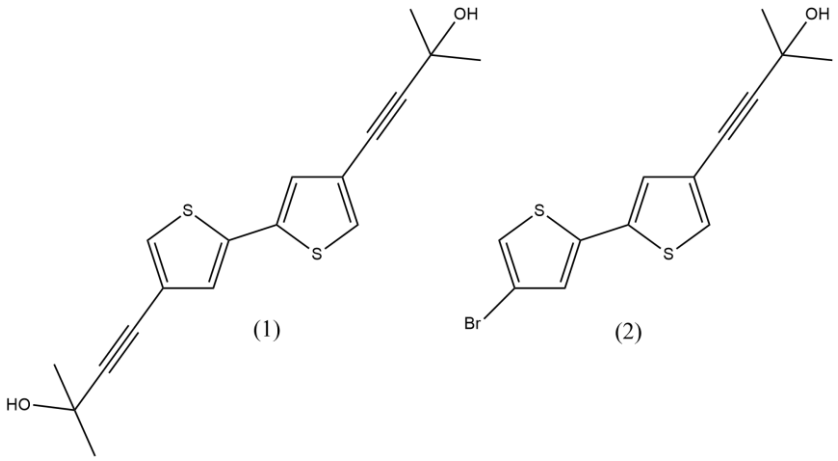

The syntheses of (1) and (2) exploit a Sonogashira type reaction. Synthesis conditions for (1) are given below and are the same reported by M. I. Pilo et al.[186] with some minor changes:

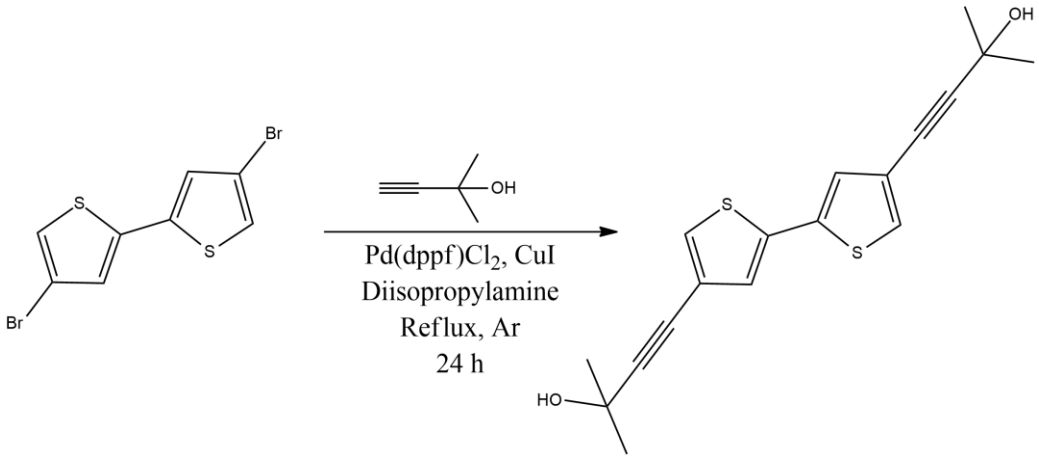

The used catalyst is $Pd(dppf)Cl_2$ which works as a pre-catalyst but is more stable than Pd(0)-catalysts. Pd(0) is, thus, generated *in situ*.

A solution of 0.3000 g ($9.26 \cdot 10^{-4}$ mol) of 4,4′-dibromo-2,2′-bithiophene, 0.0075 g ($9.26 \cdot 10^{-5}$ mol) of $Pd(dppf)Cl_2 \cdot CH_2Cl_2$ and 0.0053 g ($2.78 \cdot 10^{-5}$ mol) of CuI in 8 mL of diisopropylamine was prepared in a 25 mL double necked flask equipped with a

condenser, a small magnet and Ar inlet. After 1 h, 2-methyl-3-butin-2-ol (186 μL = $1.85 \cdot 10^{-3}$ mol) was added. The mixture was then refluxed and left under vigorous stirring for 24 h, until the complete disappearance of the substrate and possibly also the mono-coupling product (criteria: TLC on alumina with petroleum ether/ethyl acetate 2:3 as eluent). After cooling to room temperature, the mixture was added with 50 mL of CH_2Cl_2 and washed with 50 mL of saturated $NaHCO_3$ solution and then with 3 x 50 mL of water. The organic phase was then treated with $MgSO_4$, filtered and the solvent was evaporated under reduced pressure. The residue was purified through chromatographic column on alumina using a gradient elution, starting from petroleum ether/ethyl acetate 3:1 to 2:3.

Yield: 83%

^1H NMR ($CDCl_3$, ppm) (figure 71): δH = 7.29 (d, 2H), 7.13 (d, 2H), 1.94 (s, 2H), 1.61 (s, 12H)

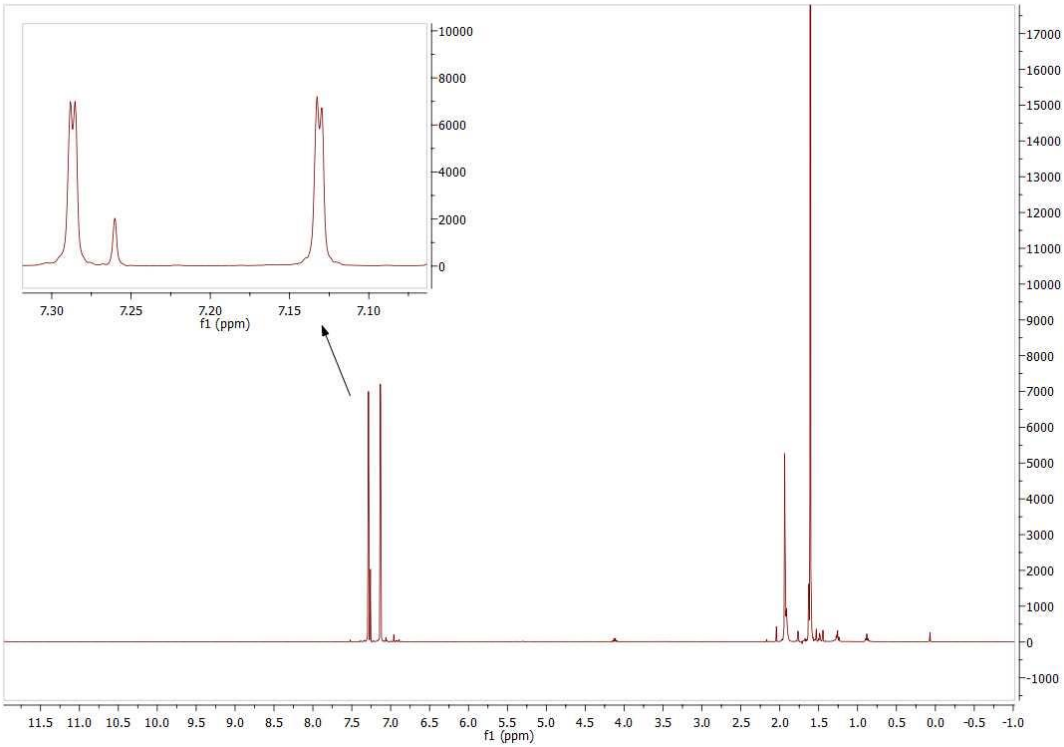

Figure 71: ^1H NMR spectrum of 4,4′-([2,2′-bithiophene]-4-4′-diyl)bis(2-methylbut-3-yn-2-ol) (1)

Using 1:1 mole ratio of the 4,4′-dibromo-2,2′-bithiophene and 2-methyl-3-butin-2-ol, it is possible to obtain the mono-coupled product (2).

^{1}H NMR ($CDCl_3$, ppm) (figure 72): δH = 7.30 (d, 1H), 7.14 (d, 1H), 7.12 (d, 1H), 7.06 (d, 1H), 2.13 (s, 1H), 1.61 (s, 6H)

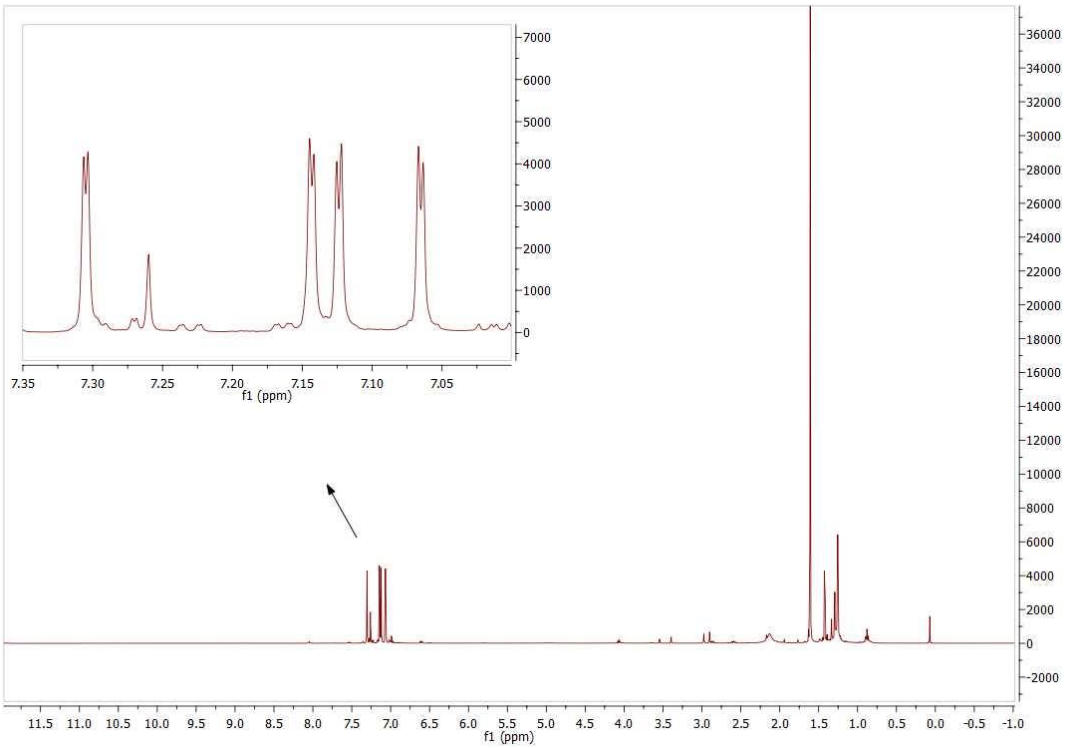

Figure 72: ^{1}H NMR spectrum of 4-(4′-bromo-[2,2′-bithiophen]-4-yl)-2-methylbut-3-yn-2-ol (2)

2.3.4 Synthesis of 4,4′-diethynil-2,2′-bithiophene (3)

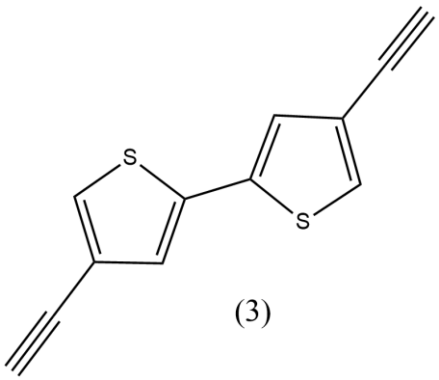

(3)

The synthesis of (3) is a triple bonds deprotection step, whose conditions are reported below:

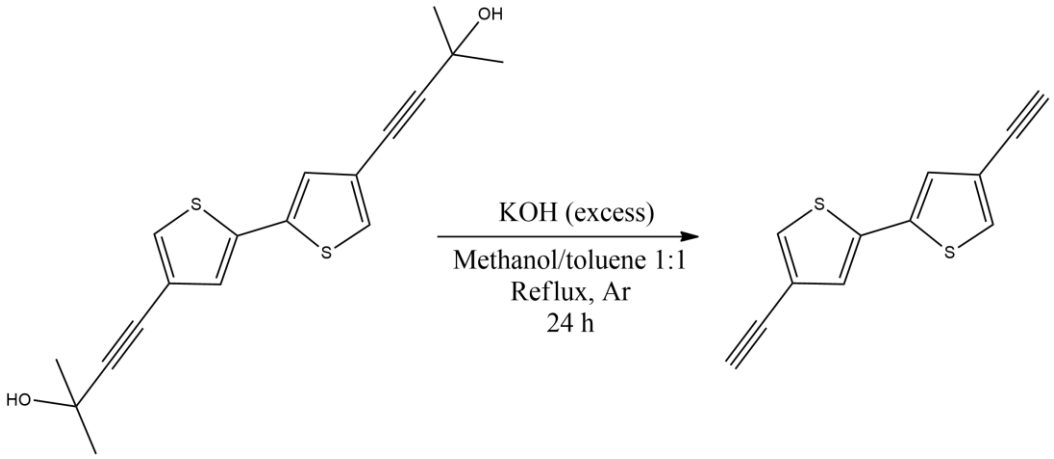

A solution of 0.2500 g ($7.56 \cdot 10^{-4}$ mol) of (1) in 10 mL of methanol/toluene 1:1 was prepared in a 25 mL double necked flask, equipped with a condenser, a small magnet and Ar inlet. An excess of KOH was then added. The mixture was then refluxed and left under vigorous stirring for 24 h, until the disappearance of (1) (criteria: TLC on silica gel with petroleum ether/ethyl acetate 5:1). After cooling to room temperature, the mixture was added with 50 mL of water and the product extracted with 3 x 50 mL of CH_2Cl_2. The organic phase was then washed with saturated NH_4Cl solution, treated with $MgSO_4$, filtered and the solvent was evaporated under reduced pressure. Usually, the obtained product does not need purification on column.

Yield: 95%

^1H NMR ($CDCl_3$, ppm) (figure 73): δH = 7.40 (d, 2H), 7.20 (d, 2H), 3.04 (s, 2H)

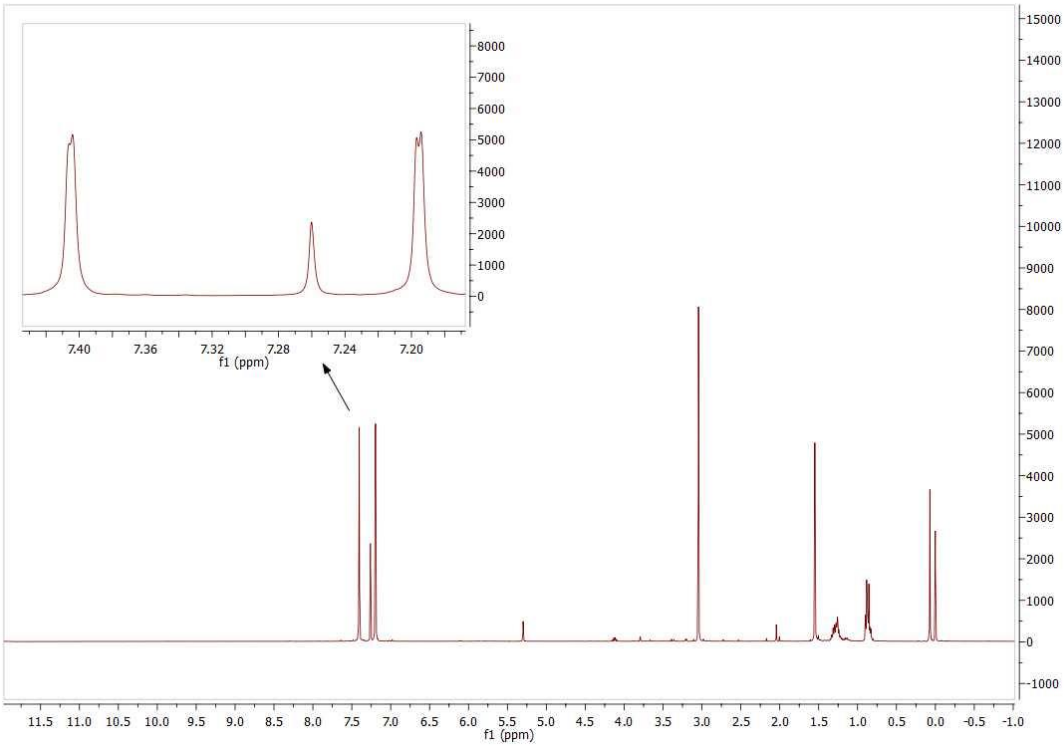

Figure 73: ^{1}H NMR spectrum of 4,4′-diethynil-2,2′-bithiophene (3)

2.3.5 Synthesis of 4,4′-([2,2′-bithiophene]-4,4′-diylbis(ethyne-2,1-diyl))dianiline (4)

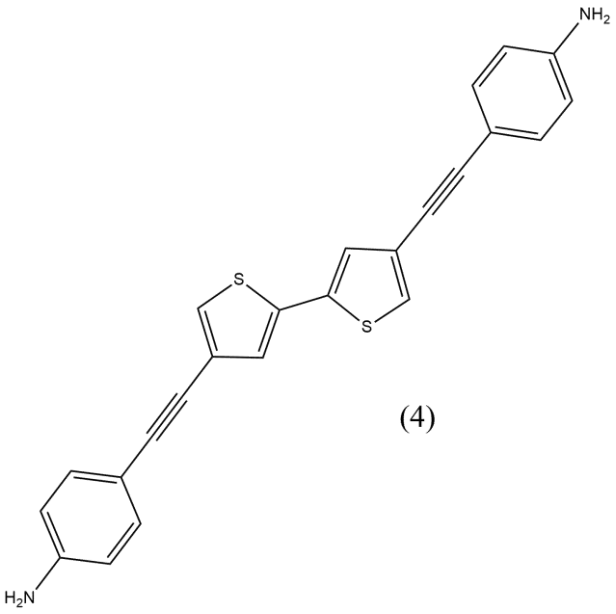

(4)

The synthesis of (4) is divided into two steps: first Sonogashira coupling between the aryl halide N-Boc-4-iodoaniline and (3), then deprotection reaction of NH-Boc derivative.

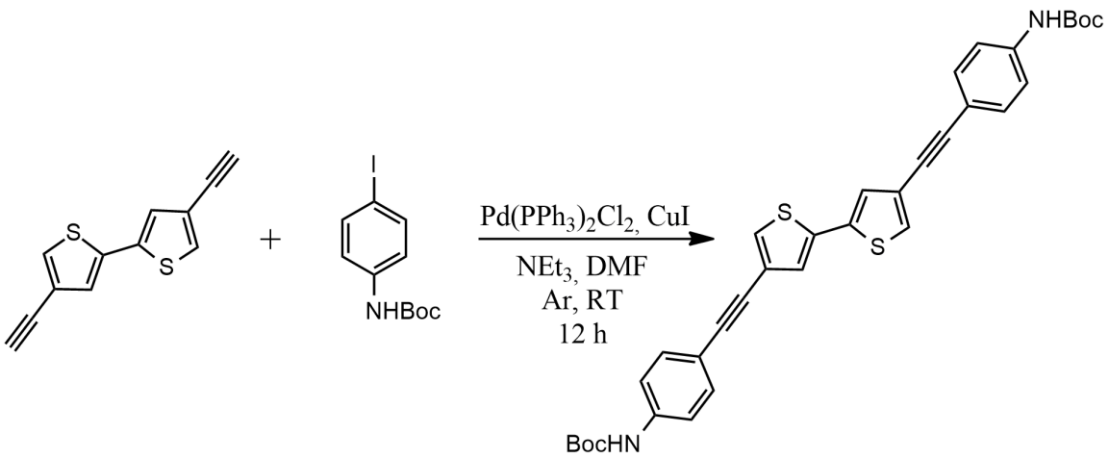

A solution of 0.5360 g ($1.68 \cdot 10^{-3}$ mol) of N-Boc-4-iodoaniline, 0.0590g ($8.40 \cdot 10^{-5}$ mol) of $PdCl_2(PPh_3)_2$ and 0.0320 g ($1.68 \cdot 10^{-4}$ mol) of CuI in 8 mL of triethylamine (NEt_3) and 1 mL of N,N-dimethylformamide (DMF) was prepared in a 25 mL double necked flask, equipped with a condenser, a small magnet and Ar inlet. After 1 h, a solution of 0.1800 g ($8.40 \cdot 10^{-4}$ mol) of (3) in 3 mL of DMF (carefully degassed) was slowly (30-45 min) added using a dropping funnel. The reaction proceeds at room temperature and under vigorous stirring for 12 h, until the disappearance of the (3) (criteria: TLC on silica gel with hexane/ethyl acetate 20:1). It is important to note that, with this eluent mixture, it is possible to distinguish well the two starting reagents but the product is not eluted, as well as the catalyst. When (3) completely disappears, it is possible to change the ratio of the eluent in 5:2 to distinguish the three spots relating to the unreacted N-Boc-4-iodoaniline, the desired product and the catalyst.

The mixture is then added with 25 mL of water and the product extracted with 25 mL of CH_2Cl_2. The organic phase was then washed with 3 x 25 mL of water to completely remove DMF, and finally with a saturated NaCl solution, treated with abundant $MgSO_4$, filtered and the solvent was evaporated under reduced pressure. The residue

was purified on chromatographic column on silica gel using hexane/ethyl acetate 5:1 until the complete removal of unreacted aryl halide and then with the same eluent mixture but in ratio 5:2.

Yield: 26%

^{1}H NMR ($CDCl_3$, ppm) (figure 74): δH = 7.44 (AA'BB', 4H), 7.37 (d, 2H) and 7.35 (AA'BB', 4H) partially overlapping, 7.25 (d, 2H), 6.55 (s, 2H), 1.53 (s, 18H)

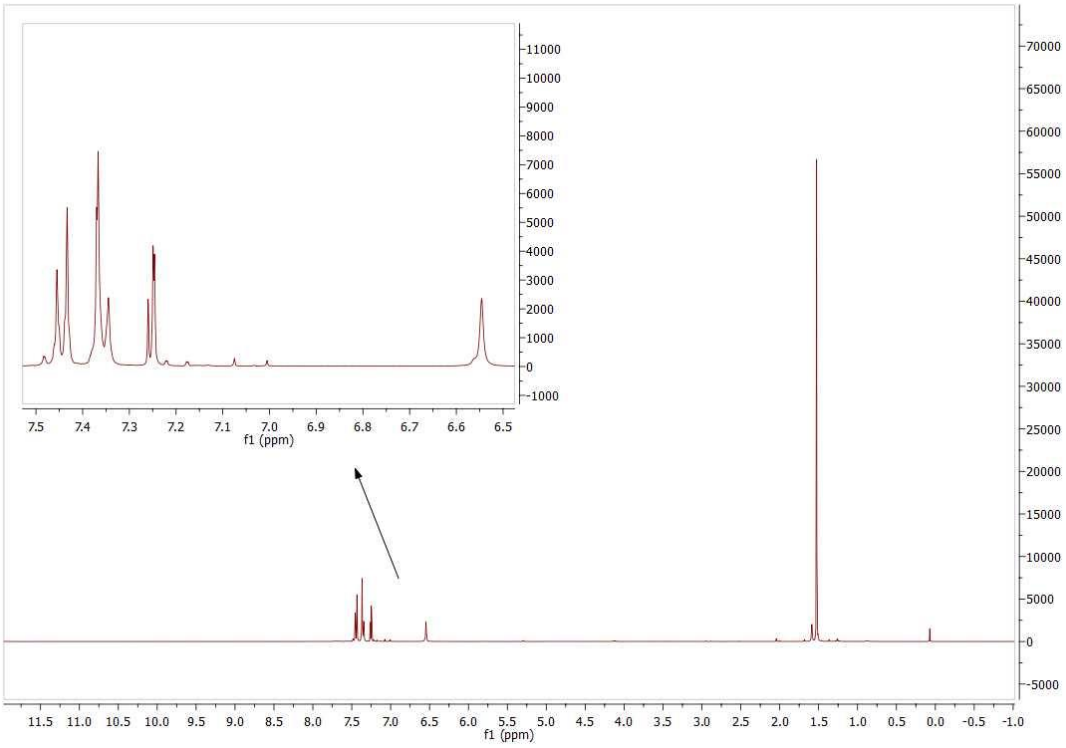

Figure 74: ^{1}H NMR spectrum of the di-tert-butyl(([2,2'-bithiophene]-4,4'-diylbis(ethyne-2,1-diyl))bis(4,1-phenylene)dicarbamate

The obtained product is then made to react according to the conditions shown below.

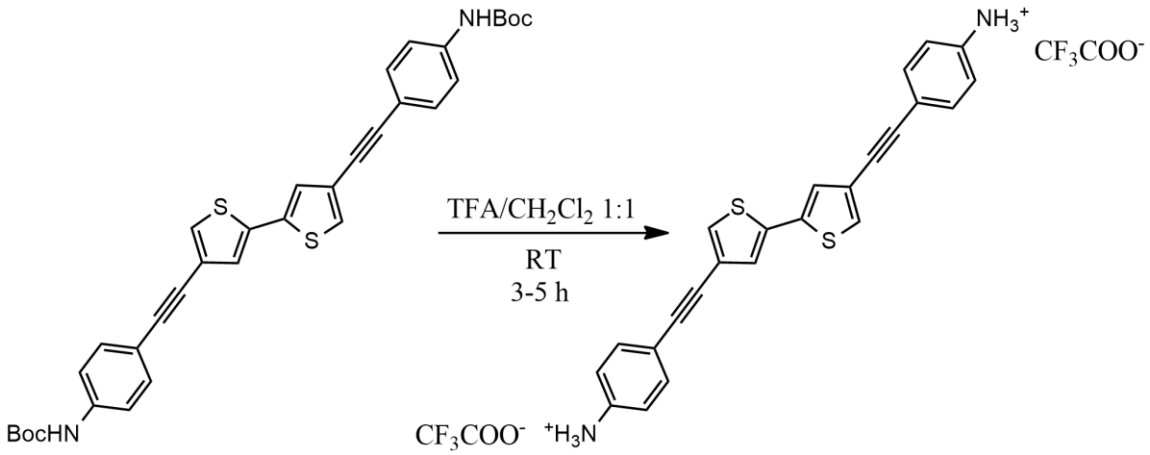

0.1300 g ($2.08 \cdot 10^{-4}$ mol of protected product were dissolved in 9 mL 1:1 of CH_2Cl_2/trifluoroacetic acid (TFA) in a 25 mL double necked flask equipped with a small magnet. The reaction proceeds at room temperature for 5 h until the disappearance of the substrate (criteria: TLC on silica gel with ethyl acetate/hexane 3:2 as eluent). The resulting solution was evaporated under reduced pressure and the residue was triturated with anhydrous diethyl ether, filtered and washed with anhydrous diethyl ether to yield the desired product as dark solid. The obtained solid is soluble in methanol and in dimethyl sulfoxide (DMSO).

It should be noted that it is very important that the reaction residue (which may contain some traces of TFA) does not come into contact with water, to avoid possible reactions that can destroy the triple bonds[187].

Yield: 88%

^1H NMR (DMSO d_6, ppm): δH = 7.15-7.05 (m 6H), 6.55-6.45 (m, 6H) overlapping signals.

To obtain the neutral molecule, an exchange with a weakly basic resin (aminomethyl polystyrene resin cross-linked with 1% DVB (200-400 mesh), 0.5 – 0.9 mmol/g) was attempted. A small portion of the 4,4′-([2,2′-bithiophene]-4,4′-diyilbis(ethyne-2,1-diyl))dibenzeneaminium was mixed with the resin in THF for about 4 h under slow rotation. The residue was then filtered and washed with THF. Unfortunately, the resulting product did not seem to be the desired one.

2.3.6 Synthesis of 4,4′-([2,2′-bithiophene]-4,4′-diylbis(ethyne-2,1-diyl)) dibenzoic acid (5)

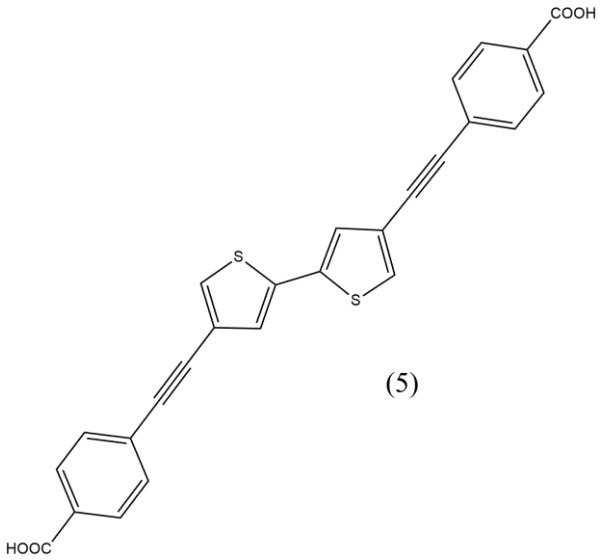

(5)

The synthesis of (5) exploits a Sonogashira-type reaction.

2.3.6.1 Synthesis Attempt 1

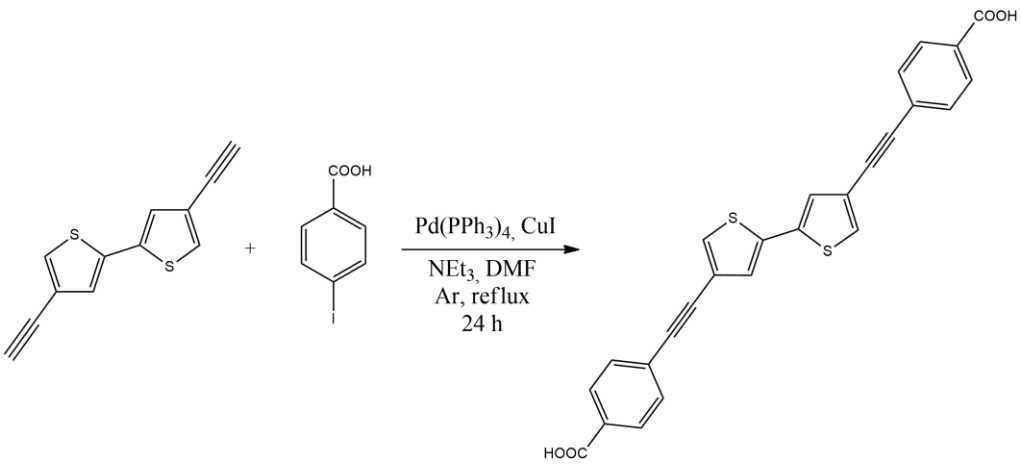

A solution of 0.0710 g ($2.86 \cdot 10^{-4}$mol) of 4-iodobenzoic acid, 0.0800 g ($3.73 \cdot 10^{-4}$mol) of (3), 0.0165 g ($1.43 \cdot 10^{-5}$ mol) of $Pd(PPh_3)_4$, 120 μL ($8.63 \cdot 10^{-4}$ mol) of triethylamine and 0.0055 g ($2.89 \cdot 10^{-5}$ mol) of CuI in 8 mL of DMF was prepared in a 25 mL double necked flask equipped with a condenser, a small magnet and Ar inlet. The mixture was then refluxed and left under vigorous stirring for 24 h, until the disappearance of 4-iodobenzoic acid (criteria: TLC on silica gel with petroleum ether/ethyl acetate 5:1 as eluent). After cooling to room temperature, the mixture was added with 70 mL of HCl 10% and the resulting mixture was extracted with 70 mL of ethyl acetate. The organic phase was then washed with 3 x 70 mL of water and with 70 mL of saturated NaCl solution, treated with $MgSO_4$, filtered and the solvent was evaporated under reduced pressure.

The ^{1}H NMR spectrum indicated that the obtained product was not the desired one.

2.3.6.2 Synthesis Attempt 2

The second attempt provides the reaction between 4,4'-dibromo-2,2'-bithiophene and 4-ethynylbenzoic acid:

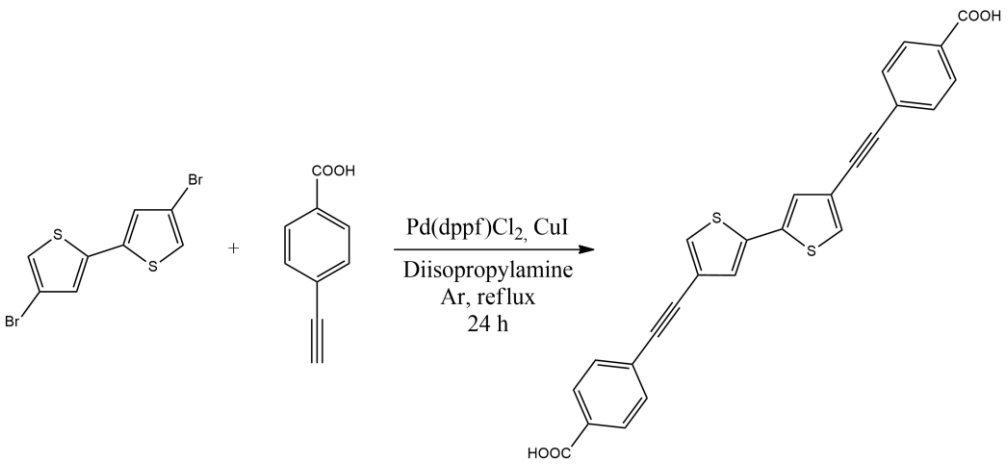

4-ethynylbenzoic acid was previously synthesized as follows:

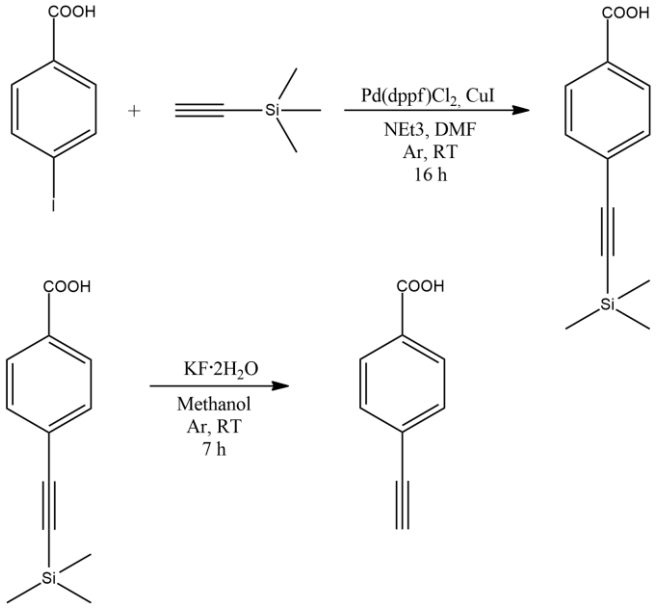

Step 1: a solution of 0.2000 g ($8.06 \cdot 10^{-4}$ mol) of 4-iodobenzoic acid, 0.0330 g ($4.04 \cdot 10^{-5}$ mol) of $Pd(dppf)Cl_2 \cdot CH_2Cl_2$, 0.0150 g ($7.88 \cdot 10^{-5}$ mol) of CuI, 340 µL ($2.45 \cdot 10^{-5}$ mol) of triethylamine in 8 mL of DMF was prepared in a 25 mL double necked flask equipped with a small magnet and Ar inlet. After 1 h, 144 µL ($1.04 \cdot 10^{-3}$ mol) of trimethylsilylacetylene were added. The reaction proceeds at room temperature under vigorous stirring for 16 h, until the disappearance of the aryl iodide (criteria: TLC on silica gel with petroleum ether/ethyl acetate 5:1).

The mixture was added with 30 mL of HCl 10% and the resulting mixture was extracted with 30 mL of ethyl acetate. The organic phase was then washed with 3 x 30 mL of water and with 30 mL of saturated NaCl solution, treated with $MgSO_4$, filtered and the solvent was evaporated under reduced pressure.

Yield: 68%

^1H NMR ($CDCl_3$, ppm) (figure 75): δH = 8.03 (d, 2H), 7.54 (d, 2H), 0.26 (s, 9H)

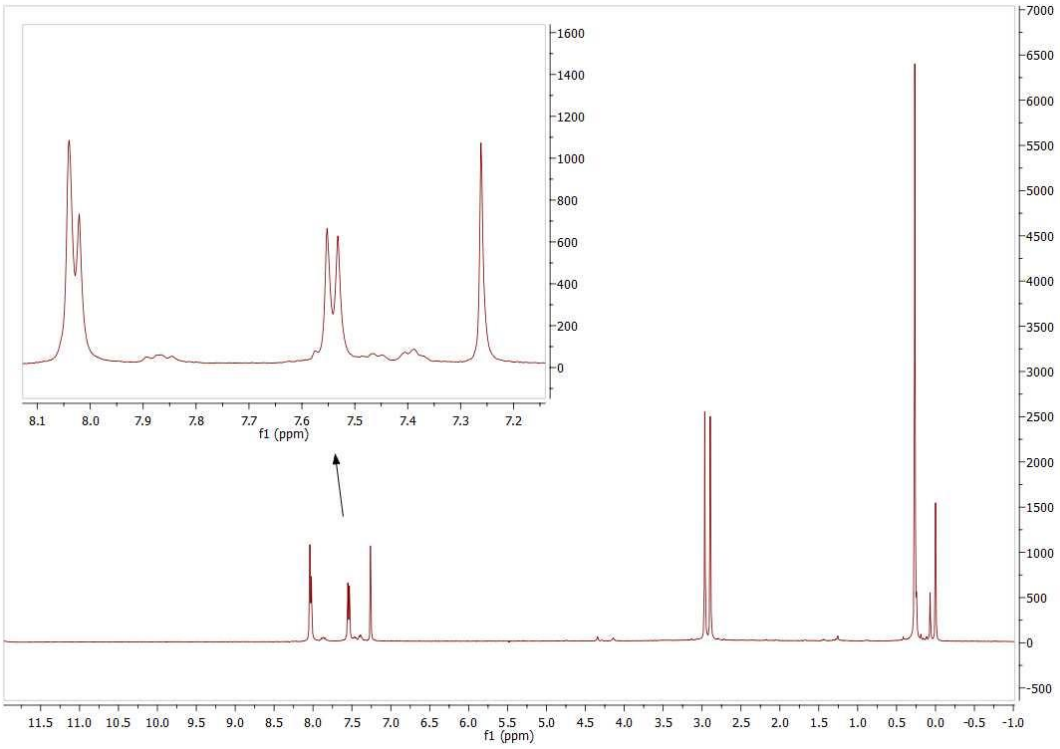

Figure 75: ^1H NMR spectrum of 4-((trimethylsilyl)ethynyl)benzoic acid

Step 2: a solution of 0.1200 g ($5.50 \cdot 10^{-4}$ mol) of 4-((trimethylsilyl)ethynyl)benzoic acid in 5 mL of methanol was prepared in a 25 mL double necked flask equipped with a small magnet and Ar inlet. 0.2600 g ($2.76 \cdot 10^{-3}$ mol) of $KF \cdot 2H_2O$ were then added. The reaction proceeds at room temperature under vigorous stirring for 7 h.

The mixture was added of 30 mL of water and the resulting mixture was extracted with 70 mL of ethyl acetate. The organic phase was then washed with 3 x 30 mL of water, treated with $MgSO_4$, filtered and the solvent was evaporated under reduced pressure.

Yield: 50%

^{1}H NMR ($CDCl_3$, ppm) (figure 76): δH = 8.05 (d, 2H), 7.58 (d, 2H), 3.26 (s, 1H)

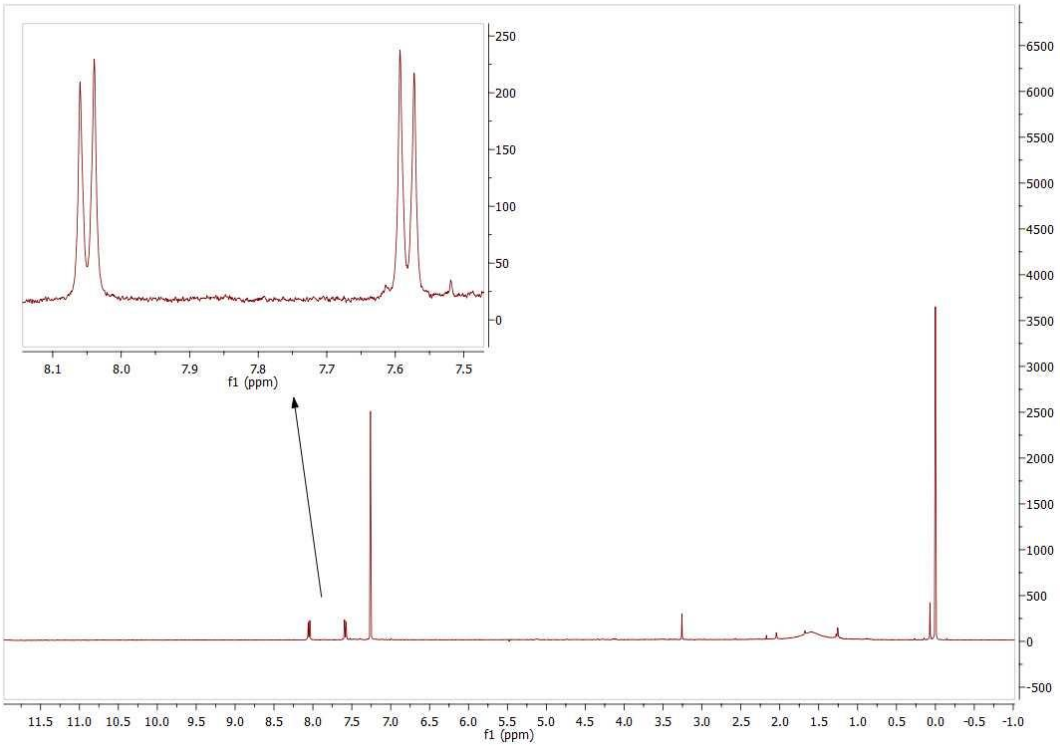

Figure 76: ^{1}H NMR spectrum of 4-ethynylbenzoic acid

Once 4-ethynylbenzoic acid was obtained, the reaction was carried out as follows:

a solution of 0.0890 g ($2.75 \cdot 10^{-4}$ mol) of 4,4'-dibromo-2,2'-bithiophene, 0.0800 g ($5.48 \cdot 10^{-4}$ mol) of 4-ethynylbenzoic acid, 0.0022 g ($2.69 \cdot 10^{-6}$ mol) of $Pd(dppf)Cl_2 \cdot CH_2Cl_2$ and 0.0016 g ($8.40 \cdot 10^{-6}$ mol) of CuI in 8 mL of diisopropylamine was prepared in a 25 mL double necked flask equipped with a condenser, a small magnet and Ar inlet. The mixture was then refluxed and left under vigorous stirring for 24 h, until the disappearance of the aryl halide (criteria: TLC on alumina with petroleum ether/ethyl acetate 2:3 as eluent). After cooling to room temperature, the mixture was added with 50 mL of saturated $NaHCO_3$ solution and the resulting mixture was extracted with 50 mL of CH_2Cl_2. The organic phase was then washed with 3 x 50 mL of water, treated with $MgSO_4$, filtered and the solvent was evaporated under reduced pressure.

^{1}H NMR ($CDCl_3$, ppm) (figure 77): δH = 8.03 (d, 4H), 7.52 (d, 4H), 7.43 (s, 2H), 7.15 (s, 2H), 7.10 (d, 2H), 7.08 (d, 2H).

Two of these signals (7.15 and 7.08 ppm) are clearly related to the starting aryl halide whereas the other four could be related to the desired product. However, an effective separation that allowed the isolation of the product was not possible.

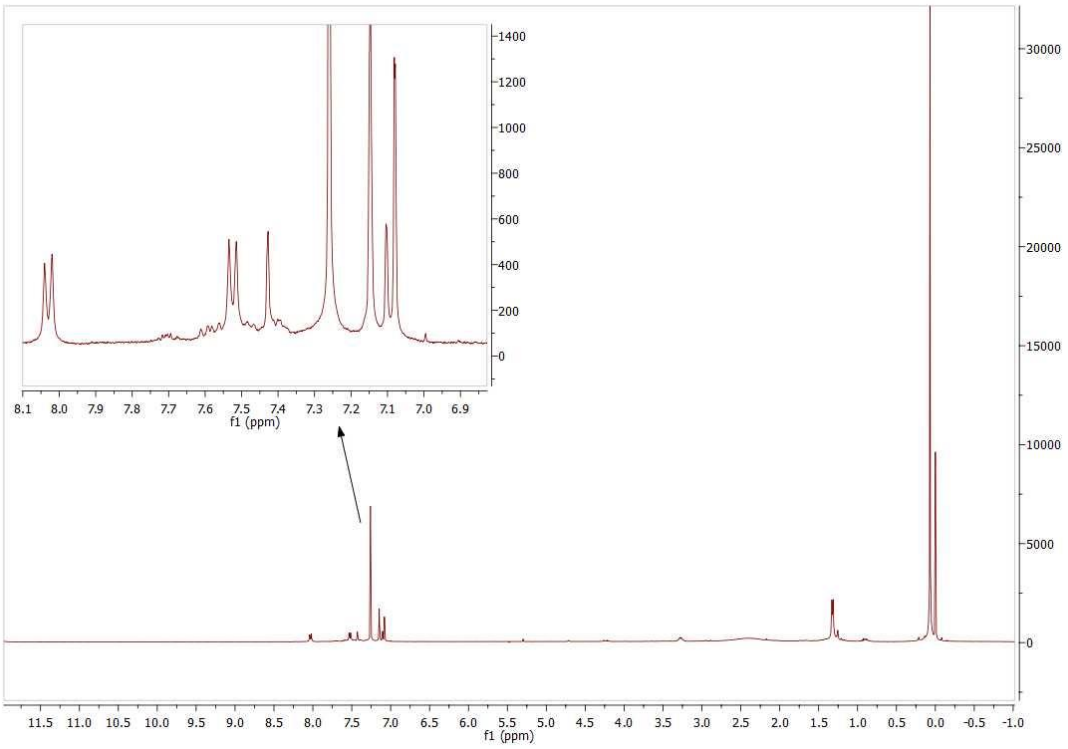

Figure 77: ^{1}H NMR spectrum of the product of the synthesis attempt 2

2.3.6.3 Synthesis Attempt 3

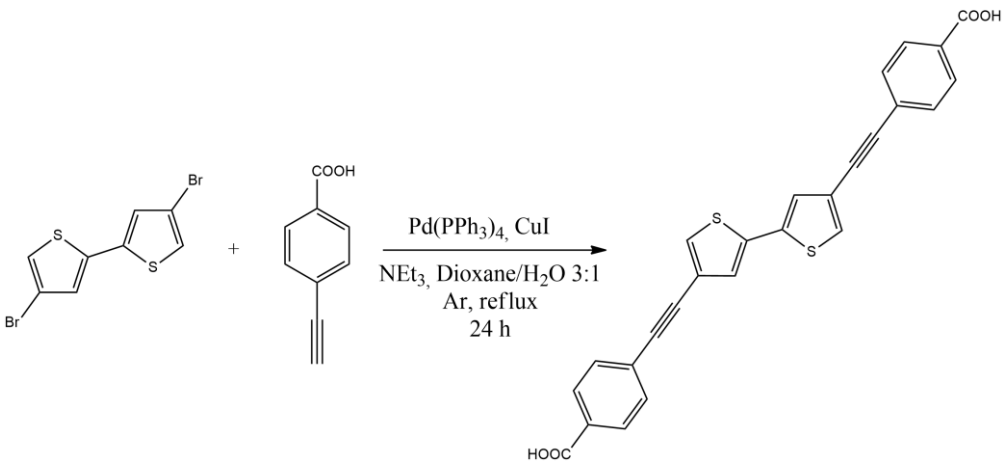

A solution of 0.0300 g ($9.26 \cdot 10^{-5}$ mol) of 4,4'-dibromo-2,2'-bithiophene, 0.0055 g ($4.76 \cdot 10^{-6}$ mol) of $Pd(PPh_3)_4$, 0.0018 g ($9.45 \cdot 10^{-6}$ mol) of CuI, 117 μL ($8.42 \cdot 10^{-4}$ mol) of triethylamine in 8 mL of dioxane/H_2O 3:1 was prepared in a double necked flask equipped with a condenser, a small magnet and Ar inlet. Then, 0.0300 g ($2.05 \cdot 10^{-4}$ mol) of 4-ethynylbenzoic acid were added. The mixture was then refluxed and left under vigorous stirring for 24 h. After 24 h the TLC on silica gel with petroleum ether/ethyl acetate 95:5 as eluent, showed only the two spots of the starting reagents.

2.3.6.4 Synthesis Attempt 4

By attributing the failure of the previous reactions to the presence of -COOH group[188,189], the reaction was carried out using the corresponding methyl ester (methyl-4-ethynylbenzoate) instead of 4-ethynylbenzoic acid, with a final hydrolysis step.

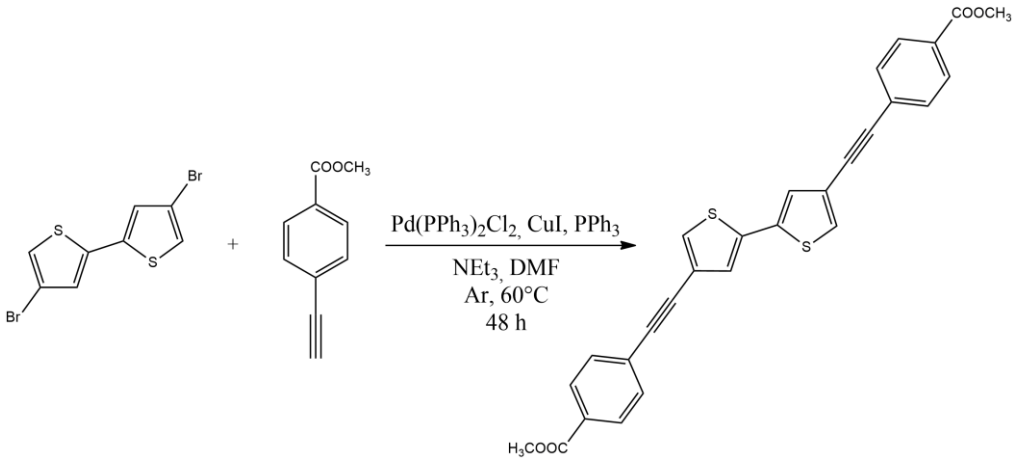

Methyl-4-ethynylbenzoate was previously synthesized as follows:

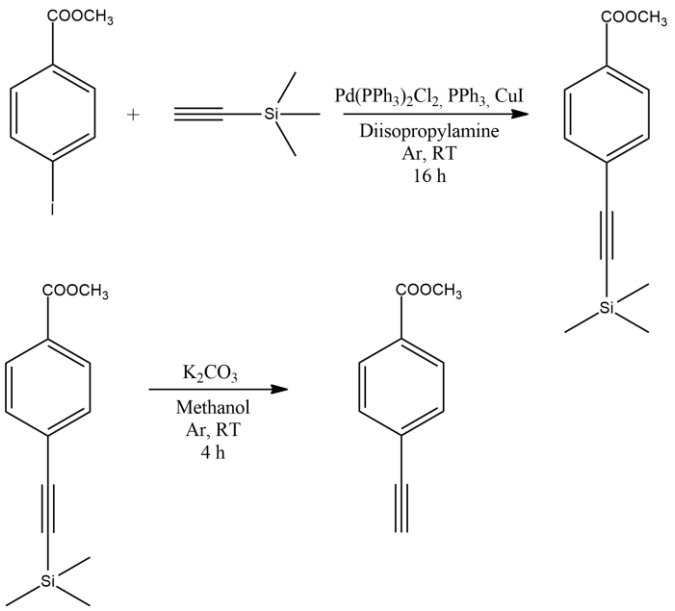

Step 1: a solution of 0.2000 g ($7.63 \cdot 10^{-4}$ mol) of methyl-4-iodobenzoate, 0.0110 g ($1.57 \cdot 10^{-5}$ mol) of $Pd(PPh_3)_2Cl_2$, 0.0060 g ($3.15 \cdot 10^{-5}$ mol) of CuI, 0.008 g ($3.05 \cdot 10^{-5}$ mol) of PPh_3 in 10 mL of diisopropylamine was prepared in a 25 mL double necked flask equipped with a small magnet and Ar inlet. After 1 h, 137 µL ($9.89 \cdot 10^{-4}$ mol) of trimethylsilylacetylene were added. The reaction proceeds at room temperature under vigorous stirring for 16 h, until the disappearance of aryl iodide (criteria: TLC on silica gel with petroleum ether/ethyl acetate 10:1 as eluent).

The mixture was added with 50 mL of water and the resulting mixture was extracted with 50 mL of CH_2Cl_2. The organic phase was then washed with 3 x 50 mL of water, treated with $MgSO_4$, filtered and the solvent was evaporated under reduced pressure.

Yield: 90%

^1H NMR ($CDCl_3$, ppm) (figure 78): δH = 7.96 (d, 2H), 7.51 (d, 2H), 3.91 (s, 3H), 0.25 (s, 9H)

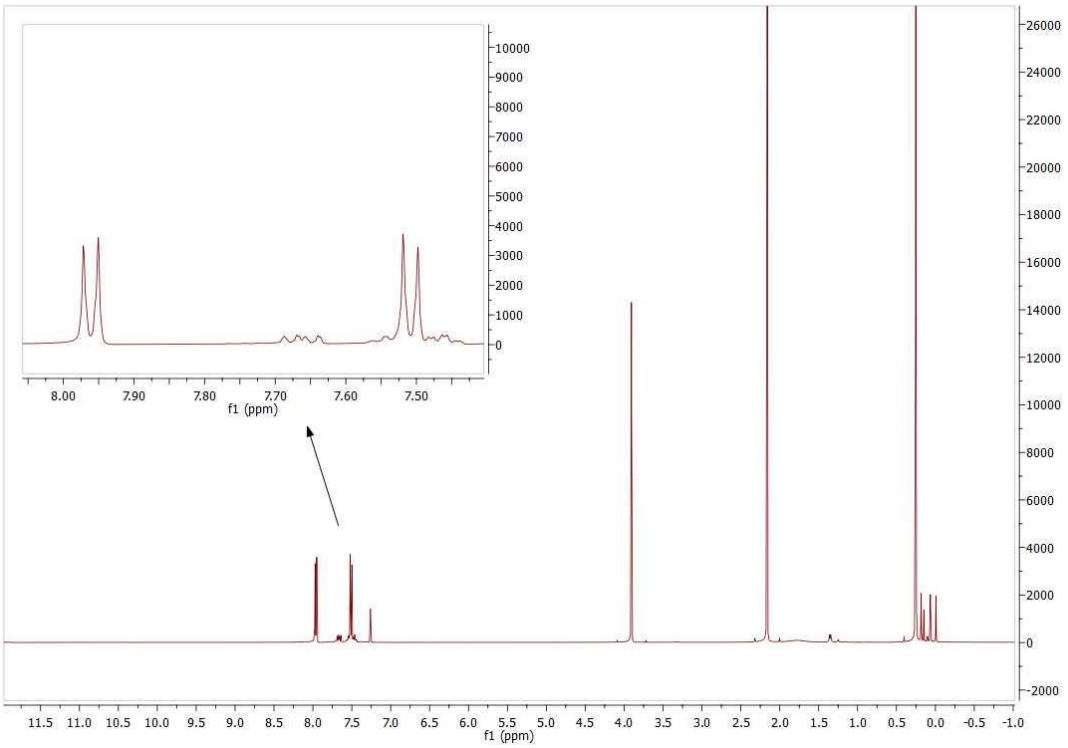

Figure 78: ^{1}H NMR spectrum of methyl-4-((trimethylsilyl)ethynyl)benzoate

Step 2: a solution of 0.1500 g ($6.93 \cdot 10^{-4}$ mol) of methyl-4-((trimethylsilyl)ethynyl)benzoate in 5 mL of methanol was prepared in a 25 mL double necked flask equipped with a small magnet and Ar inlet. 9.3 mg ($6.73 \cdot 10^{-5}$ mol) of K_2CO_3 were then added. The reaction proceeds at room temperature under vigorous stirring for 4 h, until the disappearance of the substrate.

The mixture was added with 50 mL of saturated $NaHCO_3$ solution and the resulting mixture was extracted with 3 x 30 mL of CH_2Cl_2. The organic phase was then washed with 3 x 50 mL of water, treated with $MgSO_4$, filtered and the solvent was evaporated under reduced pressure.

Yield: 79%

^{1}H NMR ($CDCl_3$, ppm) (figure 79): δH = 7.99 (d, 2H), 7.55 (d, 2H), 3.92 (s, 3H), 3.23 (s, 1H)

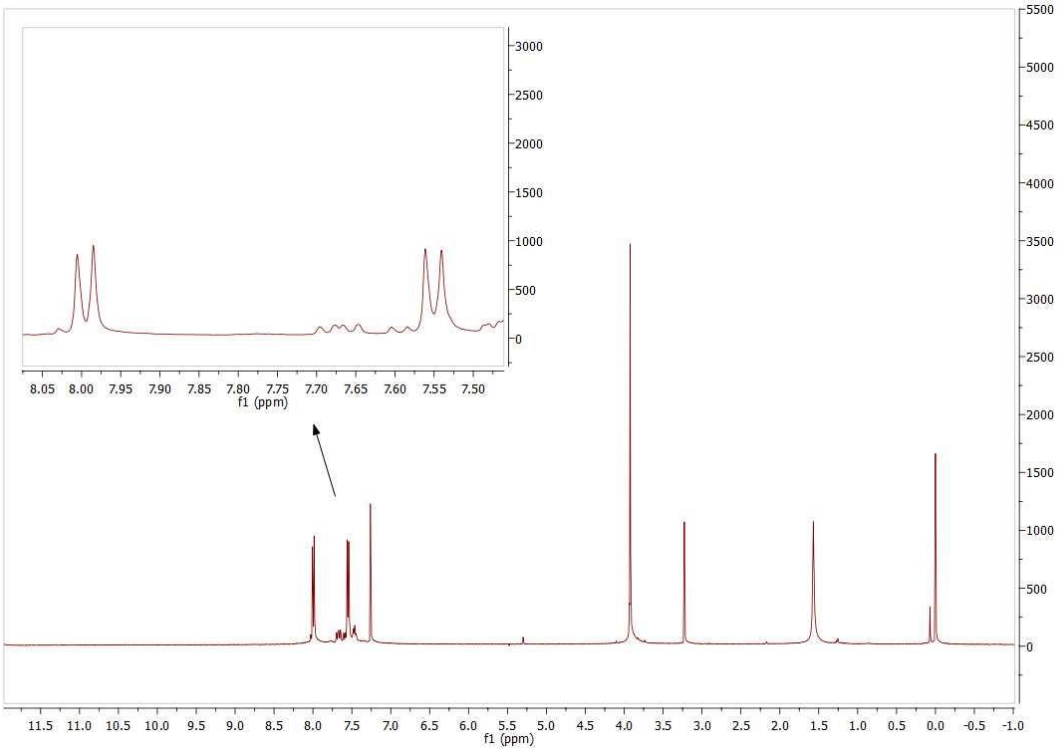

Figure 79: ^{1}H NMR spectrum of methyl-4-ethynylbenzoate

Once methyl-4-ethynylbenzoate was obtained, the reaction was carried out as follows: a solution of 0.0600 g ($1.85 \cdot 10^{-4}$ mol) of 4,4'-dibromo-2,2'-bithiophene, 0.0800 g ($4.99 \cdot 10^{-4}$ mol) of methyl-4-ethynylbenzoate, 0.013 g ($1.85 \cdot 10^{-5}$ mol) of $Pd(PPh_3)_2Cl_2$, 0.0100 g ($3.81 \cdot 10^{-5}$ mol) of PPh_3, 0.0070 g ($3.67 \cdot 10^{-5}$mol) of CuI in 10 mL of triethylamine was prepared in a double necked flask equipped with a condenser, a small magnet and Ar inlet. 5 mL of DMF were then added in order to enhance the solubility of the ethynylbenzoate. The mixture was then heated to 60 °C and left under vigorous stirring for 48 h, until the disappearance of the aryl halide (criteria: TLC on silica gel with petroleum ether/ethyl acetate 95:5).

After cooling to room temperature, the mixture was added with 50 mL of water and the resulting mixture was extracted with 3 x 50 mL of CH_2Cl_2. The organic phase was then washed with 3 x 50 mL of water, treated with $MgSO_4$, filtered and the solvent was evaporated under reduced pressure.

From ^{1}H NMR spectrum, the obtained product it is not the desired one and it is still present a big amount of unreacted starting aryl bromide.

2.3.6.5 Synthesis Attempt 5

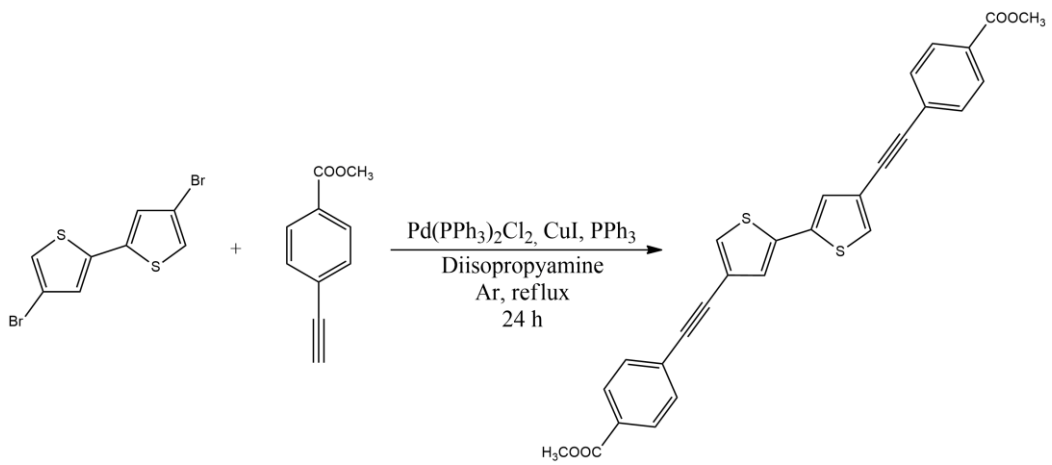

A solution of 0.0760 g ($2.34 \cdot 10^{-4}$ mol) of 4,4'-dibromo-2,2'-bithiophene, 0.0750 g ($4.68 \cdot 10^{-4}$ mol) of methyl-4-ethynylbenzoate, 0.0070 g ($9.97 \cdot 10^{-6}$ mol) of $Pd(PPh_3)_2Cl_2$, 0.0033 g ($1.73 \cdot 10^{-5}$ mol) of CuI, 0.0049 g ($1.87 \cdot 10^{-5}$mol) of PPh_3 in 10 mL of diisopropylamine was prepared in a 25 mL double necked flask equipped with a condenser, a small magnet and Ar inlet. The mixture was then refluxed and left under vigorous stirring for 24 h until the disappearance of the aryl bromide (criteria: TLC on silica gel with petroleum ether/ethyl acetate 1:1).

After cooling to room temperature, the mixture was added with 50 mL of CH_2Cl_2 and washed with saturated NH_4Cl solution. The organic phase was then treated with $MgSO_4$, filtered and the solvent was evaporated under reduced pressure. The residue was purified on chromatographic column on silica gel using petroleum ether/ethyl acetate 1:1 as eluent.

The ^1H NMR spectrum evidences the presence of a large amount of unreacted aryl halide, and signals attributable to the homocoupling product of the terminal alkynes. No evidence of the desired coupling product is present.

2.3.6.6 Synthesis Attempt 6

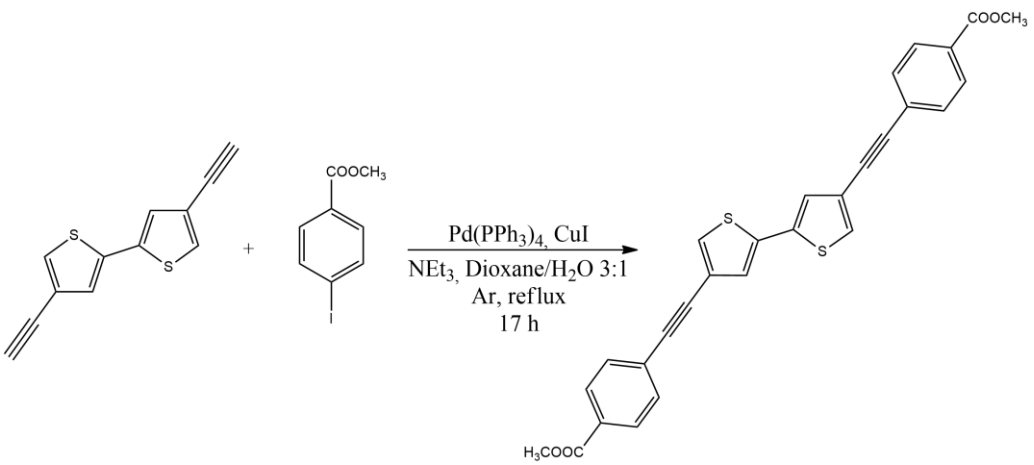

A solution of 0.0900 g ($4.20 \cdot 10^{-4}$ mol) of 4,4'-diethynyl-2,2'-bithiophene, 0.2200 g ($8.40 \cdot 10^{-4}$ mol) of methyl-4-iodobenzoate, 0.0480 g ($4.15 \cdot 10^{-5}$mol) of $Pd(PPh_3)_4$, 0.0160 g ($8.40 \cdot 10^{-5}$ mol) of CuI, 232 µL ($1.67 \cdot 10^{-3}$ mol) of triethylamine in 8 mL dioxane/H_2O 3:1 was prepared in a 25 mL double necked flask equipped with a condenser, a small magnet and Ar inlet. The mixture was then refluxed and left under vigorous stirring for 17 h, until the disappearance of the substrates (criteria: TLC on alumina with petroleum ether/ethyl acetate 95:5).

After cooling to room temperature, the mixture was filtered off, the filter washed with CH_2Cl_2 and the solvent evaporated under reduced pressure. The residue was purified on chromatographic column on alumina using petroleum ether/ethyl acetate 95:5.

From the ^1H NMR two products can be observed: the desired one and the homocoupling product of the terminal alkynes. Unfortunately, it was not possible to obtain an efficient separation.

2.3.6.7 Synthesis Attempt 7: One-Pot Sonogashira Method

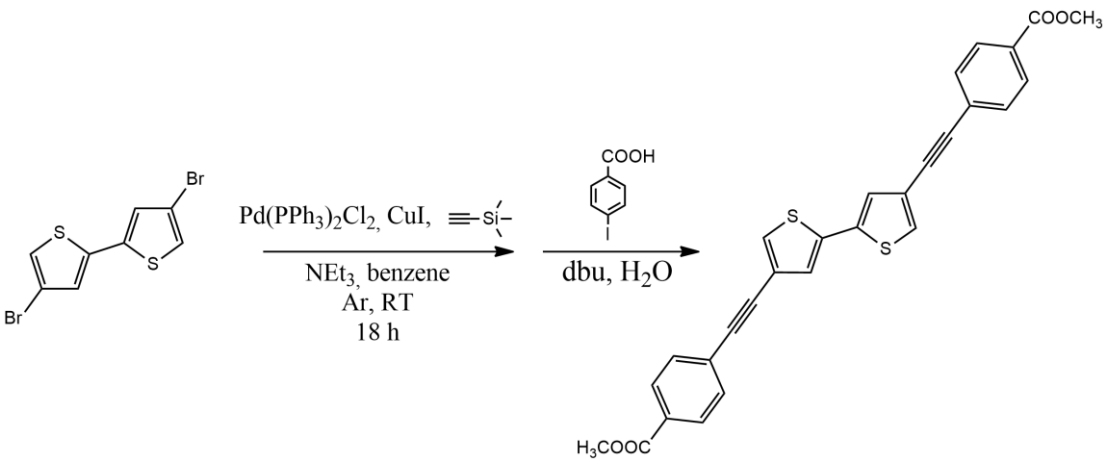

In this synthesis attempt the reaction conditions reported by M. J. Mio et al.[173] were used.

A solution of 0.2600 g ($8.02 \cdot 10^{-4}$ mol) of 4,4'-dibromo-2,2'-bithiophene, 0.0340 g ($4.84 \cdot 10^{-5}$ mol) of $Pd(PPh_3)_2Cl_2$, 0.0320 g ($1.68 \cdot 10^{-4}$ mol) of CuI, 1.4 mL ($1.01 \cdot 10^{-2}$ mol) of triethylamine in 4 mL of benzene was prepared in a 25 mL double necked flask equipped with a small magnet and Ar inlet. The reaction proceeds at room temperature under vigorous stirring for 18 h in the absence of light. After 18 h, 0.3970 g ($1.60 \cdot 10^{-3}$ mol) of 4-iodobenzoic acid, 2.9 mL ($1.94 \cdot 10^{-2}$ mol) of 1,8-diazabicyclo[5.4.0]undec-7-ene (dbu) and 6 mL (40 mol%) of water were added. After 18 h the reaction was monitored with TLC on silica gel with hexane/ethyl acetate 9:1 as eluent. The TLC showed only the spots related to the unreacted starting reagents.

2.3.7 Synthesis of 4′-(2,2′:5′,2′′-terthien-3′-ethynyl)-2,2′:6′,2′′-terpyridine (TAT) (6)

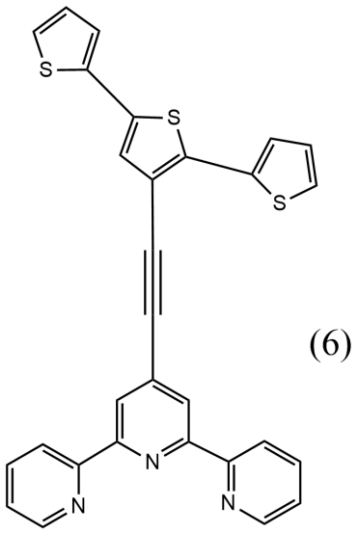

(6)

In this synthesis the reaction conditions reported by P. Manca et al.[146] were used with some minor changes.

The synthesis of (6) is divided into four steps: a first Suzuki coupling between 2,3,5-tribromothiophene and thiophene-2-boronic acid, a successive Sonogashira coupling between the obtained 3′-bromo-2,2′:5′,2′′-terthiophene and 2-methyl-3-butyn-2-ol, then a deprotection step of triple bond and finally another Sonogashira coupling between the obtained 3′-ethynyl-2,2′:5′,2′′-terthiophene and 4′-chloro-2,2′:6′,2′′-terpyridine.

1° Step: synthesis of 3′-bromo-2,2′:5′,2′′-terthiophene (7)

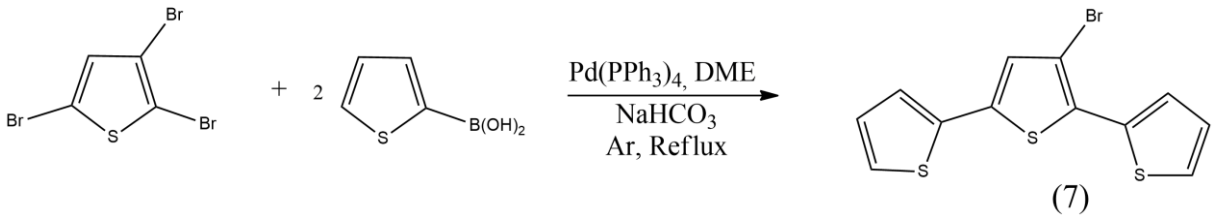

(7)

A solution of 0.5000 g ($1.56 \cdot 10^{-3}$ mol) of 2,3,5-tribromothiophene and 0.1080 g ($9.35 \cdot 10^{-5}$ mol) of $Pd(PPh_3)_4$ in 15 mL of 1,2-dimethoxyethane (DME) was prepared in a 25 mL

double necked flask equipped with a condenser, a small magnet and Ar inlet. The solution was stirred for 10 minutes at room temperature. Then 0.6080 g ($4{,}75 \cdot 10^{-3}$ mol) of thiophene-2-boronic acid were added, immediately followed by 1 M $NaHCO_3$ solution (5.5 mL). Then the reaction mixture was refluxed with vigorous stirring for 4-6 hours until the solution appears brown and clear. TLC on silica gel using petroleum ether as eluant evidences the presence of (7). After cooling to room temperature, 15 mL of distilled water were poured onto the residue and the resulting mixture was extracted with diethyl ether (3 x 30 mL). The organic phase was then washed with saturated NaCl solution, treated with $MgSO_4$, filtered and the solvent was evaporated under reduced pressure. The residue was purified on chromatographic column on silica gel using petroleum ether as eluant to give a green oil.

Yield: 68%

^1H NMR ($CDCl_3$, ppm) (figure 80): δH = 7.33 (dd, 1H), 7.25 (dd, 1H), 7.15 (dd, 1H), 7.07 (dd, 1H), 6.98 (dd, 1H), 6.98 (s, 1H) overlapped, 6.92 (dd, 1H).

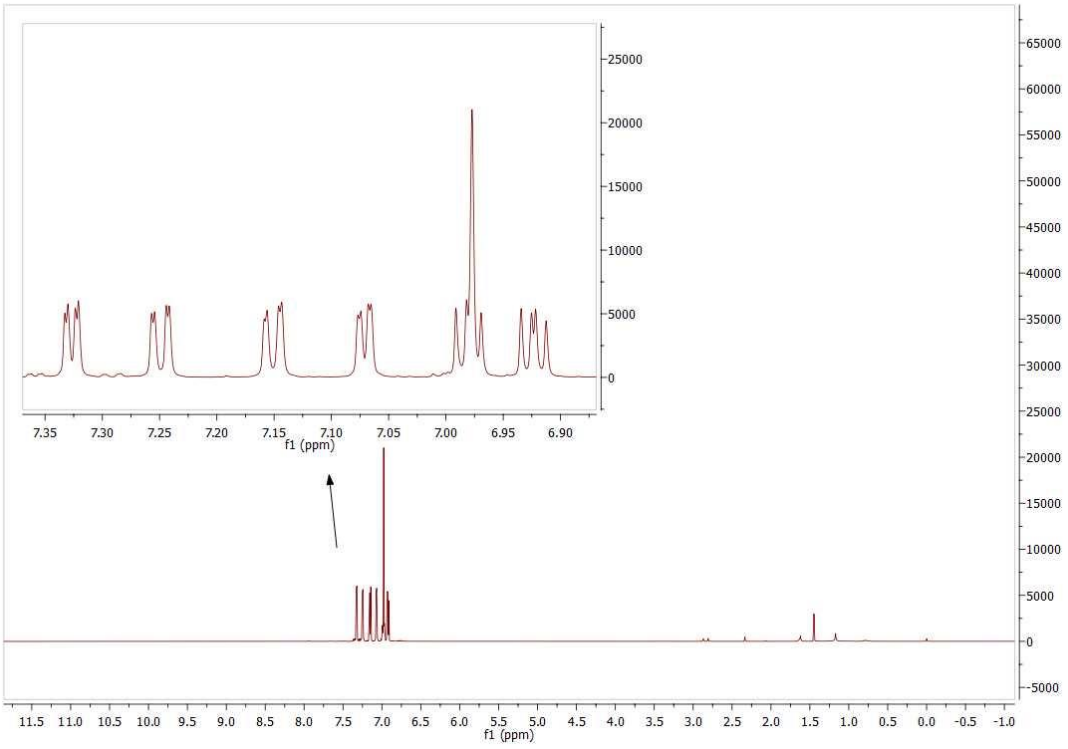

Figure 80: ^1H NMR spectrum of 3′-bromo-2,2′:5′,2′′-terthiophene (7)

2° Step: synthesis of 3'-(3-hydroxy-methylbut-1-ynil)-2,2':5,2''-terthiophene (8)

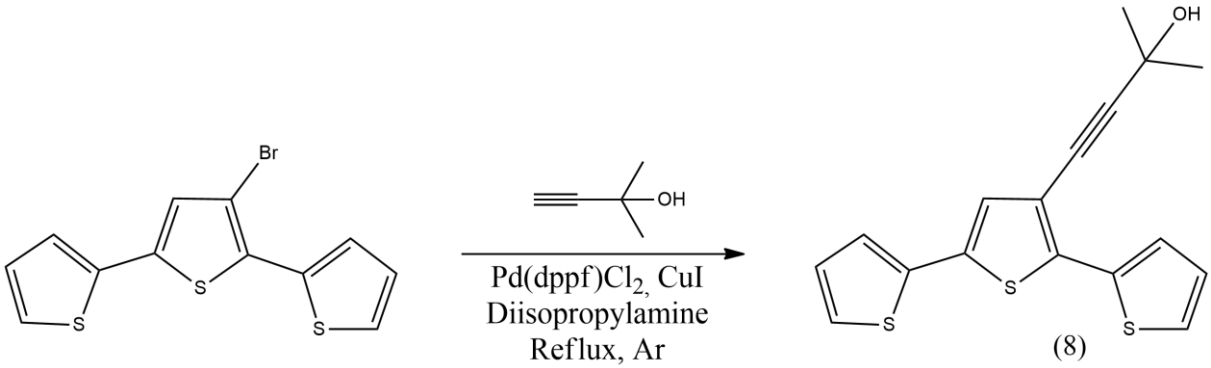

A solution of 0.3300 g ($1.01 10^{-3}$ mol) of (7), 0.0082 g ($1.00 \cdot 10^{-5}$ mol) of $Pd(dppf)Cl_2 \cdot CH_2Cl_2$ and 0.0057 g ($2.99 \cdot 10^{-5}$ mol) of CuI in 10 mL of diisopropylamine was prepared in a 25 mL double necked flask equipped with a condenser, a small magnet and Arinlet. Then 98 μL ($1.01 \cdot 10^{-3}$ mol) of 2-methyl-3-butyn-2-ol were added. The reaction mixture was refluxed for 24 hours under stirring, until the disappearance of (7) (criteria: TLC on silica gel using n-hexane/ethyl acetate 5:1 as eluant). Then the mixture was cooled at room temperature and 25 mL of CH_2Cl_2 were added. The organic resulting phase was washed first with 25 mL of saturated $NaHCO_3$ solution and then with 25 mL of H_2O. The extract was treated with $MgSO_4$, filtered and the solvent evaporated under reduced pressure. The residue was purified on chromatographic column on silica gel using n-hexane/ethyl acetate 5:1 as eluant to give a green oil.

Yield: 84%

^1H NMR ($CDCl_3$, ppm) (figure 81): δH = 7.34 (dd, 1H), 7.19 (dd, 1H), 7.12 (dd, 1H), 7.05 (dd, 1H), 6.98 (s, 1H), 6.94 (dd, 1H), 6.90 (dd, 1H), 2.23 (s, 1H), 1.57 (s, 6H).

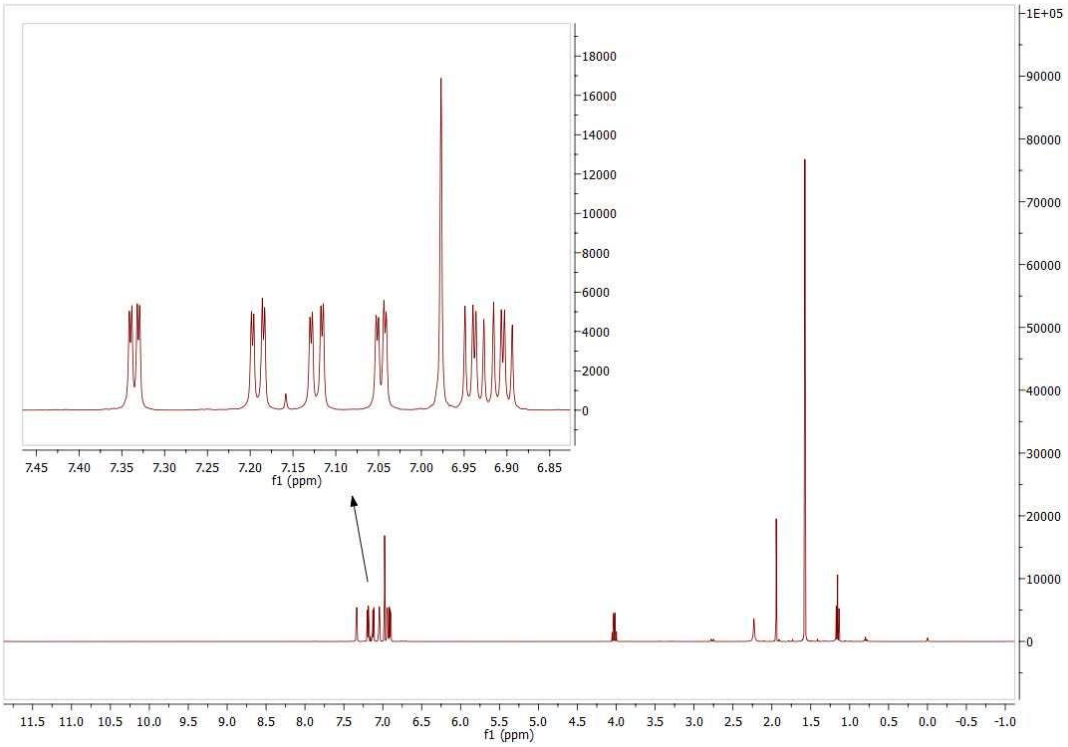

Figure 81: ^{1}H NMR spectrum of 3′-(3-hydroxy-methylbut-1-ynil)-2,2′:5,2′′-terthiophene (8)

3° Step: synthesis of 3′-(ethynyl)-2,2′:5′,2′′-terthiophene (9)

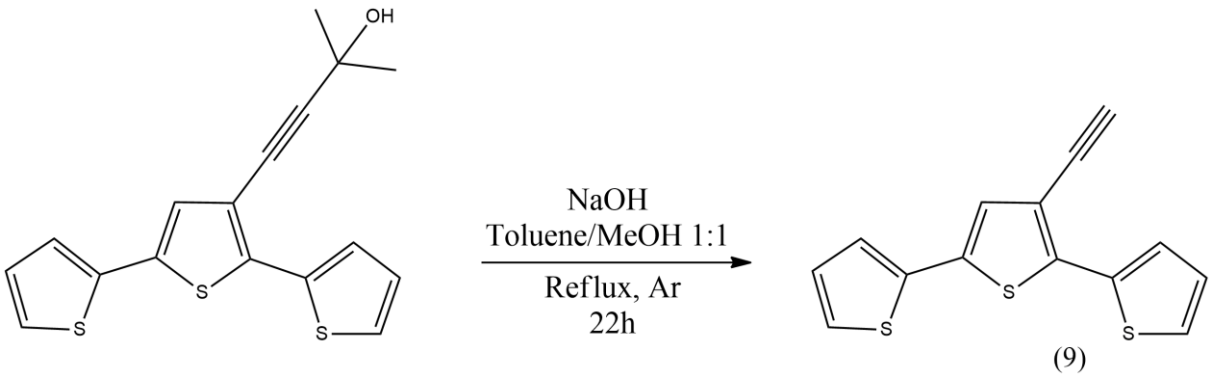

(9)

A solution of 0.2450 g ($7.41 \cdot 10^{-4}$ mol) of (8) in 10 mL of methanol/toluene 1:1 was prepared in a 25 mL double necked flask equipped with a condenser, a small magnet and Ar inlet. An excess of NaOH was then added. The mixture was then refluxed and left under vigorous stirring for 24 hours, until the disappearance of (8) (criteria: TLC on silica gel using n-hexane/ethyl acetate 5:1 as eluant). After confirmation of disappearance of the substrate, the solvent was removed under reduced pressure. 25

mL of H_2O were poured onto the residue and the resulting mixture was extracted with CH_2Cl_2 (3x50 mL). The resulting organic phase was then washed with 200 mL of saturated NH_4Cl solution, treated with $MgSO_4$, filtered and the solvent was evaporated under reduced pressure. The residue was purified on chromatographic column on silica gel using n-hexane/ethyl acetate 5:1 as eluant to obtain a brown oil.

Yield: 95%

^1H NMR ($CDCl_3$, ppm) (figure 82): δH = 7.46 (dd, 1H), 7.22 (dd, 1H), 7.15 (dd, 1H), 7.08 (dd, 1H), 7.05 (s, 1H), 6.97 (dd, 1H), 6.93 (dd, 1H), 3.29 (s, 1H).

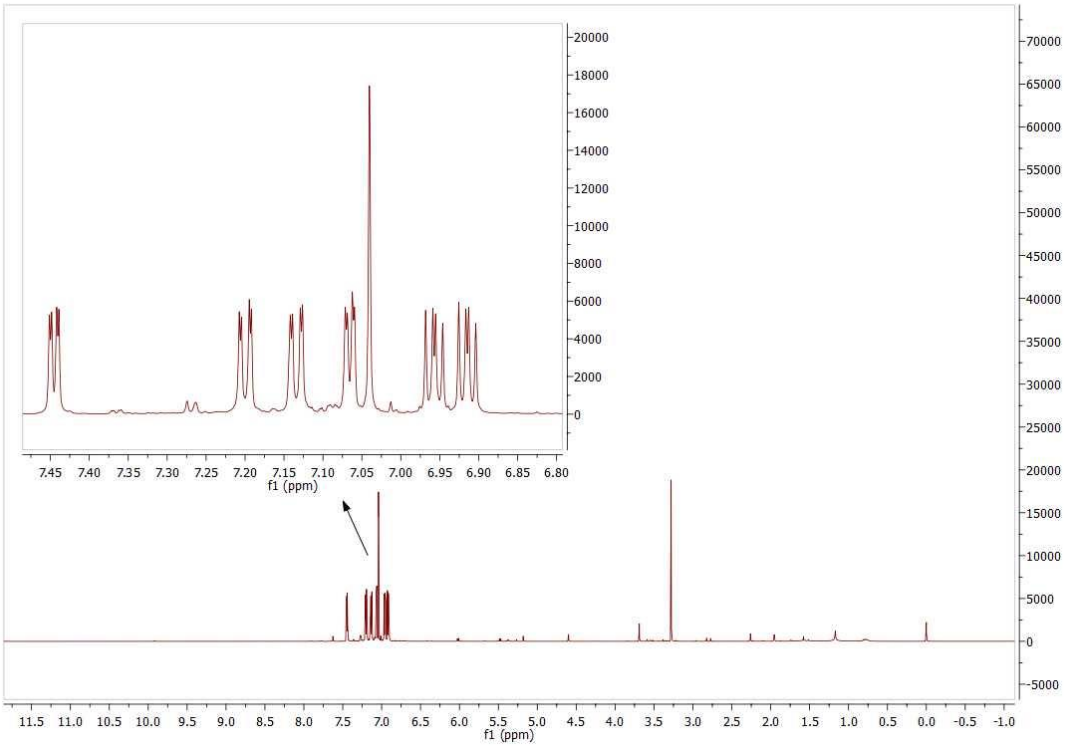

Figure 82: ^1H NMR spectrum of 3′-(ethynyl)-2,2′:5′,2′′-terthiophene (9)

4° Step: synthesis of 4'-(2,2':5',2''-terthien-3'-ethynyl)-2,2':6',2''-terpyridine (TAT) (6)

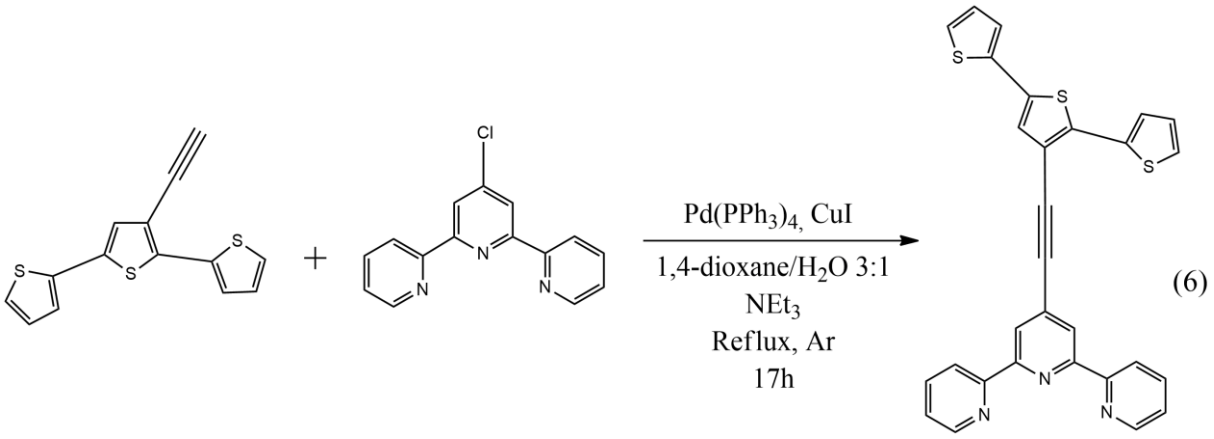

(6)

A solution of 0.2480 g ($9.24 \cdot 10^{-4}$ mol) of 4'-chloro-2,2':6',2''-terpyridine, 0.0534 g ($4.62 \cdot 10^{-5}$ mol) of $Pd(PPh_3)_4$, 0.0176 g ($9.24 \cdot 10^{-5}$ mol) of CuI, 257 µL ($1.85 \cdot 10^{-3}$ mol) of triethylamine in 10 mL of 1,4-dioxane/H_2O 3:1 was prepared in a 25 mL double necked flask equipped with a condenser, a small magnet and Ar inlet. Then 0.2400 g ($8.81 \cdot 10^{-4}$ mol) of (9) in 6 mL of 1,4-dioxane/H_2O 3:1 were added. The reaction mixture was then refluxed under Ar for 17 hours until the disappearance of (9) (criteria: TLC on alumina using petroleum ether/ethyl acetate 95:5 as eluant). After cooling to room temperature, the mixture was filtered off, the filter washed with CH_2Cl_2 and the solvent evaporated under reduced pressure. The residue was purified on chromatographic column on alumina (150 mesh) using petroleum ether/ethyl acetate 95:5 as eluant. The obtained product is a yellow solid.

Yield: 40%

^1H NMR (CD_2Cl_2, ppm) (figure 83): δH = 8.72 (ddd, 2H), 8.64 (ddd, 2H), 8.62 (s, 2H), 7.90 (td, 2H), 7.59 (dd, 1H), 7.45 (dd, 1H), 7.38 (ddd, 2H), 7.32 (dd, 1H), 7.28 (s, 1H), 7.26 (dd, 1H), 7.15 (dd, 1H), 7.08 (dd, 1H).

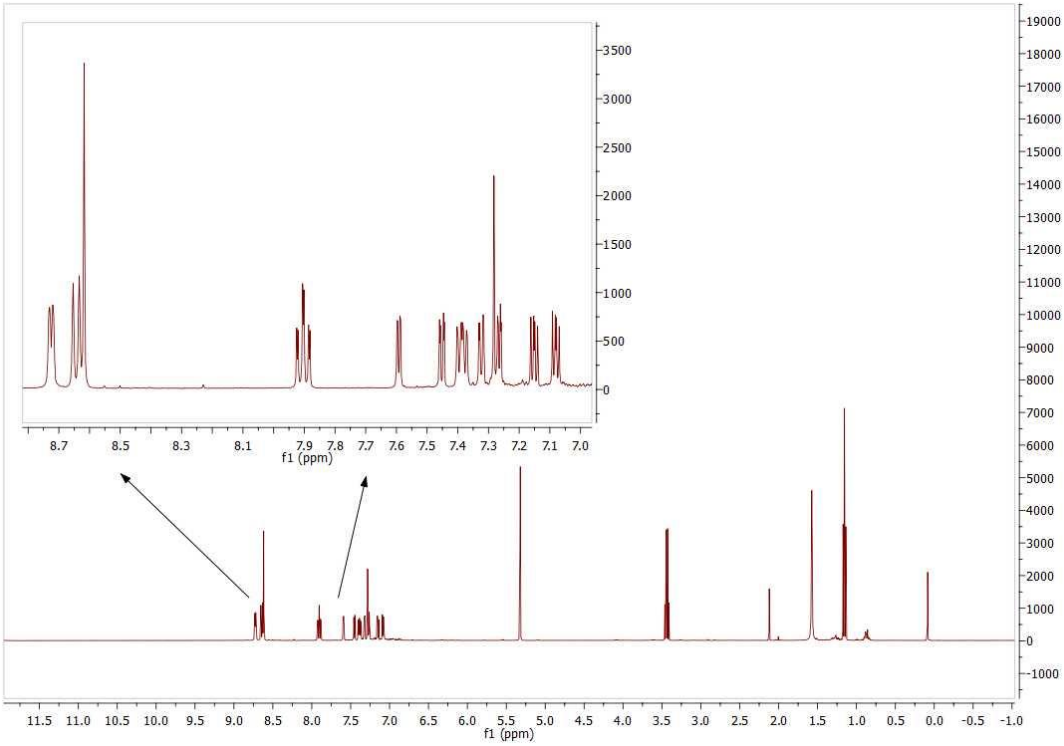

Figure 83: ^{1}H NMR spectrum of 4′-(2,2′:5′,2′′-terthien-3′-ethynyl)-2,2′:6′,2′′-terpyridine (TAT) (6)

2.3.8 Synthesis of [(TAT)Ru(TpyCOOH)][PF$_6$]$_2$ (10)

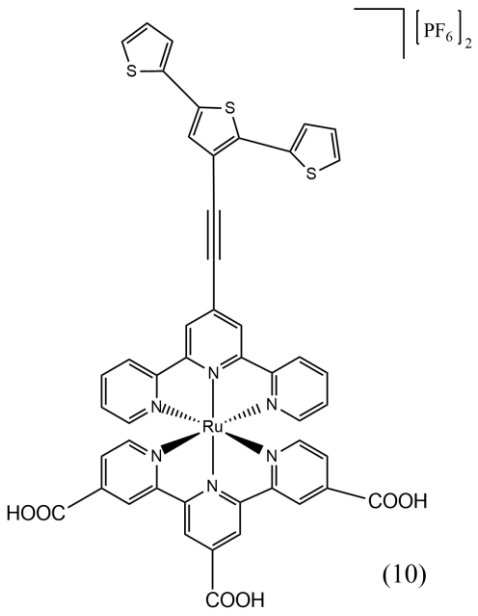

(10)

In this synthesis the reaction conditions reported by P. Manca et al.[101] were used.

The synthesis of the heteroleptic ruthenium(II) complex, $[(TAT)Ru(TpyCOOH)]^{2+}$ (TAT = 4′-(2,2′:5′,2′′-terthien-3′-ethynyl)-2,2′:6′,2′′-terpyridine; TpyCOOH = 4,4′,4′′-tricarboxylate-2,2′:6′,2′′-terpyridine) is divided into two steps: a first reaction between TAT and $RuCl_3 \cdot 3H_2O$ and a successive second reaction between the obtained $[(TAT)RuCl_3]$ and TpyCOOH.

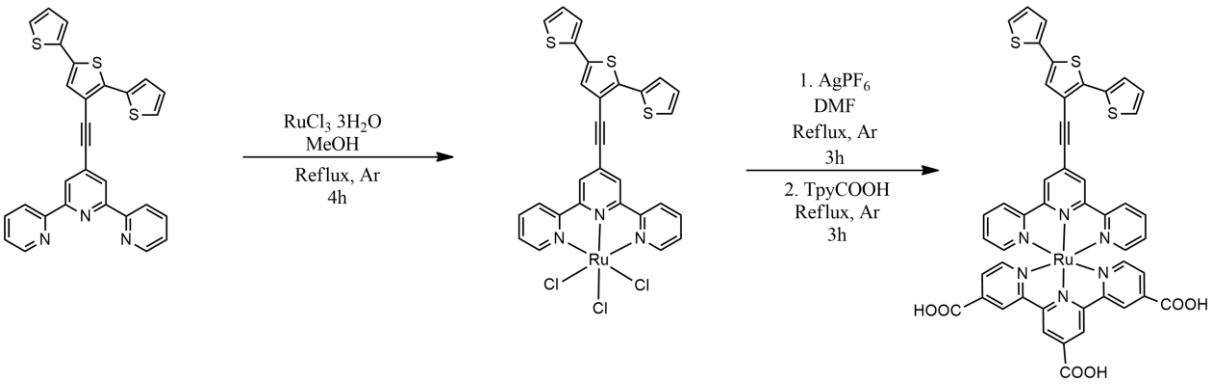

1° Step: Synthesis of $[(TAT)RuCl_3]$

0.0730 g ($1.45 \cdot 10^{-4}$ mol) of TAT were dissolved in 10 mL of hot methanol in a 25 mL double necked flask equipped with a condenser, a small magnet and Ar inlet. Then 0.0380 g ($1.45 \cdot 10^{-4}$ mol) of $RuCl_3 \cdot 3H_2O$ were added. The solution was stirred and refluxed for 4 hours. The resulting precipitate was filtered off and washed with CH_3CN, with $CHCl_3$ to remove unreacted TAT and with Et_2O to remove unreacted $RuCl_3$.

Yield: 68%

2° Step: Synthesis of $[(TAT)Ru(TpyCOOH)][PF_6]_2$ (10)

0.0700 g ($9.80 \cdot 10^{-5}$ mol) of $[(TAT)RuCl_3]$ were dissolved in 10 mL of DMF in a 25 mL double necked flask equipped with a condenser, a small magnet and Ar inlet. 0.0740 g ($2.28 \cdot 10^{-4}$ mol) of silver hexafluorophosphate ($AgPF_6$) were added. The solution was

refluxed for 3 hours. After cooling to room temperature, the solution was filtered over a pad of celite to remove AgCl and then reacted with 0.0370 g ($1.02 \cdot 10^{-4}$ mol) of TpyCOOH refluxing for 3 hours. After cooling to room temperature, the solvent was removed under vacuo and the residue was dissolved in CH_3CN and precipitated with Et_2O. The product is a dark red solid.

Yield: 62%

^1H NMR (d_6-DMSO, ppm): δH = 9.70 (m, 2H), 9.39 (s, 2H) partially overlapping, 9.37 (s, 2H) partially overlapping, 9.34 (s, 2H), 8.84-8.76 (m, 2H), 8.50-8.45 (m, 2H), 8.38 (d, 2H), 8.24 (d, 1H) partially overlapping, 8.21 (d, 1H) partially overlapping, 8.10-8.03 (m, 3H), 8.00-7.86 (m, 4H), 7.71 (dd, 1H), 7.61 (dd, 1H)

CHAPTER 3

RESULTS AND DISCUSSION

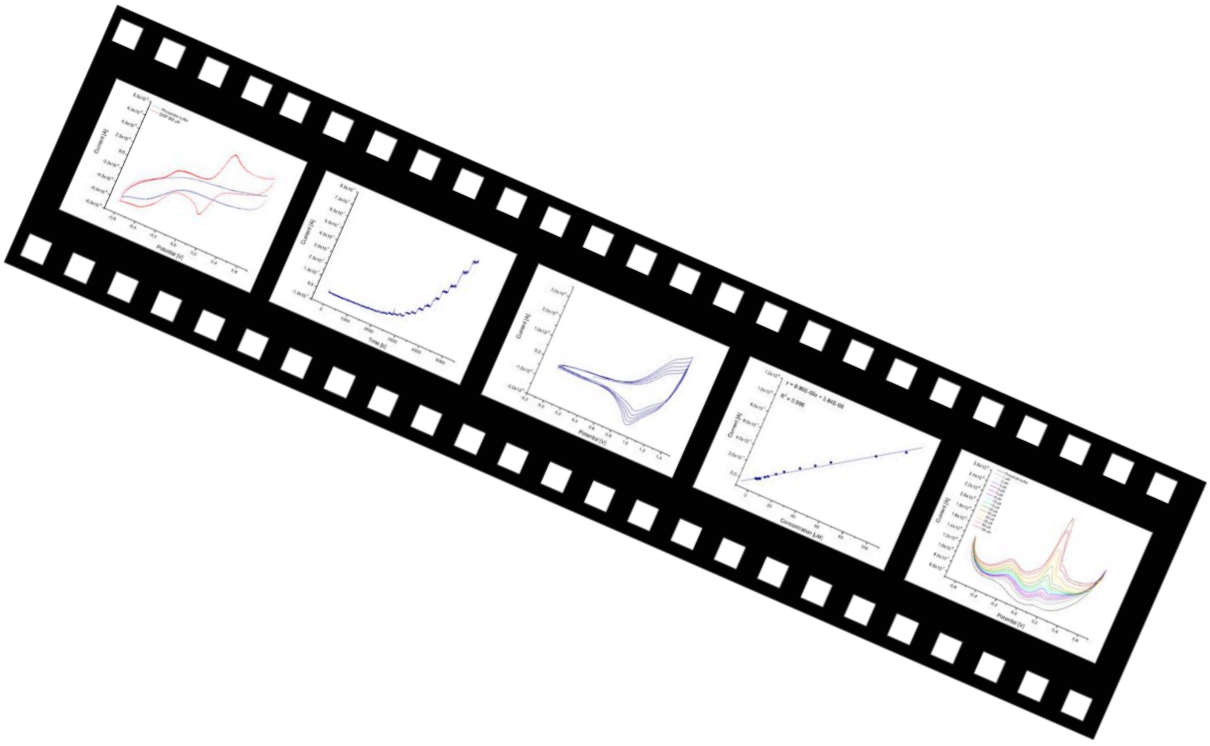

3.1 Electrochemical Characterization of Monomers and of Their Corresponding Polymers

All the voltammetric studies were performed using $CH_2Cl_2/TEAPF_6$ or $CH_3CN/TEAPF_6$ or $CH_2Cl_2/TBABF_4$ 0.1 M or 0.01 M as solvent/electrolyte systems, depending on the considered monomer species. Monomer concentrations were chosen between $2 \cdot 10^{-3}$ and 10^{-2} M in order to allow the subsequent electropolymerization step. All these measurements were carried out in a three-electrode cell configuration with Ag/AgCl as reference, graphite bar or Pt wire as counter and platinum, gold or glassy carbon disk as working electrodes.

3.1.1 4,4′-([2,2′-bithiophene]-4-4′-diyl)bis(2-methylbut-3-yn-2-ol) (1)

(1) was characterized and then electropolymerized in $CH_3CN/TEAPF_6$ 0.1 M using a monomer concentration of 10^{-2} M, scanning the potential between 0 and 1.5 V with a platinum disk as working electrode[9]. The voltammetric response (figure 84) shows a peak at about 1.4 V attributable to the oxidation of the thiophene fragment. It is also possible to observe a return peak at about 1.1 V.

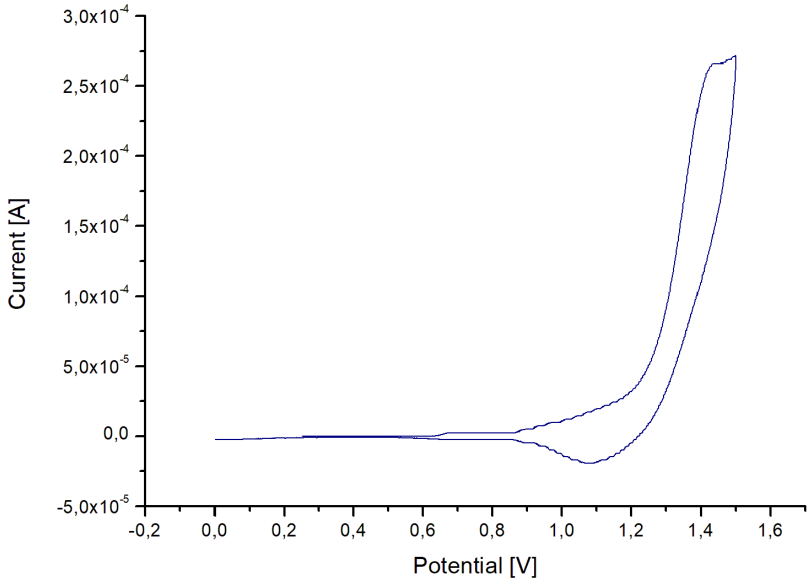

Figure 84: CV characterization of 10^{-2} M 4,4′-([2,2′-bithiophene]-4-4′-diyl)bis(2-methylbut-3-yn-2-ol) (1) in $CH_3CN/TEAPF_6$; potential scan rate: 100 mV s^{-1}

Subsequent scans showed progressive increases in current, typical of an anodic polymerization behaviour (figure 85), and a simultaneous formation of a red-coloured film.

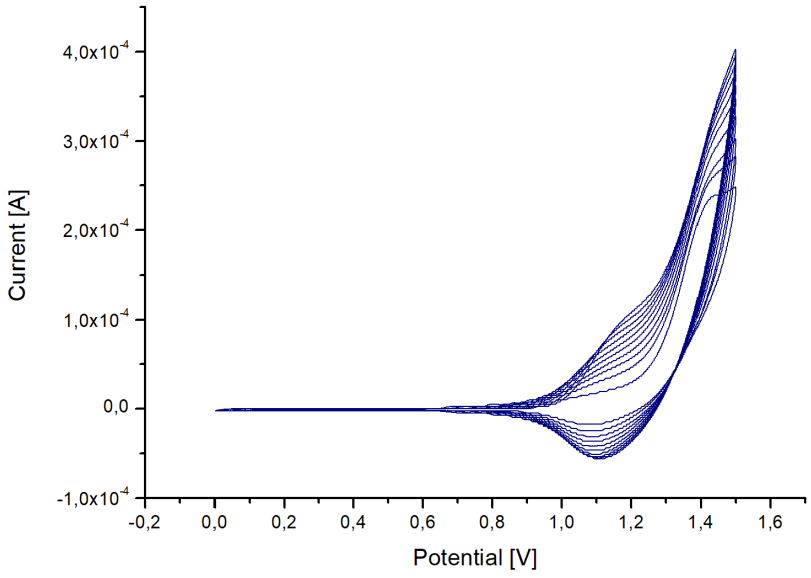

Figure 85: cyclic voltammograms of 10^{-2} M 4,4′-([2,2′-bithiophene]-4-4′-diyl)bis(2-methylbut-3-yn-2-ol) (1) on platinum disk electrode in $CH_3CN/TEAPF_6$ 0.1 M (10 scans); potential scan rate: 100 mV s^{-1}

In addition to the potentiodynamic polymerization, the potentiostatic one was also performed by setting the potential at 1.35 V for a time interval necessary to reach a charge density value of 10 mC (≈ 320 mC cm^{-2}). The obtained film was then neutralized setting the potential at 0 V for 60 s. In figure 86 the characterizations of the films obtained by cyclic voltammetry (10 scans) and chronoamperometry are reported. Characterizations were performed in the same solvent/electrolyte system without the monomer.

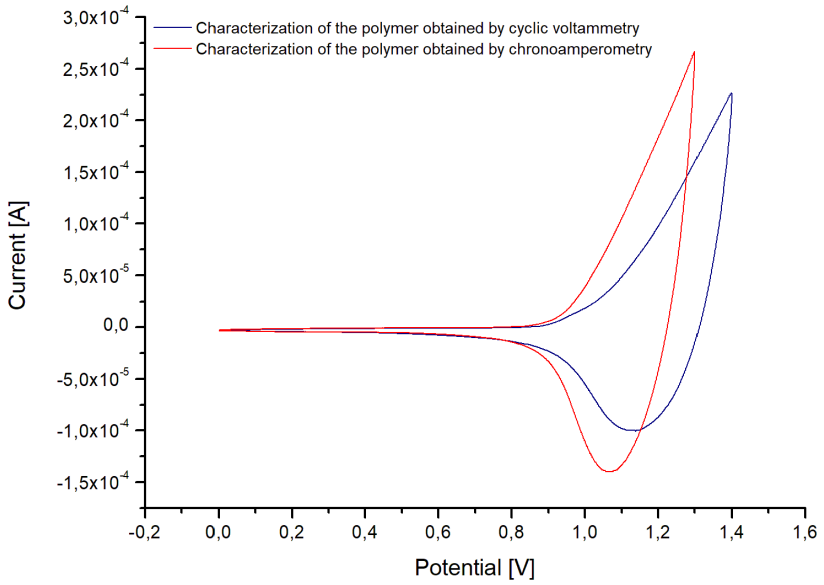

Figure 86: (blue line) CV characterization of poly[4,4′-([2,2′-bithiophene]-4-4′-diyl)bis(2-methylbut-3-yn-2-ol)] in $CH_3CN/TEAPF_6$ obtained by cyclic voltammetry (10 scans) and (red line) CV characterization of poly[4,4′-([2,2′-bithiophene]-4-4′-diyl)bis(2-methylbut-3-yn-2-ol)] in $CH_3CN/TEAPF_6$ obtained by chronoamperometry (Q_{dep} = 320 mC cm^{-2}); potential scan rate 100 mV s^{-1}

In both of them doping processes are not particularly evident because they occur at potentials very close to that in which the scan is reversed: 1.30 and 1.35 for the film obtained in chronoamperometry and in cyclic voltammetry, respectively. However, reduction peaks at about 1.1 V are well visible and attributable to polymer dedoping processes.

3.1.2 4-(4′-bromo-[2,2′-bithiophen]-4-yl)-2-methylbut-3-yn-2-ol (2)

(2) was characterized in $CH_3CN/TEAPF_6$ 0.1 M using a monomer concentration of 10^{-2} M, scanning the potential between 0 and 1.6 V with a platinum disk as working electrode. The voltammetric response (figure 87) shows a peak at 1.53 V attributable, also in this case, to the oxidation of the thiophene fragment, with a return peak at about 1.2 V.

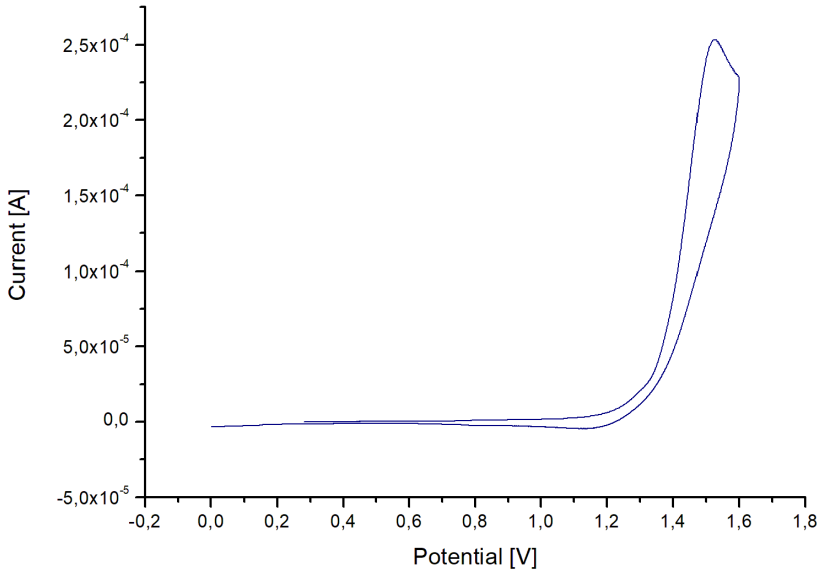

Figure 87: CV characterization of 10^{-2} M 4-(4′-bromo-[2,2′-bithiophen]-4-yl)-2-methylbut-3-yn-2-ol (2) in $CH_3CN/TEAPF_6$; potential scan rate: 100 mV s^{-1}

Even for (2) subsequent scans showed progressive increases in current, typical of an anodic polymerization behaviour (figure 88), and a simultaneous formation of a deep-red coloured film.

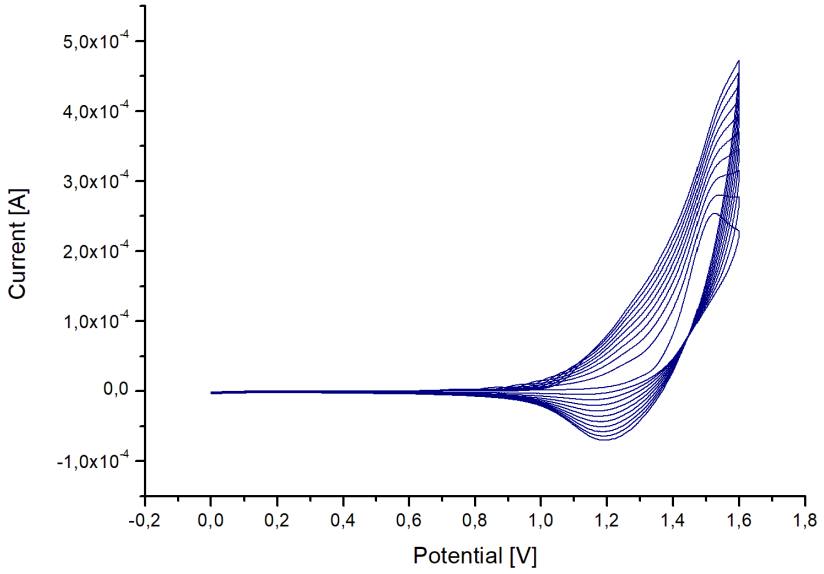

Figure 88: cyclic voltammograms of 10^{-2} M 4-(4′-bromo-[2,2′-bithiophen]-4-yl)-2-methylbut-3-yn-2-ol (2) on platinum disk electrode in $CH_3CN/TEAPF_6$ 0.1 M (10 scans); potential scan rate: 100 mV s^{-1}

Electrodeposition of the polymer film was performed using cyclic voltammetry (10 scans) and chronoamperometry at 1.55 V until a charge density value of 10 mC (≈ 320 mC cm^{-2}) has been reached. In figure 89 characterizations of the films obtained by cyclic voltammetry and chronoamperometry are reported. In the first one (blue line) it is possible to observe a slightly marked peak at about 1.30 V, probably attributable to oligomers, and a much more visible reduction peak at about 1.2 V ascribable to the polymer dedoping process. Polymer doping peak is, instead, not well visible because, as in the previous case, it occurs at potential of about 1.5 where the scan is reversed. In the latter (red line), two oxidation peaks, one well visible at about 1.1 V and one slightly evident at about 1.25 V, are present and it is possible to observe a dedoping peak at 1.2 V, that is sharper than that observed for the film obtained by the potentiodynamic technique. Even in this case the doping peak of the polymer is not well visible and the distinguishable oxidation peaks could be attributed to oligomers of different chain length.

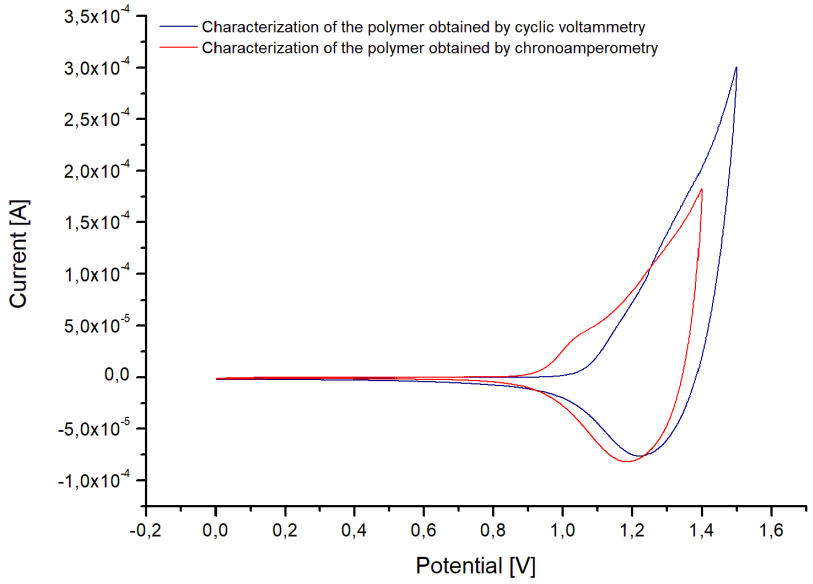

Figure 89: (blue line) CV characterization of poly[4-(4′-bromo-[2,2′-bithiophen]-4-yl)-2-methylbut-3-yn-2-ol] in $CH_3CN/TEAPF_6$ obtained by cyclic voltammetry (10 scans) and (red line) CV characterization of poly[4-(4′-bromo-[2,2′-bithiophen]-4-yl)-2-methylbut-3-yn-2-ol] in $CH_3CN/TEAPF_6$ obtained by chronoamperometry (Q_{dep} = 320 mC cm^{-2}); potential scan rate 100 mV s^{-1}

3.1.3 4,4′-diethynil-2,2′-bithiophene (3)

(3) was characterized in $CH_3CN/TEAPF_6$ and in $CH_3CN/TBABF_4$ 0.1 M using a monomer concentration of 10^{-2} M, scanning the potential between 0 and 1.4 V and between 0 and 1.6 V, both with platinum and gold as working electrodes.

Between 0 and 1.4 V, in both investigated solvent/electrolyte systems, for the first two/three scans neither oxidation nor reduction processes are particularly evident (figure 90a). However, what can be observed is the sudden increase in current around 1.3 V which could be attributable to the beginning of the polymerization of the monomer. After the second or third scan, an oxidation peak began to appear at about 0.9 V and it could be related to the oxidation of oligomers (figure 90b).

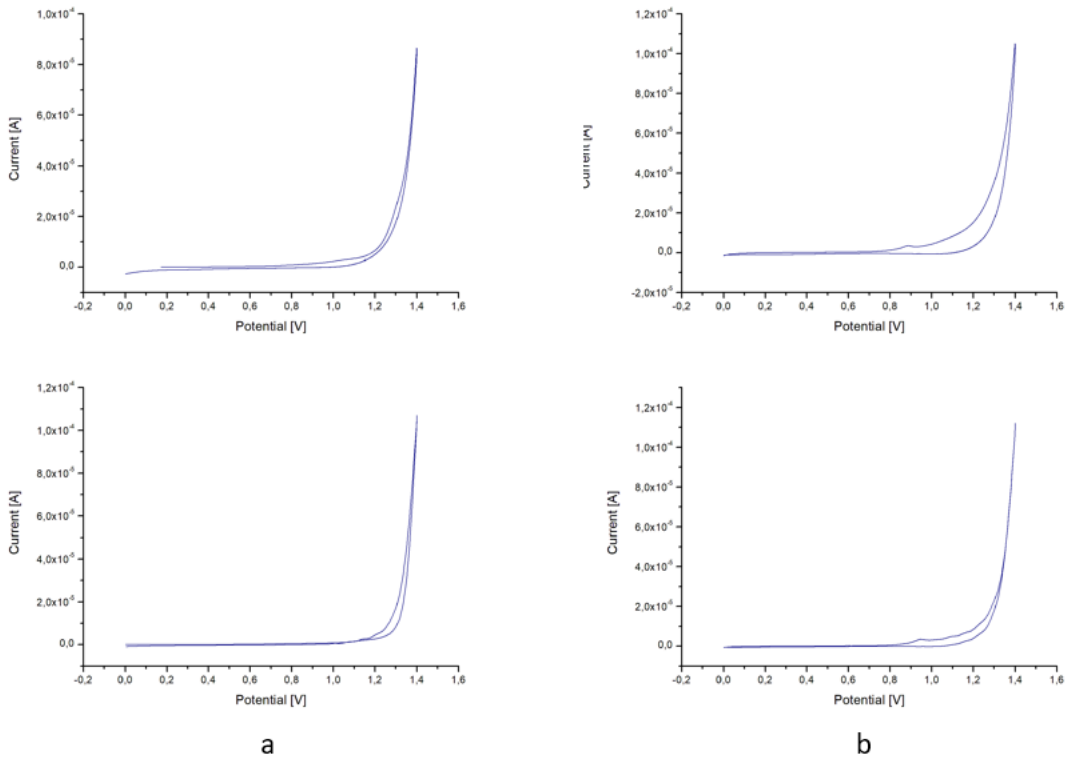

Figure 90: CV characterization of 10^{-2} M of 4,4'-diethynil-2,2'-bithiophene (3) on platinum disk electrode (a) first scan in $CH_3CN/TEAPF_6$ 0.1 M (top) and in $CH_3CN/TBABF_4$ 0.1 M (down); (b) third scan in $CH_3CN/TEAPF_6$ 0.1 M (top) and in $CH_3CN/TBABF_4$ 0.1 M (down); potential scan rate 100 mV s^{-1}

An increasing of the number of scans shows a shift of the oligomer oxidation peak to increasingly anodic values, thus reflecting an oxidation process that is, gradually, more difficult (figure 91). Nevertheless, at potential values higher than 1.3 V, for subsequent scans, the current shows an increase suggesting, however, a possible formation of a polymer film.

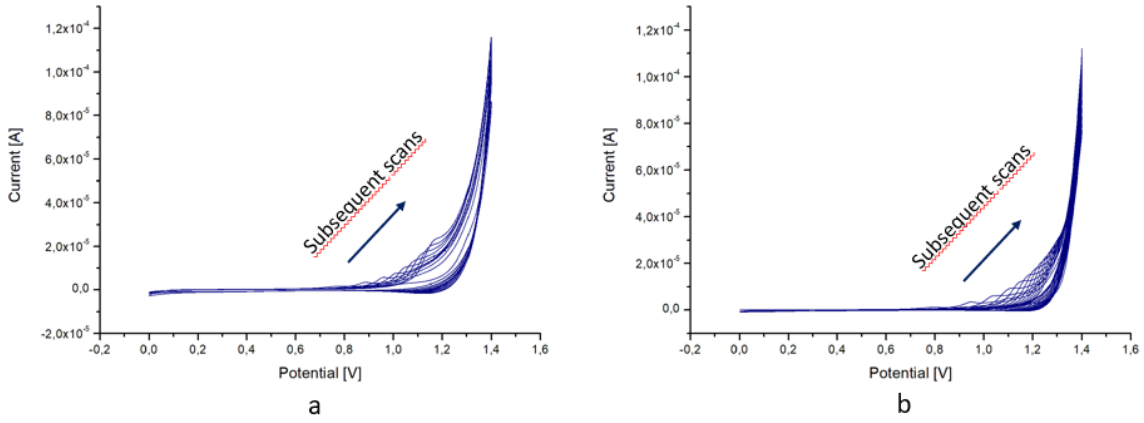

Figure 91: cyclic voltammograms of 10^{-2} M 4,4′-diethynil-2,2′-bithiophene (3) on platinum disk electrode in (a) $CH_3CN/TEAPF_6$ 0.1 M (10 scans) and (b) $CH_3CN/TBABF_4$; potential scan rate: 100 mV s^{-1}

Actually, yellow and green films were observed on the electrode surfaces when the process was performed in $CH_3CN/TEAPF_6$ and $CH_3CN/TBABF_4$, respectively.

The obtained films were characterized in the same solvent/electrolyte systems without monomer (figure 92). In the former (figure 92a) it is possible to note an oxidation peak at about 1.15 V attributable to oligomers and a reduction peak at about 1.25 V that is ascribable to a polymer dedoping process whose associated doping is not clearly visible. In the latter (figure 92b) the oxidation peak of the oligomers appears at about 1.25 V. Dedoping polymer peak is just slightly shifted at higher potential value than that observed in figure 92a.

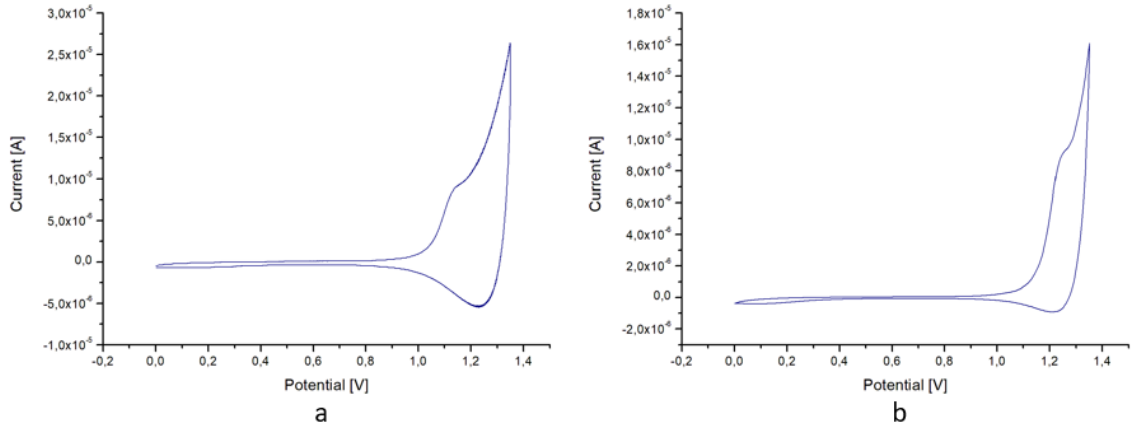

Figure 92: CV characterization of poly(4,4′-diethynil-2,2′-bithiophene) obtained by cyclic voltammetry (10 scans) (a) obtained in $CH_3CN/TEAPF_6$ 0.1 M and (b) in $CH_3CN/TBABF_4$ 0.1 M; potential scan rate 100 mV s^{-1}

Other tests were performed by chronoamperometry by setting the potential at 1.17 V, 1.2 V and 1.3 V until a charge value of 1.5 mC (≈ 48 mC cm^{-2}) was reached. Then, the obtained film (also in this case yellow- and green-coloured) were neutralized at 0 V for 60 s. The only appreciable characterization was that of the obtained green film at 1.3 V in $CH_3CN/TBABF_4$ (figure 93a). The others, on the other hand, in addition to not highlighting any type of process, also showed lower current values (figure 93b).

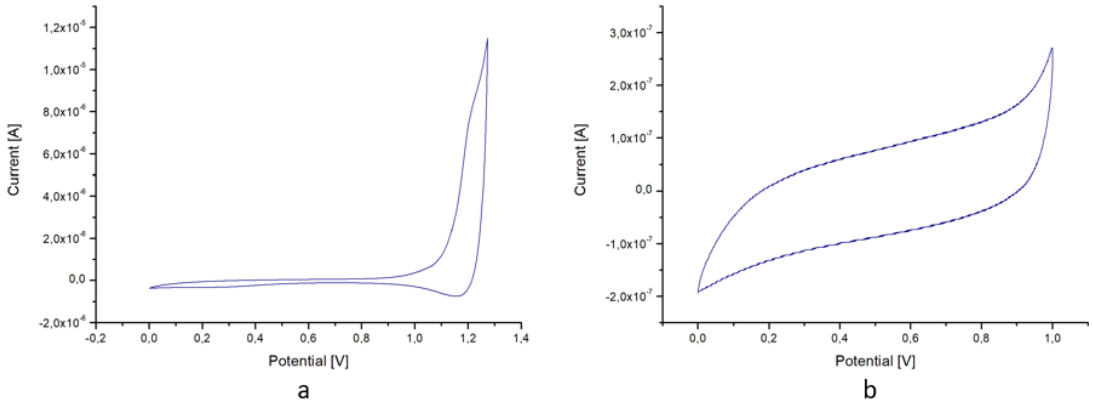

Figure 93: CV characterization of poly(4,4'-diethynil-2,2'-bithiophene) obtained by chronoamperometry at (a) 1.30 V vs. Ag/AgCl in $CH_3CN/TBABF_4$ 0.1 M and (b) 1.17 V vs. Ag/AgCl in $CH_3CN/TEAPF_6$ 0.1 M; potential scan rate 100 mV s^{-1}

Scanning the potential between 0 and 1.6 V in $CH_3CN/TEAPF_6$ 0.1 M, using gold electrode, it was observed, no earlier than the fourth scan, a broad oxidation peak at about 1.5 V and a reduction peak at about 1.2. After the first fourth scans, in which no redox process seemed to occur, a typical polymerization behaviour occurred (figure 94), which, however, was not observed with the platinum electrode.

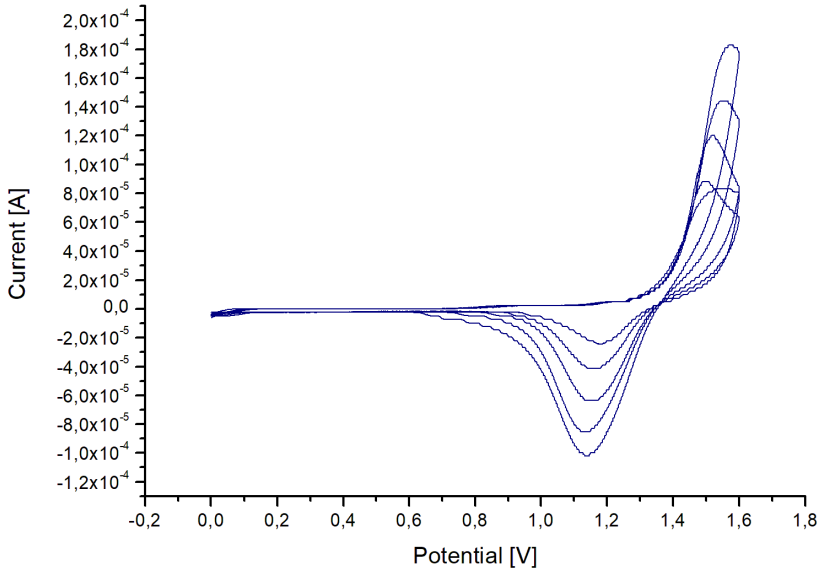

Figure 94: cyclic voltammograms of 10^{-2} M 4,4′-diethynil-2,2′-bithiophene (3) on gold disk electrode in $CH_3CN/TEAPF_6$ 0.1 M from the fourth to the ninth scan; potential scan rate: 100 mV s^{-1}

The obtained deep-red coloured film was characterized in the same solvent/electrolyte system without monomer, highlighting a very well-marked reduction peak at about 1.15 V but no oxidation processes are clearly visible but it is identifiable at about 1.5 V (when the scan is reversed) (figure 95).

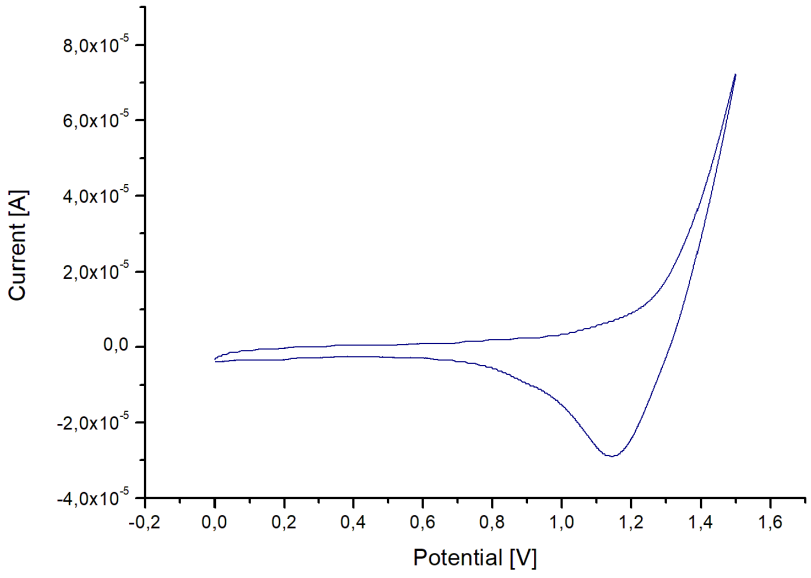

Figure 95: CV characterization of poly(4,4′-diethynil-2,2′-bithiophene) obtained by cyclic voltammetry (10 scans) on gold disk electrode in $CH_3CN/TEAPF_6$ 0.1 M; potential scan rate: 100 mV s^{-1}

Nevertheless, this polymerization process was not reproducible. In particular, an analogous behaviour to that shown in figure 95 has been observed only a few times and with the freshly prepared monomer solution. A hypothesis on the difficulty of polymerization could be related to a high sensitivity of the monomer to humidity.

3.1.4 4,4′-([2,2′-bithiophene]-4,4′-diyilbis(ethyne-2,1-diyl))dibenzeneaminium (4)

(4) was characterized in $CH_3CN/TEAPF_6$ and in CH_2Cl_2 (with 1% of methanol to increase solubility)/$TEAPF_6$ 0.1 M using a concentration of $5 \cdot 10^{-3}$ M using both platinum and glassy carbon electrodes. In $CH_3CN/TEAPF_6$ the voltammograms show a very similar behaviour for platinum and glassy carbon: two oxidation peaks at about 0.9 V and 1.4 V (anticipated for platinum electrode) (figure 96).

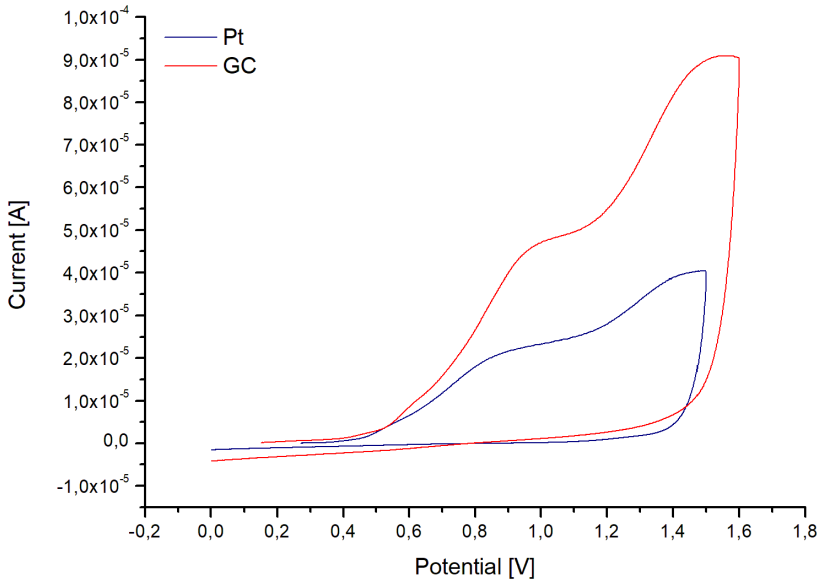

Figure 96: CV characterization of $5 \cdot 10^{-3}$ M 4,4′-([2,2′-bithiophene]-4,4′-diyilbis(ethyne-2,1-diyl))dibenzeneaminium in $CH_3CN/TEAPF_6$ 0.1 M on platinum (blue line) and glassy carbon (red line) electrodes; potential scan rate: 100 mV s^{-1}

In CH_2Cl_2/$TEAPF_6$ it is possible to observe with the platinum electrode three anodic peaks at about 0.9 V, 1.1 V and 1.45 V with the last one more sharped (figure 97a) and only one peak at 1.55 with glassy carbon (figure 97b). In all cases no reduction peaks are visible.

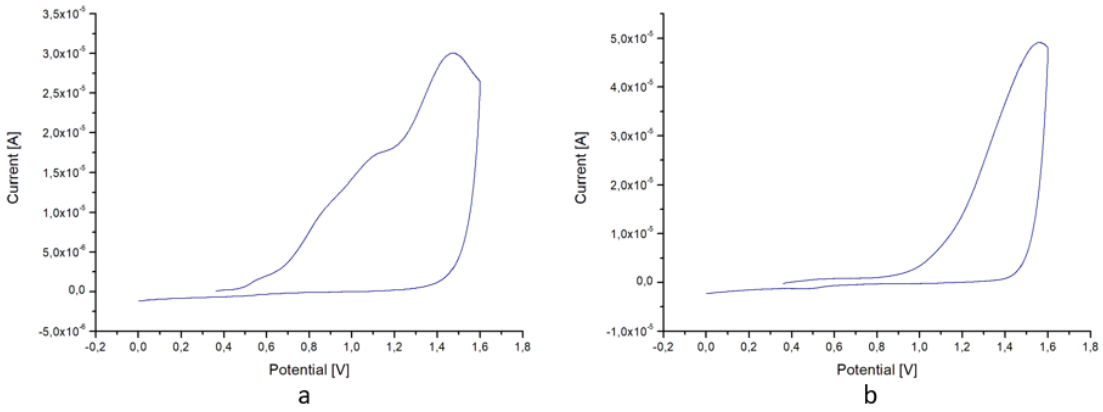

Figure 97: CV characterization of $5 \cdot 10^{-3}$ 4,4′-([2,2′-bithiophene]-4,4′-diyilbis(ethyne-2,1-diyl))dibenzeneaminium in CH_2Cl_2/$TEAPF_6$ 0.1 M on (a) platinum and (b) glassy carbon electrodes; potential scan rate: 100 mV s^{-1}

At each successive scan the current decreased (figure 98) and no film deposition was observed.

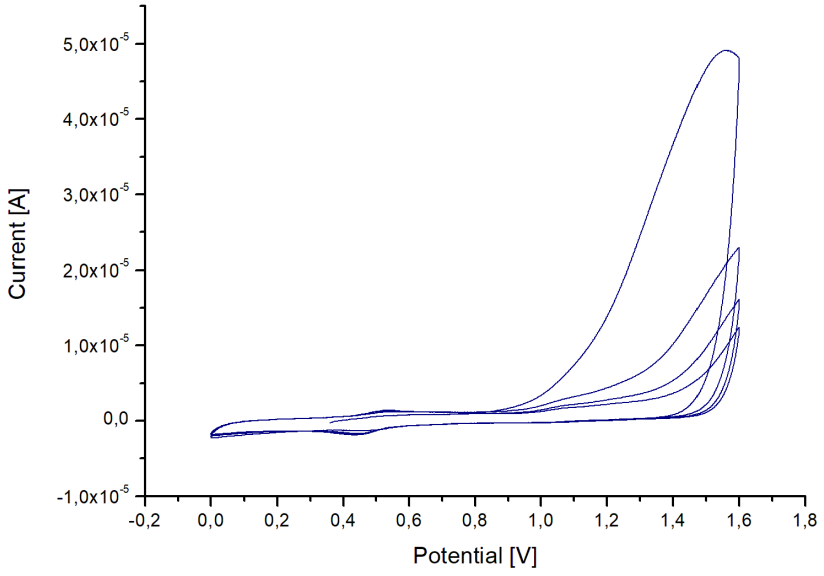

Figure 98: cyclic voltammograms of $5 \cdot 10^{-3}$ M 4,4′-([2,2′-bithiophene]-4,4′-diyilbis(ethyne-2,1-diyl))dibenzeneaminium on glassy carbon disk electrode in CH_2Cl_2/$TEAPF_6$ 0.1 M; potential scan rate: 100 mV s^{-1}

However, in CH_2Cl_2 added with methanol, on GC electrode a blue deposit was observed but the characterization did not show neither oxidation nor reduction processes (figure 99).

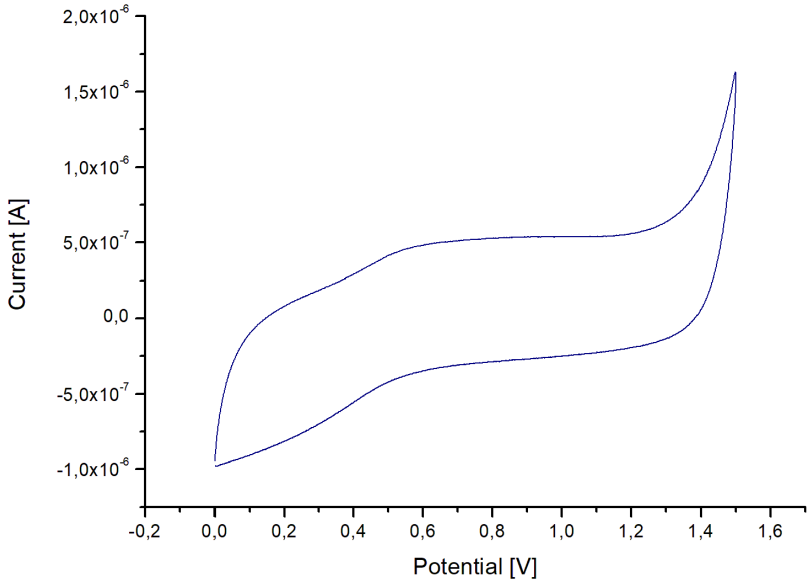

Figure 99: CV characterization of the blue layer deposited by cyclic voltammetry on a glassy carbon electrode in CH_2Cl_2/$TEAPF_6$ 0.1 M; potential scan rate: 100 mV s^{-1}

Polymerization/deposition tests were also carried out by chronoamperometry at 1.4 V and 1.5 V on GC in the same solvent/electrolyte system, showing only in the latter case blue deposit layer which characterization (figure 100) is not so different from that obtained with the potentiodynamic technique.

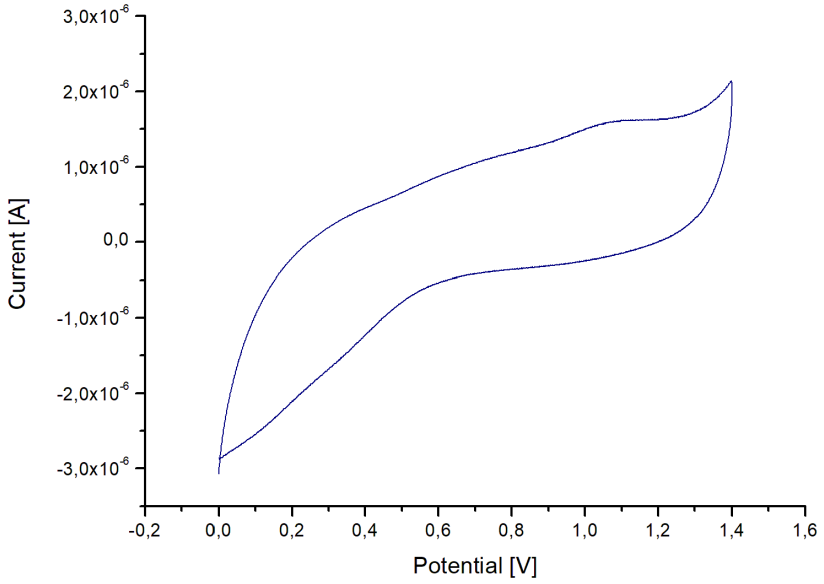

Figure 100: CV characterization of the blue layer deposited by chronoamperometry at 1.50 V vs. Ag/AgCl on a glassy carbon electrode in CH_2Cl_2/$TEAPF_6$ 0.1 M; potential scan rate: 100 mV s^{-1}

To overcome the low solubility of the monomer in CH_2Cl_2, a polymerization test was performed using as solvent/electrolyte system CH_2Cl_2/CH_3CN 4:1/$TEAPF_6$ 0.1 M. Even in this case the first scan shows two oxidation peaks at about 0.9 V and 1.2 V, slightly lower than those observed in the analysis performed using only CH_3CN or CH_2Cl_2 (with methanol) (figure 101).

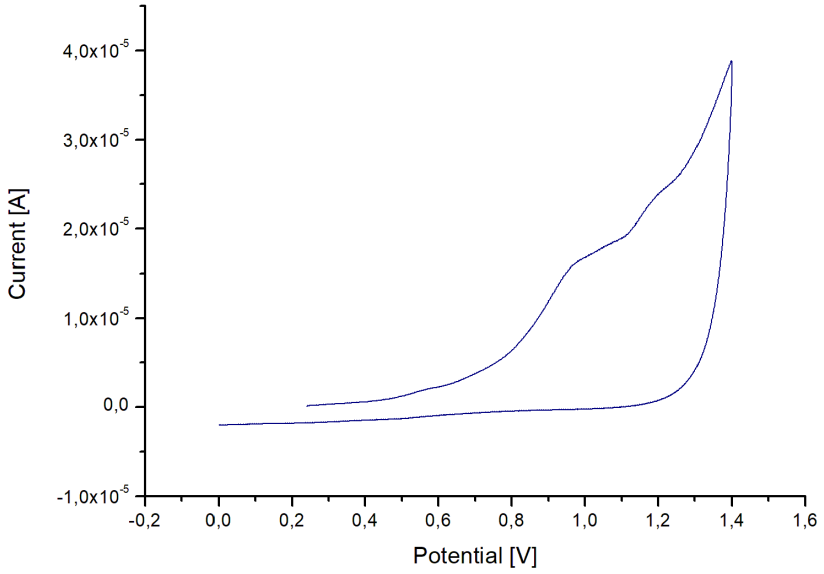

Figure 101: CV characterization of $5 \cdot 10^{-3}$ M 4,4′-([2,2′-bithiophene]-4,4′-diyilbis(ethyne-2,1-diyl))dibenzeneaminium in CH_2Cl_2/CH_3CN(4:1)/$TEAPF_6$ 0.1 M on glassy carbon electrode; potential scan rate: 100 mV s^{-1}

Attempts of polymerization/deposition were carried out scanning the potential between 0 and 1.4 V and 0 and 1.2 V. No typical polymerization behaviour, neither deposition of a film, was observed.

3.1.5 4′-(2,2′:5′,2′′-terthien-3′-ethynyl)-2,2′:6′,2′′-terpyridine (TAT) (6)

(6) was characterized in $CH_2Cl_2/TEAPF_6$ 0.1 M using a monomer concentration of $2 \cdot 10^{-3}$ M, scanning the potential between 0 and 1.6 V with gold, platinum and glassy carbon electrodes. In figure 102 the characterization with the platinum electrode is reported. Two anodic peaks are observed: a first one at 1.15 V attributable to the oxidation of the thiophene fragment, and a second at 1.46 V ascribable to the terpyridine moiety[146]. An associated cathodic peak centred at 0.9 V is also well visible.

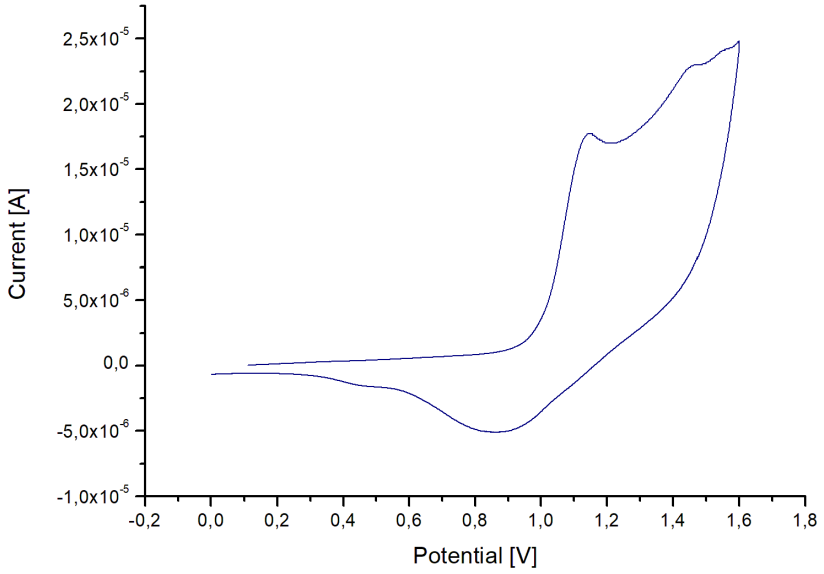

Figure 102: CV characterization of $2 \cdot 10^{-3}$ M 4′-(2,2′:5′,2′′-terthien-3′-ethynyl)-2,2′:6′,2′′-terpyridine (TAT) (6) on platinum electrode in CH_2Cl_2/$TEAPF_6$ 0.1 M; potential scan rate: 100 mV s^{-1}

Scanning the potential between 0 and 1.2 V the current increases for each successive scan showing the classical behaviour of an anodic polymerization process. In figure 103 the polymerization processes by cyclic voltammetry performed using platinum disk electrode is reported.

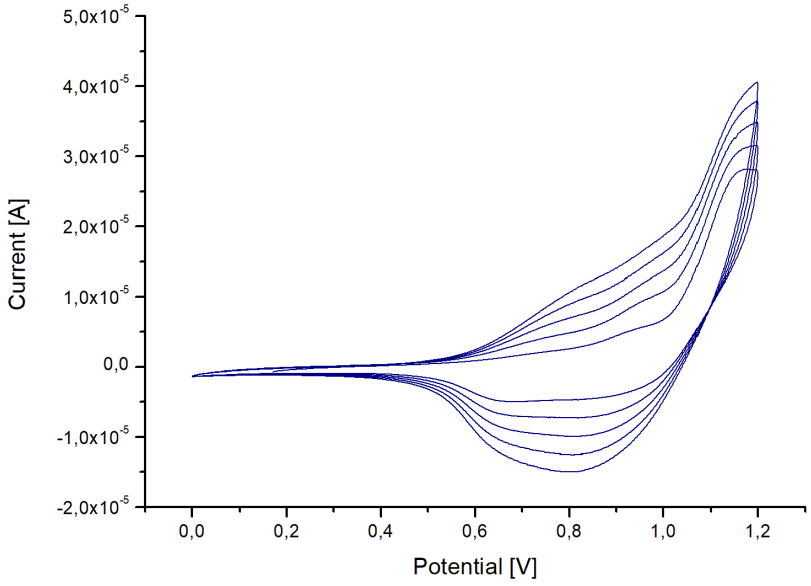

Figure 103: cyclic voltammograms of $2 \cdot 10^{-3}$ M 4′-(2,2′:5′,2′′-terthien-3′-ethynyl)-2,2′:6′,2′′-terpyridine (TAT) (6) in CH_2Cl_2/$TEAPF_6$ 0.1 M on platinum; potential scan rate: 100 mV s^{-1}

The polymerization process was also performed by chronoamperometry in order to control the charge density and consequently the thickness of the film. The process was carried out setting the potential at 1.16 V, until a charge of 1 mC (≈ 32 mC cm^{-2} for platinum and ≈ 15 mC cm^{-2} for glassy carbon) was reached. Then, the polymer films were neutralized at 0 V for 60 s. Characterizations were performed using $CH_3CN/TEAPF_6$ 0.1 M instead of $CH_2Cl_2/TEAPF_6$ 0.1 M in such a way to make a comparison with the characterization reported by Manca et al.[146]. Figure 104 shows in both cases oxidation peak at about 0.98 V and an associated reduction peak at about 0.85 V attributable to the polymer doping and dedoping processes, respectively.

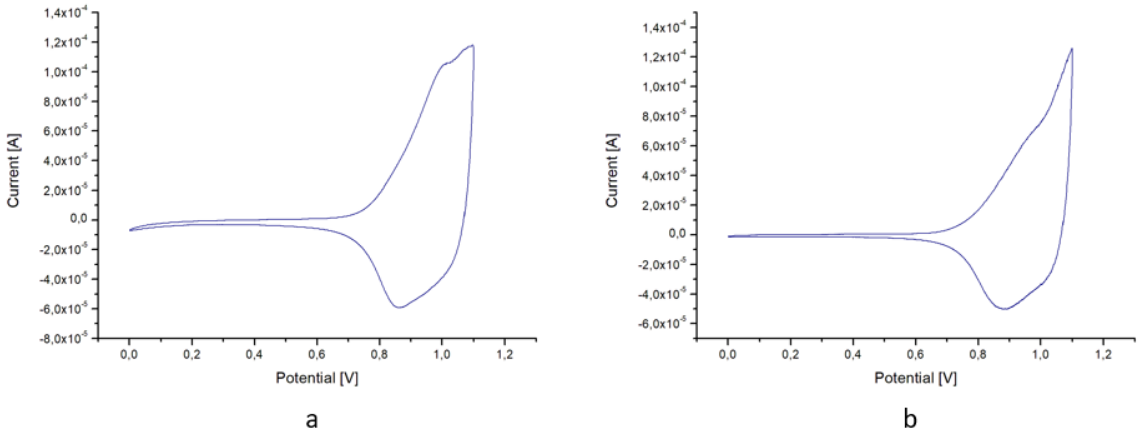

Figure 104: CV characterization in $CH_3CN/TEAPF_6$ 0.1 M of poly[4′-(2,2′:5′,2′′-terthien-3′-ethynyl)-2,2′:6′,2′′-terpyridine] poly(TAT) obtained by chronoamperometry at 1.16 V vs. Ag/AgCl in $CH_2Cl_2/TEAPF_6$ 0.1 M on (a) platinum and (b) glassy carbon electrodes; potential scan rate: 100 mV s^{-1}

3.1.6 [(TAT)Ru(TpyCOOH)][PF_6]$_2$ (10)

(10) was characterized in $CH_2Cl_2/TEAPF_6$ 0.1 M using a monomer concentration of $5 \cdot 10^{-3}$ M with platinum, gold and glassy carbon electrodes. Characterization performed with platinum electrode shows two oxidation peaks: a first one at 1.06 V and a second at about 1.4 V attributable to the terthiophene and metal oxidations, respectively[101]. In the voltammogram two reduction peaks at about 1.2 V and 0.95 V are also visible

(figure 105a). With gold electrode the oxidation peaks are slightly shifted at higher potentials (figure 105b) and with glassy carbon oxidation peaks are not very evident and reduction peaks are shifted towards more cathodic values (1.07 V and 0.84 V) (figure 105c).

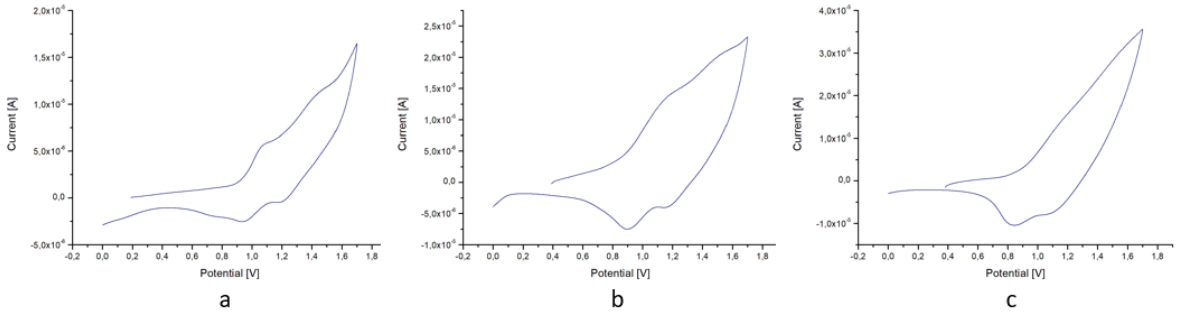

Figure 105: CV characterization of $5 \cdot 10^{-3}$ M [(TAT)Ru(TpyCOOH)][PF_6]$_2$ in CH_2Cl_2/TEAPF_6 0.1 M on (a) platinum, (b) gold and (c) glassy carbon electrodes; potential scan rate: 100 mV s^{-1}

Scanning the potential between 0 and 1.3 V the current increases for each successive scan proving that a polymerization process occurs on the terthiophene moiety. In figure 106 polymerization process performed by cyclic voltammetry on gold electrode is reported.

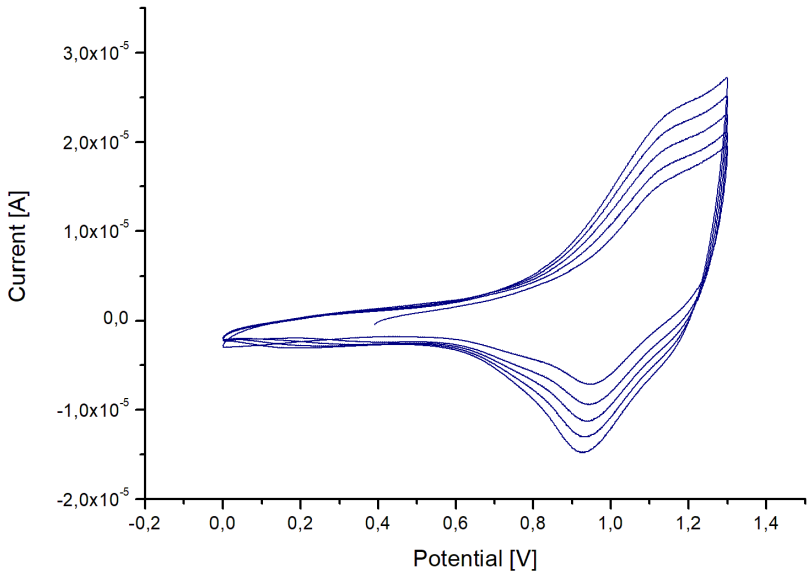

Figure 106: cyclic voltammograms of $5 \cdot 10^{-3}$ M [(TAT)Ru(TpyCOOH)][PF_6]$_2$ in CH_2Cl_2/TEAPF_6 0.1 M on gold electrode; potential scan rate: 100 mV s^{-1}

Figure 107 reports the characterizations in CH_2Cl_2 and in CH_3CN of poly[(TAT)Ru(TpyCOOH)] obtained on platinum disk electrode by cyclic voltammetry (20 scans). It is possible to note that in both voltammograms a sharped reduction peak, assignable to a polymer dedoping process, centred at 0.89 V in CH_2Cl_2 and at 1.07 V in CH_3CN is well visible. Doping peak, instead, is just barely visible in the characterization performed with CH_3CN at a potential value of 1.13 V.

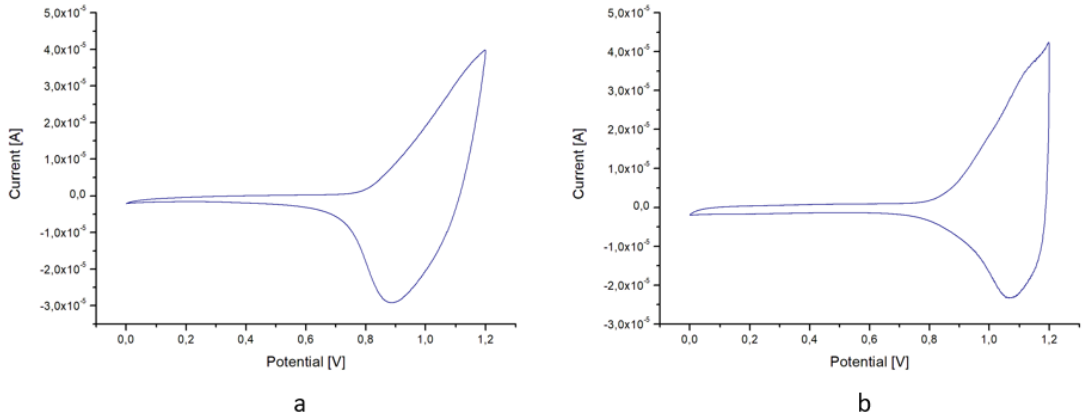

Figure 107: CV characterization of poly[(TAT)Ru(TpyCOOH)] obtained by cyclic voltammetry (20 scans) on platinum disk electrode in (a) $CH_2Cl_2/TEAPF_6$ and (b) in $CH_3CN/TEAPF_6$; potential scan rate: 100 mV s^{-1}

As for TAT, polymerization process was also performed by chronoamperometry in order to manage the film thickness. The process was carried out setting the potential at 1.05 V[101] until a charge value of 1 mC was reached. The obtained deep-red polymer films were then neutralized at 0 V for 60 s.

Figure 108 reports characterizations in $CH_3CN/TEAPF_6$ of polymer films obtained by chronoamperometry on gold ($Q_{dep} \approx 32$ mC cm^{-2}) and glassy carbon ($Q_{dep} \approx 15$ mC cm^{-2}). Characterizations were performed using $CH_3CN/TEAPF_6$ 0.1 M instead of $CH_2Cl_2/TEAPF_6$ 0.1 M in such a way to make a comparison with the characterization reported by Manca et al.[101].

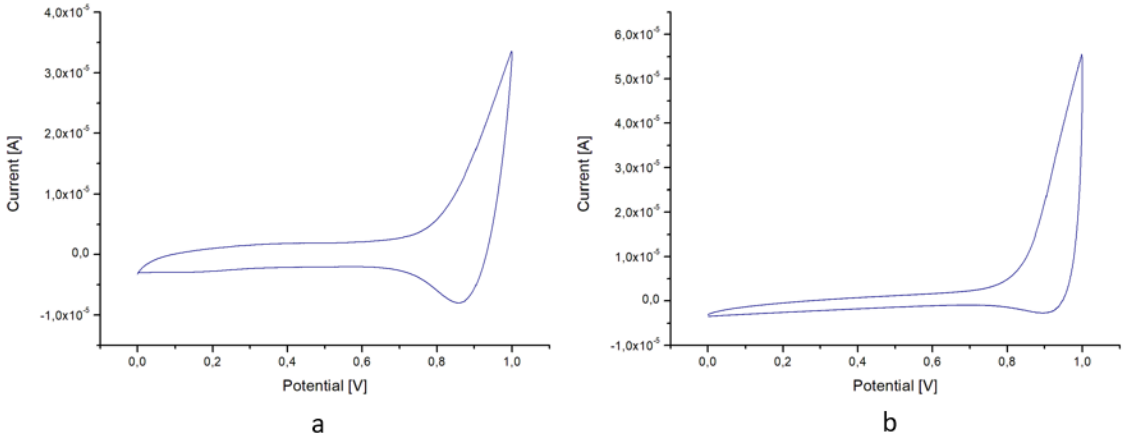

Figure 108: CV characterization of poly[(TAT)Ru(TpyCOOH)] obtained by chronoamperometry in $CH_3CN/TEAPF_6$ on (a) gold and (b) glassy carbon electrodes; potential scan rate: 100 mV s^{-1}

With gold electrode dedoping process at about 0.87 V is observed, whereas with glassy carbon electrode it is shifted at about 0.92 V. Doping peaks are not clearly evident because they occur at a potential close to, or coinciding with, the one in which the scan is reversed.

The films obtained on gold and glassy carbon electrodes by chronoamperometry were used for tyrosinase-based biosensors construction.

3.1.7 4,7-bis(5-(pyridine-2-yl)thiophen-2-yl)benzo[c][1,2,5] thiadiazole (TBT) (11)

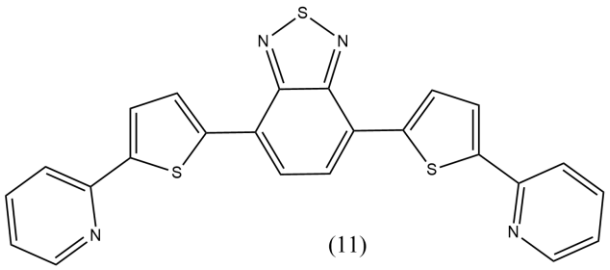

(11)

(11) was synthesized by a Stille cross-coupling reaction, in Wrocław University of Science and Technology, Wrocław, Poland by Dr. Zając[190]. It was characterized in $CH_2Cl_2/TBABF_4$ 0.01 M using a monomer concentration of $2 \cdot 10^{-3}$ M, scanning the

potential between 0.4 and 1.7 V with a gold disk electrode. It is possible to observe a pre-peak at 1.24 V and a second peak centred at 1.45 V (figure 109a). Successive scans show progressive increases in current, usually associable to an anodic polymerization process (figure 109b).

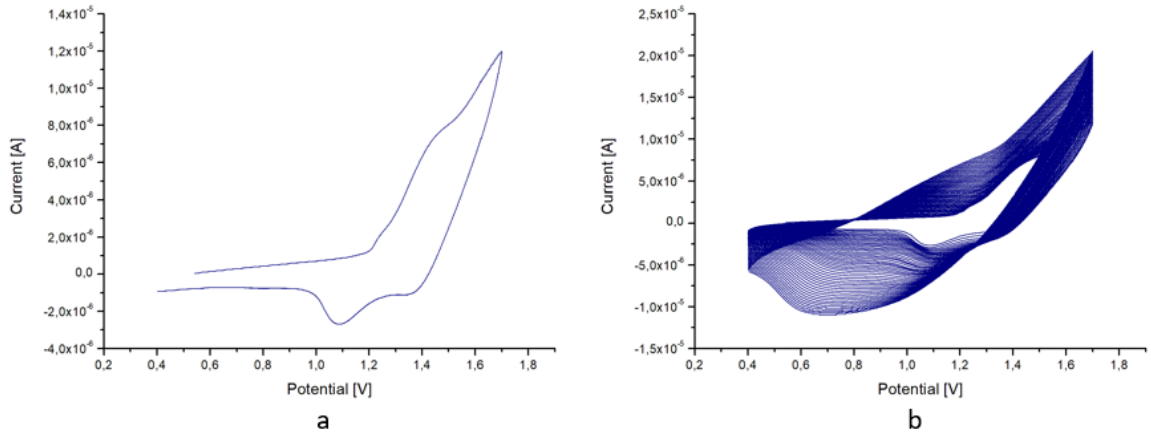

Figure 109: cyclic voltammograms of $2 \cdot 10^{-3}$ M 4-7-bis(5-pyridin-2-yl)thiophen-2-yl)benzo[c][1,2,5]thiadiazole (TBT) on a gold-disk electrode in CH_2Cl_2/$TBABF_4$ solvent system: (a) first scan, (b) 50 subsequent scans; potential scan rate: 100 mV s^{-1}

After 50 scans a deep-red coloured film appeared on gold disk electrode. The nature of the film deserves special considerations as it is known that pyridine can polymerize, when properly functionalized, by cathodic reduction as in the case of vinylpyridine[191]. On the contrary, few examples of polymerization for anodic oxidation have been reported. A hypothesis about the nature of the obtained film can be based on the electrochemical behaviour of acridine, reported by K. Yasukoucki[192]. In particular, acridine gives an oxidation product which can be described as an oligomer species resulting from C-C and C-N linkages. In agreement with this reference, we assume that the film derived from TBT can be supposed to originate from the activation of the pyridine ring (probably facilitated from the presence of the thiophene fragment), giving a pyridinium radical cation that results in an oligomerization product with a C-N linked structure[193] as showed in figure 110.

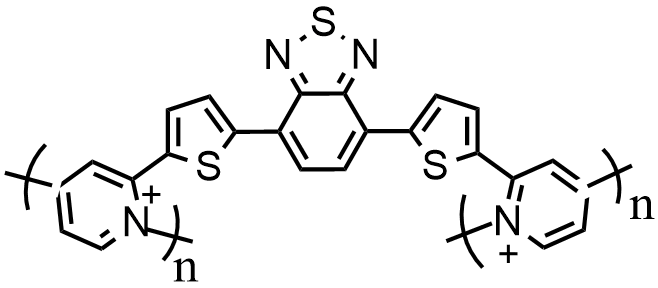

Figure 110: proposed growing unit of 4-7-bis(5-pyridin-2-yl)thiophen-2-yl)benzo[c][1,2,5]thiadiazole (TBT)

Electrochemical characterization was performed in CH_2Cl_2/$TBABF_4$ 0.01 M without monomer. The response shows a highly broad anodic process at about 1.2–1.4 V and a corresponding cathodic process between 1.1 and 0.5 V (figure 111), which could be associable to polymer doping and dedoping processes, respectively.

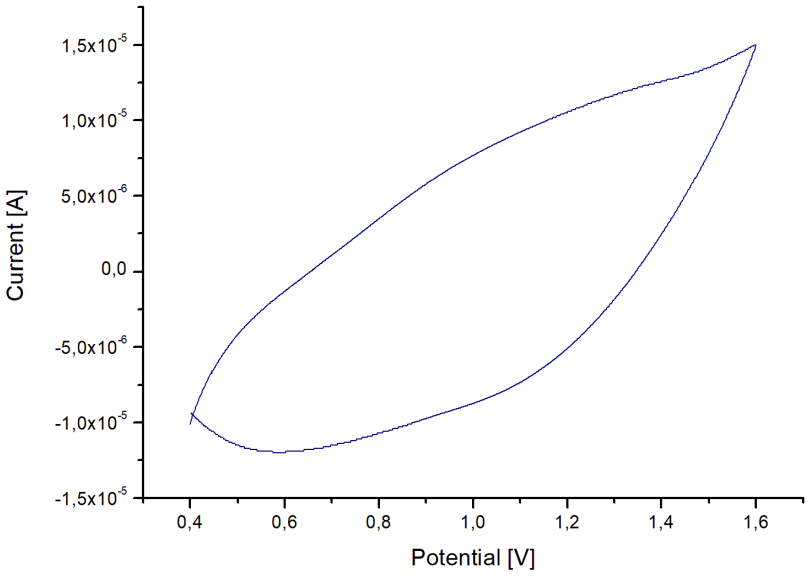

Figure 111: CV characterization of the TBT-film on gold electrode in CH_2Cl_2/$TBABF_4$ 0.1 M. Potential scan rate: 100 mV s^{-1}

The obtained film had a charge of 1.8 mC (Q_{dep} ≈ 60 mC cm^{-2}), measured by integrating the current passed during the electrochemical polymerization process.

SEM analysis was performed in order to examine the morphology and the surface features of the obtained film (figure 112).

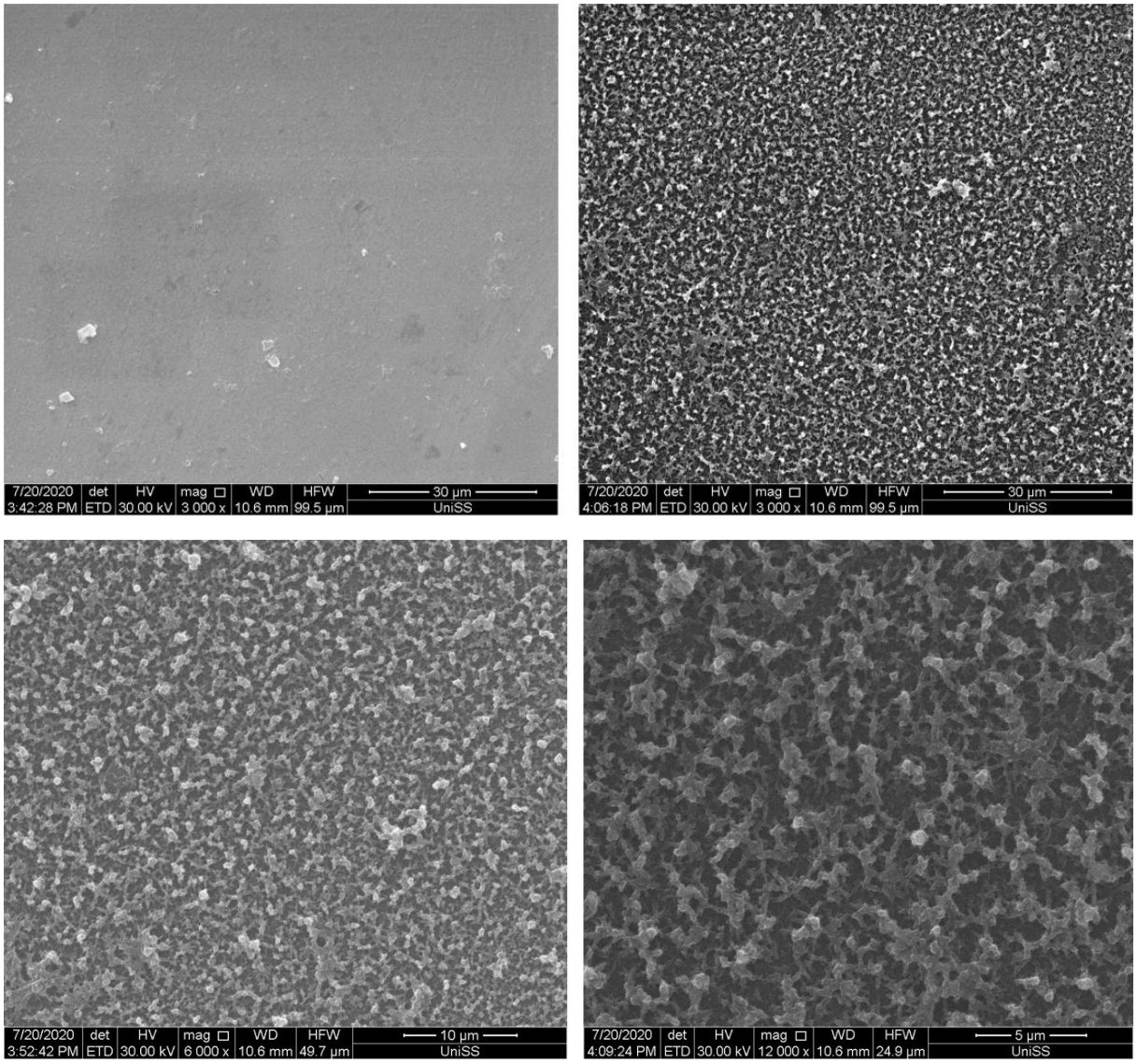

Figure 112: SEM images of (a) bare ITO coated glass and TBT-film (Qdep = 13 mC cm-2) at different magnification (b) 3000 x (c) 6000 x and (d) 12000 x

SEM images suggest the formation of polymer film homogenously distributed and with a porous structure, both advantageous features for the development of biosensors. As a matter of fact, the homogeneous porous structure can increase the specific surface area, thus determining an increase in the sensitivity of the biosensor, as well as facilitate the electron transfer between the active sites of the enzyme and the electrode surface[194].

The obtained film was used for a tyrosinase-based biosensor construction.

3.1.8 Bis(4-thiophen-2-yl)tetraphenylsilane (TTP) (12)

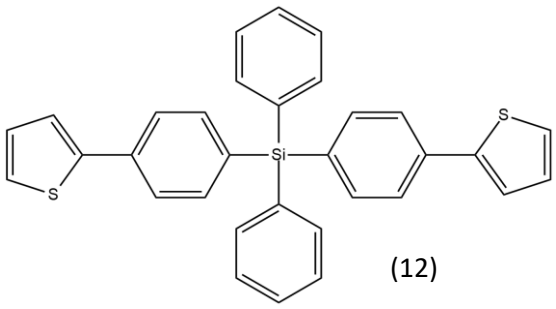

(12)

(12) was also synthesized in Wrocław University of Science and Technology, Wrocław, Poland by Dr. Zając[195].

(12) was characterized in CH_2Cl_2/$TEAPF_6$ 0.1 M using a monomer concentration of 10^{-2} M, scanning the potential between -0.15 and 1.35 V with both gold and glassy carbon electrodes. Voltammetric responses show an oxidation peak at about 1.25 V and a reduction peak at about 1.15 V for both the gold electrode and the glassy carbon one (figure 113).

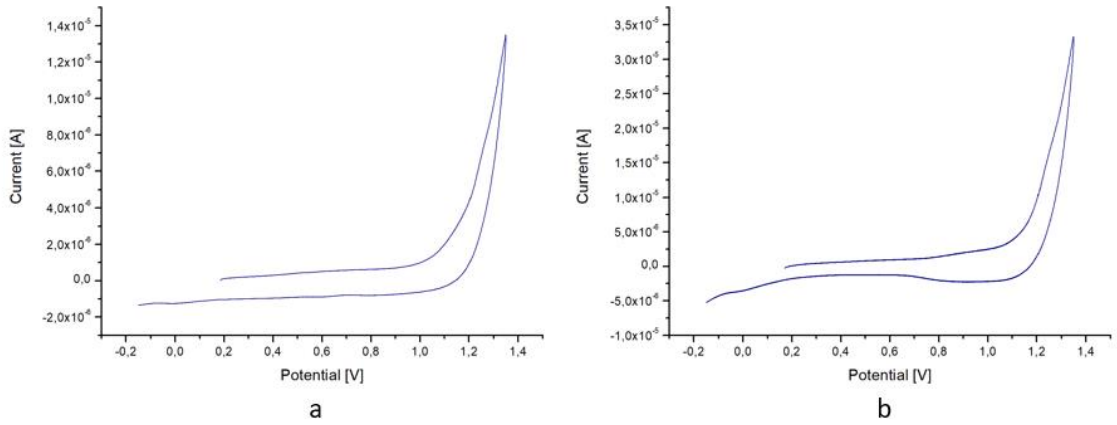

Figure 113: CV characterization of 10^{-2} M bis(4-thiophen-2-yl)tetraphenylsilane (TTP) (12) in CH_2Cl_2/$TEAPF_6$ 0.1 M on (a) gold and (b) glassy carbon electrodes; potential scan rate: 100 mV s^{-1}

Subsequent scans, similarly to what occurs with the monomer (3), show a shift of the oligomer oxidation peak to increasingly anodic values, thus reflecting an oxidation process that is, gradually, more difficult. Nevertheless, at potential values higher than

1.1 V, for subsequent scans, the behaviour suggests an anodic polymerization process. A contemporary formation of a green-yellow coloured film confirms it. In figure 114 polymerization processes performed by cyclic voltammetry for both gold and glassy carbon electrodes are reported.

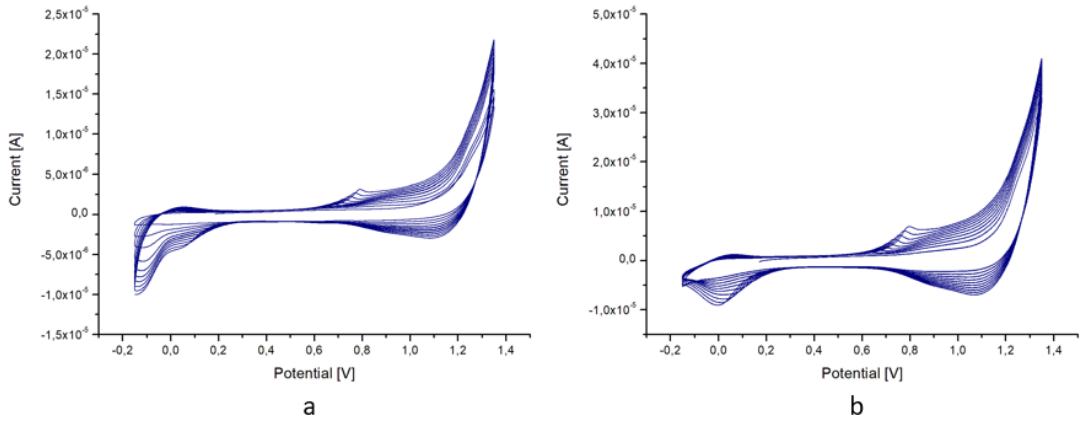

Figure 114: cyclic voltammograms of 10^{-2} M bis(4-thiophen-2-yl)tetraphenylsilane (TTP) (12) in CH_2Cl_2/$TEAPF_6$ 0.1 M on (a) gold and (b) glassy carbon electrodes; potential scan rate: 100 mV s^{-1}

Electropolymerization was also carried out by chronoamperometry, setting the potential at 1.3 V until a charge value of 1 mC (≈ 32 mC cm^{-2} for gold electrode) and 3 mC (≈ 43 mC cm^{-2} for glassy carbon electrode) were reached. Then, the obtained polymer films were neutralized at 0 V for 60 s. In figure 115 characterizations of the polymers obtained by chronoamperometry are reported.

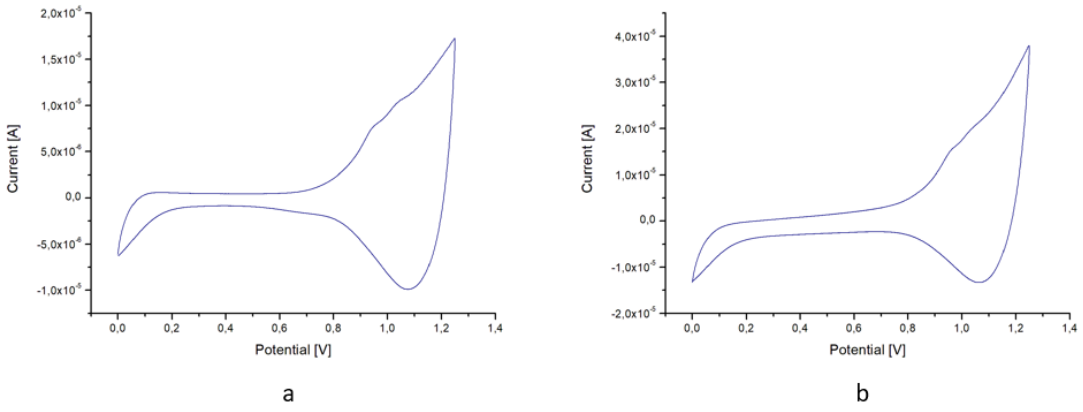

Figure 115: CV characterization of poly[bis(4-thiophen-2-yl)tetraphenylsilane] (poly(TTP)) obtained by chronoamperometry at 1.3 V vs. Ag/AgCl in CH_2Cl_2/$TEAPF_6$ 0.1 M on (a) gold and (b) glassy carbon electrodes; potential scan rate: 100 mV s^{-1}

In both voltammograms two anodic peaks at 0.95 V and 1.04 V, ascribable to oxidation of oligomers of different chain length, are observable. Moreover, a marked reduction peak centred at 1.07 V occurs, attributable to a dedoping process associated to a doping at about 1.25 V.

3.2 Spectroscopic Characterizations

Monomers and some polymers used for biosensors construction were also characterized from the spectroscopic point of view using UV-Vis spectroscopy.
Energy gap value (E_{gOPT}) was calculated based on λ_{onset} (nm) value, that is λ corresponding to the 10% of the maximum absorbance, according to the equation:

$$E = \frac{hc}{\lambda_{onset}}$$

where h is the Plank's constant = $6.626 \cdot 10^{-34}$ J s, c is the speed of light in vacuum = $2.998 \cdot 10^{8}$ m s^{-1}. Being 1 J = $6.242 \cdot 10^{18}$ eV, the equation becomes:

$$E\ [eV] = \frac{1239.81}{\lambda}$$

3.2.1 Dithiophene-based Monomers

UV-Vis spectra of (1), (2) and (3) (figure 116) were acquired in CH_3CN using a monomer concentration of $5 \cdot 10^{-5}$ M, scanning wavelengths from 900 to 235 nm.

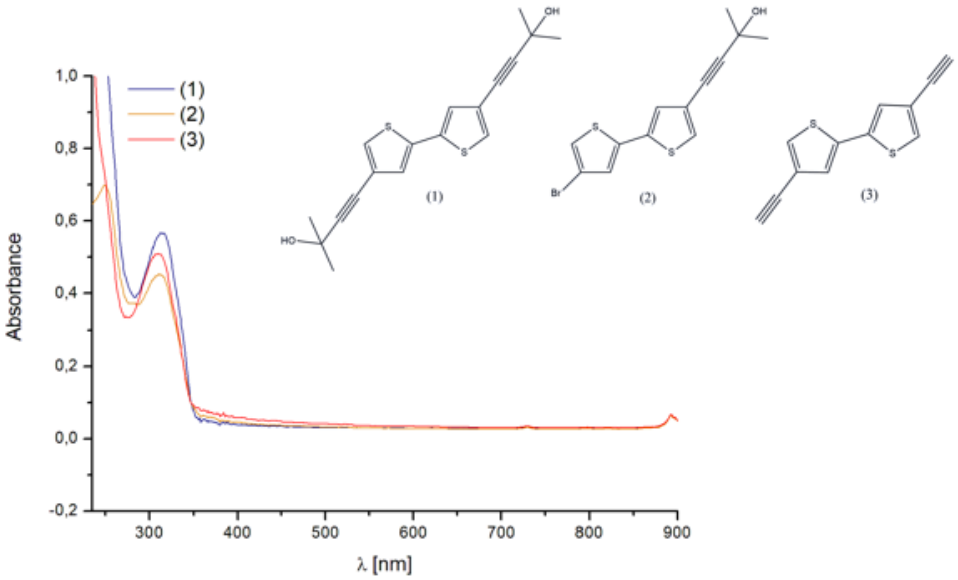

Figure 116: UV-Vis spectra of $5 \cdot 10^{-5}$ M 4,4′-([2,2′-bithiophene]-4-4′-diyl)bis(2-methylbut-3-yn-2-ol) (1) (blue line), 4-(4′-bromo-[2,2′-bithiophen]-4-yl)-2-methylbut-3-yn-2-ol (2) (orange line) and 4,4′-diethynil-2,2′-bithiophene (3) (red line)

In table 11 the optical features obtainable from the spectra are summarized:

Table 11: optical properties of dithiophene-based monomers

Monomer	**λ_{max} [nm]**	**ε[L mol^{-1} cm^{-1}]**	**λ_{onset} [nm]**	**E_{gOPT} [eV]**
(1)	315	11400	351	3.53
(2)	312	9000	398	3.11
(3)	311	10200	434	2.85

3.2.2 4′-(2,2′:5′,2′′-terthien-3′-ethynyl)-2,2′:6′,2′′-terpyridine (TAT)

UV-Vis spectrum of TAT (figure 117) was acquired in CH_2Cl_2 using a monomer concentration of $5 \cdot 10^{-5}$ M, scanning wavelengths from 900 to 235 nm.

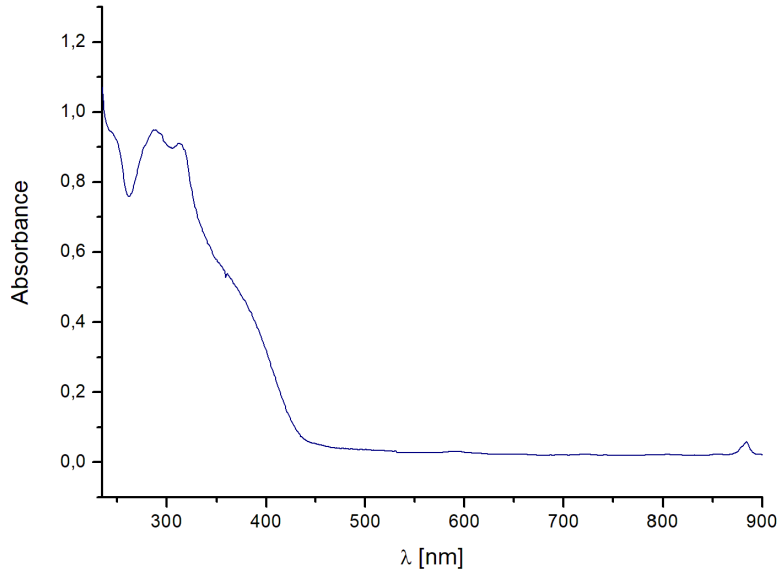

Figure 117: UV- Vis spectrum of $5 \cdot 10^{-5}$ M 4′-(2,2′:5′,2′′-terthien-3′-ethynyl)-2,2′:6′,2′′-terpyridine (TAT)

In table 12 the optical features obtainable from the spectrum are summarized:

Table 12: optical properties of TAT

Monomer	λ_{max} [nm]	ε[L mol^{-1} cm^{-1}]	λ_{onset} [nm]	E_{gOPT} [eV]
TAT	289	19000	429	2.89

3.2.3 Bis(4-thiophen-2-yl)tetraphenylsilane (TTP)

UV-Vis spectrum of TTP (figure 118) was acquired in CH_2Cl_2 using a monomer concentration of $5 \cdot 10^{-5}$ M, scanning wavelengths from 900 to 235 nm.

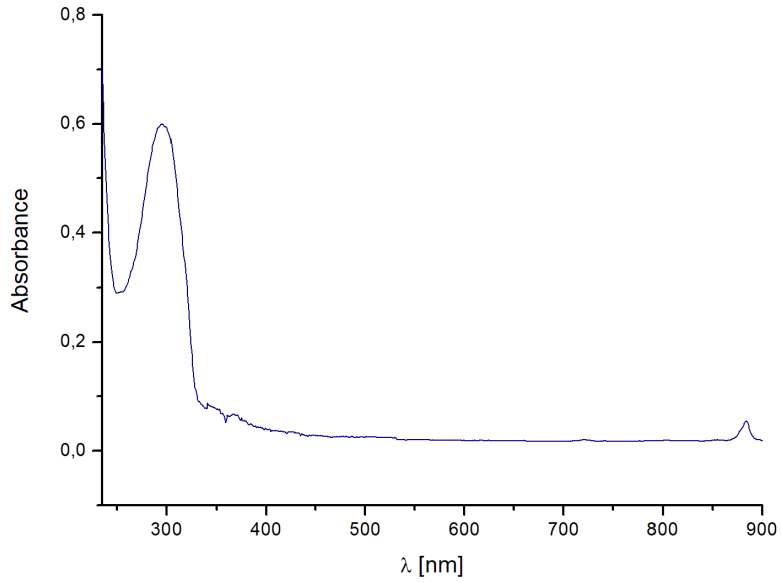

Figure 118: UV- Vis spectrum of $5 \cdot 10^{-5}$ M bis(4-thiophen-2-yl)tetraphenylsilane (TTP)

In table 13 the optical features obtainable from the spectrum are summarized:

Table 13: optical properties of TTP

Monomer	**λ_{max} [nm]**	**ε[L mol^{-1} cm^{-1}]**	**λ_{onset} [nm]**	**E_{gOPT} [eV]**
TTP	296	12000	374	3.31

3.2.4 Poly[(TAT)Ru(TpyCOOH)]

Poly[(TAT)Ru(TpyCOOH)] was deposited by chronoamperometry at 1.05 V (Q = 10 mC) and then neutralized at 0 V for 60 s on indium tin oxide (ITO). The spectrum (figure 119) was recorded putting the glass inside an empty cuvette, scanning wavelengths from 900 to 300 nm.

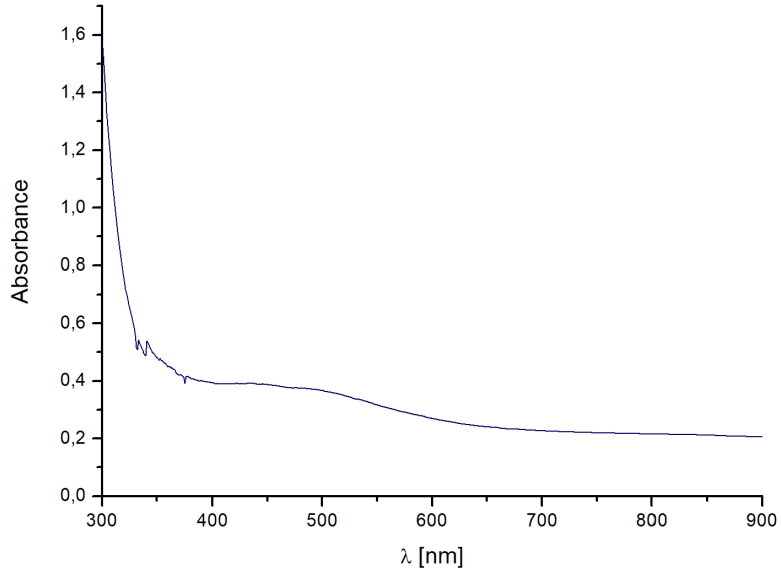

Figure 119: UV-Vis spectrum of poly[(TAT)Ru(TpyCOOH)] on ITO glass

In table 14 the optical features obtainable from the spectrum are summarized:

Table 14: optical properties of poly[(TAT)Ru(TpyCOOH)]

Polymer	**λ_{max} [nm]**	**λ_{onset} [nm]**	**E_{gOPT} [eV]**
Poly[(TAT)Ru(TpyCOOH)]	438	671	1.85

3.2.5 Poly(TTP)

Poly(TTP) was deposited by chronoamperometry at 1.3 V (Q = 10 mC) and then neutralized at 0 V for 60 s on indium tin oxide (ITO). The spectrum (figure 120) was recorded putting the glass inside an empty cuvette, scanning wavelengths from 900 to 300 nm.

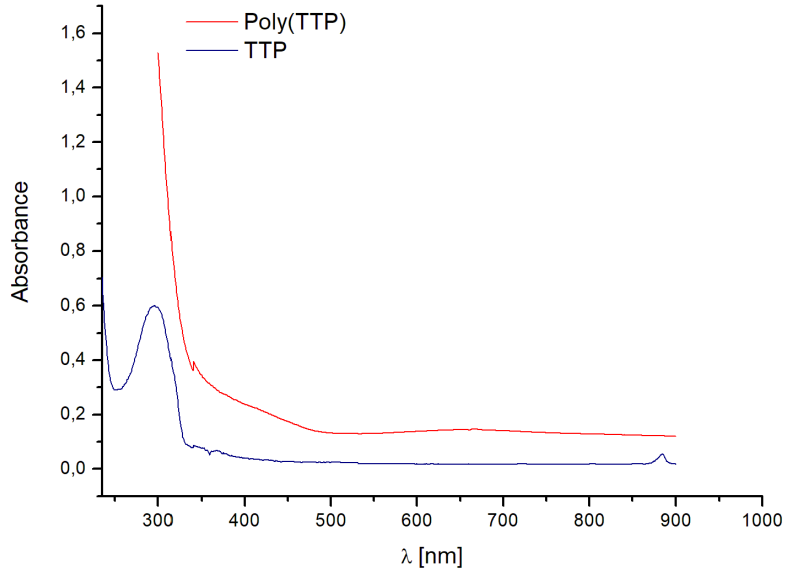

Figure 120: UV-Vis spectrum of poly(TTP) on ITO glass (red line) and TTP in CH_2Cl_2 (blue line)

In table 15 the optical features obtainable from the spectrum are summarized:

Table 15: optical properties of poly(TTP)

Polymer	λ_{max} [nm]	λ_{onset} [nm]	E_{gOPT} [eV]
Poly(TTP)	662	-	-

3.3 Biosensors Assembly

3.3.1 General Procedures for Biosensors Assembly

All the biosensors were realized by directly electrodepositing the polymer films using a voltammetric cell with a three electrodes configuration with gold (ø 2mm), platinum (ø 2mm) or glassy carbon (ø 3mm) disks as working electrodes, a platinum wire or a graphite bar as a counter and Ag/AgCl as reference. Before the deposition the working electrodes were cleaned with alumina (Al_2O_3 0.3 μm), sonicated for 15 minutes and

rinsed with distilled water and anhydrous acetone. All depositions were carried out using anhydrous solvents and in argon atmosphere. Then, the obtained polymer films were characterized in the same solvent/electrolyte systems without monomer. Afterwards, enzymes were immobilized onto the modified electrode surfaces.

3.3.2 Preparation of Diamine Oxidase (DAO) Solution and Immobilization Procedure

5 mg of diamine oxidase from *porcine kidney* (≥ 0.05 U/mg solid protein) were solubilized in 1 mL of phosphate buffer at pH 7.0. The immobilization procedure provides the dropping of 6 μL of this solution onto the modified electrode surface followed by the addition of two aliquots of 5 μL of a 2.5% glutaraldehyde solution to promote a cross-linking between enzyme molecules. The modified electrode was then stored at 4°C until the surface was dry.

3.3.3 Preparation of Tyrosinase (Tyr) Solution and Immobilization Procedure

2 mg of tyrosinase from *mushroom* (≥ 1000 U/mg solid protein) were solubilized in a phosphate-citrate buffer at pH 5.2. The immobilization procedure is based on physical absorption and cross-linking between enzyme molecules using glutaraldehyde as coupling agent. 40 μL of the enzyme solution were dropped onto the modified electrode surface, taking care that the surface did not dry out. After 2 hours 40 μL of 40% glutaraldehyde solution were added on the electrode surface to cross-link the enzyme. After 10 minutes the unbound protein was washed away dipping the electrode in phosphate buffer at pH 7.0 (2 x 15 minutes), acetate buffer at pH 5.2 (2 x 15 minutes) and Tris-HCl buffer at pH 7.2 (45 minutes). The biosensor was stored at 4°C in phosphate buffer when not in use.

The immobilization procedure is reported by S. Baluta et al.[113] for laccase immobilization but it has also proved effective for tyrosinase.

3.4 Biosensors for Histamine Detection

Biosensors for histamine detection were prepared immobilizing diamine oxidase (DAO) on poly(3,4-ethylenedioxythiophene) (PEDOT) and on poly[(TAT)Ru(TpyCOOH)] films.

At first, DAO was entrapped in a conducting film resulting from the polymerization of a commercial monomer (3,4-ethylenedioxythiophene, EDOT) according with the method described by Al Layla et al.[8] for the determination of several diamines. This choice was made with the aim of verifying the efficacy of the enzyme. Once the efficiency of the enzyme was verified, a second biosensor which involves the use of poly[(TAT)Ru(TpyCOOH)] for the electrode surface modification was assembled. The aim was to obtain a second-generation biosensor, since, as anticipated in the section 1.3.1, the only AO-based biosensor of this type is that reported by Niculescu et al.[69] based on the use of a polymer deriving from an Os complex. The idea that a conducting polymer film of a Ru complex, similarly to what reported by Niculescu et al., could also in our case facilitate the electron transfer between the enzyme and the electrode, was at the basis of our purpose. However, the obtained biosensor showed acceptable results only by working as a first-generation device, thus allowing the determination of histamine by determining hydrogen peroxide, a by-product of the enzyme reaction. More details about these two biosensors are discussed in the following paragraphs.

3.4.1 Pt/PEDOT/DAO

PEDOT films with entrapped DAO were obtained on platinum surfaces using the polymerization conditions reported by Al Layla et al.[8]: 0.028 M EDOT, 0.05 M sodium dodecyl sulphate (SDS) as supporting electrolyte, and 20 mg DAO in 0.05 M phosphate buffer at pH 7.0 The electropolymerization was carried out by chronoamperometry at 0.9 V *vs*. Ag/AgCl. In figure 121 the characterizations of the PEDOT/DAO films with a

deposited charge of $1.4 \cdot 10^{-2}$ C ($Q_{dep} \approx 445$ mC cm^{-2}) and $2.3 \cdot 10^{-2}$ C ($Q_{dep} \approx 730$ mC cm^{-2}), respectively, are reported.

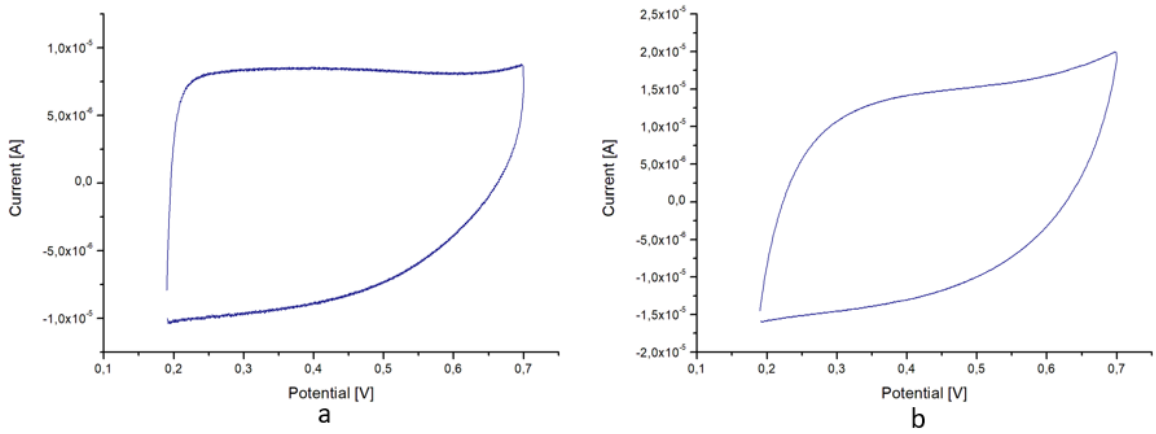

Figure 121: CV characterizations of PEDOT/DAO films deposited on platinum electrode in phosphate buffer/SDS 0.05 M by chronoamperometry at 0.9 V vs. Ag/AgCl with a Q_{dep} of (a) 445 mC cm^{-2} and (b) ≈ 730 mC cm^{-2}

Then, both biosensors were tested in presence of histamine using chronoamperometry. The best results were obtained with the film with a charge value of 445 mC cm^{-2}. Amperometric measurements were performed in phosphate buffer at pH 8.2 in open-air atmosphere and in a stirred solution, setting the potential at 0.7 V *vs*. Ag/AgCl to detect oxidation current of H_2O_2.

In figure 122 the chronoamperometric response obtained adding aliquots of histamine 9 mM is reported, in a concentration range between 0.04 and 2.5 mM.

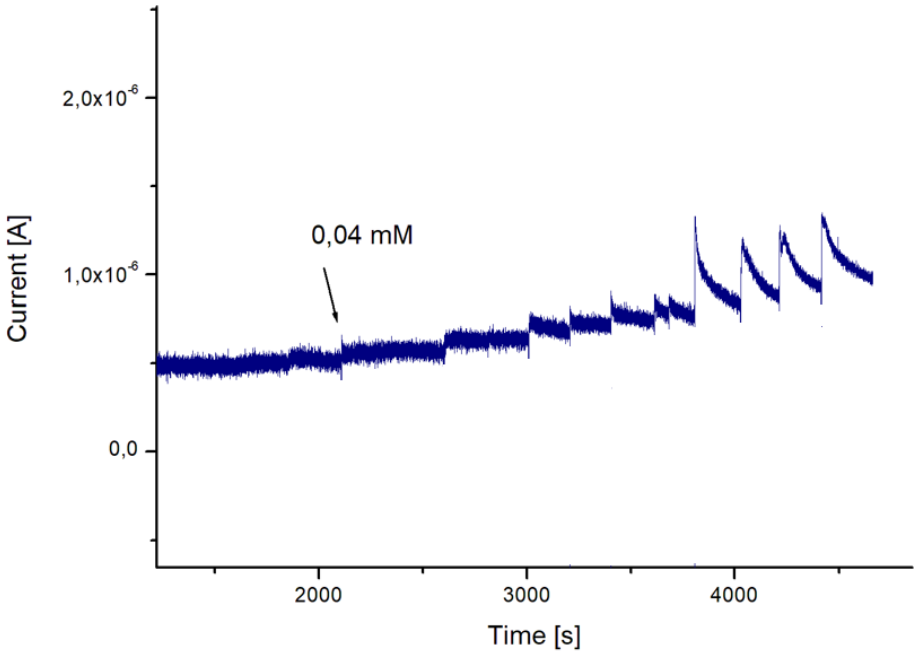

Figure 122: current/time response of Pt/PEDOT/DAO in 0.1 M phosphate buffer (pH 8.2) with histamine concentration between 0.02 and 2.5 mM

The corresponding calibration curve (figure 123) shows a linear response between 0.04 and 2.5 mM, with a coefficient of determination ($R^2 = 0.986$) equal or better than those reported in the reference article for other biogenic amines (putrescine ($R^2 = 0.986$), cadaverine ($R^2 = 0.984$) and 1,3 diamine propane ($R^2 = 0.957$)).

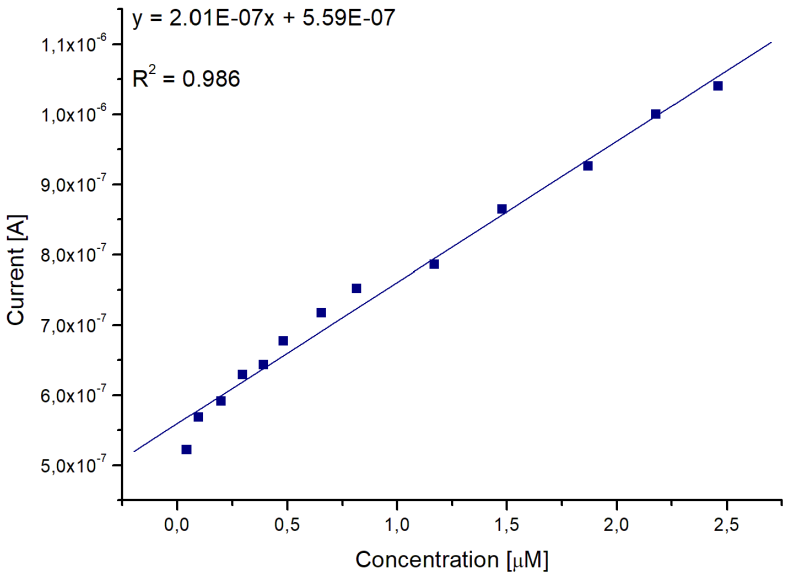

Figure 123: calibration curve obtained with the biosensor Pt/PEDOT/DAO in a concentration range between 0.04 and 2.5 mM

3.4.2 Pt/poly([(TAT)Ru(TpyCOOH)]/DAO

Unlike EDOT, which can polymerize in aqueous solution, [(TAT)Ru(TpyCOOH)][PF_6]$_2$ requires an organic solvent as it is not soluble in an aqueous medium.

The biosensor was assembled using the procedure described in section 3.3.1 and DAO enzyme was immobilized according to the procedure described in section 3.3.2. Poly[(TAT)Ru(TpyCOOH)] was obtained onto a platinum disk by cyclic voltammetry (20 scans) using the conditions described in section 3.1.6.

In figure 124 the polymerization process occurred on platinum disk electrode is reported. Characterizations of the so-obtained film were recorded both in CH_2Cl_2/$TEAPF_6$ and CH_3CN/$TEAPF_6$ 0.1 M and are reported in figure 107.

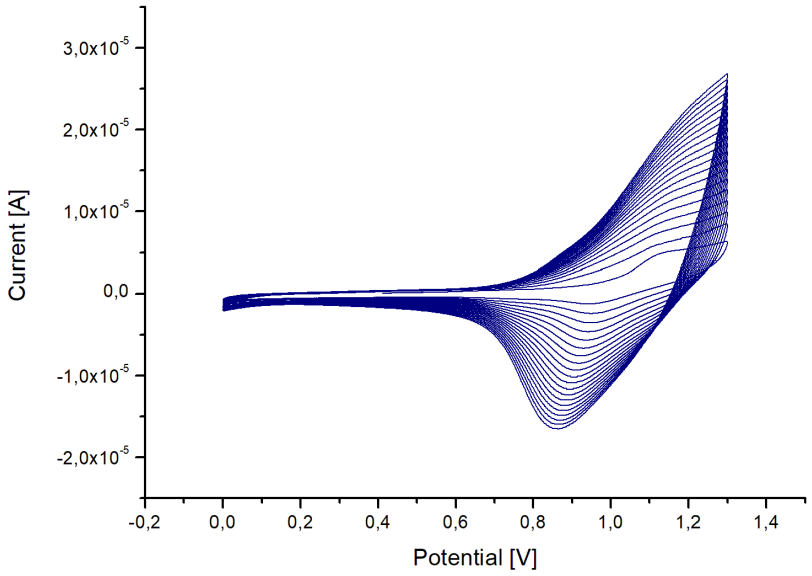

Figure 124: cyclic voltammograms of $5 \cdot 10^{-3}$ M [(TAT)Ru(TpyCOOH)][PF_6]$_2$ in CH_2Cl_2/$TEAPF_6$ 0.1 M on platinum disk electrode (20 scans); potential scan rate: 100 mV s^{-1}

SEM images of a poly[(TAT)Ru(TpyCOOH)] (figure 125) show the presence of different domains on the same film. Such a feature is reasonably attributable to potentiodynamic technique used in the polymerization step, which unlike the potentiostatic one, leads to the formation of more inhomogeneous films.

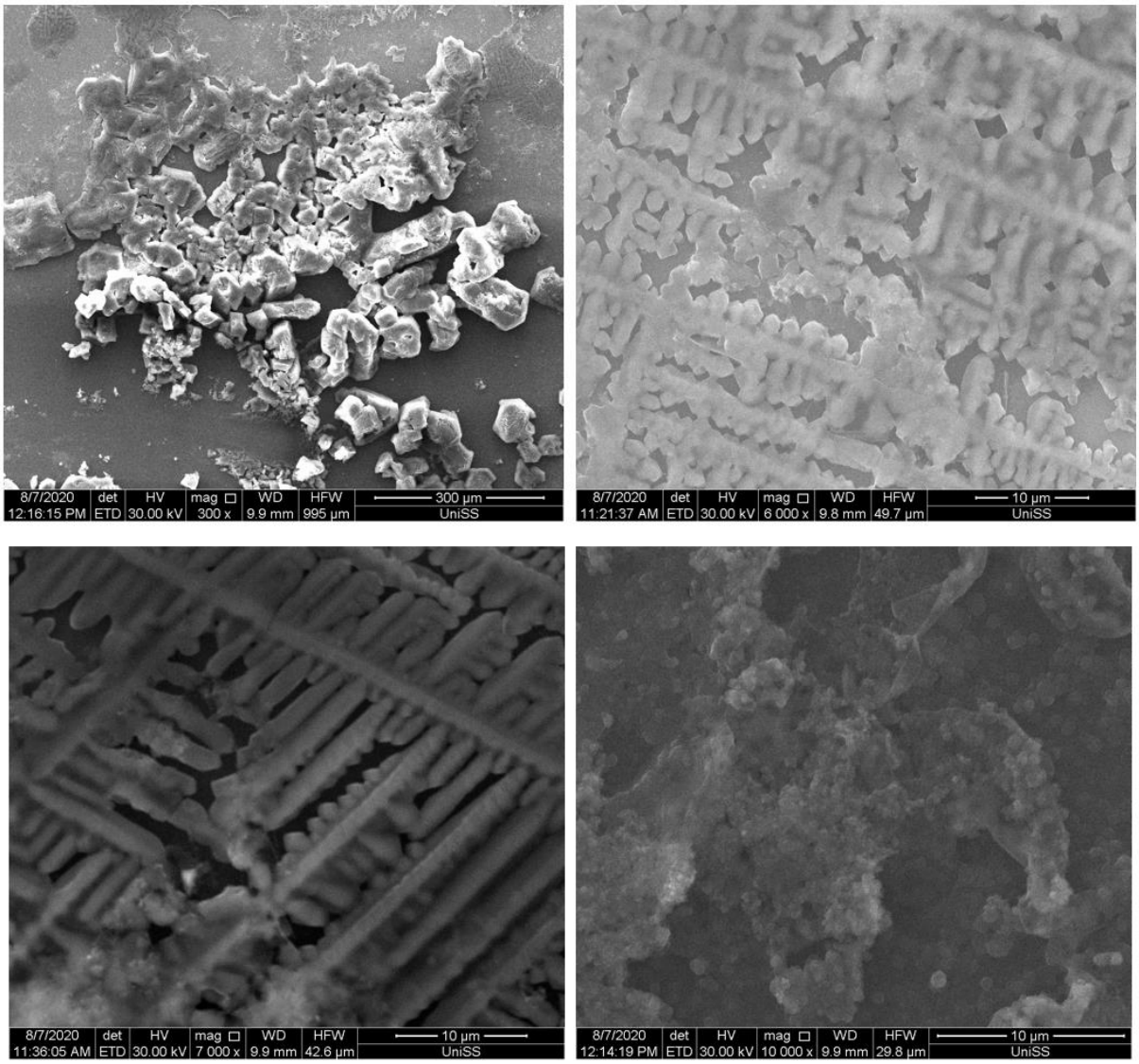

Figure 125: SEM images of poly[(TAT)Ru(TpyCOOH) deposited by cyclic voltammetry on ITO glass at different magnification (a) 300 x (b, c, d) 7000 x on different polymer regions

With this biosensor several tests have been carried out in presence of histamine by chronoamperometry under mild stirring, progressively adding aliquots of 5 mM histamine solution. The first tests involved the use of potassium ferricyanide ($K_3Fe(CN)_6$) as a redox mediator, operating at 0.25 V *vs.* Ag/AgCl chosen on the basis of the cyclic voltammogram recorded in presence of 1 mM $K_3Fe(CN)_6$ (figure 126).

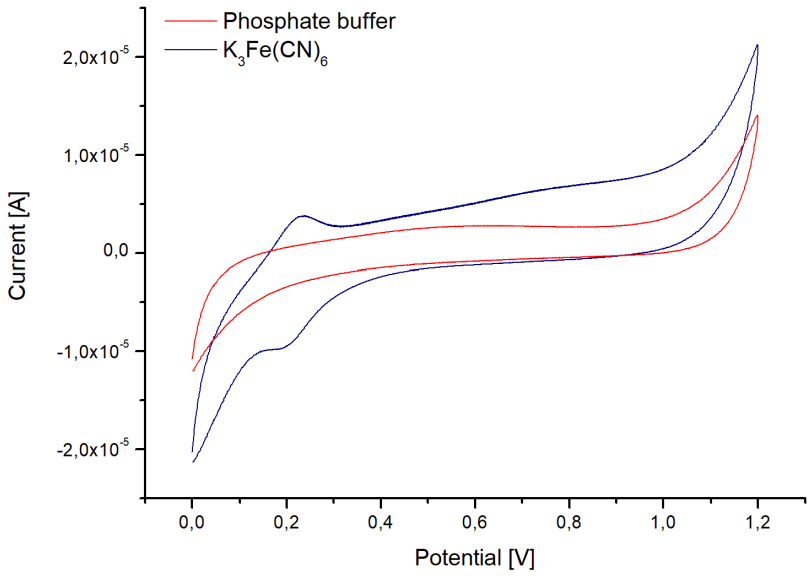

Figure 126: cyclic voltammograms of the Pt/poly[(TAT)Ru(TpyCOOH)]/DAO of the buffer solution (red line) and in presence of 1mM $K_3Fe(CN)_6$ (blue line)

However, the obtained amperometric responses showed a reduction current which gradually became less and less intense due to the dilution of the redox mediator.

A further test was then carried out at 0.7 V *vs*. Ag/AgCl with the aim of recording the oxidation current of H_2O_2, which is generated during the enzyme reaction. In this case, increasing currents have been observed (figure 127), but only in the presence of high concentrations of histamine: the visible jumps, in fact, are attributable to histamine concentrations between 85–330 μM.

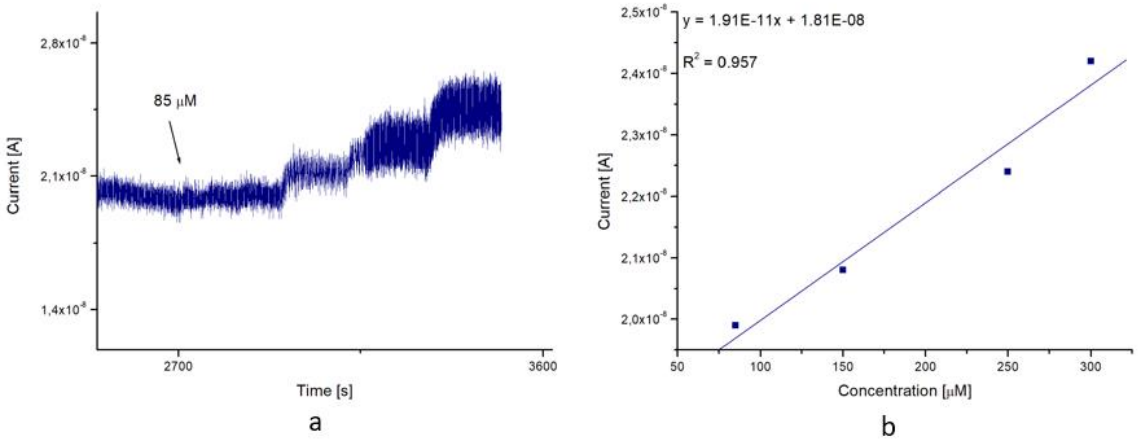

Figure 127: (a) current/time response of Pt/poly[(TAT)Ru(TpyCOOH)]/DAO in 0.1 M phosphate buffer (pH 7.0) with histamine concentration between 85 and 330 µM and (b) corresponding calibration curve

The unsatisfactory obtained results could be ascribable to an incompatibility of the enzyme with the used polymer film or perhaps, to an unsuitable immobilization method which could have caused a protein semi-misfolding, partially inactivating it.

3.5 Biosensors for Epinephrine Detection

Biosensors for epinephrine detection were prepared immobilizing tyrosinase on poly(TBT), poly[(TAT)Ru(TpyCOOH)] and poly(TTP) deposited on gold or glassy carbon electrodes as described in section 3.3.1.

3.5.1 Au/poly(TBT)/Tyr

A biosensor for epinephrine detection was realized using a conducting film from TBT as modifying agent for electrode surface. The film was deposited on gold electrode as reported in section 3.1.7.

Onto this film tyrosinase was then immobilized as reported in section 3.3.3.

The ability of the Au/TBT film/Tyr biosensor to detect epinephrine was initially tested by cyclic voltammetry. In figure 128 voltammetric curves recorded on a bare gold electrode and on the modified electrode in a 20 μM epinephrine solution are reported.

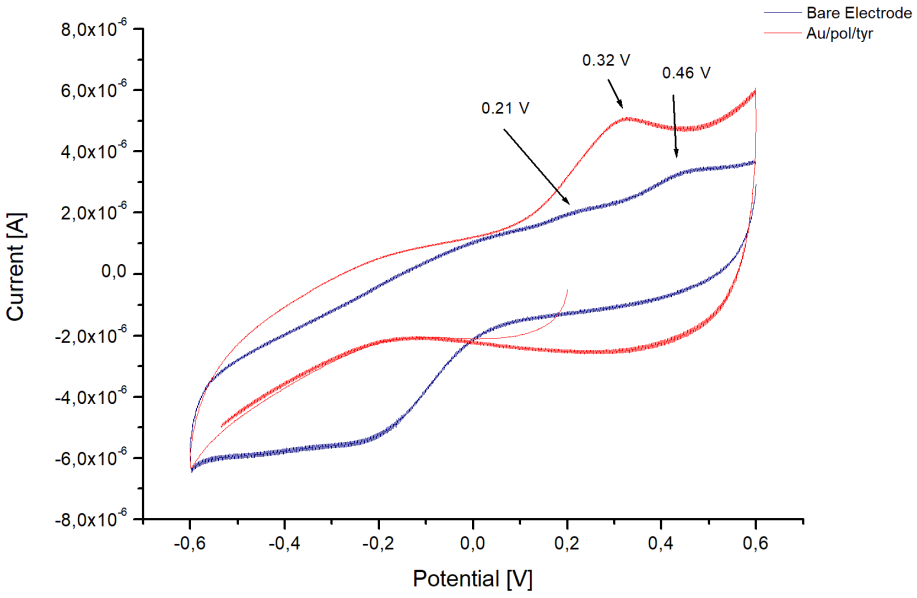

Figure 128: comparison between the bare and the Au/poly(TBT)/Tyr in presence of 20 μM EP. Potential scan rate: 100 mV s^{-1}

Two broad peaks, with low current intensity, are observed with the bare electrode, assignable to the oxidation of EP to the open-chain quinone (adrenalinequinone), which can cyclize to leucoadrenochrome, and to the oxidation of this last one to adrenochrome, respectively[196-198] (figure 129).

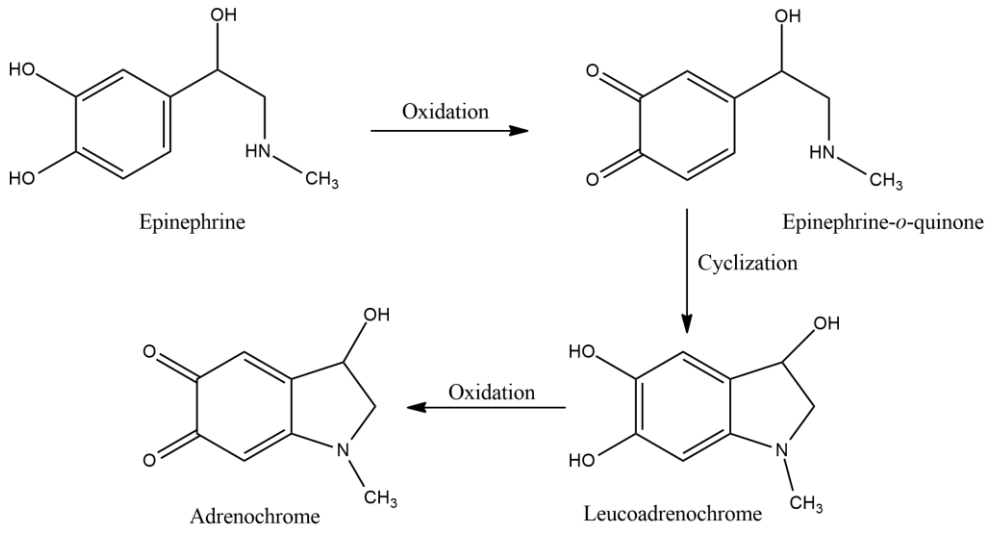

Figure 129: Schematic representation of the literature epinephrine electrochemical oxidation mechanism

Conversely, the voltammetric response obtained with tyrosinase-based electrode evidences a well-defined and more intense peak, at 0.32 V, intermediate between the peaks of the Au bare electrode. This feature suggests that the double-step oxidation process of EP occurs in a single-step on the modified electrode.

According to CV characterization, further experiments were carried out by chronoamperometry in open-atmosphere under mild stirring, setting the potential at 0.3 V *vs*. Ag/AgCl. Figure 130a reports the amperometric response in the range 0.1–50 μM of epinephrine concentration. Progressive increases in the intensity current due to consecutive known additions of epinephrine solution are observed. The current response was proportional to the concentration with a very good coefficient of determination ($R^2 = 0.996$) (figure 130b).

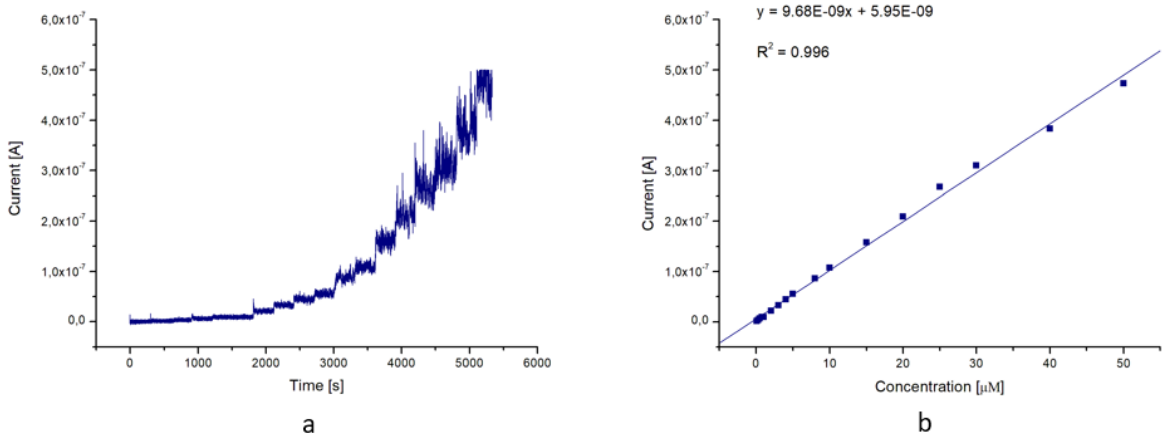

Figure 130: (a) current/time response of Au/poly(TBT)/Tyr in 0.1 M phosphate buffer (pH 7.0) with EP concentration between 0.1 and 50 µM and (b) corresponding calibration curve

LoD of the Au-TBT-Tyr biosensor was calculated using equation (1):

$$LoD = \frac{3.29\sigma_B}{b} \quad (1)$$

where σ_B is the standard deviation of blank response (11 measurements) and b is the slope of regression line.

LoQ has been calculated using equation (2):

$$LoQ = \frac{5\sigma_B}{b} \quad (2)$$

and sensitivity was calculated as the ratio of the slope of the calibration curve to the area of the electrode surface. LoD, LoQ and sensibility were determined as 0.06 µM, 0.09 µM and $3.08 \cdot 10^{-7}$ A μM^{-1} cm^{-2}, respectively. The enzyme sensor was tested for stability by replied measurements every week on a 20 µM epinephrine solution, showing a stability for times higher than 30 days.

All analytical parameters are summarized in table 16.

Table 16: analytical parameters of the calibration curve for the determination of epinephrine with Au/TBT-film/Tyr biosensor

Linearity [μM]	LoD [μM]	LoQ [μM]	R^2	Slope	Intercept	Sensitivity [A μM^{-1} cm^{-2}]	Stability [days]
0.1-50	0.06	0.09	0.996	$9.68 \cdot 10^{-9}$	$5.95 \cdot 10^{-9}$	$3.08 \cdot 10^{-7}$	>30

In addition, the calibration data allow to estimate the Hill coefficient (n_H) by graphing log [I/(I_{max}-I)] *vs.* log [C]. This dimensionless parameter gives information about the cooperativity of ligand binding. The obtained value is 1.09 ± 0.01 (R^2 = 0.984), which, being very close to unity suggests that the kinetics of enzyme reaction is in agreement with a Michaelis-Menten type kinetics. Furthermore, the value slightly higher than 1 shows that there is a positive cooperative effect between the occupied active centres, that is the affinity of the tyrosinase for EP increases after the binding of an EP molecule with the enzyme[115]. Apparent Michaelis-Menten constant (K_M) was calculated using the adapted Lineweaver-Burk equation (3):

$$\frac{1}{I} = \frac{1}{I_{max}} + \frac{K_M}{I_{max}[C]} \quad (3)$$

where I is the anodic current, I_{max} is the steady-state current and [C] is the concentration of EP. I_{max} ($4.5 \cdot 10^{-7}$ A) and K_M (35 μM) values have been calculated from the intercept and slope of equation (3), respectively. In particular, the small K_M value, measuring the affinity between the enzyme and its substrate, suggests a strong affinity between the immobilized tyrosinase and EP[199].

Finally, the effect of scan rate on biosensor response was also investigated for a 50 μM EP solution (figure 131a). A linear graph peak current *vs*. square root of scan rate with R^2 = 0.997 was obtained in the range 10-350 mV s^{-1} (figure 131b), typical of a diffusion-controlled mechanism. This means that the considered electrochemical process is limited by the rate of diffusion, that is by the rate of the mass transport of the

electroactive species towards the electrode surface, determined by a concentration gradient[200,201].

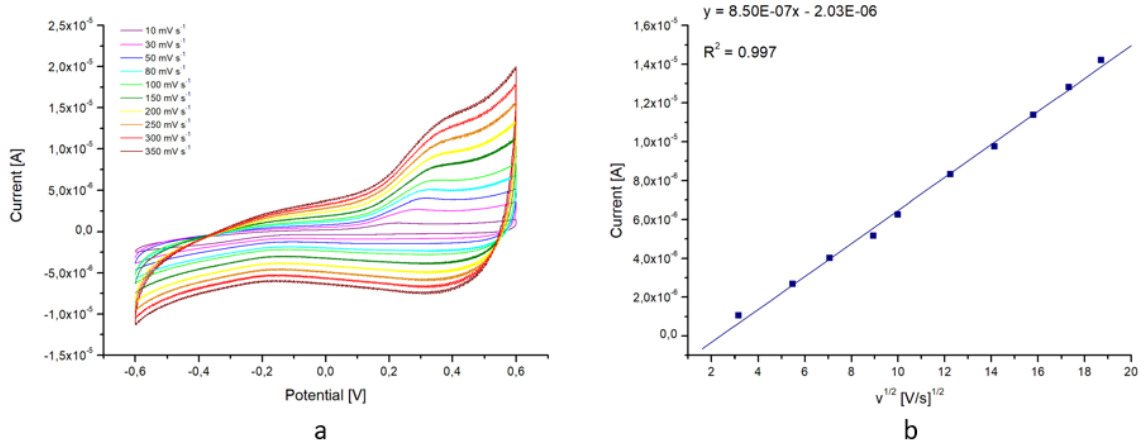

Figure 131: (a) cyclic voltammograms of Au/poly(TBT)/Tyr at different scan rates (10-350 mV s^{-1}) and (b) plot of I_p versus $v^{1/2}$

The diffusion coefficient (D [cm^2 s^{-1}]) of EP can be calculated from the slope of the graph 132b using the Randles-Sevcik equation (4):

$$i_p = 2.69 \cdot 10^5 n^{3/2} A D^{1/2} C v^{1/2} \quad (4)$$

where i_p is the maximum anodic peak current [A], n is the number of exchanged electrons, A is the electrode area [cm^2], C is the EP concentration [mol cm^{-3}], and v is the potential sweep rate [V s^{-1}]. Diffusion coefficient was estimated as $5.10 \cdot 10^{-7}$ cm^2 s^{-1}. This D value, if compared with others reported in the literature for the same analyte and with modified gold electrodes[198,202], is higher. This indicates that the electrochemical process occurs faster with our biosensor, suggesting the efficiency of the electron transfer between the electroactive species and the gold electrode, mediated by the poly(TBT) coating, is greater than that evaluated in the case of gold electrodes coated by L-cysteine self-assembled monolayers (L-cys/Au SAMs)[198] and by self-assembled iron-octacarboxyphtalocyanine complex (Cys-FeOCPc)[202].

3.5.2 Poly[(TAT)Ru(TpyCOOH)]/Tyr-based Biosensors

Other two biosensors for epinephrine detection were realized using as modifying agent for electrode surfaces a conducting metallopolymer film: poly[(TAT)Ru(TpyCOOH)][101] as reported in section 3.1.6. It was deposited on both gold and glassy carbon electrodes by chronoamperometry with a Q_{dep} of 32 mC cm^{-2} and 15 mC cm^{-2}, respectively. Characterizations of the so-obtained polymer films are reported in the same section in figure 108. Onto these films tyrosinase was then immobilized as reported in section 3.3.3.

Before using the metallopolymer species for the modification of electrode surfaces, its precursor, TAT, was also used with no good results. In figure 132 the differential pulse voltammograms recorded with GC/poly(TAT)/Tyr biosensor, in presence of increasing concentrations of epinephrine, are reported.

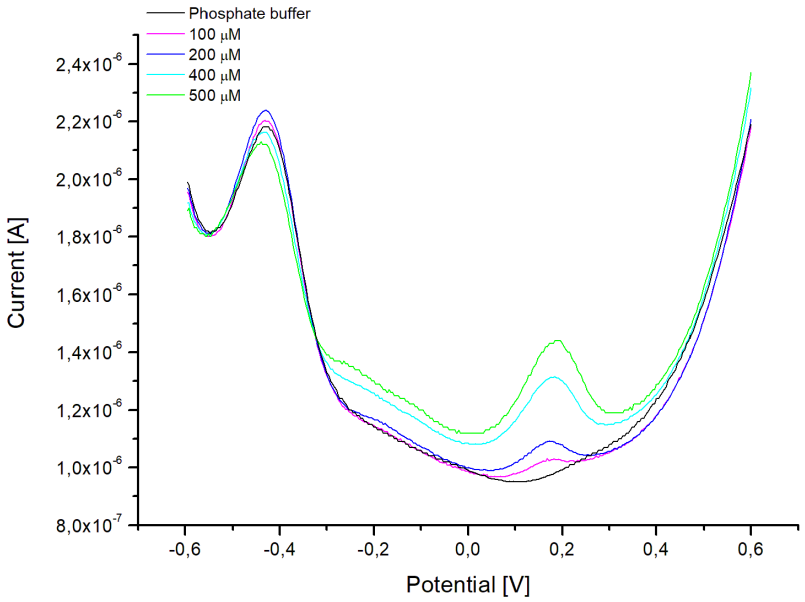

Figure 132: representative DPV scans for different concentrations of EP (potential range -0.6÷0.6 V vs. Ag/AgCl, modulation amplitude 0.05 V, step potential 0.004 V) obtained with GC/poly(TAT)/Tyr biosensor

As it possible to observe, the biosensor showed significant responses only in the presence of high concentrations of epinephrine. As a matter of fact, the first concentration reported that is the first in which a peak appears, is 100 μM.

The decision to use the metallo-polymer instead of the simple TAT ligand was, therefore, taken with the aim of improving the performances of the biosensor.

The metallopolymer film, as reported in previous studies by Manca et al.[101], has a value of E_g equal to 1.60 eV (E_{gEC}) lower than that of poly(TAT) equal to 2.04 eV (E_{gEC}). A lower energy gap can be translated into a higher conductivity; therefore, an easier electron transfer between the modified electrode and the substrate (or a mediator) can be expected, thus also a higher sensitivity of the biosensor. Actually, the performances of the metallopolymer-based biosensors proved to be decisively better than those of the aforementioned biosensor with poly(TAT).

3.5.2.1 Au/poly[(TAT)Ru(TpyCOOH)]/Tyr

The biosensor was first tested using cyclic voltammetry. In figure 133 the voltammetric responses recorded in phosphate buffer solution (0.1 M, pH 7.0) and in the presence of 550 μM epinephrine are showed. A broad anodic peak can be observed at about 0.2 V *vs*. Ag/AgCl with an associated small reduction peak at about 0.16 V.

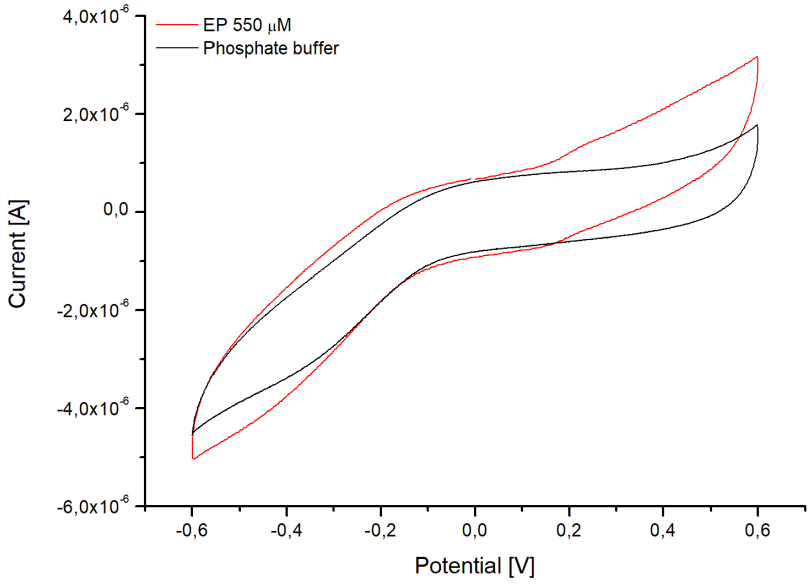

Figure 133: cyclic voltammograms of the Au/poly[(TAT)Ru(TpyCOOH)]/Tyr of the buffer solution (black line) and in presence of 550 µM EP (red line)

Further experiments were then carried out at room temperature, in open-atmosphere by both DPV and chronoamperometry.

In order to properly evaluate the analytical behaviour of the reported biosensor, DPV measurements were performed between -0.6 and 0.6 V (step potential = 0.004 V, amplitude = 0.05 V). In figure 134 the differential pulse voltammograms recorded in presence of increasing concentrations of epinephrine in a range 1-100 µM are reported. It is possible to observe two peaks at -0.2 and 0.15 V that can be attributable to two different oxidation processes: from EP to adrenalinequinone (the open-chain quinone) which can cyclize to leucoadrenochrome, and to the oxidation of this last one to adrenochrome[196-198,203].

In particular the voltammogram shows that both peaks, the second more intensely, increase as the concentration of added epinephrine increases.

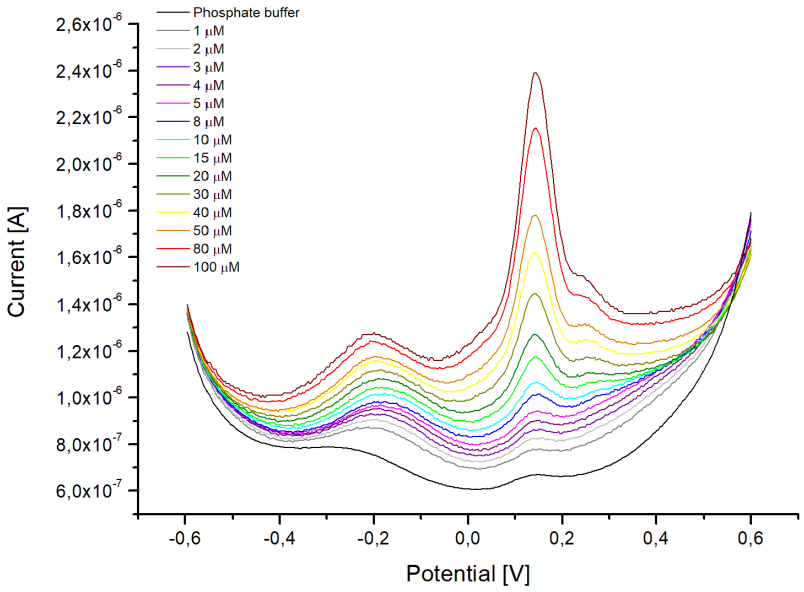

Figure 134: representative DPV scans for different concentrations of EP (potential range -0.6÷0.6 V vs. Ag/AgCl, modulation amplitude 0.05 V, step potential 0.004 V) obtained with Au/poly[(TAT)Ru(TpyCOOH)]/Tyr biosensor

The calibration curve (figure 135), obtained using the peak current values at 0.15 V, shows a very good linear response with a $R^2 = 0.998$.

The graph in figure 134, as well as all the other DPV graphs, shows the voltammograms obtained starting from the first quantifiable concentration, however the investigated concentrations started from lower values, comparable with those reported in the literature relating to biosensors usable in biological samples[109,122].

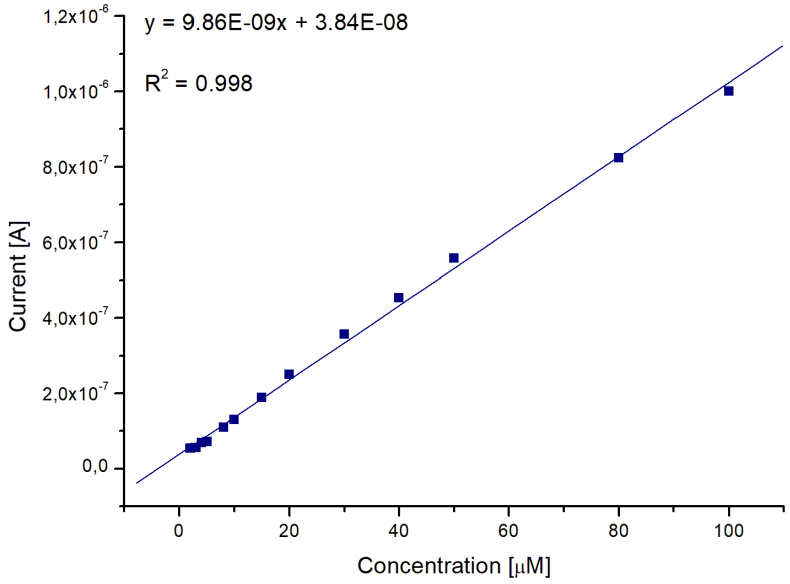

Figure 135: calibration curve calibration curve obtained with the biosensor Au/poly[(TAT)Ru(TpyCOOH)/Tyr in a concentration range between 1 and 100 µM

LoD, LoQ and sensitivity of the obtained device have been calculated using the formulas reported in section 3.5.1 and have been determined as 0.67 µM, 1.02 µM and $3.14 \cdot 10^{-7}$ A μM^{-1} cm^{-2}.

All analytical parameters are summarized in table 17:

Table 17: analytical parameters of the calibration curve (DPV data) for the determination of epinephrine with Au/poly[(TAT)Ru(TpyCOOH)]/Tyr biosensor

Linearity [µM]	LoD [µM]	LoQ [µM]	R^2	Slope	Intercept	Sensitivity [A μM^{-1} cm^{-2}]
1-100	0.67	1.02	0.998	$9.86 \cdot 10^{-9}$	$3.84 \cdot 10^{-8}$	$3.14 \cdot 10^{-7}$

Chronoamperometric measurements were carried out in order to achieve a lower LoD value. Experiments were performed under mild stirring in a 30 mL voltammetric cell, applying a constant potential of 0.18 V. After the background current reached a stable value, incremental amounts of $5.46 \cdot 10^{-3}$ M EP in aqueous solution were injected into the cell with a time interval of about 200 s and the current/time response was recorded.

Figure 136 reports the amperometric response showing progressive increases in the intensity current due to consecutive additions of EP solution, in a concentration range 1 μM–1 mM.

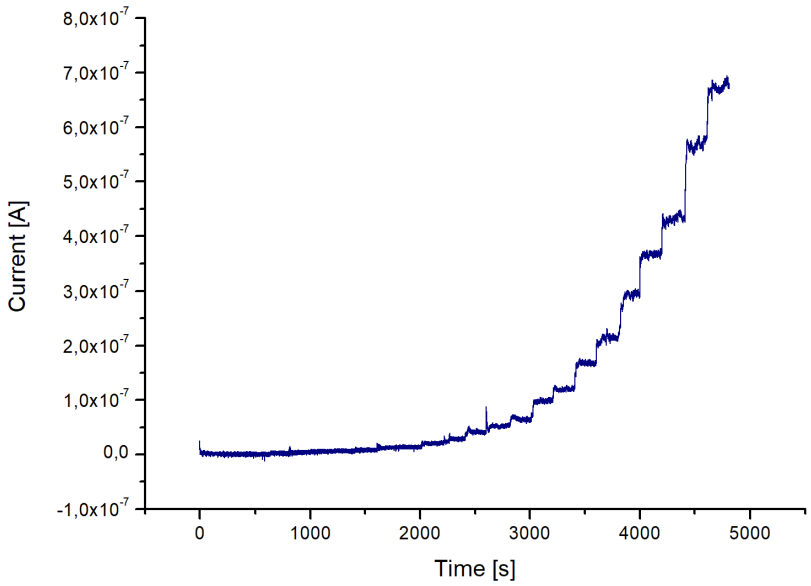

Figure 136: current/time response of Au/poly[(TAT)Ru(TpyCOOH)]/Tyr in 0.1 M phosphate buffer (pH 7.0) with EP concentration between 1 μM and 1mM

The current response was proportional to the concentration in the range 1–100 μM with a very good coefficient of determination (R^2 = 0.998) (figure 137).

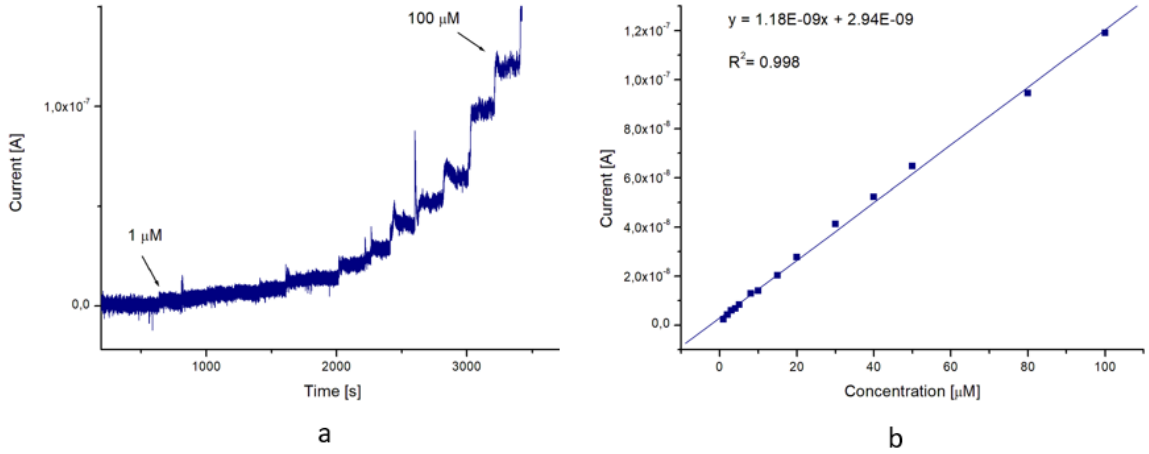

Figure 137: current/time response of Au/poly[(TAT)Ru(TpyCOOH)]/Tyr in 0.1 M phosphate buffer (pH 7.0) with EP concentration between 1 μM and 100 μM and (b) corresponding calibration curve

LoD, LoQ and sensitivity of the obtained device have been calculated using the formulas reported in section 3.5.1 and have been determined as 0.47 μM, 0.71 μM and $3.70 \cdot 10^{-8}$ A μM^{-1} cm^{-2}.

All analytical parameters are summarized in table 18:

Table 18: analytical parameters of the calibration curve (chronoamperometric data) for the determination of epinephrine with Au/poly[(TAT)Ru(TpyCOOH)]/Tyr biosensor

Linearity [μM]	LoD [μM]	LoQ [μM]	R^2	Slope	Intercept	Sensitivity [A μM^{-1} cm^{-2}]
1-100	0.47	0.71	0.998	$1.18 \cdot 10^{-9}$	$2.94 \cdot 10^{-9}$	$3.70 \cdot 10^{-8}$

The selectivity of the Au/poly[(TAT)Ru(TpyCOOH)]/Tyr biosensor was also examined. The interfering study is, in fact, a fundamental step before real samples analyses, with particular attention to biological fluids samples. Urine, blood plasma and serum etc. contain possible interfering agents such as ascorbic acid (AA), uric acid (UA), tryptophan (Trp) and L-cysteine (L-cys), therefore the effects of these substances on determination of 10 μM EP (where the peak is well-defined) were investigated. The concentrations of interfering species were varied in the ratio 1:1, 1:5 and 1:10. The peak current value recorded for only EP solution was accepted as 100% and the response in presence of interfering substances was relatively evaluated considering this value. Figure 138 reports the interference effects of AA, UA, Trp and L-cys calculated by differential pulse voltammetric measurements.

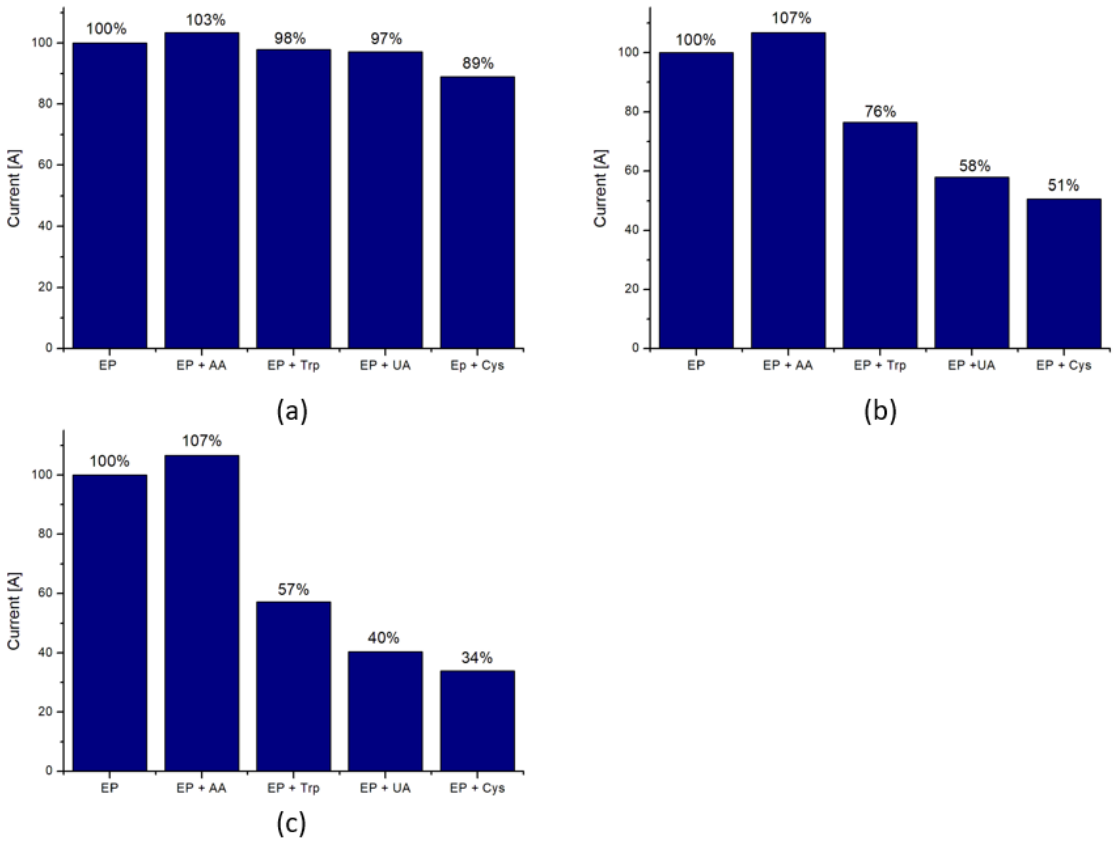

Figure 138: interference effects on 10 μM EP response of Au/poly[(TAT)Ru(TpyCOOH)]/Tyr when interfering substances are present in concentration (a) 10 μM (b) 50 μM and (c) 100 μM

It is possible to note that the effects are minimal (with the exception of L-cysteine) when the interferents are present at the same concentration of EP (figure 138a), while they become more and more significant at higher concentrations, which, however, are those of interest if the biosensor is used for analyses of biological fluids. Anyway, the interference from AA does not exceed a +7% of error, thus, allowing to consider AA influence negligible. L-cysteine, instead, is the species that most affects the voltammetric response of 10 μM EP. This may be due to the fact that, unlike the other investigated substances, for which the influence is due to their oxidation potential values very close to that of the EP (figure 139), L-cysteine has sulphur atoms in its structure which can inhibit tyrosinase active sites[204].

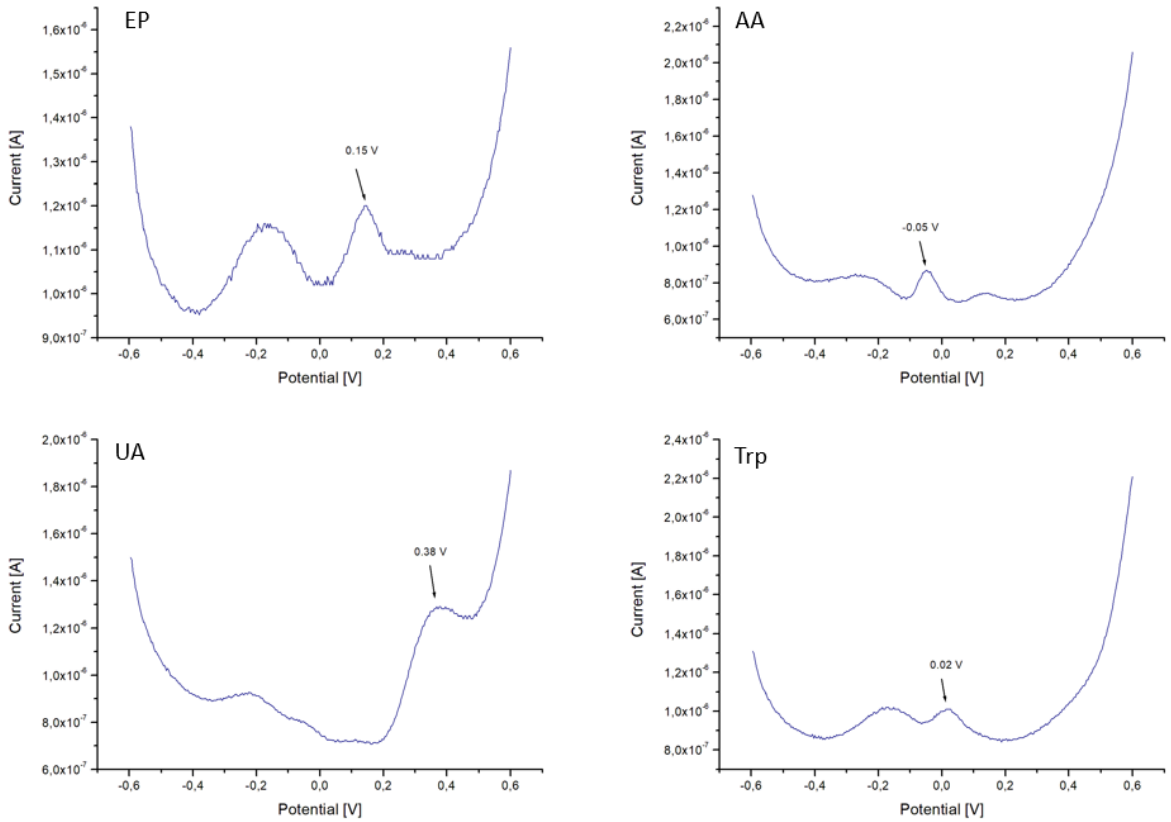

Figure 139: comparison of oxidation potential values of (a) EP, (b) AA, (c) UA and (d) Trp

Recovery tests were performed on pharmaceutical formulations as the biosensor performances, in terms of LoD and LoQ, are not suitable for investigations of biological samples. Ampoule of ADRENALINA MONICO 1 mg/1 mL ($5.46 \cdot 10^{-3}$ M) injectable solution was used diluted to 25.0 and 50.0 μM. Very good recovery values were obtained (table 19):

Table 19: recovery tests results at Au/poly[(TAT)Ru(TpyCOOH)]/Tyr (n = 5)

Sample	EP calculated	RSD%	Recovery
25.0 μM	26.9 μM	± 2.14	107.5%
50.0 μM	52.9 μM	± 1.91	105.8%

The effect of scan rate on biosensor response was also investigated for 1 mM EP at different scan rates (figure 140a). A linear graph peak current *vs*. scan rate with R^2 =

0.999 was obtained in the range 30-500 mV s^{-1} (figure 140b), typical of an absorption-controlled mechanism. In this type of processes the current is limited by the amount of space available on the electrode surface to absorb the species of interest[200,201]. For an electrode-absorbed species, the current response is described by the Laviron equation (5):

$$i_p = \frac{n^2 F^2 v A \Gamma}{RT} \quad (5)$$

where i_p is the maximum peak current, n is the number of exchanged electrons, F is the Faraday constant [C mol^{-1}], v is the potential sweep rate [V s^{-1}], A is the electrode area [cm^2], Γ is the surface coverage of the redox species [mol cm^{-2}], R is the ideal gas constant [J K^{-1} mol^{-1}] and T is the temperature [K].

Γ was calculated as $1.27 \cdot 10^{-8}$ mol cm^{-2}. This value is about 2-fold higher than those calculated by Apetrei and Apetrei[115] and by Apetrei et al.[205]. This suggests that the number of active sites is superior in the metallopolymer film than in the SWCNT[115] and in SWCNT modified with iron(II) phtalocyanine (SWCNT/FePc)[205]. Therefore, it is possible to deduce that metallopolymer film shows an improvement of the enzyme activity respect to the enzyme support used by Apetrei, probably due to the high surface area provided by the metallopolymer matrix that offers, besides, a more suitable environment for tyrosinase[206].

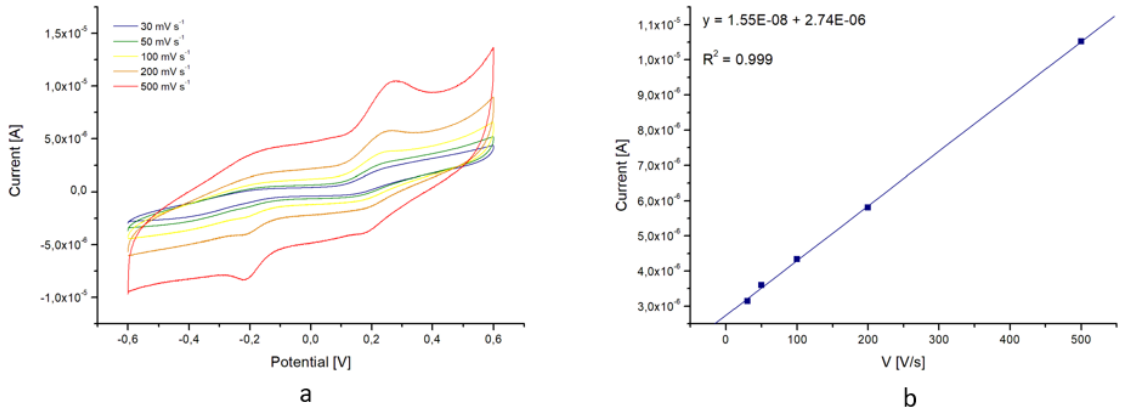

Figure 140: (a) cyclic voltammograms of Au/poly[(TAT)Ru(TpyCOOH)]/Tyr at different scan rates (30-500 mV s^{-1}) and (b) plot of I_P vs. v

Moreover, Hill coefficients are also evaluated as 1.06 ± 0.02 from DPV data and 1.28 ± 0.01 for chronoamperometric measurements.

Apparent Michaelis-Menten constant (K_M) was calculated using the adapted Lineweaver-Burk equation reported in section 3.5.1 from the data deriving from the measurements performed by DPV. In the case of chronoamperometric measurements, in fact, the Hill coefficient greater than 1.15 does not allow to calculate the K_M value because it indicates an enzyme reaction that does not fit a Michaelis-Menten type of kinetics[115,207]. A value of n_H of 1.28 shows a strong cooperative effect between the occupied active centres, that is the affinity of the tyrosinase for EP increases after the binding of an EP molecule with the enzyme. The different behaviour of the same biosensor in analysing data recorded with different techniques is reasonably ascribed to the conditions to which the device is subjected to perform the measurements. During DPV measurements the electrode, with the immobilized enzyme, was subjected to a continuous potential variation passing from a cathodic value to an anodic one for the entire series of measurements. In chronoamperometry, on the other hand, the electrode was polarized at the same potential value for the total duration of the experiment.

I_{max} and K_M were calculated as $8.33 \cdot 10^{-7}$ A and 46 μM. This K_M value is slightly higher than that obtained in the case of Au/poly(TBT)/Tyr, demonstrating that the enzyme, in

this configuration, has a slightly lower affinity for EP than when it is immobilized on TBT films. However, the biosensor has a greater affinity for EP than that reported by other authors who immobilized tyrosinase on a single-walled carbon nanotube-modified glassy carbon electrode[115].

3.5.2.2 GC/poly[(TAT)Ru(TpyCOOH)]/Tyr

The biosensor obtained by immobilizing Tyr on a GC/poly[(TAT)Ru(TpyCOOH)] modified electrode was initially tested using cyclic voltammetry. In figure 141 the voltammetric responses recorded in phosphate buffer solution (0.1 M, pH 7.0) and in the presence of 500 μM epinephrine are showed. A small anodic peak can be observed at about 0.25 V *vs*. Ag/AgCl.

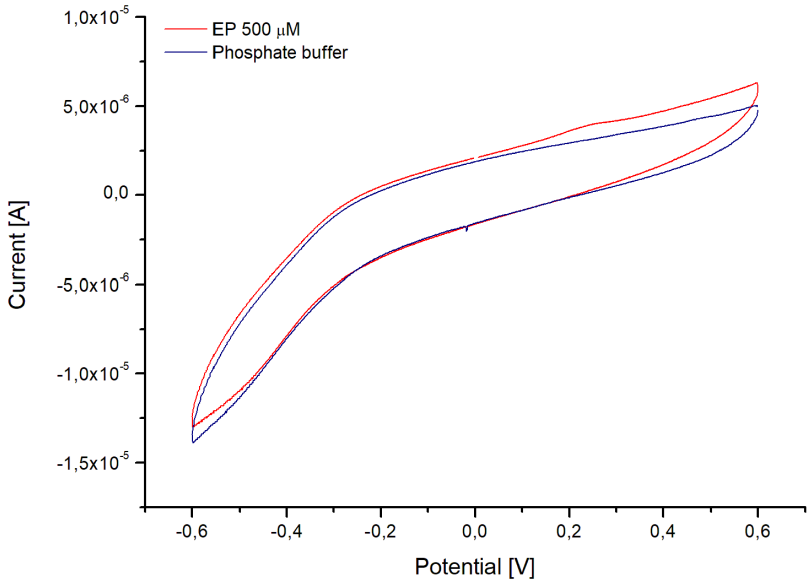

Figure 141: cyclic voltammograms of the GC/poly[(TAT)Ru(TpyCOOH)]/Tyr of the buffer solution (blue line) and in presence of 500 μM EP (red line)

Further experiments to better evaluate the behaviour of the biosensor were than carried out at room temperature, in open-atmosphere by DPV.

DPV measurements were performed in anodic direction between -0.6 and 0.6 V (step potential = 0.004 V, amplitude = 0.05 V). In figure 142 the differential pulse voltammograms recorded in presence of increasing concentrations of EP in a range 3.7-250 μM are reported. Differently from what observed with the analogue Au/poly[(TAT)Ru(TpyCOOH)]/Tyr biosensor, only one intense peak is evident at 0.15 V which increases with increasing epinephrine concentration.

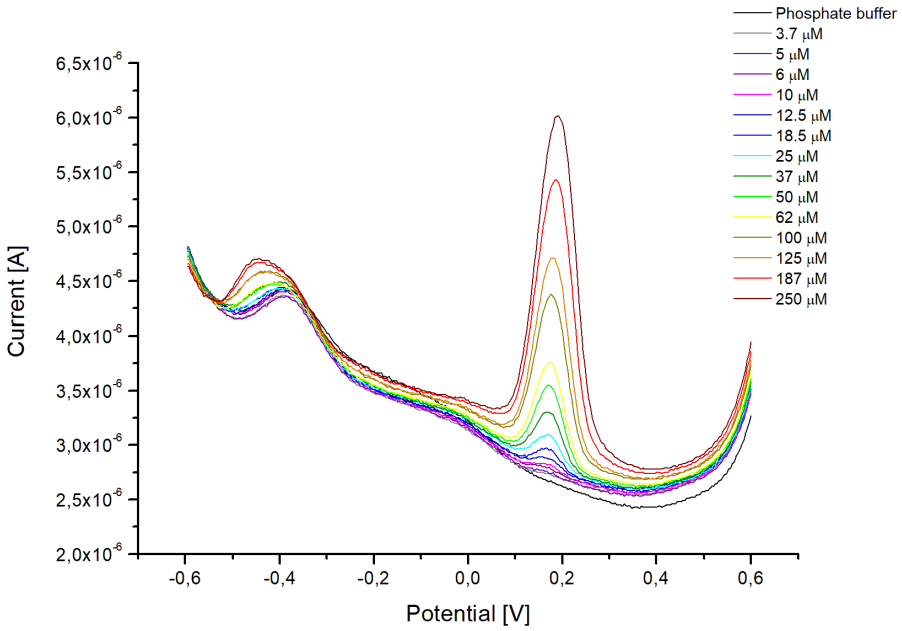

Figure 142: representative DPV scans for different concentrations of EP (potential range -0.6÷0.6 V vs. Ag/AgCl, modulation amplitude 0.05 V, step potential 0.004 V) obtained with GC/poly[(TAT)Ru(TpyCOOH)]/Tyr biosensor

The calibration curve (figure 143) evidences a very good linear response in the whole investigated range with a $R^2 = 0.997$.

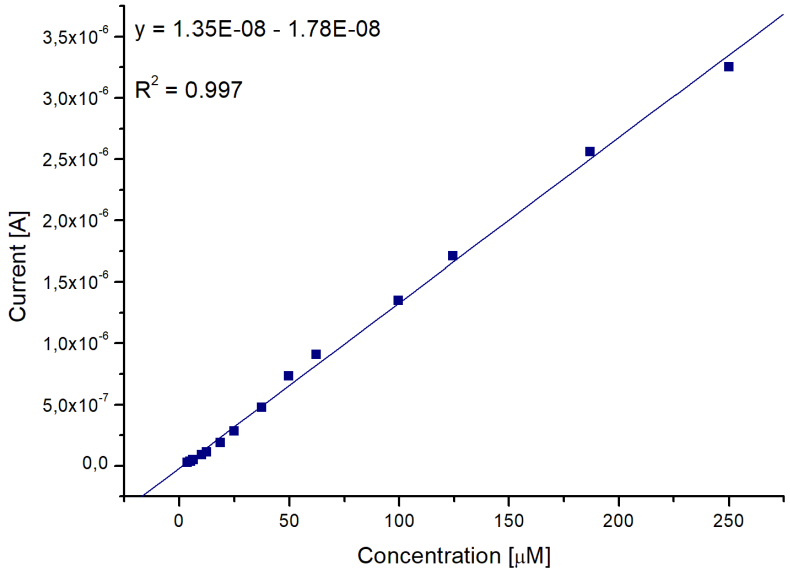

Figure 143: calibration curve calibration curve obtained with the biosensor GC/poly[(TAT)Ru(TpyCOOH)/Tyr in a concentration range between 3.7 and 250 μM

LoD, LoQ and sensitivity of the obtained device have been calculated using the formulas reported in section 3.5.1 and have been determined as 2.45 μM, 3.73 μM and $1.93 \cdot 10^{-7}$ A μM^{-1} cm^{-2}.

All analytical parameters are summarized in table 20:

Table 20: analytical parameters of the calibration curve for the determination of epinephrine with GC/poly[(TAT)Ru(TpyCOOH)]/Tyr biosensor

Linearity [μM]	LoD [μM]	LoQ [μM]	R^2	Slope	Intercept	Sensitivity [A μM^{-1} cm^{-2}]
3.7-250	2.45	3.73	0.997	$1.35 \cdot 10^{-8}$	$1.78 \cdot 10^{-8}$	$1.93 \cdot 10^{-7}$

With this device LoD and LoQ are slightly higher than those calculated for the biosensor configuration with gold electrode. Nevertheless, the obtained values are comparable (or better than) to other reported in literature, and the biosensor can be applied for pharmaceutical formulations investigations, also allowing to determine more concentrated EP solution as the linear range is larger.

Recovery tests were performed using diluted ampoule of ADRENALINA MONICO 1 mg/1mL ($5.46 \cdot 10^{-3}$ M) injectable solution at concentrations of 25.0 and 100.0 μM.

Good recovery values were obtained (table 21):

Table 21: recovery tests results at GC/poly[(TAT)Ru(TpyCOOH)]/Tyr (n = 5)

Sample	EP calculated	RSD%	Recovery
25.0 μM	26.1 μM	± 2.84	104.2%
100.0 μM	89.4 μM	± 1.59	89.4%

Selectivity was also examined, verifying the effects, on 10 μM EP, of the interferents already evaluated for the Au/poly[(TAT)Ru(TpyCOOH)]/Tyr biosensor.
The concentrations of interfering substances were varied in the ratio 1:1, 1:5 and 1:10. The peak current value recorded for only EP solution was accepted as 100% and the response in presence of interfering substances was relatively evaluated considering this value: figure 144 reports the interference effects of AA, UA, Trp and L-cys calculated on differential pulse voltammetric measurements.

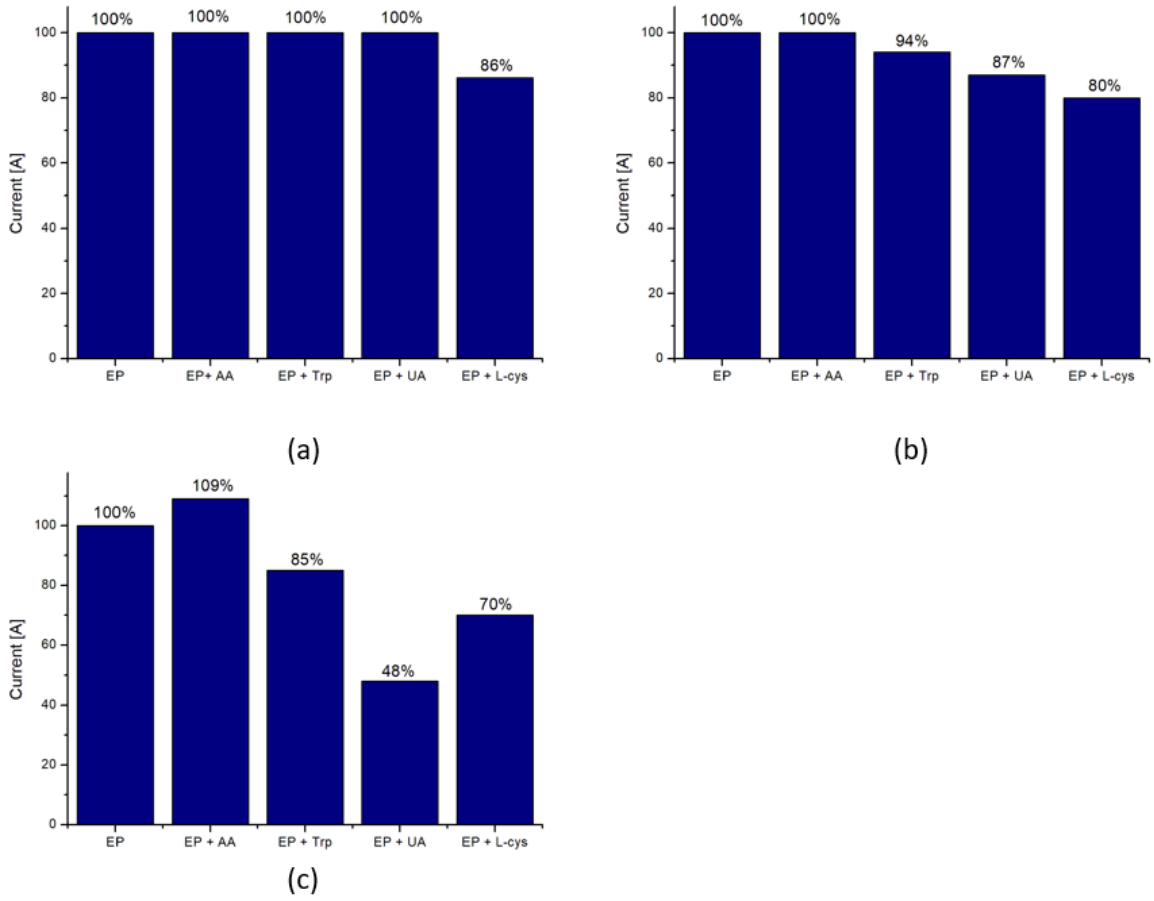

Figure 144: interference effects on 10 μM EP response at GC/poly[(TAT)Ru(TpyCOOH)]/Tyr when interfering substances are present in concentration (a) 10 μM (b) 50 μM and (c) 100 μM

As can be noted from the graphs, the effects of the interferents (with the exception of L-cysteine) are completely absent if the concentrations of EP and interfering substance are equal. A slightly more considerable effect occurs when interferents are present in a concentration 5-fold higher but, however, the error in determination is still acceptable, as it is less than or equal to (in the case of cysteine) -20%. At 10-fold higher concentration the interfering's influence becomes more and more significative but still tolerable at least as regards AA and Trp, with recoveries of 109% and 85%, respectively.

The effect of scan rate on biosensor response was also investigated for 1 mM EP at different scan rates (figure 145a). A linear graph peak current *vs*. scan rate with R^2 = 0.995 was obtained in the range 30-500 mV s^{-1} (figure 145b), typical of an absorption-controlled mechanism as in the case of the Au/poly[(TAT)Ru(TpyCOOH)]/Tyr

biosensor. Using Laviron equation (5), Γ was calculated as $1.04 \cdot 10^{-8}$ mol cm^{-2}, comparable to that obtained for the gold analogue device. The small difference could be due to the different way in which the metallopolymer is arranged on different materials and also to the different thickness of the films.

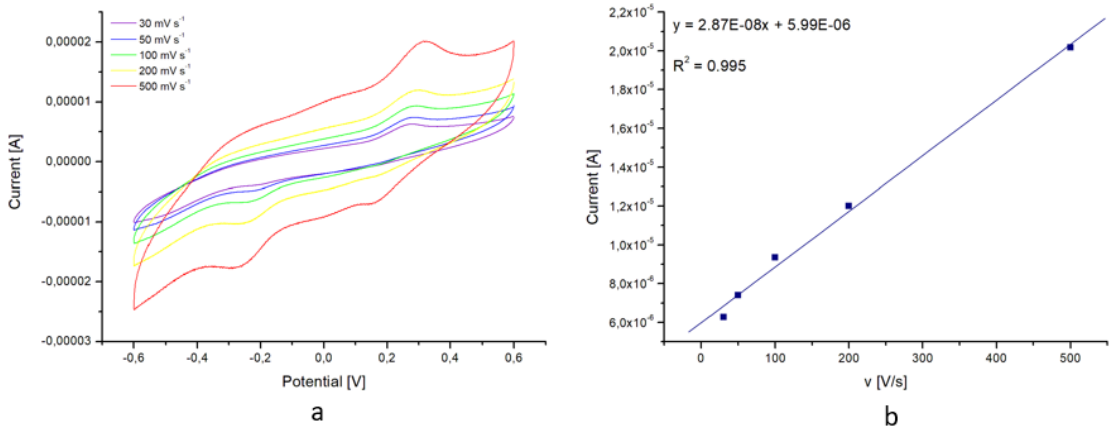

Figure 145: (a) cyclic voltammograms of GC/poly[(TAT)Ru(TpyCOOH)]/Tyr at different scan rates (30-500 mV s^{-1}) and (b) plot of I_P vs. v

In addition, from calibration data, Hill coefficient was evaluated as 1.77 ± 0.02. The value significantly deviating from 1 indicates that the kinetics of the enzymatic reaction does not fit the Michaelis–Menten type.

The differences in the various performances and features of the two poly[(TAT)Ru(TpyCOOH)]-based biosensors can be attributable to the different electrode material (gold and glassy carbon) which can interact differently with both the polymer film and the enzyme. Furthermore, it should also be remembered that the deposited films do not have the same thickness, as they have different charge density values. The thickness, considering that these are polyterthiophene-based films, can be calculated according to the equation (6):

$$d = \alpha Q_{dep} \quad (6)$$

where d is the thickness [nm], α is the experimental value [nm cm^2 mC^{-1}] and Q_{dep} is the charge density [mC cm^{-2}]. According to literature[208] an α value equal to 2.6 nm cm^2 mC^{-1} was used.

The film deposited on gold electrode possessed a thickness of about 80 nm instead that deposited on glassy carbon electrode had a thickness of about 40 nm (due to the fact that the electrode area was double for the glassy carbon electrode).

3.5.3 Poly(TTP]/Tyr-based Biosensors

Tyrosinase-based biosensors were also constructed using poly(TTP) as modifying agent for electrode surfaces. Poly(TTP) was deposited on gold and glassy carbon electrodes by chronoamperometric technique with a Q_{dep} of about 32 mC cm^{-2} (d ≈ 83 nm) and 43 mC cm^{-2} (d ≈ 110 nm), respectively, as described in section 3.1.8. Characterization of the so-obtained polymer films are illustrated in figure 115. Onto these films tyrosinase was then immobilized as reported in section 3.3.3.

The two obtained devices, Au/poly(TTP)/Tyr and GC/poly(TTP)/Tyr, were employed for the determination of EP and dopamine (DOP).

3.5.3.1 Au/poly(TTP)/Tyr

The biosensor was first tested using cyclic voltammetry. In figure 146 the voltammetric responses recorded in phosphate buffer solution (0.1 M, pH 7.0) and in the presence of 1 mM EP are showed. A very broad anodic peak can be observed at about 0.2 V *vs*. Ag/AgCl with an associated reduction peak at about 0.14 V.

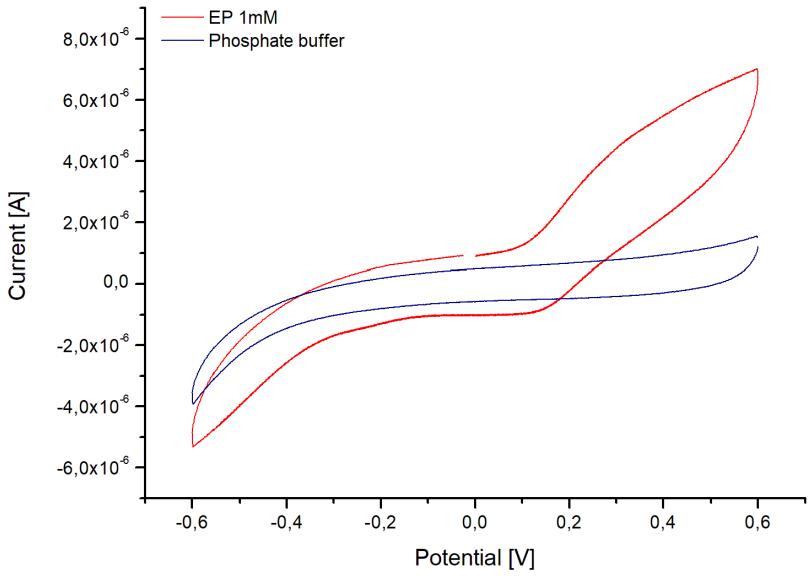

Figure 146: cyclic voltammograms of the Au/poly(TTP)/Tyr of the buffer solution (blue line) and in presence of 1 mM EP (red line)

Further experiments were than carried out at room temperature, in open-atmosphere by DPV in order to better understand the observed redox processes.

DPV measurements were performed between -0.6–0.6 V (step potential = 0.004 V and amplitude = 0.05 V). In figure 147 the differential pulse voltammograms recorded in presence of increasing concentrations of EP in a range 4-500 μM are reported. It is possible to observe an intense peak at about 0.15 V that can be reasonably ascribable to the oxidation of EP to EP open-chain quinone. At the highest concentration, voltammograms show a broad and ill-defined peak that can be attributable to the oxidation of leucoadrenochrome to the adrenochrome, as previously described for Au/poly[(TAT)Ru(TpyCOOH)]/Tyr biosensor.

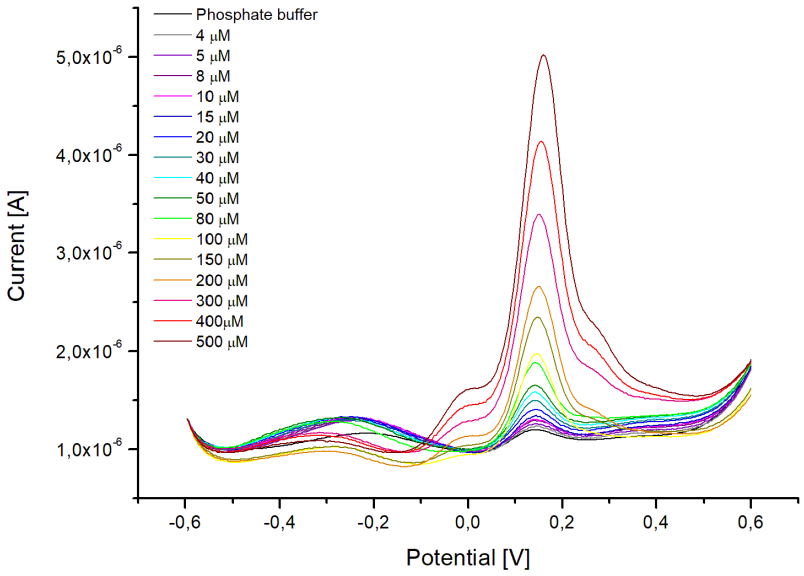

Figure 147: representative DPV scans for different concentrations of EP (potential range -0.6÷0.6 V vs. Ag/AgCl, modulation amplitude 0.05 V, step potential 0.004 V) obtained with Au/poly(TTP)/Tyr biosensor

The calibration curve (figure 148) obtained on the peak at 0.15 V shows a very good linear response in the whole investigated range with a $R^2 = 0.998$

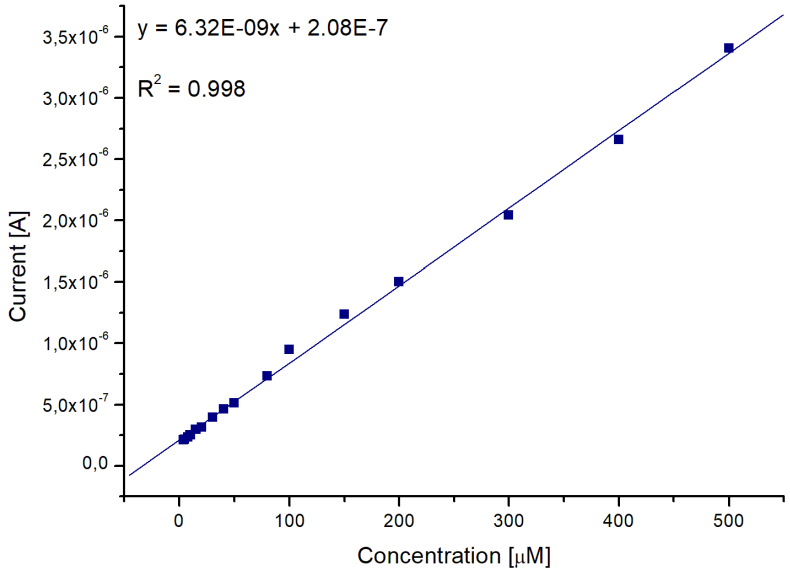

Figure 148: calibration curve calibration curve obtained with the biosensor Au/poly(TTP)/Tyr in a concentration range between 4 and 500 µM

LoD, LoQ and sensitivity of the obtained device have been calculated using the formulas reported in section 3.5.1 and have been determined as 2.07 μM, 3.14 μM and $2.01 \cdot 10^{-7}$ A μM^{-1} cm^{-2}.

All analytical parameters are summarized in table 22:

Table 22: analytical parameters of the calibration curve for the determination of epinephrine with Au/poly(TTP)/Tyr biosensor

Linearity [μM]	LoD [μM]	LoQ [μM]	R^2	Slope	Intercept	Sensitivity [A μM^{-1} cm^{-2}]
4-500	2.07	3.14	0.998	$6.32 \cdot 10^{-9}$	$2.08 \cdot 10^{-7}$	$2.01 \cdot 10^{-7}$

As can be deduced from the data shown in the table 22, this device has performances comparable to those of the biosensor GC/poly[(TAT)Ru(TpyCOOH)/Tyr with the advantage of having a slightly wider linear response range. Even in this case the application of the biosensor is suitable just for the analyses of pharmaceutical formulations, since the lowest quantifiable concentration is much higher than the concentrations of epinephrine in biological fluids.

Recovery tests were performed using diluted ampoule of ADRENALINA MONICO 1 mg/1mL ($5.46 \cdot 10^{-3}$ M) injectable solution at concentrations of 25.0 and 50.0 μM.

Good recovery value was obtained for the lower concentration of 25.0 μM whereas a large overestimation can be observed as regards the highest concentration of 50 μM (table 23):

Table 23: recovery tests results at Au/poly(TTP)/Tyr (n = 5)

Sample	EP calculated	RSD%	Recovery
25 μM	26.0 μM	± 3.08	104.1%
50 μM	62.0 μM	± 7.65	124.1%

Selectivity was also examined, verifying the effects, on 10 μM EP, of the interferents already evaluated for the biosensors described in the previous paragraph.

The concentrations of interfering substances were varied to be in the ratio 1:1, 1:5 and 1:10. The peak current value recorded for only EP solution was accepted as 100% and the response in presence of interfering substances was relatively evaluated considering this value: in figure 149 the interference effects of AA, UA, Trp and L-cys calculated on differential pulse voltammetric measurements are reported.

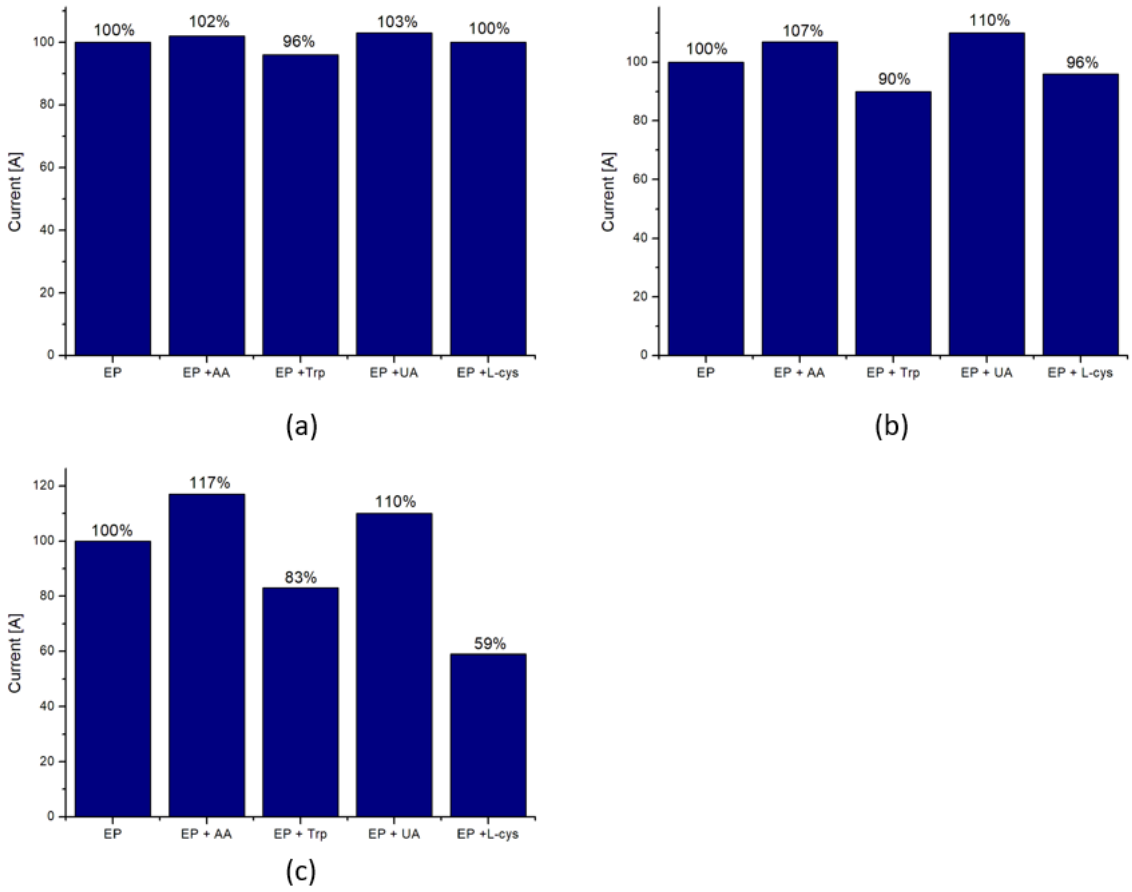

Figure 149: interference effects on 10 μM EP response of Au/poly(TTP)/Tyr when interfering substances are present in concentration (a) 10 μM (b) 50 μM and (c) 100 μM

From the interference bar graphs it is evident that in the presence of a concentration equal to that of EP the effect of the interferents is negligible, with a maximum of -4% error as regards tryptophan. At higher interfering substances concentrations, the effect becomes slightly more considerable, however reaching a maximum error of ± 10%. A

more significant effect occurs with interferent concentrations 10-fold higher than those of the analyte, however remaining within a ± 20% error, with the exception of L-cysteine.

This biosensor shows LoD and LoQ higher than Au/poly[(TAT)Ru(TpyCOOH)]/Tyr. Concerning selectivity, Au/poly(TTP/Tyr seems to suffer in a minor extent the influence of UA, Trp and L-Cys, while the effect of AA is slightly higher than on the case of Au/poly[(TAT)Ru(TpyCOOH)]/Tyr (figure 150).

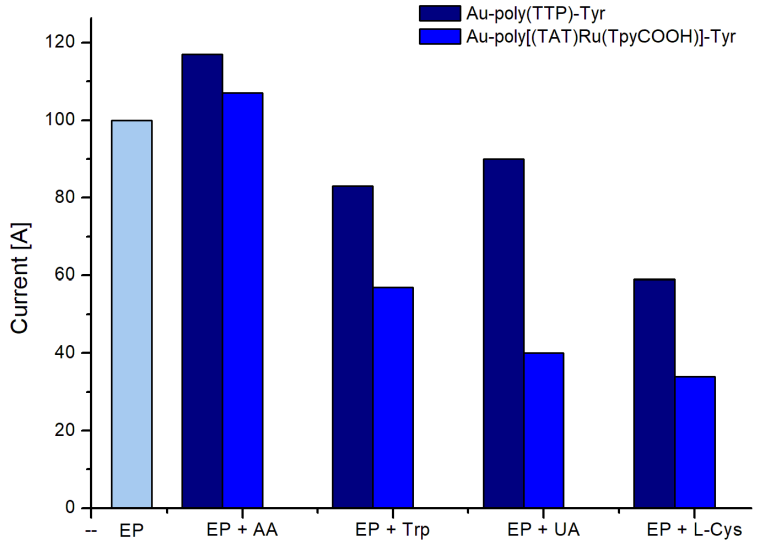

Figure 150: comparison of the selectivity of the Au/poly(TTP)/Tyr and Au/poly[(TAT)Ru(TpyCOOH)]/Tyr biosensors when EP:int is 1:10

The effect of scan rate on biosensor response was also investigated for 1 mM EP at different scan rates (figure 151a). A linear graph peak current *vs*. square root of scan rate with $R^2 = 0.991$ was obtained in the range 30-500 mV s^{-1} (figure 151b), typical of a diffusion-controlled mechanism.

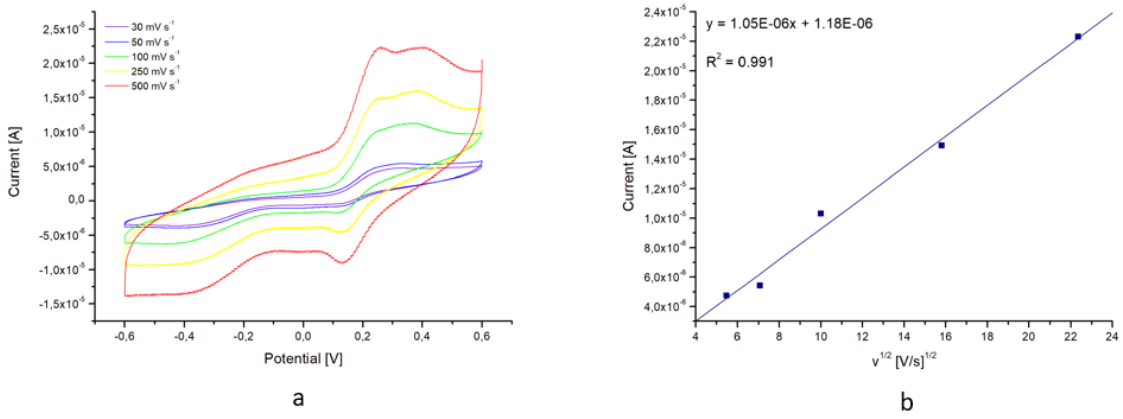

Figure 151: (a) cyclic voltammograms of Au/poly(TTP)/Tyr at different scan rates (30-500 mV s^{-1}) and (b) plot of I_p vs. $v^{1/2}$

The diffusion coefficient D of EP can be calculated from the slope of the graph 156b using the Randles-Sevcik equation reported in section 3.5.1.

Diffusion coefficient was estimated as $1.93 \cdot 10^{-9}$ cm^2 s^{-1}. This value is comparable to that calculated by Agboola et al.[202] of $2.62 \cdot 10^{-9}$ cm^2 s^{-1}, whereas it differs by almost two-fold with respect to that evaluated for the biosensor Au/poly(TBT)/Tyr of $5.10 \cdot 10^{-7}$ cm^2 s^{-1}. So, the electrochemical process is supposed to occur more slowly at the Au/poly(TTP)/Tyr system than at the analogue with poly(TBT). This difference may be due to the different effectiveness of the two polymer films in mediating the electron transfer between the electroactive species and the electrode.

3.6 Biosensors for Dopamine Detection

Au/poly(TTP)/Tyr and GC/poly(TTP)/Tyr were tested in presence of DOP, as DOP is another tyrosinase substrate. As a matter of fact, also DOP (figure 152) is a neurotransmitter belonging to the catecholamine group with a structure, differing from EP for the lack of an -OH substituent on the alkyl-chain and a methyl substituent on the terminal -NH.

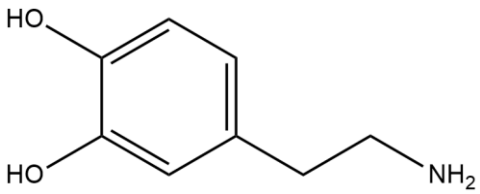

Figure 152: structure of dopamine

Analogously to what reported for EP, concentrations of DOP in bodily fluids are indicative of the body state and related to stress conditions[209,210]. In particular high levels of DOP can be observed in presence of cardiotoxicity that can lead to rapid heartbeat rate, hypertension and also to heart failure. On the other hand, low concentrations are typical of Parkinson's disease, schizophrenia, Alzheimer's disease and depression[211-216]. Therefore, also in this case, the development of sensitive biosensors for DOP determination in biological fluids (blood, urine, human cerebrospinal fluid) would be desirable. Methods for the determination of DOP require to reach lower LoD and LoQ due to the very low physiological concentration of DOP. Actually, in agreement with the Human Metabolome Database, the physiological concentration in blood is less than 130 pM, whereas in human cerebrospinal fluid and urine the levels of dopamine are ≈ 5 nM and less than 1 μmol/mmol creatinine, respectively[212,217].

3.6.1 Au/Poly(TTP]/Tyr

The biosensor was first tested using cyclic voltammetry. In figure 153 the voltammetric responses recorded in phosphate buffer solution (0.1 M, pH 7.0) and in the presence of 550 μM DOP are showed.

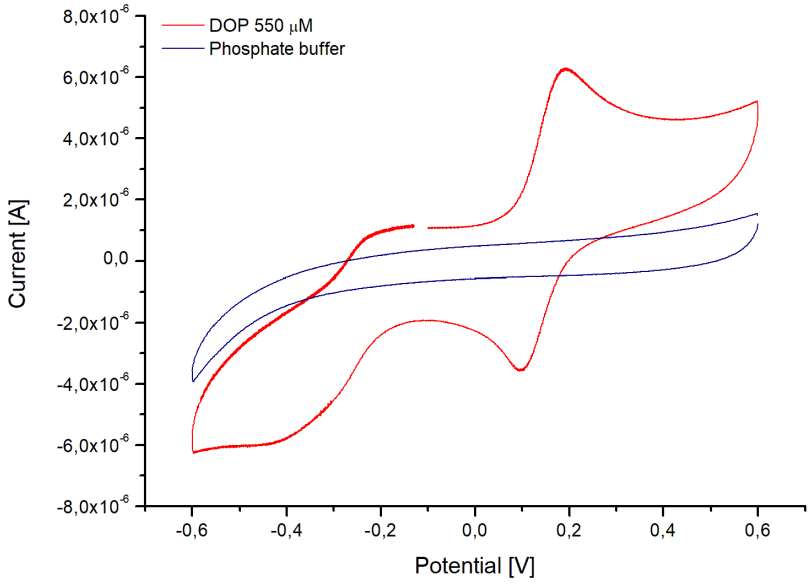

Figure 153: cyclic voltammograms of the Au/poly(TTP)/Tyr of the buffer solution (blue line) and in presence of 550 μM DOP (red line)

The cyclic voltammogram shows four electrochemical processes: it is possible to observe an anodic peak at about 0.19 V with an associated cathodic one at about 0.1 V and another broader anodic peak, significantly less intense, at about -0.23 V with associated a reduction peak at about -0.43 V. The most intense anodic peak can be reasonably, in analogy to what happens for EP, associable to the oxidation of DOP to dopamine-*o*-quinone which can cyclize to leukoaminochrome and the less anodic peak can be ascribable to the oxidation of this last one to aminochrome[218] (figure 154).

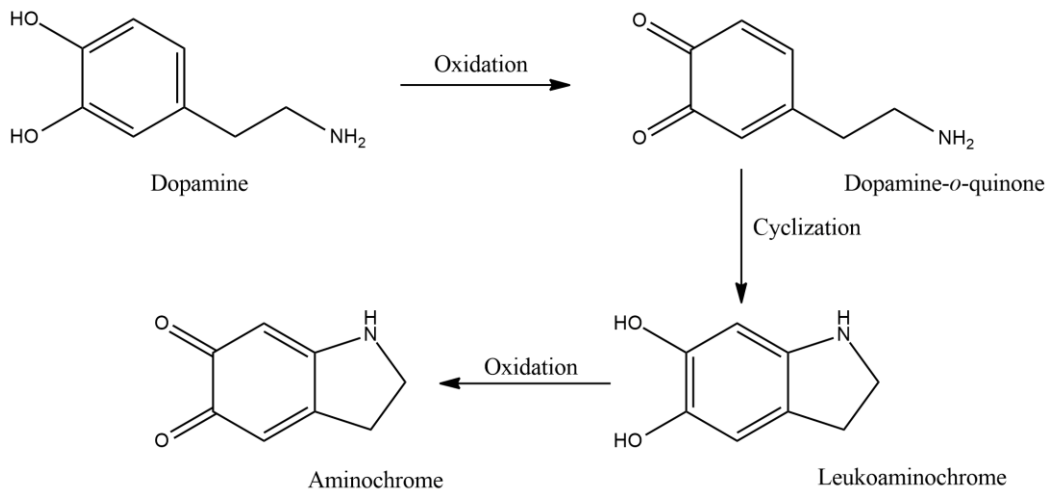

Figure 154: Schematic representation of the literature dopamine electrochemical oxidation mechanism

Further experiments were than performed at room temperature, in open-atmosphere, by DPV.

DPV measurements were carried out in anodic direction between -0.6÷0.6 V (step potential = 0.004 V and amplitude = 0.05 V). In figure 155 the differential pulse voltammograms recorded in presence of increasing concentrations of DOP in a range 2-15 μM are reported. From the graph it is possible to distinguish two peaks at about -0.23 and 0.13 V corresponding to the oxidation of leukoaminochrome and of dopamine, respectively. In particular the voltammogram shows that both peaks, the second more intensely, increase as the concentration of added dopamine increases.

The biosensor was tested up to concentrations of 100 μM, however showing a reduced linear range, probably due to a phenomenon of enzyme saturation or electrode passivation.

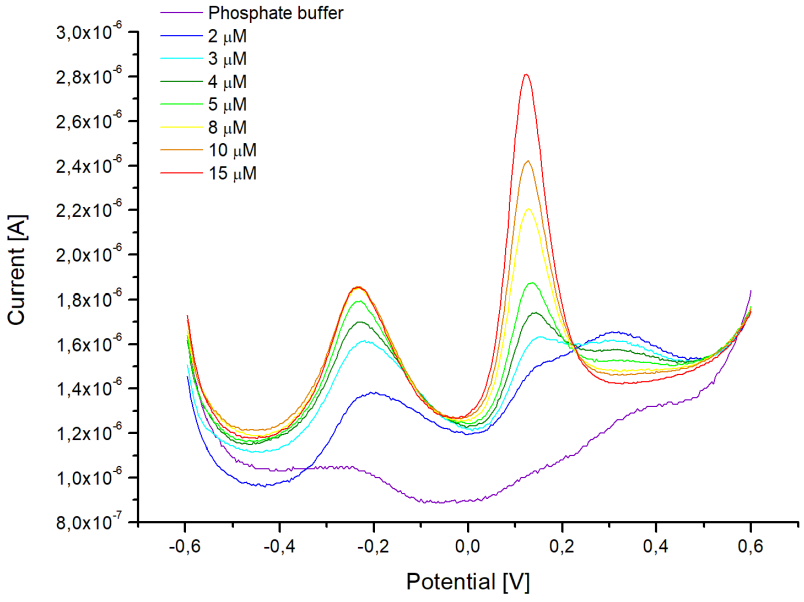

Figure 155: representative DPV scans for different concentrations of DOP (potential range -0.6÷0.6 V vs. Ag/AgCl, modulation amplitude 0.05 V, step potential 0.004 V) obtained with Au/poly(TTP)/Tyr biosensor

The calibration curve (figure 156) obtained on the more intense peak shows an acceptable linear response in the narrow range with a $R^2 = 0.990$.

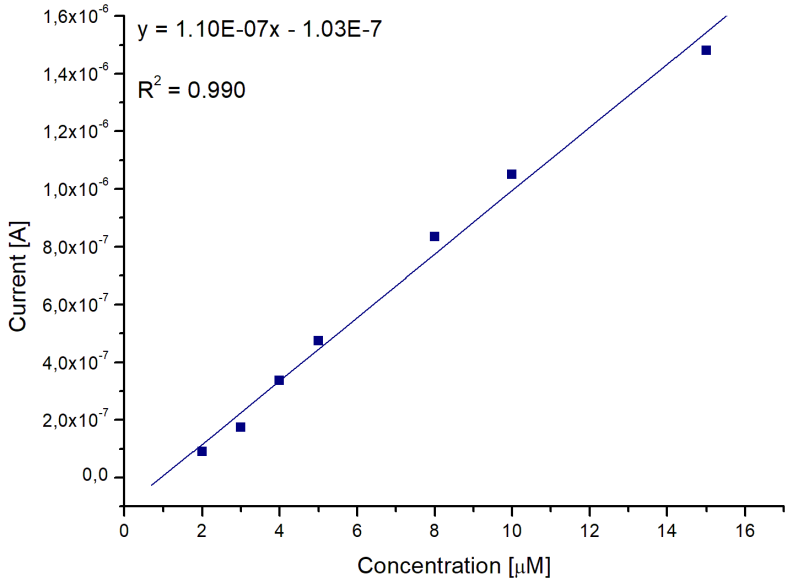

Figure 156: calibration curve calibration curve obtained with the biosensor Au/poly(TTP)/Tyr in a concentration range between 2 and 15 μM

LoD, LoQ and sensitivity of the obtained device have been calculated using the formulas reported in section 3.5.1 and have been determined as 0.24 μM, 0.37 μM and $3.50 \cdot 10^{-6}$ A μM^{-1} cm^{-2}.

All analytical parameters are summarized in table 24:

Table 24: analytical parameters of the calibration curve for the determination of dopamine with Au/poly(TTP)/Tyr biosensor

Linearity [μM]	LoD [μM]	LoQ [μM]	R^2	Slope	Intercept	Sensitivity [A μM^{-1} cm^{-2}]
2-15	0.24	0.37	0.990	$1.10 \cdot 10^{-7}$	$1.03 \cdot 10^{-7}$	$3.50 \cdot 10^{-6}$

Although the obtained LoD and LoQ values are comparable to (or better than) others reported in literature[219-221], even in the case of optical biosensors which are normally more sensitive methods[222-224], the values are not suitable for carrying out analyses on biological samples.

Nevertheless, the device can be useful for pharmaceutical formulations investigations.

However, since the performances were not optimal, it was decided to use the same poly(TTP)-tyrosinase configuration on the glassy carbon electrode with the aim to check if some enhancement is possible.

3.6.2 GC/Poly(TTP]/Tyr

The biosensor was first tested using cyclic voltammetry. In figure 157 the voltammetric responses recorded in phosphate buffer solution (0.1 M, pH 7.0) and in the presence of 80 μM DOP are showed. Conversely to what has been observed with the modified-gold electrode, the cyclic voltammetric analysis shows only one broad oxidation peak at about 0.11 V attributable to the oxidation of DOP to dopamine-*o*-quinone with the associated cathodic peak at about 0.10 V.

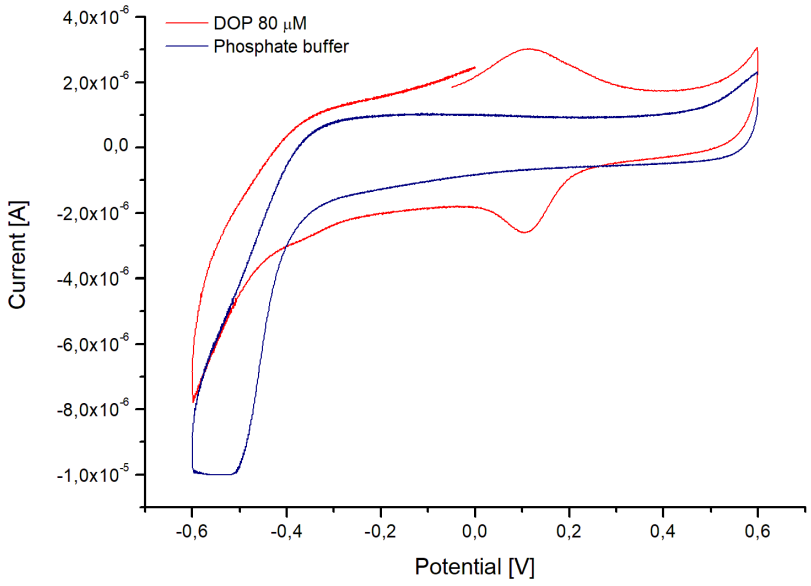

Figure 157: cyclic voltammograms of the GC/poly(TTP)/Tyr of the buffer solution (blue line) and in presence of 80 μM DOP (red line)

Further experiments were than performed at room temperature, in open-atmosphere, by DPV.

DPV measurements were carried out between -0.6 and 0.6 V (step potential = 0.004 V and amplitude = 0.05 V). It is possible to observe only one peak at 0.1 V that increases as the concentration of DOP increases.

The biosensor was tested up to concentrations of 100 μM, even in this case showing a reduced linear range probably due to a phenomenon of enzyme saturation.

In figure 158 are reported the differential pulse voltammograms recorded in presence of increasing concentrations of DOP in a range 0.5-10 μM.

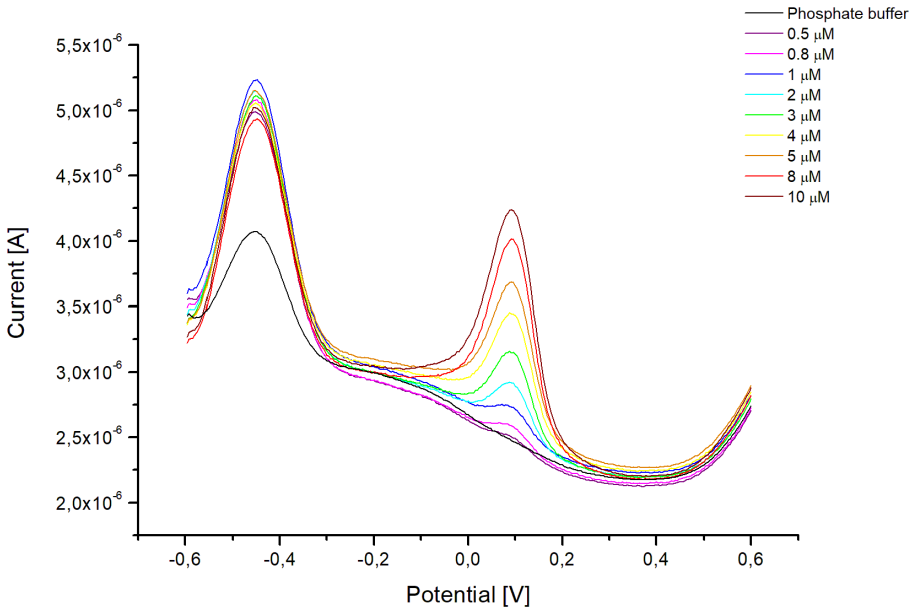

Figure 158: representative DPV scans for different concentrations of DOP (potential range -0.6÷0.6 V vs. Ag/AgCl, modulation amplitude 0.05 V, step potential 0.004 V) obtained with GC/poly(TTP)/Tyr biosensor

The calibration curve obtained using the current peak values at 0.1 V (figure 159) shows a good linear response in the narrow range with a $R^2 = 0.994$.

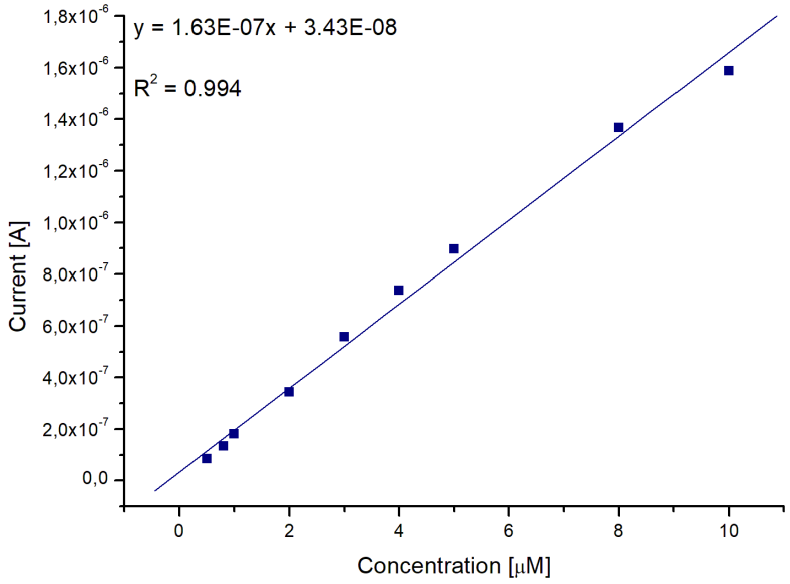

Figure 159: calibration curve calibration curve obtained with the biosensor GC/poly(TTP)/Tyr in a concentration range between 0.5 and 10 µM

LoD, LoQ and sensitivity of the obtained device have been calculated using the formulas reported in section 3.5.1 and have been determined as 0.23 µM, 0.35 µM and $2.33 \cdot 10^{-6}$ A μM^{-1} cm^{-2}.

All analytical parameters are summarized in table 25:

Table 25: analytical parameters of the calibration curve for the determination of dopamine with GC/poly(TTP)/Tyr biosensor

Linearity [µM]	LoD [µM]	LoQ [µM]	R^2	Slope	Intercept	Sensitivity [A μM^{-1} cm^{-2}]
0.5–10	0.23	0.35	0.994	$1.63 \cdot 10^{-7}$	$3.43 \cdot 10^{-8}$	$2.33 \cdot 10^{-6}$

As can be deduced from the data reported in table 25, this device has better performances than those of the biosensor Au/poly(TTP)/Tyr, not as regards LoD and LoQ which are absolutely comparable, but for what concerns linearity which starts from a value of about an order of magnitude lower. Compared to (bio)sensors reported

in the literature, this device is better performing from the point of view of LoD but not regarding the linear response range which is very narrow. In table 26 analytical performances of our biosensors and other (bio)sensors reported in literature are compared.

Table 26: comparison of amperometric (bio)sensors for determination of DOP

(Bio)sensor	Linearity [μM]	LoD [μM]	R^2	Reference
MWNT-Nafion-Tyr	5-23	0.52	-	225
Eggshell-Tyr	50-250	25	0.9719	226
Tyr-SWNTs-PPy-GCE	5-50	5	0.998	220
CDs-CS-GCE	0.1-30	0.0112	0.996	227
GME	4-100	2.64	0.988	228
GO/GCE	1.0-15.0	0.27	-	229
Graphene-diamond	5-2000	0.20	-	219
Au-CoP	10-50	0.98	-	221
Au-CoP-Tyr	2-30	0.43		221
γ-WO_3 NPs/GCE	0.1-50, 50-600	0.024	-	230
Au/poly(TTP)/Tyr	2-15	0.24	0.990	This work
GC/poly(TTP)/Tyr	0.5-10	0.23	0.994	This work

CDs-CS: carbon dots-chitosan; GME: graphene modified electrode; CoP: cobalt(II) porphyrin; γ-WO_3 NPs: tungsten trioxide nanoparticles with monoclinic structure;

With this biosensor, recovery and selectivity tests were carried out.

Recovery tests were performed using diluted ampoule of DOPAMINA CLORIDRATO S.A.L.F. 10 mg/2mL (0.026 M) injectable solution at concentrations of 1.0 and 5.0 μM. Good recovery values were obtained (table 27):

Table 27: recovery tests results at GC/poly(TTP)/Tyr (n = 5)

Sample	DOP calculated	RSD%	Recovery
1 μM	0.98 μM	± 9.61	97.6%
5 μM	4.66 μM	± 11.2	93.1%

Selectivity was examined, verifying the effects, on 5 μM DOP, of the interferents already evaluated for the biosensors described in the previous paragraphs.

The concentrations of interfering substances were varied to be in the ratio 1:1, 1:5 and 1:10. The peak current value recorded for only DOP solution was accepted as 100% and the response in presence of interfering substances was relatively evaluated considering this value: in figure 160 the interference effects of AA, UA, Trp and L-cys calculated on differential pulse voltammetric measurements are reported.

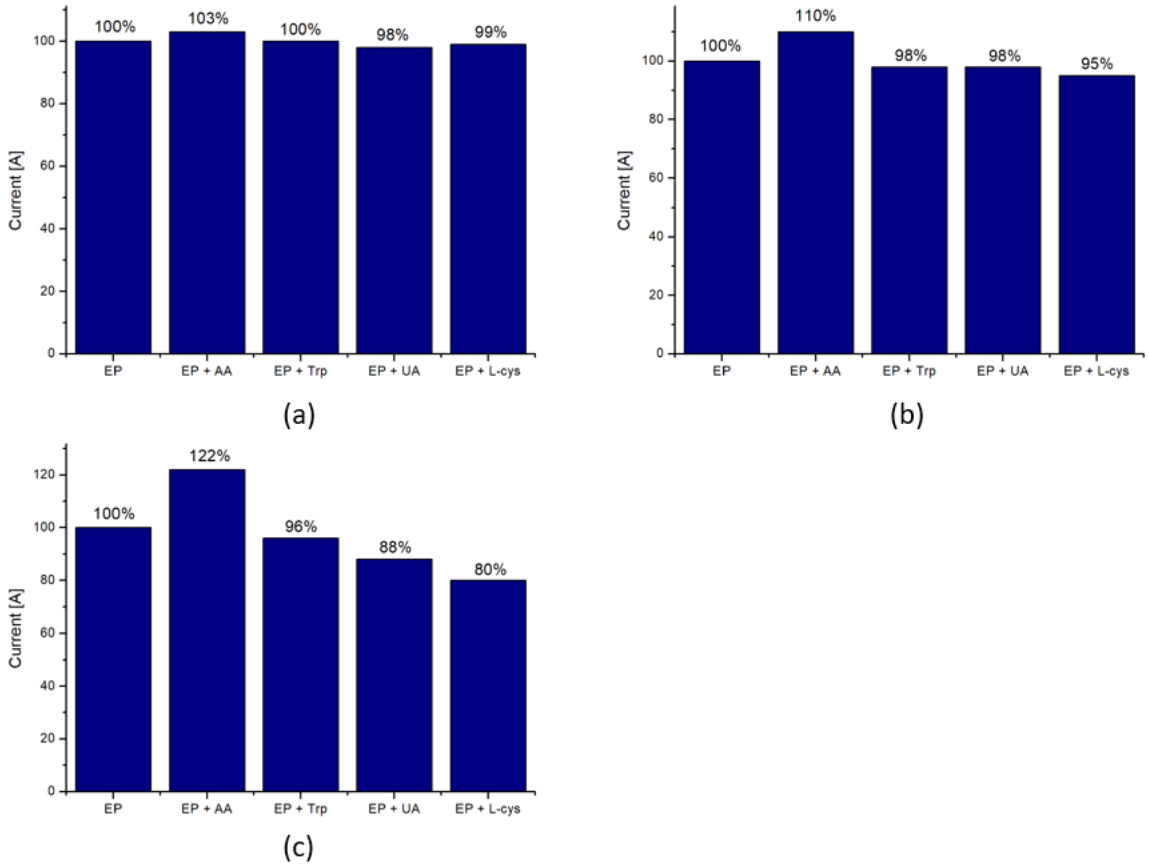

Figure 160: interference effects on 5 μM DOP response at GC/poly(TTP)/Tyr when interfering substances are present in concentration (a) 5 μM (b) 25 μM and (c) 50 μM

Plots in figure 160 evidence that in the presence of a concentration equal to that of DOP the effect of the interferents is negligible, with a maximum of +3% error in presence of 5 μM AA. At higher interfering substances concentrations, the effect becomes slightly more significative, however reaching a maximum error of +10% for AA and remaining almost constant for the other interferents. A more considerable effect occurs with interferent concentrations 10-fold higher than those of DOP, reaching a +22% error in the case of AA and -20% in the case of L-cysteine. The higher interference effect of AA on the determination of DOP, compared to EP, is reasonably due to the fact that the oxidation potential of DOP is closer to that of AA than that of EP. The interference from L-Cys, on the other hand, is always attributed to its tendency to inhibit the enzyme.

The effect of scan rate on biosensor response was also investigated for 10 μM DOP at different scan rates (figure 161a). A linear graph peak current *vs*. square root of scan rate with $R^2 = 0.990$ was obtained in the range 30-500 mV s^{-1} (figure 161b), typical of a diffusion-controlled mechanism.

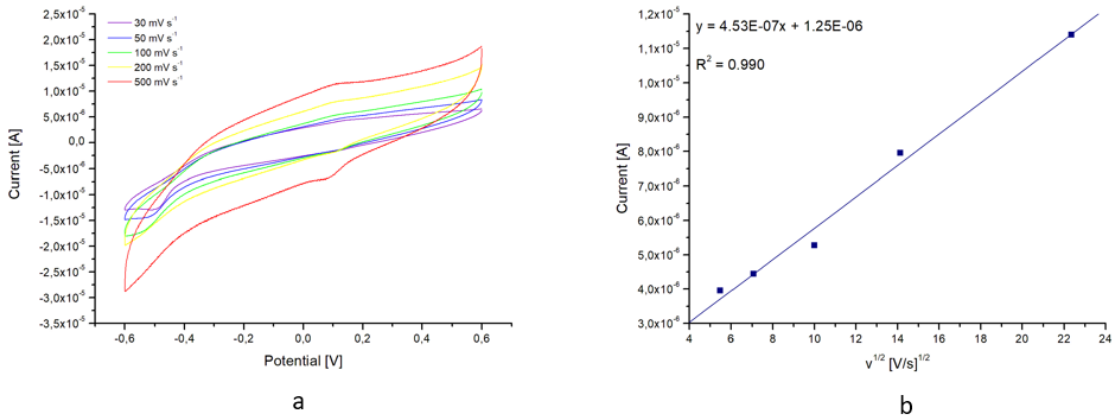

Figure 161: (a) cyclic voltammograms of GC/poly(TTP)/Tyr at different scan rates (30-500 mV s^{-1}) and (b) plot of I_P vs. $v^{1/2}$

The diffusion coefficient D of DOP can be calculated from the slope of the graph 162b using the Randles-Sevcik equation reported in section 3.5.1.

Diffusion coefficient was calculated as $7.12 \cdot 10^{-7}$ $cm^2 s^{-1}$. This value, compared to others reported in the literature[227,229,230] relating to modified GCE electrodes, it is lower, meaning that the electrochemical process occurs more slowly in the case of our biosensor. Table 28 shows some of the diffusion coefficients reported in the literature.

Table 28: comparison of diffusion coefficients obtained with different GC-modified electrodes for dopamine detection

(Bio)sensor	Diffusion Coefficient [$cm^2 s^{-1}$]	Reference
GO/GCE	$2.26 \cdot 10^{-6}$	229
CDs-CS/GCE	$3.68 \cdot 10^{-6}$	227
γ-WO_3 NPs/GCE	$1.4025 \cdot 10^{-5}$	230
β-WO_3 NPs/GCE	$1.613 \cdot 10^{-5}$	230
GC/poly(TTP)/Tyr	$7.12 \cdot 10^{-7}$	This work

GO: graphene oxide; β-WO_3 NPs: tungsten trioxide nanoparticles with orthorhombic structure;

Hill coefficient was also evaluated as 1.06 ± 0.02. The value, that differ from unity only minimally, suggests that the kinetics of enzyme reaction is in agreement with a Michaelis-Menten type kinetics. Furthermore, the value slightly higher than 1 shows that there is a positive cooperative effect, similarly to what is described in the case of the Au/poly(TBT)/Tyr biosensor for the determination of EP.

Moreover, apparent Michaelis-Menten constant (K_M) was calculated using the adapted Lineweaver-Burk equation reported in section 3.5.1.

I_{max} and K_M were calculated as $9.43 \cdot 10^{-6}$A and 57 μM, respectively. The obtained K_M value is very similar to that reported by Tsai et al.[225] of 60 μM, who immobilized tyrosinase on multiwalled carbon nanotube-Nafion-nanobiocomposite-modified glassy carbon electrode. Florescu and David[221], who anchor tyrosinase on CoP-modified gold report a value of 92.68 μM. Considering that generally the values of K_M

for the immobilized tyrosinase are between 60 and 200 μM[221], a value of 57 indicates that the affinity of the enzyme for dopamine is increased. This may be due to a particular rearrangement of the protein on the TTP film which has modified its conformation making the active site more suitable for the dopamine binding.

FINAL SUMMARY

This thesis work was devoted to the design and development of thiophene-conducting polymer-based biosensors for histamine, epinephrine and dopamine detection. Syntheses (including unsuccessful syntheses approaches) of monomers suitable for the obtainment of conductive polymers and metallopolymers to be used for the modification of electrode surfaces are reported. The monomers obtained were characterized by spectroscopic (^{1}H NMR and UV-Vis) and electrochemical (CV) techniques and their behaviour and ability to electropolymerize were discussed. The electrochemical characterizations of the electrogenerated polymers are also reported. Finally, development of biosensors was accurately described, and the analytical parameters were evaluated.

In a first step of the research, a classical thiophene-based conducting polymer (PEDOT, poly(3,4-ethylenedioxythiophene)) was used and compared to a metal-containing system ([(TAT)Ru(TpyCOOH), TAT = 4'-(2,2':5',2''-terthien-3'-ethynyl)-2,2':6',2''-terpyridine, TpyCOOH = 4,4',4''-tricarboxylate-2,2':6,2''–terpyridine), previously reported by the research group where this PhD work was performed. The conducting polymers were used as immobilizing agents of the enzyme DAO (diamine oxidase) for histamine detection. In particular, two biosensors, Pt/PEDOT/DAO and Pt/poly[(TAT)Ru(TpyCOOH)]/DAO, were designed and investigated. The PEDOT-based biosensor was developed with the aim to check the suitability of the arrangement, according to a biosensor previously reported [8]. The encouraging results obtained were the basis for the development of an analogue arrangement using the electrogenerated metal-containing polymer (poly[(TAT)Ru(TpyCOOH)]). Numerous attempts to find an adequate configuration, including different approaches for the enzyme immobilization, use of a redox mediator as well as use of different thicknesses of the film were performed. Unfortunately, results obtained show that a so-designed system is not suitable for histamine detection.

The experience gained at the beginning of the work suggested to focus the attention to different analytes, specifically epinephrine (EP) and dopamine (DOP), well-known neurotransmitters. To this end, electrogenerated films deriving from TBT (4,7-bis(5-(pyridin-2-yl)thiophen-2-yl)benzo[c][1,2,5]thiadiazole), from TTP (bis(4-(thiophen-2-yl)tetraphenylsilane)) and from the previously cited (TAT)Ru(TpyCOOH) were used as immobilizing agent, and tyrosinase (Tyr) was used as bioreceptor. Concerning EP detection, four biosensors (Au/poly(TBT)/Tyr, Au/poly[(TAT)Ru(TpyCOOH)]/Tyr, GC/poly[(TAT)Ru(TpyCOOH)]/Tyr and Au/poly(TTP)/Tyr) were developed. All of these biosensors showed analytical performances comparable to (or better than) literature data in terms of linearity range, LoD, and LoQ. Although LoD values indicate that these biosensors are not suitable for the use in biological samples, they can be used for pharmaceutical formulations analysis as most of the electrochemical (bio)sensors for EP detection reported in literature. A comparison between analytical parameters of the developed biosensors and some analogue systems reported in literature is summarized in Table 29.

Table 29: comparison of amperometric biosensors for determination of EP

Biosensor	Linearity [μM]	LoD [μM]	LoQ [μM]	R^2	Method	Ref.
GCE/SWCNT/Tyr	10-110	2.54	-	0.977	CA	115
CPE/MWCNT/Nafion/Tyr	5-500	0.3	-	0.9985	DPV	111
GCE/MWCNTs/Tyr	0.6-100	0.514	1.71	0.997	DPV	203
GCE/Eggshell membrane/Tyr	30-300	10	-	0.9734	DPV	231
Graphene-modified SPE/Tyr	1-27.5	0.656	-	-	CA	232
Au/poly(TBT)/Tyr	0.1-50	0.06	0.09	0.996	CA	193 and this work
Au/poly(Ru-complex)/Tyr	1-100 1-100	0.67 0.47	1.02 0.71	0.998 0.998	DPV CA	233 and this work
GC/poly(Ru-complex)/Tyr	3.7-250	2.45	3.73	0.997	DPV	233 and this work
Au/poly(TTP)/Tyr	4-500	2.07	3.14	0.998	DPV	This work

Poly(Ru-complex): poly[(TAT)Ru(TpyCOOH)]

From the summarized data it is possible to note that the analytical performances of our biosensors are in accordance with, and in some cases better than, those reported in literature for other Tyr-based devices, demonstrating a remarkable effectiveness of the polymer matrices used for the immobilization of the bio-element.

Hill coefficient (n_H) and Michaelis-Menten constant (K_M) were evaluated. The calculated values are compared in table 30.

Table 30: comparison of n_H and K_M of tyrosinase-based amperometric biosensors for EP detection

Biosensor	n_H	K_M [μm]	Ref.
Au/poly(TBT)/Tyr	1.09 ± 0.01	35	193 and this work
Au/poly(Ru-complex)/Tyr	1.06 ± 0.01	46	233 and this work
GC/poly(Ru complex)/Tyr	1.77 ± 0.02	-	233 and this work
GCE/SWCNT/Tyr	1.07 ± 0.03	60	[115]

As it is possible to observe, the smallest K_M value, corresponding to a higher affinity of the enzyme to its substrate, was obtained for the Au/poly(TBT)/Tyr biosensor, that is the device with the lowest LoD value.

In the case of the GC/poly[(TAT)Ru(TpyCOOH)]/Tyr biosensor it was not possible to calculate K_M as the enzymatic process does not fit Michaelis-Menten kinetics model, as can be deduced from the high value of Hill coefficient.

The effect of scan rate on biosensor response was also investigated. In particular, in the case of poly[(TAT)Ru(TpyCOOH)]-based biosensors, the influence of scan rate on the

peak current showed a linear relationship between 30 and 500 mV s^{-1}, typical of an absorption-controlled mechanism. Moreover, values of the surface coverage of the redox species Γ were calculated and compared with literature data (table 31). Table 31 suggests that the used metallopolymer films show an enhancement in enzymatic activity respect to the SWCNT and SWCNT modified with FePc. Probably, the metallopolymer matrix offers a more suitable environment for tyrosinase anchoring, in addition to a higher surface area.

Table 31: comparison of the surface coverage of the redox species of tyrosinase-based biosensors

(Bio)sensor	**Γ [mol cm^{-2}]**	**Ref.**
GCE/SWCNT/Tyr	$2.34 \cdot 10^{-10}$	115
SPE/SWCNT/FePc/Tyr	$8.92 \cdot 10^{-10}$	205
Au/poly(Ru-complex)/Tyr	$1.27 \cdot 10^{-8}$	233 and this work
GC/poly(Ru-complex)/Tyr	$1.04 \cdot 10^{-8}$	233 and this work

FePc: iron(II)phtalocyanine;

Conversely, for TBT- and TTP-based biosensors, linear graphs of peak current *vs.* square root of scan rate were obtained, typical of a diffusion-controlled mechanism. Estimated values of the diffusion coefficient D are compared with literature data (table 32). It is possible to note that the value of Au/poly(TBT)/Tyr is comparable to that reported for the L-Cys/Au SAMs device, whereas it is almost two-fold higher than that reported for the TTP-modified one (which is absolutely comparable with that of Au/Cys/FeOCPc). These data suggest that the electrochemical process occurs faster at

the Au/poly(TBT)/Tyr than at the analogue with poly(TTP), highlighting the different effectiveness of the two polymers in mediating the electron transfer.

Table 32: comparison of diffusion coefficients obtained with different (bio)sensors for epinephrine detection

(Bio)sensor	D [$cm^2\ s^{-1}$]	Ref.
GCE/SWCNT/Tyr	$7.87 \cdot 10^{-6}$	115
Au/Cys-FeOCPc	$2.62 \cdot 10^{-9}$	202
L-Cys/Au SAMs	$1.48 \cdot 10^{-7}$	198
Au/poly(TBT)/Tyr	$5.10 \cdot 10^{-7}$	193 and this work
Au/poly(TTP)/Tyr	$1.93 \cdot 10^{-9}$	This work

Selectivity was tested for Au/poly[(TAT)Ru(TpyCOOH)]/Tyr, GC/poly[(TAT)Ru(TpyCOOH)/Tyr and Au/poly(TTP)/Tyr using typical interfering substances that can be found in biological fluids: AA, Trp, UA and L-Cys. Interference studies on Au/poly(TBT)/Tyr are, currently, in progress. Bar graphs here reported (figure 162) are useful visual tool to compare the selectivity of the aforementioned devices.

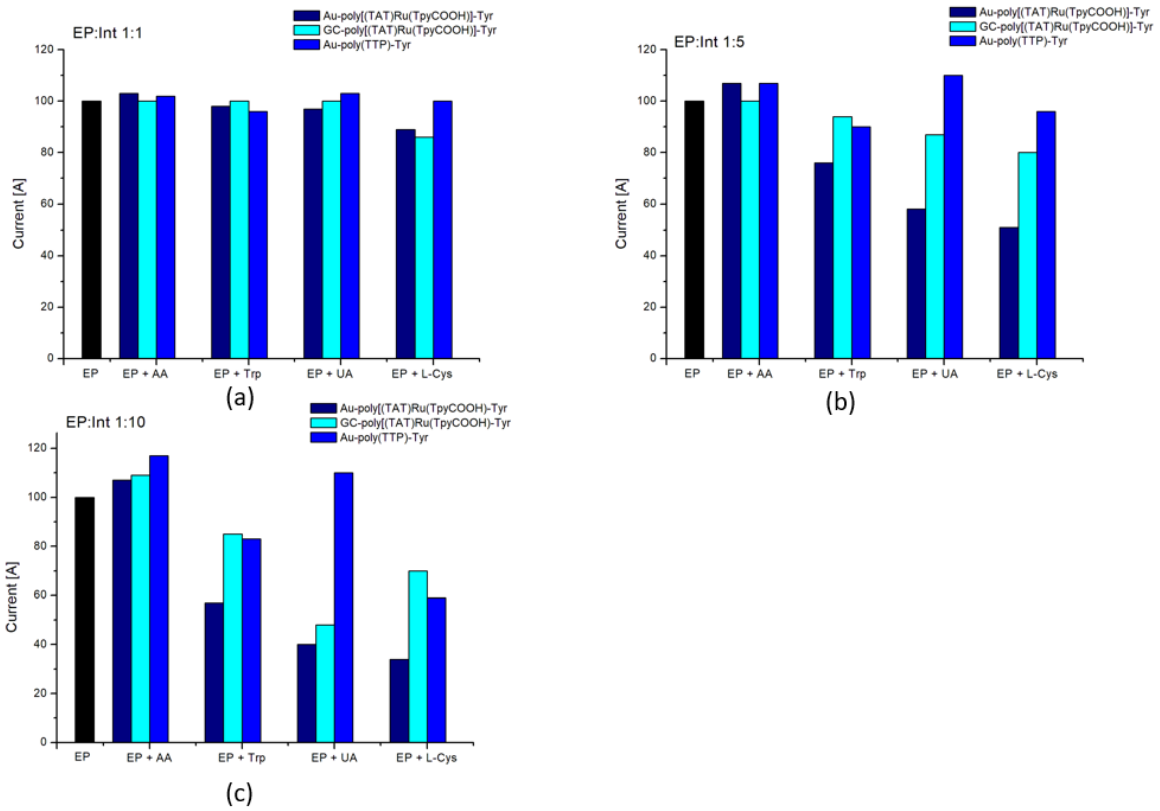

Figure 162: comparison of the selectivity of the Au/poly[(TAT)Ru(TpyCOOH)]/Tyr, GC/poly[(TAT)Ru(TpyCOOH)]/Tyr and Au/poly(TTP)/Tyr biosensors

This comparison suggests that, as far as interferents effect is concerned, both the electrode material and its coating play a fundamental role, besides obviously the concentration of the interfering substances.

In particular, as regards the biosensors obtained using the Ru(II) complex, the electrode material seems to be a fundamental element in limiting some types of interference. As a matter of fact, the biosensor GC/poly[(TAT)Ru(TpyCOOH)]/Tyr turns out to be decidedly more selective than the gold analogue, especially when EP: Int is 1:1 or 1:5. On the 1:10 ratio, in which the electrode material and its coating probably count less than the concentration of the interferers, the behaviour is almost the same, except for the interference from AA (even though with a minimal difference). A comparison, instead, between the biosensor Au/poly[(TAT)Ru(TpyCOOH)]/Tyr and Au/poly(TTP)/Tyr can highlight how, with the same electrode material, different surface modifying agents can influence the response of the biosensor in the presence of interfering substances. Such a comparison, considering the case EP:Int 1:10,

remarkably highlights that the TTP coating is more capable to limit the influence of interfering substances (with the exception of AA) compared to the metallopolymer film. The selectivity performances of both biosensors are almost comparable (with the exception of the L-Cys) for the 1:1 ratio, whereas for the 1:5 the Au/poly(TTP)/Tyr is definitely less affected.

Both poly[(TAT)Ru(TpyCOOH)-Tyr-based biosensors and the Au/poly(TTP)/Tyr one have been tested on real samples (epinephrine injection solutions) all showing very good recovery values on the 25 μM sample, from 104.1% of the Au/poly(TTP)/Tyr to 107.5% of the Au/poly[(TAT)Ru(TpyCOOH)]/Tyr. Concerning the tested highest concentrations, the Au/poly[(TAT)Ru(TpyCOOH)]/Tyr showed a recovery of 105.8% whereas the GC/poly[(TAT)Ru(TpyCOOH)]/Tyr and Au/poly(TTP)/Tyr showed an underestimation of 10.6% and a overestimation of 24.1%, respectively. These under- and overestimated values at higher concentrations may be due to the interference of metabisulphite present in the formulations[106], which however seems to interfere in different way with regard to the metallopolymer-based biosensors (decrease in recovery) and the TTP-based one (increase in recovery).

Finally, TTP/Tyr-based devices (Au and GC modified with TTP and Tyr) were employed for dopamine detection. The modified-GC one gave very good results from the point of view of LoD and LoQ and also of selectivity with a maximum interference effect of 20% (in presence of L-Cys) and 22% (in presence of AA) for DOP:int ratio 1:10. In particular the biosensors showed LoD values of 0.24 μM (Au/poly(TTP)/Tyr) and 0.23 μM (GC/poly(TTP)/Tyr), comparable to (or better than) those reported in literature (table 26). However, the GC-modified one possesses a better linear range than the Au-modified, even if in both cases the linear ranges are rather narrow: 0.5-10 μM and 2-15 μM for the GC- and Au-modified, respectively. For the modified-GC device the effect of scan rate on biosensor response was also investigated, as well as the biochemical parameters of n_H and K_M. Briefly, regarding the effect of scan rate, a diffusion-controlled mechanism has been identified, with a diffusion coefficient of $7.12 \cdot 10^{-7}$ cm^2 s^{-1}. This value is the lowest if compared with others found in literature

related to modified GC electrodes, meaning that the electrochemical process occurs more slowly in the case of GC/poly(TTP)/Tyr.

From the point of view of biochemical parameters, calculated K_M value of 57 μM proved that tyrosinase, immobilized on TTP, has very high affinity towards DOP. Comparison tables with literature values have been previously reported in the paragraph 3.6.2.

References

[1] S. N. Sawant, *Development of Biosensors from Biopolymer Composites* in *Biopolymer Composites in Electronics*, Elsevier, **2015**

[2] N. Bhalla, P. Jolly, N. Formisano, P. Estrela, *Essays in Biochemistry*, **2016**, 60, 1-8

[3] H. Sharma, R. Mutharasan, *Sensors and Actuators B: Chemical*, **2013**, 183, 535-549

[4] J. Gonzalez-Rodriguez, M. Raveendran, *Biosensors Journal*, **2015**, 4, 1000

[5] C. R. Ispas, G. Crivat, S. Andreescu, *Analytical Letters*, **2012**, 45, 168-186

[6] P. Mehrotra, *Journal of Oral Biology and Craniofacial Research*, **2016**, 6, 153-159

[7] S. Viswanathan, H. Radecka, J. Radecki, *Monatsh Chem*, **2009**, 140, 891-899

[8] A. M. T Al Layla, Ö. Türkarslan, S. Kurbanoglu, S. T. Sulaiman, K. A. Al-Flayeh, L. Toppare, *Journal of Macromolecular Science*, **2013**, 50, 914-922

[9] R. Farre, *Biosensori Elettrochimici di Tipo Amperometrico di Potenziale Interesse nella Caratterizzazione di Produzioni Agroalimentari*, Tesi di Dottorato, Sassari, **2015**

[10] F. W. Scheller, U. Wollenberger, A. Warsinke, F. Lisdat, *Current Opinion in Biotechnology*, **2001**, 12, 35-40

[11] G. Rocchitta, A. Spanu, S. Babudieri, G. Latte, G. Madeddu, G. Galleri, S. Nuvoli, P. Bagella, M. I. Demartis, V. Fiore, R. Manetti, P. A. Serra, *Sensors*, **2016**, 16, 780

[12] G. Palleschi, *Biosensori in Medicina*, Caleidoscopio, Genova, 1989

[13] A. Mignani, *Sviluppo di Biosensori: Modifiche di Superfici Elettrodiche e Sistemi di Immobilizzazione Enzimatica*, Tesi di Dottorato, Bologna, **2008**

[14] D. R. Thévenot, K. Toth, R. A. Durst, G. S. Wilson, *Biosensors and Bioelectronics*, **2001**, 16, 121-131

[15] J. R. Stetter, W. R. Penrose, S. Yao, *Journal of The Electrochemical Society*, **2003**, 150, S11-S16

[16] K. Cammann, *Fresenius Z. Anal. Chem.*, **1977**, 287, 1-9

[17] A. D. McNaught, A. Wilkinson, *IUPAC. Compendium of Chemical Terminology, 2nd ed. (The Gold Book)*, Blackwell Scientific Publications, Oxford, **1997**

[18] M. Cremer, *Uber die Ursache der Elektromotorischen Eigenschaften der Gewebe, Zugleich ein Beitrag zur Lehre von den Polyphasischen Elektrolytketten. Z. Biol.*, **1906**, 47, 562–608

[19] O. R. Zaborsky, *Immobilization of Enzymes by Adsorption* in *Biomedical Applications of Immobilized Enzymes and Proteins*, Springer, Boston MA

[20] F. Scheller, F. Schubert, in *Biosensors*, Elsevier, Amsterdam, **1992**

[21] A. Arnau, in *Piezoelectric Transducers and Applications*, Springer, Berlin, **2004**

[22] A. E. G. Cass, G. Davis, G. D. Francis, H. A. O. Hill, W. J. Aston, I. J. Higging, E. V. Plotkin, L. D. L. Scott, A. P. F. Turner, *Anal. Chem.*, **1984**, 56, 667-671

[23] D. R. Thévenot, K. Toth, R. A. Durst, G. S. Wilson, *Pure Appl. Chem*., **1999**, 71, 2333-2348

[24] F. G. Bănică, in *Chemical Sensors and Biosensors Fundamentals and Applications*, Wiley, Croydon, **2012**

[25] L. Vial, P. Dumy, *New J. Chem*., **2009**, 33, 939-946

[26] B. Gatto, R. Pierobon, *Dall'Evoluzioni in Vitro alle Nanotecnologie: gli Aptameri come Biosensori* in *Galileo*, Collegio degli Ingegneri della Provincia di Padova, **2012**

[27] S. Song, L. Wang, J. Li, C. Fan, J. Zhao, *TrAC Trends in Analytical Chemistry*, **2008**, 27, 108-117

[28] C. Karunakaran, K. Bhargava, R. Benjamin, in *Biosensors and Bioelectronics*, Elsevier, **2015**

[29] N. A. Mungroo, S. Neethirajan, *Biosensors*, **2014**, 4, 472-493

[30] I. Palchetti, M. Mascini, *Anal. Bioanal. Chem*., **2008**, 391, 455-471

[31] A. Koyun, E. Ahlatcioğlu, Y. K. İpek, *Biosensors and Their Principles* in *A Roadmap of Biomedical Engineer and Milestones*, S. Kara (ed), InTech, Rijeka, **2012**

[32] S. V. Dzyadevych, V. N. Arkhypova, A. P. Soldatkin, A. V. El'skaya, C. Martelet, N. Jaffrezic-Renault, *ITBM-RBM*, **2008**, 29, 171-180

[33] A. Chaubey, B. D. Malhotra, *Biosensors & Bioelectronics*, **2002**, 17, 441-456

[34] G. S. Wilson, Y. Hu, *Chem. Rev*., **2000**, 100, 2693-2704

[35] J. Wang, *Chem. Rev*., **2008**, 108, 814-825

[36] S. Palanisamy, B. Unnikrishnan, S. M. Chen, *Int. J. Electrochem. Sci*., **2012**, 7, 7935-7947

[37] P. Yeh, T. Kuwana, *Chemistry Letters*, **1977**, 1145-1148

[38] C. F. Blanford, *ChemComm*, **2013**, 49, 11130-11132

[39] C. M. A. Brett, A. M. O. Brett, in *Electroanalysis*, Oxford University Press, Coimbra, **1998**

[40] F. J. Holler, D. A. Skoog, S. R. Crouch, in *Chimica Analitica Strumentale*, EdiSES, Napoli, **2009**

[41] T. Wagner, W. Vornholt, C. F. Werner, T. Yoshinobu, K. Miyamoto, M. Keusgen, M. J. Schöning, *Physics in Medicine*, **2016**, 1, 2-7

[42] N. Jaffrezic-Renault, S. V. Dzyadevych, *Sensors*, **2008**, 8, 2569-2588

[43] Y. Wang, Z. Ye, Y. Ying, *Sensors*, **2012**, 12, 3449-3471

[44] E. Katz, I. Willner, *Electroanalysis*, **2003**, 15, 913-947

[45] S. M. Borisov, O. S. Wolfbeis, *Chem. Rev.*, **2008**, 108, 423-461

[46] P. Damborský, J. Švitel, J. Katrlík, *Essays in Biochemistry*, **2016**, 60, 91-100

[47] M. S. Thakur, K. V. Ragavan, *J. Food Sci. Technol*., **2013**, 50, 625-641

[48] H. H. Nguyen, J. Park, S. Kang, M. Kim, *Sensors*, **2015**, 15, 10481-10510

[49] M. D. Marazuela, M. C. Moreno-Bondi, *Anal. Bioanal. Chem*., **2002**, 372, 664-682

[50] D. W. Kimmel, G. LeBlanc, M. E. Meschievitz, D. E. Cliffel, *Anal. Chem*., **2012**, 84, 685-707

[51] L. M. da Costa Silva, V. P. Salviano dos Santos, A. Medeiros Salgado, K. Signori Pereira, *Biosensors for Contaminants Monitoring in Food and Environment for Human and Environmental Health, State of the Art in Biosensors – Environmental and Medical Applications*, Toonika Rinken, IntechOpen, **2013**

[52] E. B. Bahadir, M. K. Sezgintürk, *Analytical Biochemistry*, **2015**, 478, 107-120

[53] T. F. McGrath, C. T. Elliott, T. L. Fodey, *Anal. Bioanal. Chem*., **2012**, 403, 75-92

[54] P. S. Panesar, S. S. Marwaha, H. K. Chopra, *Enzymes in Food Processing Fundamentals and Potential Applications*, I.K. International Publishing House Pvt. Ltd., New Delhi, **2010**

[55] A. Pizzariello, M. Stredansky, S. Miertus, *La Chimica e l'Industria*, **2001**, 83, 1-7

[56] Y. Özogul, F. Özogul, *Food: Analysis, Occurrence and Toxicity*, **2019**, 1-17

[57] M. H. Silla Santos, *International Journal of Food Microbiology*, **1996**, 29, 213-231

[58] X. Yang, B. Feng, X. He, F. Li, Y. Ding, J. Fei, *Microchimica Acta*, **2013**, 180, 935-956

[59] P. Sebastian, P. Herr, U. Fischer, *S. Afr. J. Enol. Vitic.*, **2011**, 32, 300-309

[60] B. Ten Brink, C. Damink, H. M. L. J. Joosten, J. H. J. Huis in't Veld, *Int. J. Food Microbiol.*, **1990**, 11, 73-84

[61] A. R. Shalaby, *Food Research International*, **1996**, 29, 675-690

[62] R. R. Eitenmiller, S. C. De Souza, *Seafood Toxins*, **1984**, 431-442

[63] E. E. Snell, P. A. Recsei, *J. Biol. Chem.*, **1985**, 260, 2804-2806

[64] L. Prester, *Food Additives and Contaminants*, **2011**, 28, 1547-1560

[65] S. Lu, H. Ji, Q. Wang, B. Li, K. Li, C. Xu, C. Jiang, *Food Control*, **2015**, 50, 869-875

[66] F. Bedia Erim, *Trends in Analytical Chemistry*, **2013**, 52, 239-247

[67] F. E. Russell, Z. Maretić, *Toxicon*, **1986**, 24, 967-973

[68] EU Commission Regulation No. 1019/**2013**

[69] M. Niculescu, I. Frébort, P. Peč, P. Galuszka, B. Mattiasson, E. Csöregi, *Electroanalysis*, **2000**, 12, 369-375

[70] S. Ohnuma, M. Higa, S. Hamanaka, K. Matsushima, W. Yamamuro, *Internal Medicine*, **2001**, 40, 833-835

[71] A. Lonvaud-Funel, *FEMS Microbiology Letters*, **2001**, 199, 9-13

[72] S. L. Taylor, R. R. Eitenmiller, *Food Science and Technology*, **1986**, 17, 91-128

[73] C. K. Murray, G. Hobbs, R. J. Gilbert, *The Journal of Hygiene*, **1982**, 88, 215-220

[74] S. L. Taylor, *Histamine Poisoning Associated with Fish, Cheese and Other Foods*, **1985**, World Health Organization

[75] F. Franzen, K. Eysell, *Biologically Active Amines Found in Man: Their Biochemistry, Pharmacology, and Pathophysiological Importance*, **1969**, Oxford by Pergamon Press

[76] B. A. Bartholomew, P. R. Berry, J. C. Rodhouse, R. J. Gilbert, C. K. Murray, *Epidemiol. Infect.*, **1987**, 99, 775-782

[77] J. D. Henion, *Journal of Chromatography*, **1981**, 213, 475-480

[78] H. S. Marks, C. R. Anderson, *Journal of Chromatography A*, **2005**, 1094, 60-69

[79] H. Zhai, X. Yang, L. Li, G. Xia, J. Chen, H. Huang, S. Hao, *Food Control*, **2012**, 25, 303-308

[80] R. Romero-González, M. I. Alarcón-Flores, J. L. Martinez Vidal, A. Garrido Frenich, *Journal of Agricultural and Food Chemistry*, **2012**, 60, 5324-5329

[81] B. M. De Borba, J. S. Rohrer, *Journal of Chromatography A*, **2007**, 1155, 22-30

[82] G. J. Soleas, M. Carey, D. M. Goldberg, *Food Chemistry*, **1999**, 64, 49-58

[83] P. Lehtonen, M. Saarinen, M. Vesanto, M. L. Riekkola, *Zeitschrift fur Lebensmittel-Untersuchung und-Forschung*, **1992**, 194, 434-437

[84] T. Tang, T. Shi, K. Qian, P. Li, J. Li, Y. Cao, *Journal of Chromatography B*, **2009**, 877, 507-512

[85] J. S. Li, H. Wang, K. J. Huang, H. S. Zhang, *Analytica Chimica Acta*, **2006**, 575, 255-261

[86] L. Mureşan, R. Ronda Valera, I. Frébort, I. C. Popescu, E. Csöregi, M. Nistor, *Microchimica Acta*, **2008**, 163, 219-225

[87] K. Kivirand, T. Rinken, *Analytical Letters*, **2011**, 44, 2821-2833

[88] N. Verma, V. Hooda, A. Gahlaut, A. Gothwal, V. Hooda, *Critical Reviews in Biotechnology*, **2019**

[89] B. Shkodra, B. D. Abera, G. Cantarella, A. Douaki, E. Avancini, L. Petti, P. Lugli, *Biosensors*, **2020**, 10, 35

[90] V. K. Bajpai, C. Oh, I. Khan, Y. Haldorai, S. Gandhi, H. Lee, X. Song, M. Kim, A. Upadhyay, L. Chen, Y. S. Huh, Y. K. Han, S. Shukla, *Chemosphere*, **2020**, 243, 125404

[91] L. S. John Ho, R. Fogel, J. L. Limson, *Talanta*, **2020**, 208, 120474

[92] K. Pospiskova, I. Safarik, M. Sebela, G. Kuncova, *Microchimica Acta*, **2013**, 180, 311-318

[93] P. Bouvrette, K. B. Male, J. H. T. Luong, B. F. Gibbs, *Enzyme and Microbial Technology*, **1997**, 20, 32-38

[94] S. Tombelli, M. Mascini, *Analytica Chimica Acta*, **1998**, 358, 277-284

[95] M. A. Alonso-Lomillo, O. Domínguez-Renedo, P. Matos, M. J. Arcos-Martínez, *Analytica Chimica Acta*, **2010**, 665, 26-31

[96] C. M. Keow, F. A. Bakar, A. B. Salleh, L. Y. Heng, R. Wagiran, L. S. Bean, *Food Chemistry*, **2007**, 105, 1636-1641

[97] K. Zeng, H. Tachikawa, Z. Zhu, V. L. Davidson, *Anal. Chem*., **2000**, 72, 2211-2215

[98] L. Bao, D. Sun, H. Tachikawa, V.L. Davidson, *Anal. Chem*., **2002**, 74, 1144-1148

[99] M. Niculescu, T. Ruzgas, C. Nistor, I. Frébort, M. Šebela, P. Peč, E. Csöregi, *Anal. Chem*., **2000**, 72, 5988-5993

[100] A. Boffi, G. Favero, R. Federico, A. Macone, R. Antiochia, C. Tortolini, G. Sanzò, F. Mazzei, *Anal. Bioanal. Chem*., **2015**, 407, 1131-1137

[101] P. Manca, M. I. Pilo, G. Sanna, G. Bergamini, P. Ceroni, R. Boaretto, S. Caramori, *Syntetic Metals*, **2015**, 200, 109-116

[102] I. M. Apetrei, C. Apetrei, *Sensors*, **2016**, 16, 422

[103] W. Henao-Escobar, L. del Torno-de Román, O. Domínguez-Renedo, M. A. Alonso-Lomillo, M. J. Arcos-Martínez, *Food Chemistry*, **2016**, 190, 818-823

[104] Y. T. Lin, C. H. Chen, M. S. Lin, *Sensors and Actuators B*, **2018**, 255, 2838-2843

[105] A. Geto, M. Tessema, S. Admassie, *Synthetic Metals*, **2014**, 191, 135-140

[106] D. Brondani, C. W. Scheeren, J. Dupont, I. Cruz Vieira, *Sensors and Actuators B*, **2009**, 140, 252-259

[107] F. S. Felix, M. Yamashita, L. Angnes, *Biosensors and Bioelectronics*, **2006**, 21, 2283-2289

[108] J. Feher, in *Quantitative Human Physiology*, **2012**, Elsevier

[109] H. Beitollahi, M. M. Ardakani, B. Ganjipour, H. Naeimi, *Biosensors and Bioelectronics*, **2008**, 24, 362-368

[110] P. S. Dorraji, F. Jalali, *Sensors and Actuators B*, **2014**, 200, 251-258

[111] Ş. Alpat, K. Özdemir, S. K. Alpat, *Journal of Sensors*, **2016**, 2016, ID5653975

[112] L. G. Shaidarova, A. V. Gedmina, I. A. Chelnokova, G. K. Budnikov, *Journal of Analytical Chemistry*, **2008**, 63, 979-984

[113] S. Baluta, A. Lesiak, J. Cabaj, *Electroanalysis*, **2018**, 30, 1-11

[114] E. Wierzbicka, M. Szultka-Młyńska, B. Buszewski, G. D. Sulka, *Sensors and Actuators B*, **2016**, 237, 206–215

[115] I. M. Apetrei, C. Apetrei, *International Journal of Nanomedicine*, **2013**, 8, 4391-4398

[116] P. Solich, Ch. K. Polydorou, M. A. Koupparis, C. E. Efstathiou, *Journal of Pharmaceuticals and Biomedical Analysis*, **2000**, 20, 781-789

[117] M. H. Sorouraddin, J. L. Manzoori, E. Kargarzadeh, A. M. Haji Shabani, *Journal of Pharmaceuticals and Biomedical Analysis*, **1998**, 18, 877-881

[118] W. K. Adeniyi, A. R. Wright, *Spectrochimica Acta Part A*, **2009**, 74, 1001-1004

[119] V. Carrera, E. Sabater, E. Vilanova, M. A. Sogorb, *Journal of Chromatography B*, **2007**, 847, 88-94

[120] Y. Zhao, S. Zhao, J. Huang, F. Ye, *Talanta*, **2011**, 85, 2650-2654

[121] X. Liu, D. Ye, L. Luo, Y. Ding, Y. Wang, Y. Chu, *Journal of Electroanalytical Chemistry*, **2012**, 65, 1-5

[122] T. Thomas, R. J. Mascarenhas, P. Martis, Z. Mekhalif, B. E. Kumara Swamy, *Materials Science and Engineering*, **2013**, C 33, 3294-3302

[123] R. N. Goyal, S. Bishnoi, *Talanta*, **2011**, 84, 78-83

[124] A. B. Moghaddam, M. R. Ganjali, A. A. Saboury, A. A. Moosavi-Movahedi, P. Narouzi, *J. Appl. Electrochem*., **2008**, 38, 1233-1239

[125] P. K. Robinson, *Essays in Biochemistry*, **2015**, 59, 1-41

[126] J. B. Sumner, *J. Biol. Chem*., **1926**, 69, 435-441

[127] D. L. Nelson, M. M. Cox, *I Principi di Biochimica di Lehninger*, Zanichelli

[128] W. W. Cleland, *Biochimica et Biophysica Acta*, **1963**, 67, 104-137

[129] F. Buffoni, G. Ignesti, *Molecular Genetics and Metabolism*, **2000**, 71, 559-564

[130] H. G. Schwelberger, E. Bodner, *Biochimica et Biophysica Acta*, **1997**, 1340, 152-164

[131] M. Kanteev, M. Goldfeder, A. Fishman, *Protein Science*, **2015**, 24, 1360-1369

[132] A. Nawaz, T. Shafi, A. Khaliq, H. Mukhtar, I. ul Haq, *International Journal of Biotechnlogy and Bioengineering*, **2017**, 3, 142-148

[133] Á. Sánchez-Ferrer, J. N. Rodríguez-López, F. García-Carmona, *Biochimica et Biophysica Acta*, **1995**, 1247, 1-11

[134] A. Sassolas, L. J. Blum, B. D. Leca-Bouvier, *Biotechnology Advances*, **2012**, 30, 489-511

[135] S. Kurbanoglu, C. Erkmen, B. Uslu, *Trends in Analytical Chemistry*, **2020**, 124, 115809

[136] H. P. Sneha, K. C. Beulah, P. S. Murthy, *Enzym. Food Biotechnol*., **2019**, Chapter 37, 645-658

[137] I. Migneault, C. Dartiguenave, M. J. Bertrand, K. C. Waldron, *Biotechniques*, **2004**, 5, 790-802

[138] F. M. Richards, J. R. Knowles, *J. Mol. Biol*., **1968**, 37, 231-233

[139] P. Monsan, G. Puzo, H. Mazarguil, *Biochimie*, **1975**, 57, 1281-1292

[140] P. M. Hardy, A. C. Nicholls, H. N. Rydon, *J. Chem. Soc. Perkin Trans*., **1976**, 1, 958-962

[141] P. M. Hardy, G. J. Hughes, H. N. Rydon, *J. Chem. Soc. Perkin Trans*., **1979**, 1, 2282-2288

[142] T. Tashima, I. Masahiro, T. Kuroda, S. Yagi, N. Terumichi, *J. Org. Chem*., **1991**, 56, 694-697

[143] D. R. Walt, V. Agayn, *Trends in Analytical Chemistry*, **1994**, 13, 425-430

[144] B. Nordén, E. Krutmeijer, *The Nobel Prize in Chemistry, 2000: Conductive Polymers*, Kungl. Vetenskapsakademien (The Royal Swedish Academy of Sciences)

[145] T. K. Das, S. Prusty, *Polymes-Plastics Technology and Engineering*, **2012**, 51, 1487-1500

[146] P. Manca, M. I. Pilo, G. Casu, S. Gladiali, G. Sanna, R. Scanu, N. Spano, A. Zucca, C. Zanardi, D. Bagnis, L. Valentini, *Journal of Polymer Science Part A: Polymer Chemistry*, **2011**, 49, 3513-3523

[147] G. Ruggeri, *Polimeri Conduttori, CnS – La Chimica nella Scuola*, Novembre – Dicembre **2002**

[148] H. Shirakawa, E. J. Louis, A. G. McDiarmid, C. K. Chiang, A. J. Heeger, *J. C. S. Chem. Comm.*, **1977**, 474, 578-580

[149] B. Scrosati, *Materials Science Forum*, **1989**, 42, 207-220

[150] T-H. Le, Y. Kim, H. Yoon, *Polymers*, **2017**, 9, 150

[151] P. Manca, *Elettrosintesi, Caratterizzazione e Proprietà di Politiofeni Funzionalizzati con Unità Chelanti all'Azoto*, Tesi di Dottorato, Sassari, **2009**

[152] J. Roncali, *Chem. Rev*., **1992**, 92, 711-738

[153] M. Szajda and J. N. Lam, "*Thiophenes and their Benzo Derivatives: Structure", in "Comprehensive Heterocyclic Chemistry II, Vol. 2"*, Editor, C. W. Bird, Pergamon Press, Oxford, **1996**

[154] M. H. Palmer, R. H. Findlay, *Tetrahedron Letters*, **1972**, 41, 4165-4168

[155] S. Gronowitz, *Advances in Heterocyclic Chemistry*, **1963**, 1, 1-124

[156] B. Krische, M. Zagorska, *Synthetic Metals*, **1989**, 28, C263-C268

[157] T. Yamamoto, K. Sanechika, A. Yamamoto, *J. Polym. Sci.: Polymer Letters Edition*, **1980**, 18, 9-12

[158] J. W-P. Lin, L. P. Dudek, *J. Polym. Sci.: Polym. Chem. Ed*., **1980**, 18, 2869-2873

[159] K. Tamao, K. Sumitani, M. Kumada, *Journal of the American Chemical Society*, **1972**, 94, 4374-4376

[160] Tourillon G., Garnier F., *J. Electroanal.Chem*.,**1982**, 135, 173-178

[161] J. Heinze, B. A. Frontana-Uribe, S. Ludwigs, *Chem. Rev*., **2010**, 110, 4724-4771

[162] A. Czerwinski, H. Zimmer, C.V. Pham, H. B. Mark, *J. Electrochem.Soc*., **1985**, 132, 2669-2672

[163] K. Tanaka, T. Shichiri, T. Yamabe, *Synthetic Metals*, **1986**, 16, 207-214

[164] M. Gratzl, D.F. Hsu, A. M. Riley, J. Janata, *J. Phys.Chem*., **1990**, 94, 5973-5981

[165] J-C. Eloi, L. Chabanne, G. R. Whittell, I. Manners, *Materialtoday*, **2008**, 11, 28-36

[166] P. G. Pickup, *J. Mater. Chem*., **1999**, 9, 1641-1653

[167] B. J. Holliday, T. M. Swager, *Chem. Commun*., **2005**, 23-36

[168] R. Cozzi, P. Protti, T. Ruaro, in *Analisi Chimica: Moderni Metodi Strumentali*, ESU, Milano, **1987**

[169] I. P. Beletskaya, A. V. Cheprakov, *Chem. Rev*., **2000**, 100, 3009-3066

[170] A. Suzuki, *Angew. Chem. Int. Ed*., **2011**, 50, 6723-6737

[171] S. S. Gujral, S. Khatri, P. Riyal, *Indo Global Journal of Pharmaceutical Sciences*, **2012**, 2, 351-367

[172] M. Toyota, C. Komori, M. Ihara, *J. Org. Chem*., **2000**, 65, 7110-7113

[173] M. J. Mio, L. C. Kopel, J. B. Braun, T. L. Gadzikwa, K. L. Hull, R. G. Brisbois, C. J. Marwworth, P. A. Grieco, *Organic Letters*, **2002**, 4, 3199-3202

[174] K. Sonogashira, *Journal of Organometallic Chemistry*, **2002**, 653, 46-49

[175] K. Sonogashira, Y. Tohda, N. Hagihara, *Tetrahedron Letters*, **1975**, 50, 4467-4470

[176] S. Thorand, N. Krause, *J. Org. Chem.,* **1998**, 63, 8551-8553

[177] B. Witulski, J. R. Azcon, C. Alayrac, A. Arnautu, V. Collot, S. Rault, *Synthesis*, **2005**, 5, 771-780

[178] A. V Ustinov, V. A. Korshun, *Russian Chemical Bulletin International Edition*, **2006**, 55, 1268-1274

[179] P. Espinet, A. M. Echavaren, *Angew. Chem. Int. Ed*., **2004**, 43, 4704-4734

[180] C. Len, S. Bruniaux, F. Delbecq, V. S. Parmar, *Catalysts*, **2017**, 7, 146

[181] R. Chinchilla, C. Nájera, *Chem. Rev*., **2007**, 107, 874-922

[182] T. Posset, J. Blümel, *J. Am. Chem. Soc*., **2006**, 128, 8394-8395

[183] N. Miyaura, K. Yamada, A. Suzuki, *Tetrahedron Letters*, **1979**, 36, 3437-3440

[184] N. Miyaura, A. Suzuki, *J.C.S. Chem. Comm*., **1979**, 866-867

[185] A. J. J. Lennox, G. C. Lloyd-Jones, *Chem. Soc. Rev*., **2014**, 43, 412

[186] M. I. Pilo, R. Farre, J. I. Lachowicz, E. Masolo, A. Panzanelli, G. Sanna, N. Senes, A. Sobral, N. Spano, *Journal of Analytical Methods in Chemistry*, **2018**, Article ID 1849439

[187] L. Hintermann, A. Labonne, *Synthesis*, **2007**, 8, 1121-1150

[188] Z. Gu, Z. Li, Z. Liu, Y. Wang, C. Liu, J. Xiang, *Catalysis Communications*, **2008**, 9, 2154-2157

[189] M. Bérubé, D. Poirier, *Organic Letters*, **2004**, 6, 3127-3130

[190] D. Zając, D. Honisz, M. Łapkowski, J. Sołoducho, *Molecules*, **2021**, 26, 1216

[191] P. Manca, R. Scanu, A. Zucca, G. Sanna, N. Spano, M. I. Pilo, *Polymer*, **2013**, 54, 3504-3509

[192] K. Yasukoucki, I. Taniguchi, H. Yamaguchi, K. Arakawa, *J. Electroanal. Chem*., **1981**, 121, 231-240

[193] F. Meloni, K. Spychalska, D. Zając, M. I. Pilo, A. Zucca, J. Cabaj, *Electroanalysis*, **2021**, 33, 1-8

[194] T. Guo, J. Gao, X. Qin, X. Zhang, H. Xue, *Polymers*, **2018**, 10, 723

[195] D. Zając, J. Sołoducho, T. Jarosz, M. Łapkowski, S. Roszak, *Indian Journal of Applied Research*, **2017**, 7, 58-66

[196] M. D. Hawley, S. V. Tatawawadi, S. Piekarski, R. N. Adams, *Journal of the American Chemical Society*, **1967**, 89, 447-450

[197] H. M. Zhang, X. L. Zhou, R. T. Hui, N. Q. Li, D. P. Liu, *Talanta*, **2002**, 56, 1081–1088

[198] S. Wang, D. Du, Q. C. Zou, *Talanta*, **2002**, 57, 687-692

[199] G. Alarcon-Angeles, G.A. Álvarez-Romero, A. Merkoçi, *Encyclopedia of Interfacial Chemistry*, **2018**, 140-155

[200] A. J. Bard, L. R. Faulkner, in *Electrochemical Methods Fundamentals and Applications*, **2001**, John Wiley & Sons, New York

[201] N. Elgrishi, K. J. Rountree, B. D. McCarthy, E. S. Rountree, T. T. Eisenhart, J. L. Dempsey, *J. Chem. Educ*., **2018**, 95, 197-206

[202] B. O. Agboola, K. I. Ozoemena, *Electroanalysis*, **2008**, 20, 1696-1707

[203] P. Gopal, G. Narasimha, T. Madhusudana Reddy, *Process Biochemistry*, **2020**, 92, 476-485

[204] L. Qiu, M. Zhang, R. A. Sturm, B. Gardiner, I. Tonks, G. Kay, P. G. Parsons, *The Journal of Investigative Dermatology*, **2000**, 114, 21-27

[205] I. M. Apetrei, G. Bahrim, M. L. Rodriguez-Méndez, *Romanian Biotechnological Letters*, **2012**, 17, 7684-7693

[206] C. Apetrei, J. A. de Saja, J. Zurro, M. L. Rodriguez-Mendéz, *Catalysts*, **2012**, 2, 517-531

[207] J. P. Hervàs Pérez, M. Sánchez-Paniagua López, E. López-Cabarcos, B. López-Ruiz, *Biosensors and Bioelectronics*, **2006**, 22, 429-439

[208] O. A. Semenikhin, L. Jiang, T. Iyoda, K. Hashimoto, A. Fujishima, *Synthetic Metals*, **2000**, 110, 195-201

[209] S. Dalirirad, A. J. Steckl, *Sensors & Actuators B: Chemical*, **2019**, 283, 79-86

[210] A. J. Steckl, P. Ray, *ACS Sens*., **2018**, 3, 2025-2044

[211] P. Damier, E. C. Hirsch, Y. Agrid, A. M. Graybiel, *Brain*, **1999**, 122, 1437-1448

[212] F. B. K. Eddin, Y. W. Fen, *Sensors*, **2020**, 20, 1039

[213] Y. K. Lin, Y. C. Yeh, *Anal. Chem*., **2017**, 89, 11178-11182

[214] J. Soleymani, *Trends in Analytical Chemistry*, **2015**, 72, 27-44

[215] B. Sun, C. Wang, *Journal of Nanomaterials*, **2012**, ID502481

[216] X. Lin, Y. Zhang, W. Chen, P. Wu, *Sensors & Actuators B: Chemical*, **2007**, 122, 309-314

[217] Y. Cao, M. T. McDermott, *BioRxiv*, **2018**, 1-24

[218] R. P. Bacil, L. Chen, S. H. P. Serrano, R. G. Compton, *Phys. Chem. Chem. Phys*., **2020**, 22, 607-614

[219] Q. Yuan, Y. Liu, C. He, H. Sun, D. Dai, Q. Wei, G. Lai, T. Wu, A. Yu, L. Fu, K. W. A. Chee, C. T. Lin, *Biosensors and Bioelectronics*, **2018**, 111, 117-123

[220] K. Min, Y. J. Yoo, *Talanta*, **2009**, 80, 1007-1011

[221] M. Florescu, M. David, *Sensors*, **2017**, 17, 1314

[222] S. Liu, F. Shi, X. Zhao, L. Chen, X. Su, *Biosensors and Bioelectronics*, **2013**, 47, 379-384

[223] U. Baruah, N. Gogoi, A. Konwar, M. Jyoti Deka, D. Chowdhury, G. Majumdar, *J. Nanoparticles 2014*, 2014, 1-8

[224] R. Freeman, L. Bahshi, T. Finder, R. Gill, I. Willner, *Chem. Commun.*, **2009**, 764-766

[225] Y. C. Tsai, C. C. Chiu, *Sensors and Actuators B*, **2007**, 125, 10-16

[226] S. Tembe, B. S. Kubal, M. Karve, S. F. D'Souza, *Analytica Chimica Acta*, **2008**, 612, 212-217

[227] Q. Huang, S. Hu, H. Zhang, J. Chen, Y. He, F. Li, W. Weng, J. Ni, X. Bao, Y. Lin, *Analyst*, **2013**, 138, 5417-5423

[228] Y. R. Kim, S. Bong, Y. J. Kang, Y. Yang, R. K. Mahajan, J. S. Kim, H. Kim, *Biosensors and Bioelectronics*, **2010**, 25, 2366-2369

[229] F. Gao, X. Cai, X. Wang, C. Gao, S. Liu, F. Gao, Q. Wang, *Sensors and Actuators B*, **2013**, 186, 380-387

[230] A. C. Anithaa, N. Lavanya, K. Asokan, C. Sekar, *Electrochimica Acta*, **2015**, 167, 294-302

[231] S. Tembe, S. Kulkarni, M. Karve, S. F. D'Souza, *Sensors & Transducers Journal*, **2009**, 107, 111-118

[232] I. M. Apetrei, C. V. Popa, C. Apetrei, D. Tutunaru, *Romanian Biotechnological Letters*, **2014**, 19, 9801-9809

[233] F. Meloni, M. I. Pilo, G. Sanna, N. Spano, A. Zucca, *Applied Sciences – SI Advances on Coordination Chemistry with Nitrogen Ligands and Its Applications,* **2021**, 11, 2065

AKNOWLEDGEMENTS

For scientific support and collaboration, I want to thank:

- My supervisor and co-supervisor, **Prof. Antonio Zucca** and **Prof. Maria Itria Pilo** without whom this work would not have been possible.
- **Prof. Joanna Cabaj** and her research group: (**Dr. Anna Lesiak**, **Dr. Dorota Zając**, **Dr. Sylwia Baluta** and **Dr. Kamila Spychalska)** who hosted me for 8 months in their laboratory, where most of this work began to take shape.
- **Prof. Mario Sechi** and **Dr. Massimo Carraro** for their suggestions regarding organic syntheses.
- **Dr. Antonello Iacomini** for SEM images.
- **Dr. Michele Satta** for his practical help in laboratory.
- All the Professors of the Department of Chemistry and Pharmacy of the University of Sassari and of the Department of Chemical and Geological Sciences of the University of Cagliari who have dedicated their time to the advanced courses scheduled by the PhD regulations.

Usque ad finem

And here I am at the end of this sad and not well describable adventure.

Anyway, I want to thank all those who tried to illuminate my path in this period of low- light.

First of all, my wonderful parents who have supported me in these very long 3 years, encouraging and advising me every time at best.

Special thanks go to Marco and Mariangela without whom I would not have completed this PhD. I couldn't ask for better colleagues and friends!

I thank Paola and Francesca who in the darkest moment have always made me smile.
Silvia and Massimo, my photo-friends, who, in addition to daily support, also came to visit me in Poland cheering up my stay.
Monica and Laura for their constant presence even from a distance.
I strongly thank Ivana for always being present and with the right words during my entire university career.
I sincerely thank Giada, Simona, Claudio, Mauro, Mara, Valentina, Ginevra, Claudia, Valeria, Giovanni and Alessandra for their fantastic company during the months in Poland.
Agatha and Ola for making me feel at home 2000 km from home.
Friends of the T22, Matthew and Arif, and all the friends of the Italian Meeting in Wrocław.
To all of you my biggest THANKS!